# Sand transport under full-scale progressive surface waves

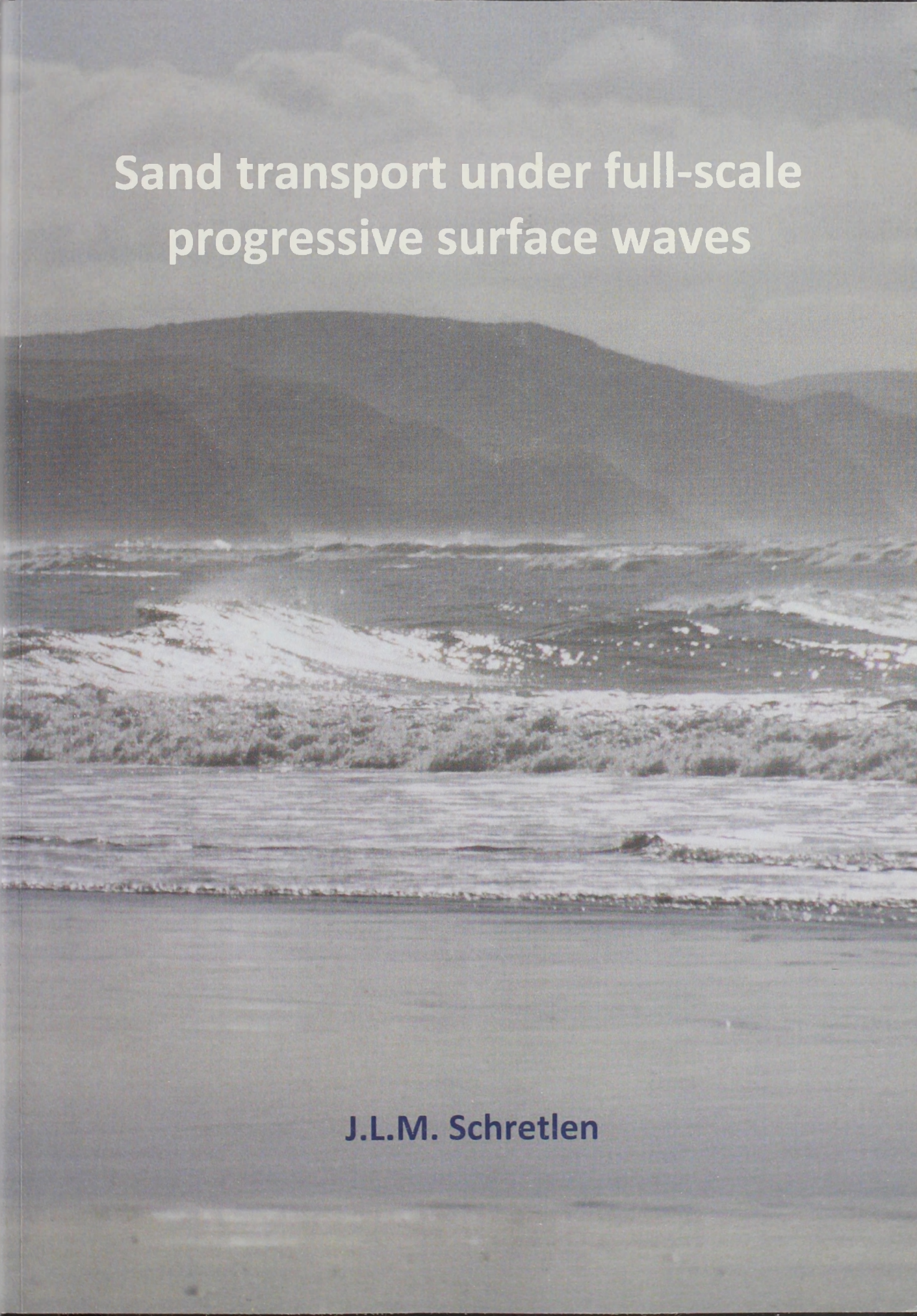

J.L.M. Schretlen

# SAND TRANSPORT UNDER FULL-SCALE PROGRESSIVE SURFACE WAVES

J.L.M. Schretlen

Promotion committee

| | |
|---|---|
| prof. dr. ir. F.J.A.M. van Houten | University of Twente, chairman/ secretary |
| prof. dr. S.J.M.H. Hulscher | University of Twente, promotor |
| dr. ir. J.S. Ribberink | University of Twente, assistant-promotor |
| | |
| prof. dr. T. O'Donoghue | University of Aberdeen |
| dr. ir. C.M. Dohmen-Janssen | University of Twente |
| prof. dr. ir. H.J. de Vriend | University of Twente |
| prof. dr.ir. L.C. van Rijn | Utrecht University |
| prof. dr. ir. M.J.F. Stive | Delft University of Technology |
| dr. B.G. Ruessink | Utrecht University |

This thesis is supported by:

The thesis is part of the 'SANTOSS' project. This project is funded by the Dutch Technology Foundation STW, applied science division of NOW and the technology programme of the Ministry of Economic Affairs of the Netherlands (project number TCB.6586) and the UK's Engineering and Physical Sciences Research Council (EPSRC) (project number GR/T28089/01).

The experiments in the GWK are performed in the framework of the SANTOSS project and of the Access programme of the Integrated Infrastructure Initiative Hydralab-III of the European Community's Sixth Framework Programme (contract no. 022441).

The cover photo is taken by Jolanthe Schretlen and shows full-scale progressive surface waves generating sheet-flow conditions at Raglan Beach, New Zealand (2004).

# SAND TRANSPORT UNDER FULL-SCALE PROGRESSIVE SURFACE WAVES

PROEFSCHRIFT

ter verkrijging van
de graad van doctor aan de Universiteit Twente,
op gezag van de rector magnificus,
prof. dr. H. Brinksma,
volgens besluit van het College voor Promoties
in het openbaar te verdedigen
op vrijdag 8 juni 2012 om 14.45 uur

door

Johanna Lidwina Maria Schretlen
geboren op 17 april 1979
te Beesel

This thesis is approved by:

| | |
|---|---|
| prof. dr. S.J.M.H. Hulscher | promotor |
| dr. ir. J.S. Ribberink | assistant-promotor |



Printed by Wöhrmann Print Service, Zutphen, The Netherlands

ISBN 978-94-6203-061-9

*Wisest is she who knows what she doesn't know (yet....)*

inspired by a quote from *Sophie's World* (Jostein Gaarder)

*"Fear is inevitable, I have to accept that, but I cannot allow it to paralyze me."*

(Isabel Allende)

## Words of thanks

The final part of writing this thesis is this section; it is not about boundary layer flow or grain sizes, but about the people I want to thank for their support throughout this whole project.

I should start with Jan and Suzanne, due to your confidence in my abilities to bring this to a good end, I had a chance to start this project in the first place. The past years you have been two very different types of supervisors, and I have been lucky to get the best of both. Jan, your eye for detail and critical questions pushed me to do a better job. After our talks, I often left your office with at least as many new ideas as solutions to the old ones (which is not always easy for someone who has trouble to decide what not to include), which was always a motivation to look beyond the obvious plans. Suzanne, it is very refreshing to also have a supervisor who has some distance from the project and can ask the right questions when I have been thinking about details to long. Apart from the research itself, some of our talks over the last couple of years have been a boost for my confidence and motivation to finish this project, and you made it possible for me to stay in the WEM group while doing so, thank you for that.

Also my 'previous two supervisors' should be mentioned here; Aart Kroon and Karin Bryan, thanks to your encouragement I considered applying for a PhD project in the first place.

If there is anything I would like to recommend to future PhD students, it is to find a research proposal which is part of a larger project. Working together in the SANTOSS project has been a privilege. Tom O'Donoghue, Jan Ribebrink, Lorna Campbell, Dominic van der A, Jebbe van der Werf, Alan Davies, Jonathan Malarkey, Shunqi Pan, Ming Lee, Rob Uittenbogaard, Wouter Kranenburg and the dedicated user-committee; in particular Richard Soulsby, Leo van Rijn, Noel Beech and Dirk-Jan Walstra. I always looked forward to our meetings together. The discussions and comments were always valuable and the positive atmosphere in which these were given have been a great motivation.

A large part of the first years of my research consisted of planning, designing and performing the new experiments. As a physical geographer used to field work I was not taken aback by the sheer size of the GWK. But I also quickly realized, there was no way I could have obtained all these measurements without the help of: the GWK staff (Joachim Grüne, Stefan Schimmels, Reinhold Schmidt-Koppenhagen and the complete technical staff); Marcel van Maarseveen, Chris Roosendaal, Bas van Dam and above all Henk Markies of the physical geography laboratory from Utrecht University and René Buijsrogge of the University of Twente for the endless designing, redesigning, calibrating, setting up and breaking down of the measurement rigs and instruments and acquisitioning systems. All the colleagues and students who helped with the measurements in one way or the other. I've been lucky to have so many of you around, I know I will forget somebody if I try to mention you all, but a special thanks for your many hours of help goes to Joris Eekhout, Michel Zuijderwijk, Maarten Kleinhans, Tommer Vermaas, Christien Huisman, Freek Huthoff and Dominic van der A.

When sitting at my desk at the WEM group, the large amount of positive, fun and motivated colleagues kept me sane. Thank you for you chats, advises, discussions and many good memories! I wouldn't dare to try to mention all of you, because I will never get it completely right, but a special word goes to; Saskia, Olav en Erik; I couldn't have asked for better office-mates, I hope I didn't bother you too much. Jebbe; thank you for getting me started the first few years, your matlab and common-research-sense advices have been valuable. Arjan; I realised it has already been 14 years, I hope we may share many more with you and Ilse.

When not generating waves in the GWK or sitting at my desk in Twente, I very much enjoyed my time at SANTOSS meetings, Hydralab or Sands meetings, conferences, summerschools at Texel

and Skallingen etc etc. Each of those was a great experience with fantastic people from all over the world. There are too many of you to mention personally, but if reading this brings back one of those good memories, this includes you as well.

Erik and Dominic, the fact that you appear in almost all of the above paragraphs shows how much we have had in common the last couple of years. Apart from colleagues I consider us to be good friends as well and I'm honoured to have you by my side as 'paranimfen'.

De laatste woorden in dit dankwoord zijn voor alle familie en vrienden die me aangemoedigd of juist afgeleid hebben wanneer het nodig was. Bedankt voor jullie enthousiasme en vertrouwen!

Lieve Lies, Gerrit, Marije, Mark, Isabel en Noor; mijn Twentse familie. Niet eens officieel, maar wat maakt dat uit als het wel zo voelt. Ik had me geen lievere schoonfamilie kunnen wensen. Nu ik in het weekend niet meer achter de laptop zit hoop ik dat jullie je bij ons net zo welkom voelen als ik altijd bij jullie doe.

Lieve mam en Sas, ook al spreek je elkaar niet elke dag, ik besef maar al te goed hoe belangrijk het voor me is om deel uit te maken van onze 3-eenheid. Ik ben ontzettend trots op wie wij alle 3 afzonderlijk en samen zijn geworden. Samen een rondje Noorwegen doen dan maar?

Allerliefste Freek, ik heb dit proefschrift niet gemaakt om wraak te nemen op jou ☺ maar nu ook deze af is, kan ik niet wachten om weer nieuwe plannen samen (waar) te maken. Ik zou een heel dankwoord kunnen schrijven voor de afgelopen jaren, maar het komt allemaal op hetzelfde neer: dankjewel en ik hou van je.

## Table of contents

## Summary

The morphology of coastal areas is constantly changing under the influence of sediments being transported to, from and along the coast. Under storm conditions with high waves and flow velocities, bed forms are being washed out and large quantities of sand are transported in a thin, mm to cm thick layer close to the bed called the sheet-flow layer. Since sand transport under storm conditions is primarily controlled by small scale near-bed processes, development of well-founded methods for predicting near-bed sand transport are critical for estimating sand budget in coastal areas. Various transport models have been developed to predict both the quantities and directions of sediment transport under storm conditions. The majority of the existing models are based on data obtained from oscillatory flow tunnel experiments. Even though oscillatory flow tunnels provide a good approximation of the flow experienced at the sea bed, theory and former experiments indicate that flow differences between full scale progressive surface waves and oscillatory flow tunnels may have a substantial effect on the net sand transport.

The research presented in this thesis focuses on the influence of surface wave effects on sand transport under sheet-flow conditions. For the first time, detailed measurements of wave boundary layer flow and sheet-flow layer transport processes under full scale surface waves are presented and analysed. These results give new insights and provide quantitative data of wave boundary flow, sheet-flow layer concentrations, sediment fluxes and net transport rates under velocity skewed surface waves for different wave conditions and types of sediment.

Before performing new measurements, an inventory of all existing (full-scale) experiments and their characterises was made (the SANTOSS database). The database is a useful resource for the design of new experiments and the development and validation of sand transport models for coastal applications. Based on this, the gaps in existing data were identified and it was determined which gaps were needed to be filled with new experiments in order to obtain a better understanding of progressive surface wave effects in sand transport processes. On basis of this database it became clear that more insight was needed in the details of the sand transport processes inside the sheet flow and wave boundary layer. In this research new measurements were carried out for various types of full-scale surface waves in the sheet-flow regime over a horizontal mobile sand bed with medium ($D_{50}$ = 0.25 mm) and fine ($D_{50}$ = 0.14 mm) sand in the large wave flume, or Groβer Wellenkanal (GWK), of the Coastal Research Centre in Hannover, Germany.

High resolution measurements of boundary layer flow characteristics under these wave conditions performed in this research, show that the measured wave boundary layer thickness and the time-dependent velocity profiles show a large similarity with those measured in oscillating flow tunnels. However, the mean horizontal flow velocity (streaming) profiles are clearly different. For all new experiments the vertical streaming profile shows a characteristic three-layer shape with 'onshore' as well as 'offshore' streaming and with alternating negative and positive shear layers in between. Above the sheet flow layer two layers are observed showing generally 'offshore' streaming. The two-layer structure is explained qualitatively by the height-dependent balance between mean pressure gradient, wave Reynolds stress and the mean (oscillatory) turbulent Reynolds stress. In the sheet flow layer all experiments show a transition to 'onshore' streaming, which is caused by the 'onshore' erosion depth always exceeding the 'offshore' component due to the velocity skewness of the oscillatory flow (erosion depth asymmetry). The streaming under progressive waves is generally

more 'onshore' than in oscillatory flow tunnels, which may be explained by the influence of the wave Reynolds stress and by advective effects (absent in tunnels). In the upper levels of the boundary layer the streaming profiles show a negative shear in the present experiments (transition to negative undertow), while tunnel experiments show here a positive shear due to the opposite direction of the mean pressure gradient (transition to positive return flow).

Apart from the flow velocities, new insights in behaviour of sediment concentrations and fluxes under progressive surface waves for both medium ($D_{50}$ = 0.25 mm) and, for the first time, fine sand ($D_{50}$ = 0.14 mm) conditions are presented. For both medium and fine sand, the maximum (crest and trough) and total mean sediment transport rates are concentrated inside the sheet flow layer. For fine sand conditions, more sand is being brought into motion, leading to a larger erosion depth and sheet-flow layer thickness than for medium sand conditions under similar wave conditions and time-dependent concentrations show a larger phase lag to the free stream flow velocity than for medium sand conditions. Despite these quantitative differences, the overall pattern of the mean flux profiles for both sand conditions are comparable. Velocity skewness generates larger onshore than offshore fluxes and the total mean transport rates are directed onshore for all experiments. The total horizontal mean sediment flux shows a two-layer structure; an onshore directed flux deep inside the pick-up layer and a (smaller) offshore directed flux above that. For medium sand conditions, the total mean flux is higher that found in oscillatory flow tunnels under similar conditions, but the behaviour and direction (onshore) is comparable. For fine sand conditions, the results differ strongly from the results previously obtained from oscillatory flow tunnel experiments. The fluxes are not only larger, but the total mean flux under progressive surface waves is positive and onshore directed instead of negative and offshore directed as found in oscillatory flows.

The measured total net sand transport rates presented in this thesis are a critical extension to the existing medium sand surface wave measurements since the amount of available data is more than doubled. In addition, it is the first time that, apart from medium sand results, transport rates are presented for full scale surface waves with a fine sand mobile bed.
The new experiments show a linear increase in transport rates with an increase in the third-order moment of the time-dependent velocity in the free stream, for both the medium and fine sand. The transition from onshore to offshore net transport with increasing flow strength as measured for fine sand conditions in oscillatory flow tunnels, is not observed under surface waves. This is in line with the results of the, independently measured, sediment fluxes inside the sheet flow layer. A likely explanation for this difference is that phase lag effects of fine sand, responsible for the transition to offshore net transport, are now overruled by progressive surface wave effects, such as a larger 'onshore' mean bed shear stress (wave Reynolds stress) and the onshore directed wave boundary layer streaming. The wave Reynolds stress leads to additional crest and trough asymmetry of the bed shear stress, additional erosion depth asymmetry and thus to more onshore sand transport. The onshore streaming leads to an additional current-related sediment flux in the onshore direction. It is shown that, since the far majority of sand is transported inside the (lower) sheet flow layer, relatively small wave induced net currents may have an important effect on the sand transport rates under these conditions.

The insights that are obtained from the new experiments are of critical importance for the development of sediment transport models. Besides performing the new experiments, the result are

compared to the existing practical sand transport models of Nielsen (2006) and Van Rijn (2007). Both are quasi-steady empirical models that use a different approach to account for surface wave streaming effects. Besides these existing models, a newly developed model of the SANTOSS-project is evaluated as well. The results of these comparisons show that the addition of individual surface wave processes as done in the development of the semi-unsteady SANTOSS model, together with the large range of conditions for which the model is developed, make the model in principle better applicable for transport rate predictions than the other two models tested here.

## Samenvatting

De morfologie van kustgebieden verandert constant als gevolg van sediment dat verplaatst wordt richting de kust, de zee en langs de kustlijn. Tijdens storm condities met hoge golven en stroomsnelheden worden beddingvormen uitgevaagd en grote hoeveelheden zand worden in een dunne laag (mm – cm dik) dichtbij de bodem verplaatst (*sheet flow*). Omdat zandtransport tijdens stormcondities voornamelijk wordt bepaald door kleinschalige processen dichtbij de bodem, is de ontwikkeling van gedegen methodes om zandtransport bij de bodem te voorspellen van cruciaal belang voor de voorspelling van de ontwikkelingen van kustgebieden. Er zijn verschillende zandtransportmodellen ontwikkeld om de kwantiteit en richting van sedimenttransport tijdens stormcondities te voorspellen. De meerderheid van de bestaande modellen is gebaseerd op data afkomstig van experimenten, uitgevoerd in tunnels met oscillerende stroming. Deze tunnels geven een goede benadering van de werkelijke stroming die dichtbij de zeebodem plaats vindt. Echter, theorie en eerdere experimenten laten zien dat kleine verschillen in de stromingsprocessen tussen oppervlaktegolven op werkelijke schaal en in tunnels met oscillerende stroming van cruciaal belang zouden kunnen zijn voor het daadwerkelijk sedimenttransport.

Het onderzoek dat in dit proefschrift gepresenteerd wordt is gericht op de invloed van deze effecten van echte golven op zandtransport in stormcondities. Voor het eerst zijn er gedetailleerde metingen van de processen in de golfgrenslaag en in de sheet-flow-laag onder oppervlaktegolven van werkelijke grootte. De resultaten geven nieuwe inzichten en kwantitatieve data van stromingen in de golfgrenslaag, sedimentconcentraties in de sheet-flow-laag, sedimentfluxen en netto zandtransporten onder verschillende typen asymmetrische oppervlaktegolven over twee verschillende soorten zandbodems (medium ($D_{50}$ = 0.25 mm) en fijn zand ($D_{50}$ = 0.14 mm).

Voor de aanvang van nieuwe experimenten, is er een inventarisatie gemaakt van de data en kenmerken van bestaande experimenten (samengevoegd in de SANTOSS database). Deze database is een waardevolle bron voor het ontwerpen van nieuwe experimenten en de ontwikkeling van zandtransportmodellen voor kustgebieden. Op basis hiervan zijn de hiaten in de bestaande data geïdentificeerd en is besloten welke van deze hiaten opgevuld moesten worden met data uit de nieuwe experimenten om in staat te zijn nieuwe inzichten te verkrijgen van de effecten van 'echte' golven op zandtransportprocessen. Duidelijk was dat er vooral meer inzicht nodig was in de details van de zandtransportprocessen binnen de golfgrenslaag en sheet-flow-laag. Om deze gedetailleerde metingen uit te kunnen voeren onder oppervlaktegolven van werkelijke grootte zijn de experimenten uitgevoerd in de golfgoot (*Großer Wellenkanal,* GWK) van het Kustenonderzoekscentrum in Hannover, Duitsland.

Gedetailleerde metingen van de stromingsprocessen in de golfgrenslaag laten zien dat de grenslaagdikte en tijdsafhankelijke snelheidsprofielen een grote overeenkomst hebben met die gemeten in tunnels met oscillerende stroming. Echter, de netto horizontale stroming is duidelijk anders. In alle gevallen van de nieuwe metingen laat het stromingsprofiel eenzelfde patroon met 3 kenmerkende lagen zien waarin kust- en zeewaartse netto stromingen elkaar afwisselen. Boven de sheet-flow-laag zijn er 2 lagen aanwezig met een netto zeewaartse stroming. Deze 2-lagenstructuur is kwalitatief verklaard door de hoogteafhankelijke verhouding tussen de netto drukgradiënt, golf Reynoldswrijving en de netto (oscillerende) turbulente Reynoldswrijving. Binnen de sheet-flow-laag laten alle experimenten zien dat er een overgang plaats vindt naar een netto kustwaartse stroming.

Deze is veroorzaakt door het feit dat de erosiediepte onder het kustwaartse deel van de golfbeweging altijd groter is dan de erosiediepte van het zeewaartse deel van de golfbeweging als gevolg van de snelheidsasymmetrie van de golf (asymmetrie van de erosiediepte). De netto stroming onder oppervlaktegolven is over het algemeen meer kustwaarts gericht dan in tunnels met oscillerende stroming, wat veroorzaakt zou kunnen worden door de invloed van de golf-Reynolds stress en advectieve effecten (welke afwezig zijn in tunnels). In de hoogste delen van de golfgrenslaag laat het netto stromingsprofiel in de huidige experimenten een negatieve schuifspanning zien (overgang naar de zeewaarste retourstroom), terwijl tunnelexperimenten hier een positieve schuifspanning laten zien als gevolg van de tegenovergestelde richting van de netto drukgradiënt.

Naast de stromingssnelheden, zijn er ook nieuwe inzichten gepresenteerd in het gedrag van de sedimentconcentraties en -fluxen onder oppervlaktegolven voor zowel een medium zand bed ($D_{50}$ = 0.25 mm) en, voor het eerst, voor een fijn zand bed ($D_{50}$ = 0.14 mm). Voor zowel medium- als fijn-zand-condities zijn de maximale (golftop en -dal) en totale netto zandtransporten geconcentreerd binnen de sheet-flow-laag. Voor fijn zand wordt er meer zand in beweging gebracht, waardoor de erosiediepte en sheet-flow-laag dikte groter zijn dan voor medium-zand-condities met dezelfde golven. Daarnaast is er een grotere vertraging in reactie van het fijne zand in relatie tot de stroming van het water. Ondanks deze kwantitatieve verschillen, is het algemene patroon van de netto fluxprofielen vergelijkbaar voor beide zandsoorten. Als gevolg van de asymmetrie in de golfbeweging en erosiediepte worden er in alle experimenten grotere kustwaartse fluxen gegenereerd dan zeewaartse fluxen en is de richting van de netto fluxen dus altijd kustwaarts. De totale horizontale netto sedimentflux laat een 2-lagen structuur zien: een kustwaarts gerichte flux in het onderste deel van de sheet-flow-laag en een (kleinere) zeewaarts gerichte flux daarboven. Voor medium-zand-condities, de totale netto flux onder oppervlaktegolven is groter dan die gemeten in tunnels met oscillerende stroming, maar het patroon en de richting zijn vergelijkbaar. Voor fijn-zand-condities laten de resultaten een groot verschil zien met de eerdere resultaten uit tunnels met oscillerende stroming. De netto fluxen zijn niet alleen groter, maar de totale netto flux onder oppervlaktegolven is kustwaarts gericht, in tegenstelling tot de tunnelmetingen waar deze zeewaarts gericht is.

De gemeten totale netto zandtransporten die gepresenteerd worden in dit onderzoek zijn een waardevolle uitbreiding van de bestaande medium-zand-metingen, aangezien de hoeveelheid data hiermee meer dan verdubbeld is. Daarnaast is dit de eerste keer dat deze data ook verkregen is voor oppervlaktegolven over een mobiele bodem bestaande uit fijn zand. De nieuwe experimenten laten voor beide zandsoorten een lineaire toename zien van het zandtransport in relatie tot een toename van het $3^{de}$-orde moment van de tijdsafhankelijke stroomsnelheid. De overgang van netto kustwaarts naar netto zeewaarts transport met toenemende stroomsnelheid zoals gemeten voor fijn-zand-condities in tunnels met oscillerende stroming is niet waargenomen onder oppervlaktegolven. Dit is in lijn met de onafhankelijk hiervan gemeten fluxen in de sheet-flow-laag. Een waarschijnlijke verklaring voor dit verschil tussen oppervlaktegolven en tunnels is dat de na-ijleffecten van fijn zand, verantwoordelijk voor de overgang naar zeewaarts transport, overgecompenseerd worden door de effecten van echte golven van de oppervlakte golven, zoals de grotere kustwaartse netto bodemschuifspanning (golf-Reynoldsstress) en de kustwaarts gerichte netto golfgrenslaagstroming. De golf-Reynoldsstress is verantwoordelijk voor een extra golftop- en golfdalasymmetrie van de bodemschuifspanning, extra asymmetrie van de erosiediepte en dus tot meer kustwaarts gericht

zandtransport. De kustwaarts gerichte stroming leidt tot een extra stromingsgerelateerde sedimentflux in de kustwaartse richting. De resultaten van dit onderzoek laten zien dat de overgrote meerderheid van het zand wordt verplaatst binnen de sheet-flow-laag, waardoor relatief kleine golf-gerelateerde netto stromingsprocessen dichtbij de bodem een bepalend effect hebben op de zandtransportprocessen onder deze condities.

De inzichten die voortgekomen zijn uit dit onderzoek en de nieuwe experimenten zijn van cruciaal belang voor de ontwikkeling van sedimenttransportmodellen. Naast de uitvoering van de nieuwe experimenten zijn de resultaten vergeleken met twee bestaande praktische zandtransportmodellen (Nielsen, 2006 en Van Rijn, 2007). Beide modellen zijn quasi-stationaire empirische modellen en gebruiken een verschillende methode om effecten van echte golven mee te nemen in hun berekeningen. Daarnaast is een nieuw semi-instationair praktisch transportmodel, ontwikkeld binnen het SANTOSS-project, geëvalueerd. De resultaten van deze vergelijkingen laten zien dat het toevoegen van de individuele effecten van echte golven, zoals gedaan is in het SANTOSS model, samen met de grote hoeveelheid data en verschillende condities waarop het model gebaseerd is, ervoor zorgen dat dit model in principe beter geschikt is om zandtransporten te voorspellen dan de andere twee geteste quasi-stationaire transportmodellen.

# 1. INTRODUCTION

## 1.1 Problem description and research background.

The morphology of coastal areas is constantly changing under the influence of sediments being transported to, from and along the coast. Under storm conditions with high waves and flow velocities, large quantities of sand are transported in a short amount of time, making these conditions of large importance to the total sand movement in coastal areas. Under these conditions, ripples are washed out and the sand is transported in a thin layer (mm's - cm's thick) close to the bed, known as the sheet-flow layer (Figure 1.1). Since these processes have a large impact on the total sand budget in coastal areas, it is important for coastal engineers, scientists and managers to be equipped with well-founded methods for predicting sand transport under these conditions. For instance, the short-term and long-term development of the coastline, impact of sea level rise, planning and design of sand nourishment schemes, sea harbours, coastal defence measures and conservation policies for the coastal environment, all require tools for predicting sand transport under waves and currents.

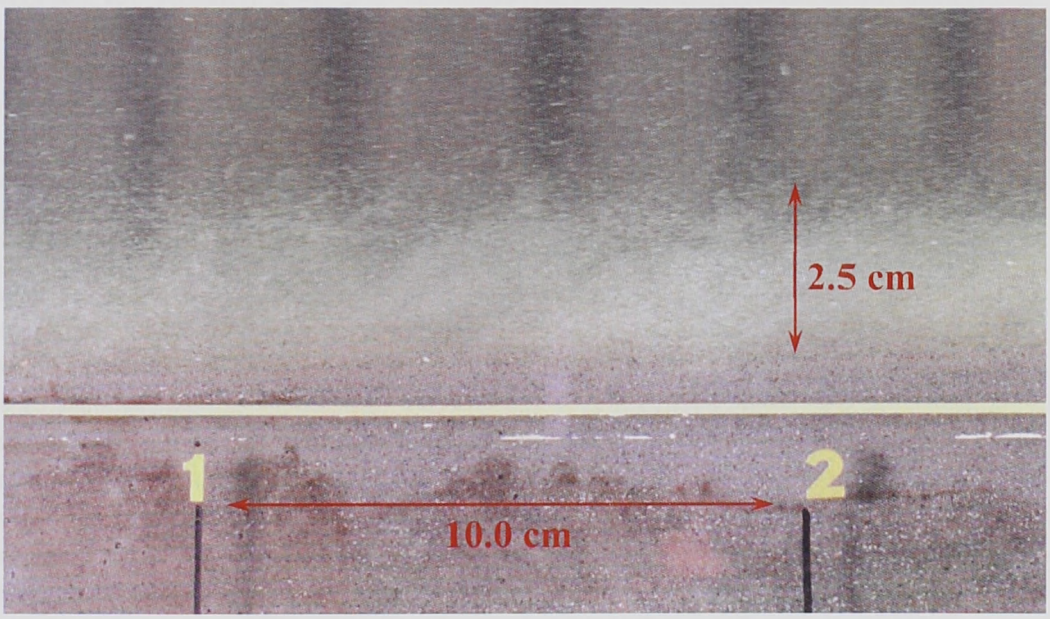


Figure 1.1. Sheet-flow layer above a mobile sand bed. Picture during oscillatory flow tunnel experiments (courtesy of J.S. Ribberink).

Under storm conditions with wave heights in the order of several meters and flow velocities in the order of meters per second, it is difficult to obtain reliable field data of the sand transport in the sheet-flow regime and even more so of the detailed processes (flow velocities and sediment concentrations) close to the bed, inside the sheet-flow layer. Therefore, many measurements that have been done in controlled laboratory settings have been of large value to the development of predictive sand transport models (see e.g. Van Rijn, 2007). Based on these data-sets practical (empirical) transport models and process based models have been developed and improved.

The research presented in this thesis focuses on the influence of surface wave effects on sand transport under sheet-flow conditions. Various transport models have been developed to predict

both the quantities and directions of sediment transport under these conditions. The majority of the existing models are based on data obtained from oscillatory flow tunnel experiments (Dibajnia & Watanabe, 1998; Dohmen-Janssen, 1999; O'Donoghue & Wright, 2004a; 2004b; Ribberink & Al Salem, 1994; Ribberink, 1998; Van der Werf, 2006).

Even though oscillatory flow tunnels provide a good approximation of the flow experienced at the sea bed, there are some fundamental differences. Figure 1.2 gives an overview of flow velocities under surface waves versus oscillatory flow tunnels. Under surface waves, each water particle moves with a horizontal and vertical velocity in an elliptical orbit. Oscillatory flow tunnels are closed with a rigid lid so there is no free surface. Here, only the (dominant) horizontal flow velocities near the sea-bed are generated, based on the wave period and amplitude of the simulated surface wave. These velocities are uniform in the x-direction.

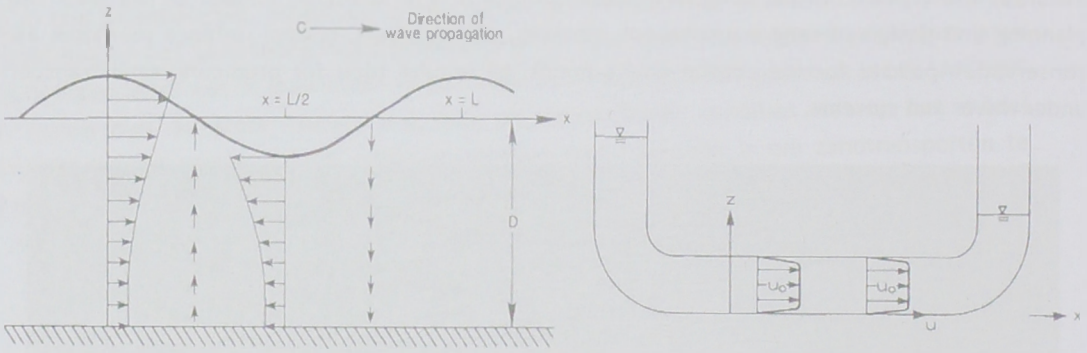


Figure 1.2. Schematisation of flow velocities under surface waves and in a oscillatory flow tunnel. The flow under surface waves (left) describes an orbital motion and varies with the water depth. The purely oscillatory flow (right) is uniform in the x-direction (from Nielsen, 1992; Fredsøe and Deigaard, 1992).

Vertical orbital motions are absent and wave-induced net currents are not fully reproduced in flow tunnels. Surface waves induce Lagrangian and Eulerian mean velocities. The Lagrangian mean velocity occurs due to the fact that i) a fluid particle in a wave will move with larger forward velocities at the top of its orbit than the backward velocities at the bottom and ii) the particles move with the wave during its forward motion and against it during its backward motion, and will therefore spend more time moving forwards than backwards (Nielsen, 1992). The Eulerian mean velocity results from the fact that i) the vertical and horizontal orbital velocities are not exactly 90° out of phase in the boundary layer as they would be in a frictionless flow, ii) wave asymmetry causes a difference in generated turbulent energy between the two half cycles and iii) return flow compensating for mass flux in the direction of wave propagation (undertow). The first process leads to an onshore-directed mean velocity, close to the bed (Longuet-Higgins, 1953), while the mean velocity resulting from the second process can be either on- or offshore-directed, depending on the relative roughness (Trowbridge & Madsen, 1984a; 1984b; Davies and Villaret, 1999). Figure 1.3 shows a flow velocity profile of Longuet-Higgins (1953), which includes the Stokes drift caused by the surface waves ($u_{s,on}$), the undertow (return flow from the beach) ($u_{m,off}$) and the boundary layer streaming ($u_{b,on}$). The Lagrangian mean velocities, as well as undertow, are absent in oscillatory flow tunnels, as well as the onshore-directed Longuet-Higgins streaming. Since under sheet-flow conditions the far majority of sand is transported within a few centimetres thick layer directly above the bed, these relatively small wave-induced net currents may be of major importance for the total net sand transport rates.

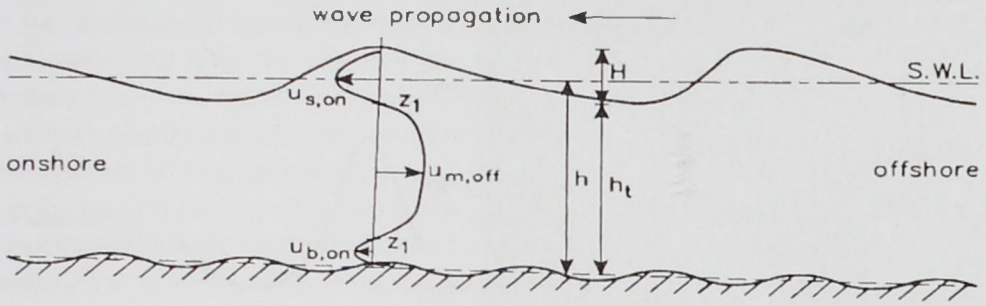


Figure 1.3. Flow velocity profile under surface waves, according to Longuet-Higgins (1953) (from: Hassan, 2003)

The few sheet flow sediment transport experiments that were done under full scale surface waves, indeed indicate that horizontal oscillatory flows and orbital flows due to surface waves result in different sediment transport rates. Based on experiments in the large wave flume in Hannover, Germany (GWK), Ribberink et al. (2000) found that the net transport rates under full-scale surface waves are approximately a factor 2 larger than for similar flow and sand conditions in a large oscillatory flow tunnel (see also Dohmen-Janssen & Hanes, 2002). Similar results were found with a 1DV transport model, the Point Sand Model (PSM), developed by Uittenbogaard (2000). This process based model is used to simulate velocities and sand transport processes under sheet-flow conditions in both a 'real wave mode' and a 'wave tunnel mode'. Previous studies indicated that the predicted sand transport rates under real waves may be 40% higher than in similar oscillatory flows (Bosboom & Klopman, 2000; Schretlen et al, 2007; Kranenburg et al., 2010).

Until now, most practical sand transport models have been developed and validated based on a selection of the existing data. Recently, various data from different conditions and measurement campaigns were for the first time combined into one large database (Schretlen and Van der Werf, 2006; Van der Werf et al., 2009). From the analyses of this database, together with an investigation of trends in the sand transport rates, it is concluded that two areas require further research. The first is the difference in sand transport processes and rates between surface waves and oscillatory tunnel flows with nominally similar oscillatory flow conditions. The second is the effect of acceleration skewness on transport processes and net transport rates. The number of existing experiments enabling analysis of 'surface wave' and 'acceleration' effects is very limited, but existing results point to the potential importance of both for the net transport rate.

## 1.2 Research objectives and questions

Based on the above, the research presented here aims to identify whether and how small-scale progressive surface wave effects occurring in the wave boundary layer and sheet-flow layer, affect the total sand transport rates under full scale surface waves. In order to do so, experiments were done under full scale surface waves in the large wave flume, or Großer Wellenkanal (GWK), of the Coastal Research Centre in Hannover, Germany, a joint research facility of the University of Hannover and the Technical University of Braunschweig. For the first time under these conditions, detailed time-dependent flow velocities were not only measured in the free stream, but also inside the wave boundary layer. With that, detailed measurements were made of the (time-dependent) sediment concentrations inside the sheet-flow and suspension layer and total sand transport rates. Also for the first time, these measurements were done for different sand types, all measurement were done for both medium sand ($D_{50}$ = 245 mm) and fine sand ($D_{50}$ = 138 mm) mobile beds.

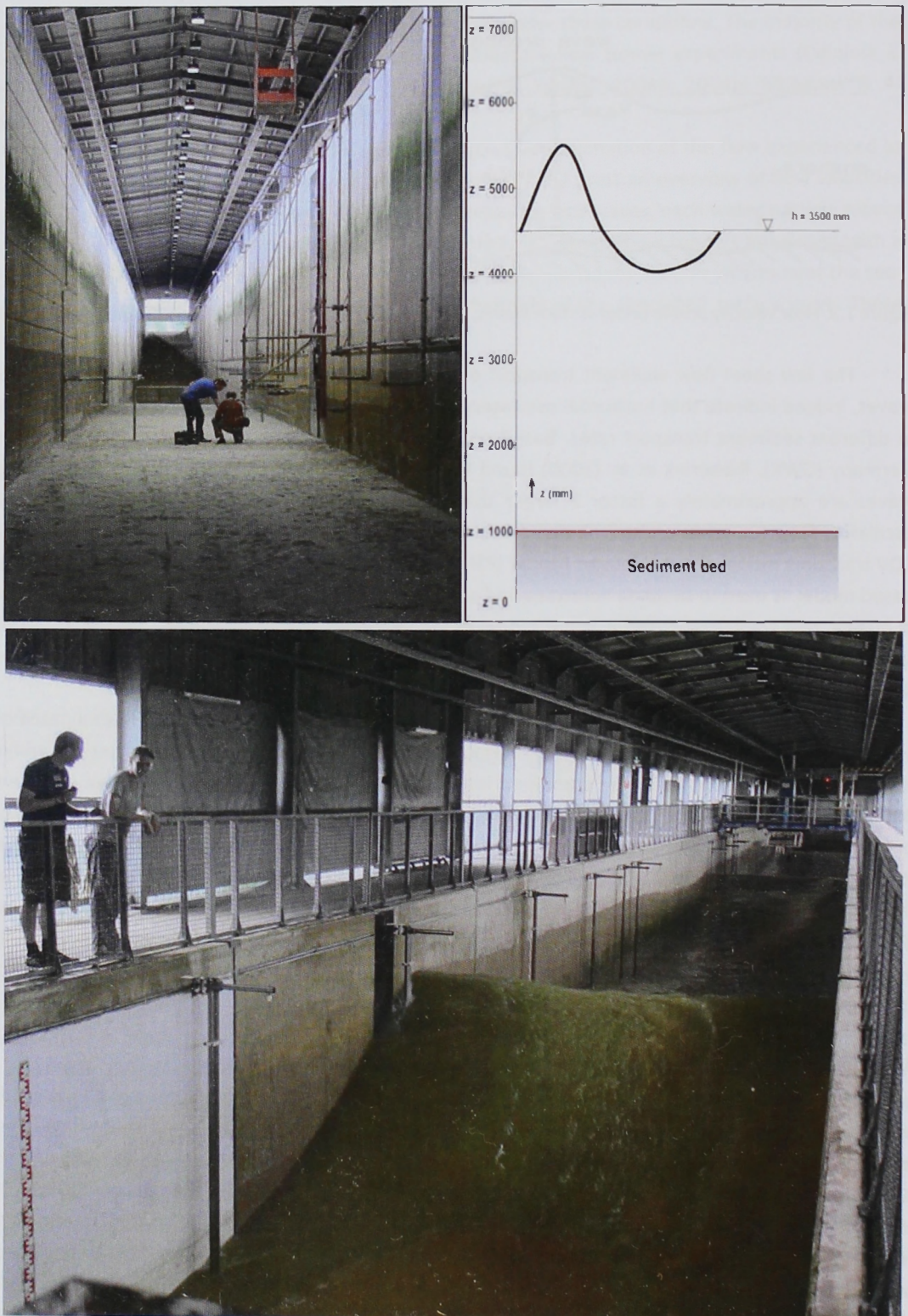


Figure 1.4 Large wave flume (GWK) without water, with measurement frame and mobile sand bed (top left), schematised cross section with dimensions of the sand bed, water depth, wave height and wave boundary layer (top right) and with water and waves (below).

Figure 1.4 shows the large wave channel without water, with the mobile sand bed and above that the instruments, placed for the detailed flow velocity and sediment concentration measurements (top left), the top right picture shows a cross section of the flume with the dimensions in mm. The flume is 7 m deep, a horizontal sand bed of 1 m thick is placed on the bed. The water depth above that is 3.5 m and 1.5 m waves are generated. The red line represents the typical thickness of the wave boundary layer, the sheet-flow layer is about 1/5 of this. The lowest part of the figure shows one of the experiments, with 1.5 m waves running through the channel. A new measurement set-up (wall frames and a buried tank with various instruments) was designed for these experiments. For the detailed measurements near the sand bed, special rigs were designed to achieve the required high spatial ($10^{-3} - 10^{-2}$ m) and high temporal ($10^{-3} - 10^{-1}$ s) measurements resolutions, while at the same time avoiding flow disturbances as much as possible and being rigid enough to withstand the wave forces. The complete measurement set-up makes it possible to measure (time-dependent) flow velocities inside the free-stream and wave boundary layer, (time-dependent) sediment concentrations inside the sheet-flow layer and suspension layer and the total net sand transport rates along the flume. It is the first time that such a complete and detailed data-set is obtained under full scale surface wave conditions with medium and fine sand mobile beds. A detailed description of the experimental conditions and the used instruments to obtain the measurements under these conditions, is given in the following Chapters of this thesis. Each Chapter is written as a separate journal paper. Therefore there is some overlap in description of the research facility in each Chapter.

The overall research questions of the complete thesis and the contents of the different Chapters are described below.

**Research questions**

1. What are the gaps in existing data and which gaps need to be covered with new experiments to obtain a better understanding of progressive surface wave effects on sand transport processes?
2. How can we measure the wave boundary layer and sheet flow layer processes near the bed under full-scale progressive surface waves?
3. To what extent do the wave boundary layer and sheet flow layer processes control the net sand transport under these wave conditions?
4. How does the grain size affect these wave boundary layer processes and the net sand transport rate?
5. How do these detailed processes and the net transport rates relate to the knowledge obtained from oscillatory flow tunnel experiments with similar conditions?
6. How do practical sand transport models account for surface wave effects and how can the new insights from the new experiments add to the development of an improved practical sand transport model?

Chapter 2 of this thesis describes the SANTOSS database which gives an overview of laboratory experiments involving sand transport processes over horizontal, mobile sand beds under full-scale non-breaking waves and non-breaking waves-plus-current conditions. Analysis of the coverage of the experiments and the measured net sand transport rates identifies the gaps in the range of test conditions and/ or the type of measurements. The database is a useful resource for the design of new experiments and the development and validation of sand transport models for coastal applications.

Chapter 3 of this thesis focuses on (time-dependent) wave boundary layer flow velocities under full scale surface waves. Most of the existing wave boundary layer measurements were carried out in i) oscillatory flow tunnels, or ii) in small scale wave flumes above fixed beds. Moreover, existing flow measuring techniques (such as laser-doppler) generally fail in situations with mobile beds because of the large sand concentrations in the wave boundary layer. The experimental work as presented in this paper was initiated to fill up this lack of knowledge. With the use of a new acoustic velocity measurement device (UVP) and with conductivity probes (CCM), high resolution flow velocity measurements were obtained inside the wave boundary layer under full-scale surface waves for the different types of mobile sand beds. The data provide new insights in the oscillatory and mean flow velocities in the wave boundary layer, including the sheet flow layer. Furthermore, existing models for wave boundary layer thickness and erosion depth are evaluated and comparisons are made with similar results from oscillatory flow tunnel experiments.

In Chapter 4, for the first time measurement results of sheet flow layer concentrations are combined with boundary layer flow velocities over the complete wave cycle under full scale surface waves, resulting in sediment flux and sediment transport measurements for both medium and fine sand conditions. Even though sheet flow layer concentrations under surface waves seem to be represented well in oscillatory flow tunnels, the wave boundary layer flow velocity results in the previous Chapter give reason to believe that such an agreement is not necessarily true for sediment fluxes, especially for fine sand conditions. The results are divided in i) time averaged concentration profiles, ii) time dependent sediment concentrations and iii) fluxes (both time averaged and time dependent). The presentation of the new experiments is followed by a comparison with existing models (for suspended and sheet-flow layer concentrations and sheet flow layer thickness) and oscillatory flow tunnel data.

In Chapter 5, total net sand transport rates, measured independently from the detailed flow velocity and sand concentration measurements shown in the previous Chapters, are presented and compared with the measured sheet-flow layer fluxes. The new transport data presented here i) are a valuable extension to the existing surface wave measurements for medium sand (it more than doubles the amount of available data up till now) and ii) gives for the first time transport rates under full scale surface waves with a fine sand mobile bed. These new results are compared with existing data and with two existing practical sand transport models (Nielsen, 2006 and Van Rijn, 2007) that use different approaches to account for surface wave streaming effects. The theoretical background of these models is described as well. Finally, a new practical sand transport model which was developed recently (Van der Werf, 2007; Ribberink et al., 2010; Van der A et al., 2010) is described and compared to the data for surface waves. It is shown how the results of the new experiments contribute to the implementation of surface wave effects into this new transport formula and how this transport model performs in comparison to the previous ones.

Chapter 6 consists of an overall discussion, conclusion and recommendations, based on the combined results of the four previous Chapters.

## References

Bosboom, J. and Klopman, G., 2000. Intra-wave sediment transport modelling, *Proceedings of the 27th International Conference on Coastal Engineering, Sydney, Australia*, pp. 2453 - 2466.

Davies, A.G. and C. Villaret. 1999. Eulerian drift induced by progressive waves above rippled and very rough beds. *Journal of Geophysical Research*, 104(C1): 1465-1488.

Dibajnia, M. and A. Watanabe. 1998. Transport rate under irregular sheet flow conditions. *Coastal Engineering* 35, 167 – 183.

Dohmen-Janssen, C.M. 1999. Grain size influence on sediment transport in oscillatory sheet flow phase lags and mobile-bed effects. *PhD-thesis*, Delft University of Technology, Delft, The Netherlands, 246 pp.

Dohmen-Janssen, C.M. and D.M. Hanes. 2002. Sheet flow dynamics under monochromatic nonbreaking waves. *Journal of Geophysical Research,* 107(C10), 3149.

Fredsøe, J. and R. Deigaard. 1992.Mechanics of coastal sediment transport. *Advanced Series on Ocean Engineering, Volume 3.* World Scientific Publishing Cp. Pte. Ltd., Singapore, 369 pp.

Hassan, W.N., 2003. Transport of size-graded and uniform sediments under oscillatory sheet-flow conditions. *PhD thesis*, University of Twente, The Netherlands.

Kranenburg, W.M. , J.S. Ribberink and R.E. Uittenbogaard. 2010. Sand transport by surface waves: can streaming explain the onshore transport?, *Proceedings of 32nd International Conference on Coastal Engineering,* ASCE, Shanghai, China.

Longuet-Higgins, M.S. 1953. Mass transport in water waves. *Philosophical Transactions of the Royal Society of London. Series A, Mathematical and Physical Sciences*, 245(903), 535 – 581.

Nielsen, P. 1992. Coastal bottom boundary layers and sediment transport. *Advanced Series on Ocean Engineering, Volume 4.* World Scientific Publishing Cp. Pte. Ltd., Singapore, 324 pp.

Nielsen, P., 2006. Sheet flow sediment transport under waves with acceleration skewness and boundary layer streaming. *Coastal Engineering*, 53: 749-758.

O'Donoghue, T. and S. Wright. 2004a. Concentrations in oscillatory sheet flow for well sorted and graded sands. *Coastal Engineering* 50, 117 – 138.

O'Donoghue, T. and S. Wright. 2004b. Flow tunnel measurements of velocities and sand flux in oscillatory sheet flow for well sorted and graded sands. *Coastal Engineering* 51, 1163 – 1184.

Ribberink, J.S. and A.A. Al-Salem. 1994. Sediment transport tin oscillatory boundary layers in cases of rippled beds and sheet flow. *Journal of Geophysical Research* 99(C6), 12707 – 12727.

Ribberink, J.S. 1998. Bed-load transport for steady flows and unsteady oscillatory flows. *Coastal Engineering* 34, 59 – 82.

Ribberink, J.S., C.M. Dohmen-Janssen, D.M. Hanes, S.R. McLean and C. Vincent. 2000. Near-bed sand transport mechanics under waves – A large-scale flume experiment (Sistex99). *Proceedings of 27th International Conference on Coastal Engineering*, ASCE, 3263-3276.

Ribberink, J.S., D.A. van der A and R.H. Buijsrogge. 2010. SANTOSS transport model – A new formula for sand transport under waves and currents. *Report SANTOSS_UT_IR3*, University of Twente, The Netherlands.

Schretlen, J.L.M. and J.J. van der Werf. 2006. SANTOSS Database, Existing data from experiments in oscillatory flow tunnels and large wave flumes. *Report SANTOSS_UT_IR1, CE&M Research Report 2006R-008/WEM-009*, University of Twente, The Netherlands.

Schretlen, J.L.M., J.J. van der Werf, J.S. Ribberink, R.E. Uittenbogaard and T. O'Donoghue. 2007. Surface wave effects on sheet-flow sand transport. *Proceedings of the 5th IAHR Symposium on River, Coastal and Estuarine Morphodynamics.* Taylor & Francis Group, 329-335.

Trowbridge, J. and O.S. Madsen. 1984a. Turbulent wave boundary layers 1. Model formulation and first-order solution. Journal of Geophysical Research, 89(C5): 7989-7997.

Trowbridge, J. and O.S. Madsen. 1984b. Turbulent wave boundary layers 2. Second-order theory and mass transport. Journal of Geophysical Research, 89(C5): 7999-8007.

Uittenbogaard, R.E., 2000. 1DV Simulation of wave current interaction. *Proceedings of the 27th International Conference on Coastal Engineering. ASCE, Sydney, Australia*, pp. 255 - 268.

Van der A, D.A., J.S. Ribberink, J.J. van der Werf and T. O'Donoghue. 2010. New practical model for sand transport induced by non-breaking waves and currents. *Proceedings of 32nd International Conference on Coastal Engineering*, Shanghai, China.

Van der Werf, J.J. 2006. Sand transport over rippled beds in oscillatory flow. *PhD-thesis*, University of Twente, Enschede, The Netherlands.

Van der Werf, J.J., J.S. Ribberink and T. O'Donoghue. 2007. Development of a new practical model for sand transport induced by non-breaking waves and currents. *Coastal Sediments 2007*, ASCE, New Orleans, USA. pp 42 – 55.

Van der Werf, J.J., J.L.M. Schretlen, J.S. Ribberink and T. O'Donoghue. 2009. Database of full-scale laboratory experiments on wave-driven sand transport processes. *Coastal Engineering* 56, 726 – 732.

Van Rijn, L.C. 2007. Unified view of sediment transport by currents and waves I: Initiation if motion, bed roughness and bed-load transport. *Journal of Hydraulic Engineering*, 133(6), 649 – 667.

# 2. DATABASE OF FULL-SCALE LABORATORY EXPERIMENTS ON WAVE-DRIVEN SAND TRANSPORT PROCESSES

**Abstract**

A new database of laboratory experiments involving sand transport processes over horizontal, mobile sand beds under full-scale non-breaking waves and non-breaking waves-plus-current conditions is described. This database combines, for the first time, data obtained from 298 experiments from 7 full-scale facilities worldwide. Analysis of the coverage of the experiments and the measured net sand transport rates identifies the following gaps in the range of test conditions and/ or the type of measurements: i) graded sand experiments, ii) wave-plus-current experiments and iii) intra-wave velocity and concentration measurements in the ripple regime. Furthermore, it highlights two areas requiring further research: i) the differences in sand transport processes and sand transport rates between real waves and tunnel flows with nominally similar near-bed oscillatory flow conditions and ii) the effects of acceleration skewness on transport rates. The database is a useful resource for the design of new experiments and the development and validation of sand transport models for coastal applications.

## 2.1 Introduction

Accurate knowledge on sediment concentrations and flow velocities in the coastal zone are essential for resolving net sediment transport rates in this area. To better understand and predict transport rates, numerous experiments were conducted in the last few decades. Most of these experiments were performed in laboratory facilities, such as oscillatory flow tunnels and wave flumes. Field conditions in the coastal zone make it difficult to obtain satisfying data of sediment transport processes, especially since variations in sediment concentrations and flow velocities occur partly on a small spatial scale (order of mm), close to the bed.

The SANTOSS database combines, for the first time, net sediment transport data obtained from various experiments worldwide. The aim is to give an overview of the available data and their characteristics. This gives the opportunity to identify gaps in the data, which is useful in the design and planning of new experiments. Besides this, the dataset is used to assess existing sand transport models and to develop and test a new practical sand transport model (SANTOSS-model, see Van der A et al., 2010 and Chapter 5 of this thesis). To develop a sand transport model which is applicable in a wide range of conditions, the data set contains data from experiments in the rippled bed as well as in the sheet flow regime. The database focuses on laboratory experiments with non-cohesive quartz sand under full scale non-breaking waves and non-breaking waves-plus-currents conditions. Where full-scale means experiments with a wave period *(T)* larger than or equal to 4 s. The database has been constructed to i) enable access to a coherent collection of sand transport data from full-scale, oscillatory flow experiments, ii) examine the coverage of existing experimental data and identify conditions requiring further experimental research and iii) develop (calibrate and/ or validate) practical models for the prediction of sand transport under waves and currents.

This Chapter is organised as follows: in Section 2.2, the laboratory facilities in which the experiments are performed and the measurements techniques used to obtain the data are described. In Section 2.3 the contents and structure of the database are given. Section 2.4 gives an overview of the characteristics of the available data and the types of measurements. In Section 2.5

*This Chapter is published in a different form as:*

Van der Werf, J.J., J.L.M. Schretlen, J.S. Ribberink and T. O'Donoghue. 2009. Database of full-scale laboratory experiments on wave-driven sand transport processes. Coastal Engineering, 56, 726 – 732.

Schretlen, J.L.M. and J.J. van der Werf. 2006. SANTOSS database, existing data from experiments in oscillatory flow tunnels and large wave flumes. Report SANTOSS_UT_IR1, CE&M Research Report 2006R-008/WEM-009, University of Twente, The Netherlands.

results of the transport rate data as implemented in the database are shown. Conclusions and recommendations are given in the final Section 2.6.

## 2.2. Laboratory facilities and measurement techniques

Not only the data itself, but also the conditions under which they are obtained are of importance. Therefore, this Section gives an overview of the characteristics of the different facilities and experimental conditions in which the experiments were conducted.

The generation of full-scale sand transport conditions in a laboratory requires a large experimental facility, capable of producing high near-bed flow velocities with periods typical of full-scale waves (with a wave period *(T)* of 4 to 15 s). Two types of facilities have this capability: large oscillatory flow tunnels and large wave flumes. The data included in the database originate from experiments carried out in 5 large oscillatory flow tunnels and 2 large wave flumes. The tunnels are the Aberdeen Oscillatory Flow Tunnel (AOFT, Aberdeen University, UK), the Cambridge Oscillatory Flow Tunnel (COFT, Cambridge University, UK), the Large Oscillating Water Tunnel (LOWT, WL|Delft Hydraulics (now Deltares), The Netherlands), the HR Pulsating Water Tunnel (PWT, HR Wallingford, UK) and the Tokyo Oscillatory Flow Tunnel (TOFT, Tokyo University, Japan). The wave flumes are the Delta Flume (Deltares (previously WL|Delft Hydraulics), The Netherlands) and the Großer Wellenkanal (GWK, University of Hannover and Technical University of Braunschweig, Germany). Table 2.1 summarizes the main characteristics of the experimental facilities. It includes test section dimensions, water depth above sediment bed *(h)* and typical flow capabilities. These include for the tunnels: flow period range *(T)*, maximum oscillatory flow velocity ($\hat{u}$) and mean (i.e. wave period averaged) current velocity ($<\bar{u}>$) (only the LOWT, PWT and TOFT are capable of generating a (co-)linear current). For the wave flumes these include: the flow period range *(T)* and maximum wave height *(H)*. More detailed descriptions of the facilities can be found in the references listed in Table 2.2 and the report accompanying the SANTOSS database (Schretlen and Van der Werf, 2006).

It is noted that oscillatory flow tunnels provide an approximation of the flow experienced at the sea bed under real waves. Phase differences in wave orbital motion, vertical orbital motions, wave-induced boundary layer streaming (Longuet-Higgins, 1953; Davies and Villaret, 1999) and undertow at higher levels above the bed are not present or are different in wave tunnels. Some of these differences in the detailed hydrodynamics may result in significant differences between tunnel and wave flume net sand transport rates for nominally similar near-bed oscillatory flows. This is discussed further in Section 2.5.

Table 2.1 Main characteristics of the experimental facilities

| Facility | Test Section | | | Typical hydraulic conditions | | | |
|---|---|---|---|---|---|---|---|
| | length (m) | width (m) | $h$ (m) | $H$ (m) | $T$ (s) | $\hat{u}$ (m/s) | $<\bar{u}>$ (m/s) |
| AOFT | 10 | 0.3 | 0.5 | - | ≤ 13 | ≤ 1.5 | - |
| COFT | 3.7 | 0.15 | 0.3 | - | ≤ 7.1 | ≤ 2.2 | - |
| LOWT | 14 | 0.3 | 0.8 | - | ≤ 12 | ≤ 1.8 | ≤ 0.55 |
| PWT | 9 | 0.51 | ≈ 2 | - | ≤ 10 | ≤ 1.1 | ≤ 0.39 |
| TOFT | 2 | 0.24 | 0.2 | - | ≤ 7 | ≤ 1.8 | ≤ 0.22 |
| Delta flume | 240 | 5 | ≤ 7 | ≤ 1.3 | ≤ 6.0 | - | - |
| GWK | 300 | 5 | ≤ 7 | ≤ 1.6 | ≤ 9.1 | - | - |

Apart from the measurement facilities, also the measurements types and the used measurement techniques are relevant. The measurements can be divided in i) sediment concentration measurements, ii) flow and sand grain velocities and iii) sand transport rates. Below, a short description of the most commonly used techniques are given. Further detail on the specific instruments can be found in Schretlen and Van der Werf (2006).

For sediment concentration measurements the five most commonly used techniques are 'Transverse Suction System' (TSS), 'Conductivity Concentration Meter' (CCM), 'OPtical Concentration Meter' (OPCON), 'Acoustic Backscatter System' (ABS) and the 'Ultra High Concentration Meter' (UHCM). The TSS is a simple and inexpensive method to measure time-averaged concentrations of suspended sediment. The principle is based on sucking samples in a direction normal to the ambient water motion at an intake velocity which, ideally, exceeds the ambient water flow velocity more than three times (Bosman et al., 1987). A concentration profile can be obtained by using several suction tubes at different heights above the bed. Dried samples are also used for grain size analyses of the suspended sediment. An OPCON-meter is specifically suited for time-dependent concentration measurements of suspended sediments (in a range of approximately 0.1 – 50 g/l). The OPCON can also supply information on the size of the particles (within a range of 10 – 1000 μm). The CCM is based on the conductivity change of sand-water mixture due to the variation of the quantity of non-conductive sand present in the measurement area. The CCM is, contrary to the OPCON-meter, capable of measuring very high sediment concentrations (100 – 1600 g/l). Therefore, the CCM is specifically suited for measuring sediment concentrations inside the sheet-flow layer. The ABS and UHCM are both acoustical instruments. The ABS is a non-intrusive technique for the monitoring of water-suspended sediment particles (concentration and particle size) and changing sea bed characteristics. In measuring volume, the UHCM is comparable to the OPCON-meter, with the main difference that OPCON is an optical instrument instead of acoustic. Because of this, the UHCM performs better in mixtures with high sediment concentrations or in turbid fluids. The UHCM can measure sediment concentrations up to 400 g/l for sand with a medium grain size ($D_{50}$ = 200 μm).

In principle, most of the flow velocity measurement techniques are based on reflection by the particles moving inside the fluid. The measured velocities are then velocities of the particles rather that the water itself. The most commonly used techniques described here include 'Laser Doppler Anemometer' (LDA), 'Electromagnetic Flow Meter' (EMF), 'Acoustic Doppler Velocity meter' (ADV), 'Ultrasonic Velocity Profiler' (UVP) and 'Particle Image Velocimetry' (PIV) with the use of High Speed Video (HSV) or camera. Measurements with LDA are based on the scattering of a laser beam by particles present in the flow. The advantage of this technique is the fact that the instrument itself can be placed outside the flow and therefore the measurements do not disturb the flow itself. A disadvantage of using laser beams is that in case of high sediment concentrations or turbid fluids, the beams are blocked and measurements are not possible. The EMF is based on the principle that any moving conductor in a magnetic field induces a voltage. The instrument itself produces a magnetic field in the surrounding water, after which the electrodes receive this electrical voltage. This is proportional to the velocity. The ADV and UVP both generate an acoustic signal which is scattered by the particles in the fluid. The reflection of this signal is recorded and through the Doppler shift principle the flow velocity of these particles can be determined. The difference between these two instruments is that the UVP measures the velocity at 128 locations along the beam axis, thereby measuring an instantaneous velocity profile. This is done only in the direction of the probe itself. The ADV measures the velocity from three directions, but only at one point instead of a profile. Besides this, the UVP is capable of measuring in fluids with higher sediment concentrations than the ADV,

though both can be applied for situations with higher concentrations compared to the LDA. The final measuring technique discussed here is PIV with the use of High Speed Video (HSV). This is based on the principle of measuring the displacement of suspended particles over a known time period. The advantages of the technique are that it is non-intrusive and an instantaneous velocity vector map can be created of the total cross-section of the flow, this compared to other techniques with which only 1 dimensional profiles or velocities at one point are measured. However, a practical issue with this technique could be that, like the LDA, it strongly relies on the visibility inside the flow.

To determine net transport rates, a Mass Conservation Technique is generally applied with the use of bed level soundings (or profile surveys) and sand traps. Bed level profiles are measured to determine the change of sand volume along the test section. Thereby the amount of sand removed from the test section is trapped in 'sand traps' on either side of the test section. If in addition the run time of the experiment is known, conclusions can be drawn concerning the net sediment transport. As the term 'Mass Conservation Technique' implies, the principle is based on the fact that the total amount of sediment present does not change throughout the experiment and the sediment continuity equation can be applied. The standard form of the Exner sediment continuity equation can be written as

$$(1-\varepsilon_0)\frac{\partial \eta}{\partial t} = -\frac{\partial q_s}{\partial x} \tag{2.1}$$

where $\varepsilon_0$ denotes bed porosity, $\eta$ is the bed level elevation, $q_s$ the volume transport rate in the $x$ direction and $t$ represents time. Strictly speaking, this form is only applicable for bed-load sediment transport. The Mass Conservation Technique and its application is explained in more detail in Dohmen-Janssen (1999), Dohmen-Janssen and Hanes (2002), Ahmed (2002) and Hassan (2003). In addition to the bed level soundings mentioned before, the changes in bed level (e.g. erosion depth or thickness of the moving layer) can additionally be analyzed by the use of video recordings. When heterogeneous sediments are concerned, the sediment collected from the sand traps is also used for analyzing the bed material composition and size distribution of the transported sand.

It should be kept in mind that differences in measurement techniques might lead to (significant) differences in net transport rates. For instance the determination of porosity of the sand bed. Dohmen-Janssen (1999) as well as Wright (2002) determined the porosity of the bed by weighing the amount of sand added to the tunnel to refill the eroded sand bed and the amount of sand eroded. The porosity is then determined by:

$$(1-\varepsilon_0) = \frac{G_{tot}}{\Delta V_{ip} * \rho_s} \tag{2.2}$$

where $\varepsilon_0$ is the porosity, $G_{tot}$ is the total dry mass of sand that left the tunnel, $\Delta V_{ip}$ is the total eroded sand volume (including pores) in the test section and $\rho_s$ the density of the sediment. Because the erosion during the experiments always developed more or less at the same location, the porosity of the eroded sand is more or less known. However, some sand may be lost from the system or the porosity may decrease due to compaction of the bed. Both lead to an overestimation of porosity when using this technique. Hassan (2003) tested this technique during various experiments and found an unrealistic variation in porosity of the bed (between 0.25 and 0.78). Previous direct measurements of the porosity indicated that a realistic value of porosity is 0.4, which was therefore

used in the analysis of his experiments. The same was used by Van der Werf and Doucette (2005) and in the analyses of the new experiments, presented in the current thesis.

Another example of possible differences in data due to analysis of the researchers is the correction of the net transport for side-wall effects. Dohmen-Janssen (1999) corrected the net transport rates as they are determined from the mass balance in the tunnel, which gives the width-averaged transport rate. Velocities and concentration however, are measured in the centerline of the tunnel. Therefore measured net sand transport rates do not correspond exactly to the measured velocities and concentrations and are therefore corrected to take this effect into account.

## 2.3 Database contents and structure

Table 2.2 lists the datasets included in the database. For each dataset the Table gives the literature reference, the facility in which the experiments were carried out, the number of experiments (number of different flow-sand bed combinations), the type of flow (wave-only or wave-plus-current), the type of sediment (well-sorted or graded), the range of median grain sizes ($D_{50}$), the range of flow periods ($T$) and the bedform regime. In total, the database contains information relating to 298 different experiments, carried out in 7 different laboratory facilities. The database contains full-scale laboratory experiments involving horizontal, mobile sand beds and non-breaking wave and non-breaking wave-plus-current flows. Experiments with artificial sediments are not included. Only experiments involving measurements of flow velocities, suspended sand concentrations and/or net sand transport rates are included. For each experiment the database contains the flow and bed conditions, information on which quantities were measured and the values of the measured net transport rate. The database does not contain detailed velocity or concentration data. The information and data are stored in five categories as follows:

1. General information: contains the literature reference, the experiment code, the experimental facility and the water depth above the sand bed.
2. Sand characteristics: contains the characteristic grain sizes ($D_{10}$, $D_{50}$ and $D_{90}$), the sand fall velocity, sand density and an indicator whether the sand was well-sorted (uniform) or graded (mixture of sizes).
3. Flow characteristics: type of flow (waves and/or currents, regular, irregular, skewness type etc.), wave/flow spectrum (for irregular waves/flows), wave height, flow period, root-mean-square orbital velocity, 'onshore' and 'offshore' velocity peaks (both are positive quantities), degree of velocity and acceleration skewness and magnitude, orientation and reference level of measured net current velocity.
4. Bed characteristics: indicates whether the bed was fixed or mobile (so far only mobile bed experiments are included), the type of bedform produced (flat bed, 2D ripples, quasi 2D ripples, 3D ripples), measured bed form height and length.
5. Measured parameters: indication of which quantities were measured (intra-wave velocities, intra-wave concentrations, wave-averaged concentrations) and the values of the measured net sand transport rates.

Further detail of the description of the database structure and comments on the included data sets can be found in the database report (Schretlen and Van der Werf, 2006).

Table 2.2 Datasets included in the SANTOSS database

| Reference | Facility | number of exp. | Flow | Sand | $D_{50}$ (mm) | $T$ (s) | Bedform regime |
|---|---|---|---|---|---|---|---|
| Sato (1987) | TOFT | 23 | IW RW | well-sorted | 0.18 | 4.0-5.5 | ripples |
| Watanabe & Isobe (1990) | TOFT | 11 | RW RW+C | well-sorted | 0.18, 0.87 | 6.0 | ripples |
| Dibajnia & Watanabe (1992) | TOFT | 23 | RW RW+C | well-sorted | 0.20 | 4.0 | s-f |
| Murray et al. (1993) | PWT | 6 | RW+C | well-sorted | 0.15 | 10 | ripples s-f |
| Ribberink & Chen (1993) | LOWT | 4 | RW | well-sorted | 0.13 | 6.5 | s-f |
| Katapodi et al. (1994) | LOWT | 4 | RW+C | well-sorted | 0.21 | 7.2 | s-f |
| Ramadan (1994) | LOWT | 10 | RW RW+C | well-sorted | 0.21 | 6.5, 7.0 | ripples s-f |
| Ribberink & Al-Salem (1994) | LOWT | 42 | IW RW | well-sorted | 0.21 | 4.0 - 12 | ripples s-f |
| Inui et al. (1995) | TOFT | 2 | RW | graded | 0.54 | 5.0 | s-f |
| Ribberink (1995) | LOWT | 5 | RW RW+C | well-sorted | 0.21 | 6.5 | s-f |
| Ribberink & Al-Salem (1995) | LOWT | 3 | RW | well-sorted | 0.21 | 6.5-9.1 | s-f |
| Hamm et al. (1998) | LOWT | 5 | RW RW+C | graded | 0.19 | 6.4-7.2 | s-f |
| Zala Flores & Sleath (1998) | COFT | 9 | RW | well-sorted | 0.41 | 5.6-7.1 | s-f |
| Dohmen-Janssen (1999) | LOWT | 23 | RW+C | well-sorted | 0.13 - 0.32 | 4.0-12 | s-f |
| Clubb (2001) | AOFT | 8 | RW | well-sorted | 0.34 | 5.0-10 | ripples |
| McLean et al. (2001) | LOWT | 4 | RW+C | well-sorted | 0.12, 0.32 | 7.2 | s-f |
| Dohmen-Janssen & Hanes (2002) | GWK | 8 | RW | well-sorted | 0.24 | 6.5, 9.1 | s-f |
| Thorne et al. (2002) | Delta flume | 12 | IW RW | well-sorted | 0.33 | 4.0-6.0 | ripples |
| Wright & O'Donoghue (2002) | AOFT | 4 | RW | well-sorted | 0.13 | 4.0-9.0 | s-f |
| Hassan (2003) | LOWT | 16 | RW RW+C | graded well-sorted | 0.13 - 0.32 | 5.0-12 | s-f |
| Thorne et al. (2003) | Delta flume | 1 | RW | well-sorted | 0.33 | 5.0 | ripples |
| O'Donoghue & Wright (2004a,b) | AOFT | 22 | RW | graded well-sorted | 0.13 - 0.46 | 5.0, 7.5 | s-f |
| Watanabe & Sato (2004) | TOFT | 12 | RW | well-sorted | 0.20 | 5.0 | s-f |
| Liu & Sato (2005) | TOFT | 6 | RW | well-sorted | 0.21, 0.30 | 4.0, 5.0 | s-f |
| Van der Werf et al. (2006) | AOFT LOWT | 22 | IW RW | well-sorted | 0.22 - 0.44 | 4.1-13 | ripples |
| Van der Werf et al. (2007) | AOFT | 13 | RW | well-sorted | 0.44 | 4.1-7.4 | ripples |
| **Total** | | **298** | | | **0.12 - 0.87** | **4.0 - 13** | |

IW = irregular orbital flow with waves only; RW = regular orb. flow, waves only; C = additional current and s-f = sheet-flow.

## 2.4 Data overview

Table 2.3 gives an overview of the experiments in terms of the type of measurements; intra-wave velocities ($u(t)$), intra-wave concentrations ($c(t)$), wave averaged concentrations ($<c(z)>$) and net sand transport rate ($<q_s>$), the type of sediment (well-sorted or graded) and the type of flow (wave-only or wave-plus-current).

Table 2.3 Overview of measurements included in the SANTOSS database
(w = only waves, w+c = waves + current).

| Sand | Flow | Regime | Type of measurements | | | |
|---|---|---|---|---|---|---|
| | | | $u(t)$ | $c(t)$ | $<c(z)>$ | $<q_s>$ |
| Well sorted | W | Ripples | 14 | 8 | 58 | 60 |
| | | Sheet-flow | 27 | 36 | 37 | 57 |
| | W+C | Ripples | 1 | 1 | 3 | 8 |
| | | Sheet-flow | 28 | 19 | 19 | 50 |
| Graded | W | Ripples | 0 | 0 | 0 | 0 |
| | | Sheet-flow | 6 | 13 | 9 | 19 |
| | W+C | Ripples | 0 | 0 | 0 | 0 |
| | | Sheet-flow | 1 | 1 | 2 | 2 |
| **Total** | | | **77** | **78** | **128** | **196** |

The information shown in Tables 2.2 and 2.3 can be used to identify gaps in the range of test conditions and/or the type of measurements. The following can be concluded on the coverage of the experiments:

- Very few graded sand experiments were carried out compared to the number of well-sorted sand experiments. And no graded sand experiments were carried out in the ripple regime or in wave flumes.
- The number of wave-only experiments far exceeds the number of wave-plus-current experiments.
- The number of experiments involving net sand transport measurements far exceeds the number of experiments involving intra-wave velocity measurements and intra-wave concentration measurements. The majority of intra-wave measurements have been carried out for sheet-flow conditions.
- Of the total of 298 experiments, only 21 were conducted under full scale surface waves in flumes and the rest (277) were performed in oscillatory flow tunnels. The wave flume experiments comprise 8 sheet-flow regime experiments carried out in the GWK by Dohmen-Janssen and Hanes (2002) (see also Ribberink et al., 2000) and 13 ripple regime experiments carried out in the Delta flume by Thorne et al. (2002, 2003). As will be discussed in Section 2.5, the sheet-flow experiments show that differences in the detailed hydrodynamics between nominally similar near-bed tunnel and real wave flows are potentially important for the net sand transport. More large wave flume experiments are needed to investigate these effects further.
- Not shown in the above Tables, but another important point is that the experiments primarily involved velocity-skewed flows with zero acceleration skewness (162 of the 189 non-sinusoidal flow experiments). As will be discussed in the next section, Watanabe and

Sato (2004) show that the net transport rates depend on acceleration skewness and more experiments are needed to investigate acceleration effects further.

As described in the introduction of this thesis (Chapter 1), the new experiments are designed to investigate the surface wave effects on sand transport processes under sheet-flow conditions. Figure 2.1 shows how the SANTOSS database can be used to give an overview of the data related to these experiments, available so far. It gives an overview of wave-alone cases with uniform sediment under sheet-flow layer conditions and the type of measurements ($u(t)$ and $c(t)$ inside the suspension layer and/or inside the sheet-flow layer, $<c(z)>$ and $<q_s>$ ). The experiments are placed in $T - \Psi_w$ space, where $T$ is the flow period and $\Psi_w$ is the mobility number defined by:

$$\Psi_w = \frac{u_w^2}{(s-1)gD_{50}} \tag{2.3}$$

where $s = \rho_s/\rho_w$ is the relative sand density with $\rho_s$ the sand density and $\rho_w$ the water density, $g$ is acceleration due to gravity and $u_w$ is a representative orbital velocity given by:

$$u_w = \sqrt{0.5\hat{u}_{on}^2 + 0.5\hat{u}_{off}^2} \tag{2.4}$$

which is the equivalent sinusoidal orbital velocity amplitude in terms of $u_{rms}$ for second-order Stokes orbital flows. $\hat{u}_{on}$ is the peak positive (onshore directed) orbital velocity and $\hat{u}_{off}$ is the peak negative (offshore directed) orbital velocity. Rippled bed conditions prevail for $\Psi_w < 100$ and flat bed, sheet flow conditions prevail for $\Psi_w > 100$. Open circles represent data from oscillatory flow tunnel experiments, black triangles from wave flumes. The following data are presented in Figure 2.1:

- Time-dependent flow velocities (with at least two points in the vertical) are only measured in oscillatory flow tunnels (Liu and Sato, 2005; Murray et al., 1993; Ramadan, 1994; Ribberink and Chen, 1993; Ribberink, 1995; Ribberink and Al-Salem, 1995; Wright and O'Donoghue, 2002; Zala Flores and Sleath, 1998).
- Time dependent concentration measurements in the suspension layer are performed in both oscillatory flow tunnels (data from Murray et al., 1993; O'Donoghue and Wright, 2004a;2004b; Ribberink and Al-Salem, 1995; Ribberink and Chen, 1993; Wright and O'Donoghue, 2002; Zala Flores and Sleath, 1998), as well as in the Large Wave Channel in Hannover (GWK) (Dohmen-Janssen and Hanes, 2002). Inside the sheet flow layer, the same measurements were done in oscillatory flow tunnels by O'Donoghue and Wright (2004a,b), Ribberink and Al-Salem (1995) and Wright and O'Donoghue (2002) and in the Large Wave Channel in Hannover by Dohmen-Janssen and Hanes (2002).
- Also time-averaged concentration measurements were performed in oscillatory flow tunnels (Murray et al., 1993; Ramadan, 1994; Ribberink and Chen, 1993; Ribberink and Al-Salem, 1994; Ribberink, 1995; Wright and O'Donoghue, 2002) and in the Large Wave Channel in Hannover (Dohmen-Janssen and Hanes, 2002).
- The net sand transport rates are measured in various oscillatory flow tunnels (Ahmed, 2002; Dibajnia and Watanabe 1992; Hassan 2003; O'Donoghue and Wright, 2004a; 2004b; Ramadan, 1994; Ribberink and Chen, 1993; Ribberink and Al-Salem, 1994; Ribberink, 1995; Watanabe and Sato, 2004; Wright and O'Donoghue, 2002) as well as in the Large Wave Channel in Hannover (GWK) (Dohmen-Janssen and Hanes,2002).

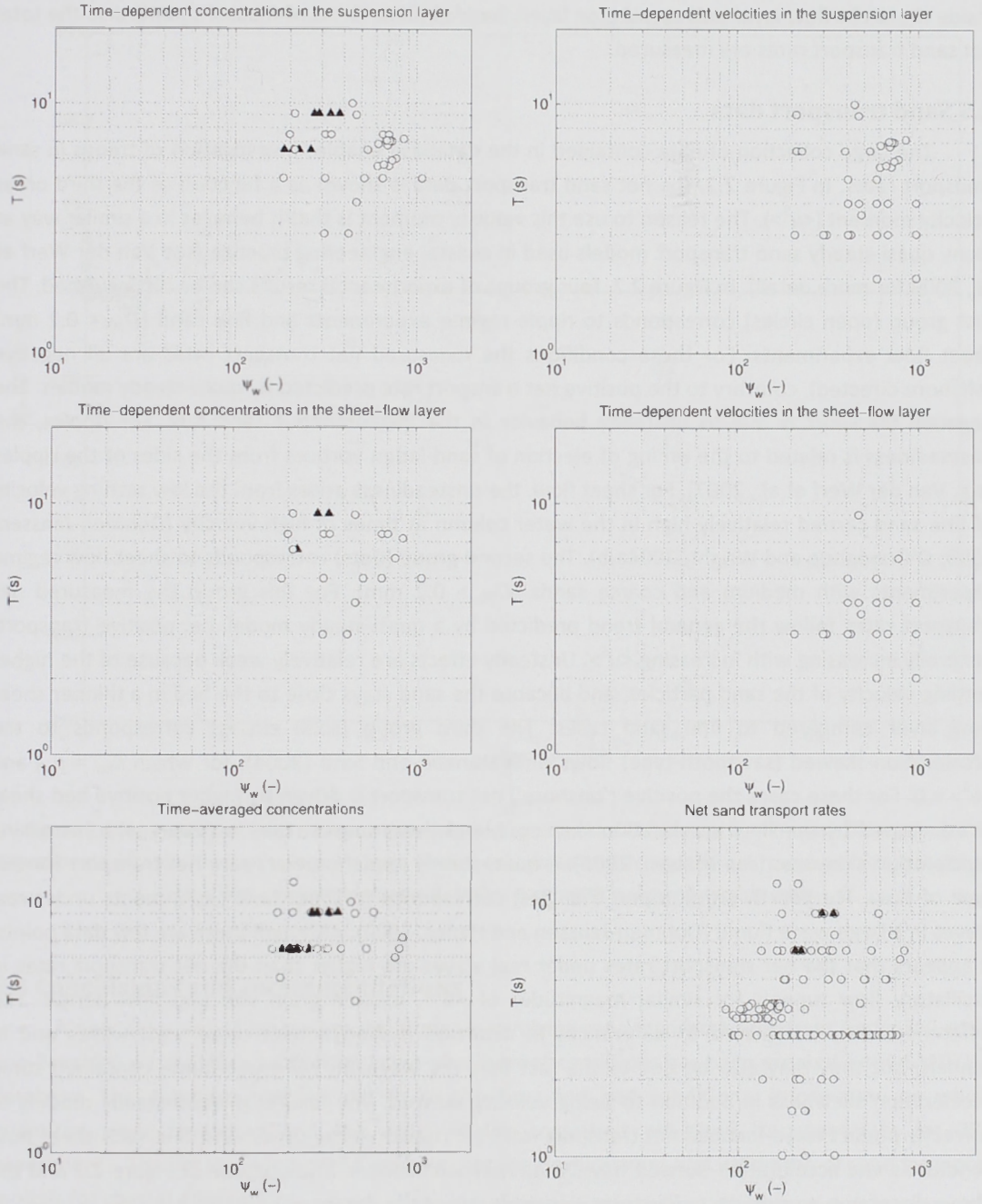


Figure 2.1 Overview of process measurements in the sheet-flow regime for wave-alone cases with uniform sediment. Open circles: oscillatory flow tunnel experiments; closed triangles: wave flume experiments.

Overall, it can be concluded that the far majority of the data concerning wave-alone cases with uniform sediment in the sheet flow regime are obtained in oscillatory flow tunnels. Only few sediment concentration and sand transport measurements are done under full scale surface wave conditions (Large Wave Channel (GWK) in Hannover) by Dohmen-Janssen and Hanes (2002) and no time-dependent flow velocities in the sheet flow layer are available under these conditions. The new experiments in the large wave flume, as presented in this thesis, are designed to fill part of these gaps; both time-dependent and time-averaged concentrations and flow velocities are measured

inside the sheet-flow layer and suspension layer. Besides these detailed measurements also the total net sand transport rates are measured.

## 2.5 Sand transport data

The large collection of data contained in the database enables investigation of trends in sand transport rates. In Figure 2.2, the net sand transport data is shown as a function of the third order velocity moment ($<u^3>$). The reason to use this velocity moment is that it behaves in a similar way as many quasi-steady sand transport models used in coastal engineering practice (see Van der Werf et al., 2009 for more detail). In Figure 2.2, four groups of experimental results can be distinguished. The first group (open circles) corresponds to ripple regime experiments and fine sand ($D_{50}$ < 0.2 mm) sheet flow experiments. For these conditions the measured net transport rates are all negative (offshore directed), contrary to the positive net transport rate predicted by quasi-steady models. The negative transport is due to unsteady behavior in the instantaneous sand flux. For ripples, the unsteadiness is related to the timing of ejection of sand-laden vortices from the sides of the ripples (e.g. Van der Werf et al., 2007). For sheet flow, the unsteadiness arises from the low settling velocity of fine sand carried relatively high in the water column at times of high velocity (Dohmen-Janssen, 1999; O'Donoghue and Wright, 2004a,b). The second group (dots) corresponds to sheet flow regime experiments with medium and coarse sands ($D_{50}$ > 0.2 mm). For this group the measured net transport rates follow the general trend predicted by a quasi-steady model, i.e. positive transport, generally increasing with increasing $<u^3>$. Unsteady effects are relatively weak because of the higher settling velocity of the sand particles, and because the sand stays close to the bed in a thinner sheet flow layer compared to fine sand cases. The third group (solid circles) corresponds to the acceleration-skewed (sawtooth-type) flows of Watanabe and Sato (2004), for which $\hat{u}_{on} = \hat{u}_{off}$ and $<u^3> = 0$. For these cases the positive ('onshore') net transport is driven by higher positive bed shear stress caused by the flow acceleration skewness, and the transport rate increases with increasing acceleration skewness (see Nielsen, 2006). A quasi-steady model predicts zero net transport for this type of flow. The fourth group (open triangles) corresponds to sheet flow experiments under real waves in a large wave flume (Dohmen-Janssen and Hanes, 2002). Although there are few data points, it appears that the net transport rates under real waves are higher than the net transport rates in oscillatory flow tunnels for similar magnitudes of $<u^3>$, median grain size and flow period. The differences may be related to differences in near-bed hydrodynamics under real waves and in tunnels, but they may also be due to the fact that the waves in the wave flume contained some acceleration skewness in addition to being velocity skewed. The failure of quasi-steady models to correctly predict wave-induced net transport rates for ripple regime conditions, fine-sand sheet flow conditions and acceleration-skewed flows is already well known. The purpose of Figure 2.2 and the above discussion is primarily to illustrate a possible use of the database.

The new experiments provide additional data of medium sand transport rates under full scale surface waves, but for the first time, also of fine sand conditions under surface waves. The results of the new experiments are described in the following Chapters of this thesis. The new data are also implemented into the database.

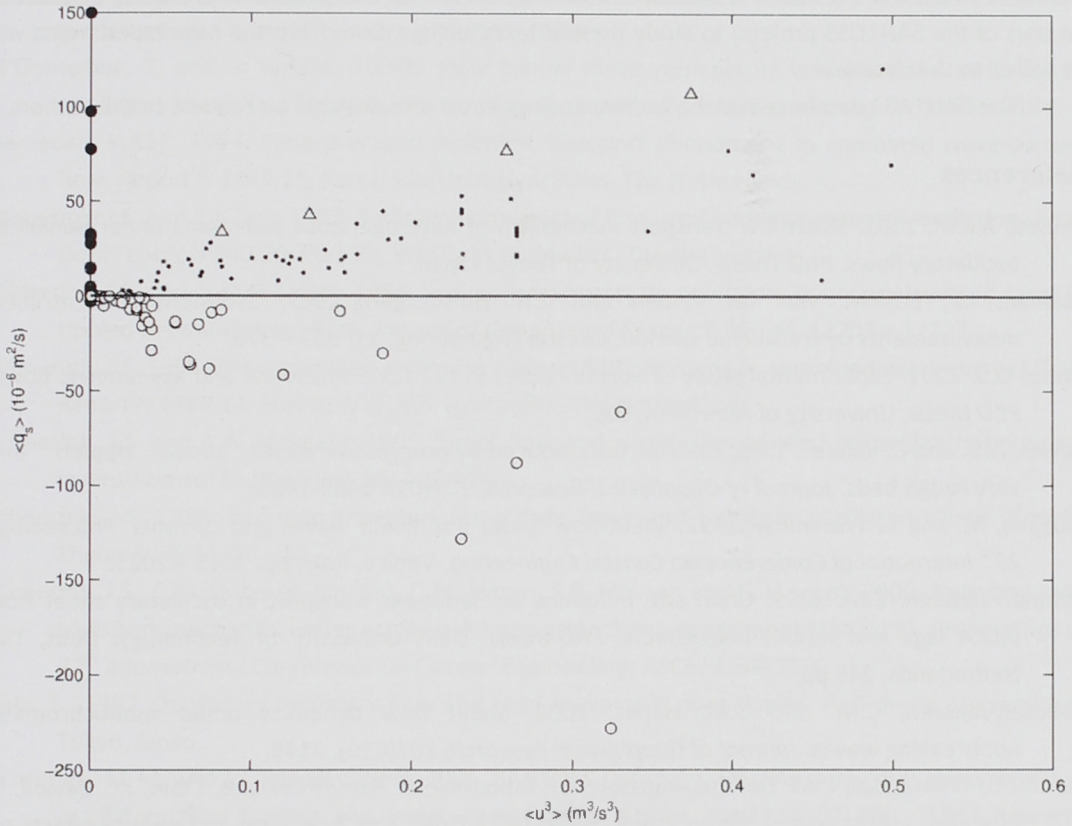


Figure 2.2 Measured net sand transport rates plotted against third-order velocity moment. Dot symbols: experiments with positive net transport; open circles: experiments with negative net transport; triangles: large wave flume experiments; solid circles: acceleration skewed experiments.

## 2.6 Conclusions and recommendations

A new database of laboratory experiments involving sand transport processes under full-scale non-breaking wave and non-breaking wave-plus-current conditions has been created – the SANTOSS database. The database contains details of the flow and bed conditions, information on which quantities were measured and the value of the measured net sand transport rate for 298 experiments. The database is a useful resource for the development and validation of sand transport models for coastal applications.

Analysis of the coverage of the experiments identified the following gaps in the range of test conditions and/or the type of measurements: (i) graded sand experiments, (ii) wave-plus-current experiments and (iii) intra-wave velocity and concentration measurements in the ripple regime. This analysis together with an investigation of trends in the sand transport rates highlights two areas requiring further research. The first is the differences in sand transport processes and sand transport rates between real waves and tunnel flows with nominally similar near-bed oscillatory flow conditions. The second is the effects of acceleration skewness on transport processes and net transport rates. The number of existing experiments enabling analysis of "surface wave" and "acceleration" effects is very limited, but results point to the potential importance of both for the net

transport rate. New oscillatory flow tunnel and large wave flume experiments are being conducted (as part of the SANTOSS project) to study these effects further. Data from the new experiments will be added to the database.

This SANTOSS database and the accompanying report are available on request to the authors.

## References


Ahmed, A.S.M. 2002. Sheetflow transport mechanism of heterogeneous sediments under nonlinear oscillatory flows. PhD Thesis, University of Tokyo, Japan.

Bosman, J.J., E.T.J.M. van der Velden and C.H. Hulsbergen. 1987. Sediment concentration measurements by transverse suction. Coastal Engineering, 11: 353 – 370.

Clubb, G.S. 2001. Experimental study of vortex ripples in full scale sinusoidal and asymmetric flows. *PhD thesis*, University of Aberdeen, UK.

Davies, A.G. and C. Villaret. 1999. Eulerian drift induced by progressive waves above rippled and very rough beds. *Journal of Geophysical Research*, 104(C1): 1465-1488.

Dibajnia, M. and A. Watanabe. 1992. Sheet-flow under non-linear waves and currents. *Proceedings 23rd International Conference on Coastal Engineering*, Venice, Italy, pp. 2015 – 2025.

Dohmen-Janssen, C.M. 1999. Grain size influence on sediment transport in oscillatory sheet flow phase lags and mobile-bed effects. *PhD-thesis*, Delft University of Technology, Delft, The Netherlands, 246 pp.

Dohmen-Janssen, C.M. and D.M. Hanes. 2002. Sheet flow dynamics under monochromatic nonbreaking waves. *Journal of Geophysical Research,* 107(C10), 3149.

Hamm, L., I. Katapodi, C.M. Dohmen-Janssen, J.S. Ribberink, P. Samothrakis, B. Cloin, J.C. Savioli, Y. Chatelus, J. Bosboom, J. Nicholson, R. Hein. 1998. Grain size, gradation and density effects on sediment transport processes in oscillatory flow conditions. *Data report, Part I,* WL|Delft Hydraulics, The Netherlands.

Hassan, W.N., 2003. Transport of size-graded and uniform sediments under oscillatory sheet-flow conditions. *PhD thesis*, University of Twente, The Netherlands.

Inui, T., M. Dibajnia, M. Isobe, A. Watanabe. 1995. A transport rate formula for mixed-size sands and its application. *Proceedings 42nd Japanese Annual Conference on Coastal Engineering*, pp. 356-360 (in Japanese).

Katapodi, I., J.S. Ribberink, P. Ruol, R. Koelewijn, C. Lodahl, S. Longo, A. Crosato, H. Wallace. 1994. Intra-wave sediment transport in oscillatory flow superimposed on a mean current. *Data report, Part III,* WL|Delft Hydraulics, The Netherlands.

Liu, H., S. Sato. 2005. Laboratory study on sheetflow sediment movement in the oscillatory turbulent boundary layer based on image analysis. *Coastal Engineering in Japan*, 47: 21-40.

Longuet-Higgins, M.S. 1953. Mass transport in water waves. *Philosophical Transactions of the Royal Society of London. Series A, Mathematical and Physical Sciences*, 245(903), 535 – 581.

McLean, S.R., J.S. Ribberink, C.M. Dohmen-Janssen, W.N. Hassan. 2001. Sand transport in oscillatory sheet flow with mean current. *Journal of Waterway, Port, Coastal, and Ocean Engineering*, 127(3): 141-151.

Murray, P.B., R.L. Soulsby, A.G. Davies. 1993. Sediment pick-up in combined wave current flow. *Data report, Report SR 364*, HR|Wallingford, UK.

Nielsen, P., 2006. Sheet flow sediment transport under waves with acceleration skewness and boundary layer streaming. *Coastal Engineering*, 53: 749-758.

O'Donoghue, T. and S. Wright. 2004a. Concentrations in oscillatory sheet flow for well sorted and graded sands. *Coastal Engineering* 50, 117 – 138.

O'Donoghue, T. and S. Wright. 2004b. Flow tunnel measurements of velocities and sand flux in oscillatory sheet flow for well sorted and graded sands. *Coastal Engineering* 51, 1163 – 1184.

Ramadan, K.A.H., 1994. Time-averaged sediment transport phenomena in combined wave-current flow. *Report H 1889.11, Part I*, WL|Delft Hydraulics, The Netherlands.

Ribberink, J.S. and Z. Chen. 1993. Sediment transport of fine sand under asymmetric oscillatory flow. *Data report H 840.20, Part VII*, WL|Delft Hydraulics, The Netherlands.

Ribberink, J.S. and A.A. Al-Salem. 1994. Sediment transport tin oscillatory boundary layers in cases of rippled beds and sheet flow. *Journal of Geophysical Research* 99(C6), 12707 – 12727.

Ribberink, J.S. 1995. Time-averaged sediment transport phenomena in combined wave-current flow. *Report H 1889.11, Part II,* WL|Delft Hydraulics, The Netherlands.

Ribberink, J.S. and A.A. Al-Salem. 1995. Sheet flow and suspension of sand in oscillatory boundary layers. *Coastal Engineering*, 25: 205-225.

Ribberink, J.S. 1998. Bed-load transport for steady flows and unsteady oscillatory flows. *Coastal Engineering* 34, 59 – 82.

Ribberink, J.S., C.M. Dohmen-Janssen, D.M. Hanes, S.R. McLean and C. Vincent. 2000. Near-bed sand transport mechanics under waves – A large-scale flume experiment (Sistex99). *Proceedings of 27th International Conference on Coastal Engineering*, ASCE, 3263-3276.

Sato, S., 1987. Oscillatory boundary flow and sand movement over ripples. *PhD thesis*, University of Tokyo, Japan.

Schretlen, J.L.M. and J.J. van der Werf. 2006. SANTOSS Database, Existing data from experiments in oscillatory flow tunnels and large wave flumes. *Report SANTOSS_UT_IR1, CE&M Research Report 2006R-008/WEM-009*, University of Twente, The Netherlands.

Thorne, P.D., J.J. Williams and A.G. Davies. 2002. Suspended sediments under waves in a large-scale flume facility. *Journal of Geophysical Research*, 107(C8).

Thorne, P.D., A.G. Davies and J.J. Williams. 2003. Measurements of near-bed intra-wave sand entrainment above vortex ripples. *Geophysical Research Letters*, 30(20), 2028.

Van der A, D.A. 2010. Effects of acceleration skewness on oscillatory boundary layers and sheet flow sand transport. PhD Thesis, University of Aberdeen, UK.

Van der A, D.A., J.S. Ribberink, J.J. van der Werf and T. O'Donoghue. 2010. New practical model for sand transport induced by non-breaking waves and currents. *Proceedings of 32nd International Conference on Coastal Engineering*, Shanghai, China.

Van der Werf, J.J. and J.S. Doucette. 2005. New measurements of the time-dependent flow and suspended sand concentration field above full-scale ripples in regular oscillatory flows in the Aberdeen oscillatory flow tunnel. Report, *EU-project SANDPIT EVK3-CT-2001-00056*, University of Twente & University of Aberdeen, Enschede, The Netherlands.

Van der Werf, J.J., J.S. Ribberink, T. O'Donoghue and J.S. Doucette. 2006. Modelling and measurement of sand transport processes over full-scale ripples in oscillatory flows. *Coastal Engineering*, 53: 657-673.

Van der Werf, J.J., J.S. Doucette, T. O'Donoghue and J.S. Ribberink. 2007. Detailed measurements of velocities and suspended sand concentrations over full-scale ripples in regular oscillatory flow. *Journal of Geophysical Research*, 112, F02012.

Van der Werf, J.J., J.L.M. Schretlen, J.S. Ribberink and T. O'Donoghue. 2009. Database of full-scale laboratory experiments on wave-driven sand transport processes. *Coastal Engineering* 26, 726 – 732.

Watanabe, A. and M. Isobe. 1990. Sand transport rate under wave-current action. *Proceeding 22nd International Conference on Coastal Engineering*, Delft, The Netherlands, pp. 2495-2507.

Watanabe, A. and S. Sato. 2004. A sheet-flow transport rate formula for asymmetric, forward-leaning waves and currents. *Proceedings 29th International Conference on Coastal Engineering*, Lisbon, Portugal, pp. 1703-1714.

Wright, S. 2002. Well-sorted and graded sand in oscillatory sheet-flow. PhD Thesis, University of Aberdeen, UK.

Wright, S. and T. O'Donoghue. 2002. Total sediment transport rate predictions in wave current sheet flow with graded sand. Oscillatory flow tunnel experiments at Aberdeen University, *Experimental report EPSRC LUBA Project*, University of Aberdeen, UK.

Zala Flores, N. and J.F.A. Sleath. 1998. Mobile layer in oscillatory sheet flow. *Journal of Geophysical Research*, 103(C6): 12,783-12,793.

# 3. BOUNDARY LAYER VELOCITIES MEASURED ABOVE MOBILE BEDS UNDER FULL SCALE PROGRESSIVE SURFACE WAVES

**Abstract**

Existing models for wave-related (cross-shore) sand transport are primarily based on data from oscillatory flow tunnel experiments. However, theory and former experiments indicate that flow differences between full scale surface waves and oscillatory flow tunnels may have a substantial effect on the net sand transport. In this paper, new high resolution measurements of boundary layer flow characteristics under full scale surface waves over a horizontal mobile sand bed with sheet flow are presented. These experiments were performed for different wave conditions with medium ($D_{50}$ = 0.25 mm) and fine ($D_{50}$ = 0.14 mm) sand in the large wave channel GWK. The measured wave boundary layer thickness and the time-dependent velocity profiles show a large similarity with those measured in oscillating flow tunnels. However, the mean horizontal flow velocity (streaming) profiles are clearly different. For all new experiments the vertical streaming profile shows a characteristic three-layer shape with 'onshore' as well as 'offshore' streaming and with alternating negative and positive shear layers in between. Above the sheet flow layer two layers are observed showing generally 'offshore' streaming. The two-layer structure is explained qualitatively by the height-dependent balance between mean pressure gradient, wave Reynolds stress and the mean (oscillatory) turbulent Reynolds stress. In the sheet flow layer all experiments show a transition to 'onshore' streaming, which is caused by the 'onshore' erosion depth always exceeding the 'offshore' component due to the velocity skewness of the oscillatory flow (erosion depth asymmetry). The streaming under progressive waves is generally more 'onshore' than in oscillatory flow tunnels, which may be explained by the influence of the wave Reynolds stress and by advective effects (absent in tunnels). In the upper levels of the boundary layer the streaming profiles show a negative shear in the present experiments (transition to negative undertow), while tunnel experiments show here a positive shear due to the opposite direction of the mean pressure gradient (transition to positive return flow).

## 3.1 Introduction

When predicting changes in coastal morphology, knowledge of sediment transport processes is essential. Under storm conditions, flow velocities are high and large quantities of sand can be transported in a relative short time span. Under these conditions, ripples on the sea bed are washed out and sand is transported in a thin layer (mm – cm) close to the bed, known as the sheet flow layer. Since the far majority of sand is transported in the first few mm – cm above the bed, detailed knowledge on the flow velocities and sheet flow layer processes in this small part of the total water column is of great importance to understand and predict sand transport under these conditions.

Various transport models have been developed to predict both the quantities and directions of this sand transport. The majority of these existing models are based on data obtained from oscillatory flow tunnel experiments (Dibajnia & Watanabe, 1998; O'Donoghue & Wright, 2004a & 2004b; Ribberink, 1998; Van der Werf, 2006; Van Rijn, 2007; Gonzalez-Rodriguez & Madsen, 2010). Even though oscillatory flow tunnels provide a good approximation of the horizontal oscillatory boundary layer flow experienced near the sea bed, there are some fundamental differences with boundary layers under progressive surface waves. Vertical orbital motions are absent and wave-induced residual currents are not fully reproduced in flow tunnels. Surface waves induce Lagrangian and Eulerian mean velocities. A Lagrangian mean velocity occurs due to the fact that i) a fluid particle in a wave will move with higher forward velocity at the top of its orbit than with backward velocity at the bottom and ii) the particles move with the wave during its forward motion and against it during its backward motion, and will therefore spend more time moving forwards than backwards (Nielsen, 1992). An Eulerian mean velocity results from the fact that i) the vertical and horizontal orbital velocities are not exactly 90° out of phase in the boundary layer as they would be in a frictionless

*This Chapter is submitted as journal paper*

Schretlen, J.L.M., J.S. Ribberink, W.M. Kranenburg and T. O'Donoghue. Boundary layer velocities measured above mobile beds under full scale progressive surface waves.

flow, ii) wave asymmetry causes a difference in generated turbulent energy between the two half wave cycles, and thereby iii) a return flow may develop, compensating for mass flux in the direction of wave propagation and driven by a mean pressure gradient (undertow). The first process leads to a vertical gradient in the wave Reynolds stress and an onshore-directed mean velocity close to the bed (Longuet-Higgins, 1953). Meantime, due to the second process the mean velocity will tend to shift from onshore to offshore, depending on the ratio of water depth and wave length and the relative roughness (Trowbridge & Madsen, 1984a & 1984b; Davies & Villaret, 1999). The Lagrangian mean velocities and undertow are absent in oscillatory flow tunnels, as well as the onshore-directed Longuet-Higgins streaming. In Appendix I the different streaming mechanisms in oscillating flow tunnels and under progressive surface waves are discussed more extensively on the basis of the wave-averaged momentum equations.

Even though the boundary layer streaming takes place in only a small part of the water column under surface waves (mm's to cm's above the bed), this thin layer with relatively small wave-induced net currents may be of major importance for the total net sand transport. Under wave-dominated sheet-flow conditions the majority of the sand is transported within a few centimetres thick layer directly above the bed. Previous experiments under full-scale surface waves (Ribberink et al., 2000; Dohmen-Janssen and Hanes, 2002) showed measured net sand transport rates which are a factor 2 larger than under similar flow and sand conditions in large oscillatory flow tunnels (Ribberink and Al-Salem, 1994). Later, Schretlen et al. (2009, 2010) showed that for fine sand ($D_{50}$ = 0.14 mm) even the direction of sheet flow net transport can be different under progressive waves than in oscillatory flows, again for nominally similar near-bed free-stream flow and sand size.

Sand transport formulae have been developed in recent years, which include progressive surface wave effects in a parameterized way (Nielsen, 2006; Gonzalez-Rodriguez and Madsen, 2010). However, these formulae still cannot fully explain the observed differences in net transport rate between progressive surface waves and oscillatory flows. Considerable uncertainty still exist about the flow parameterizations used in these formulae, which is mainly caused by the present lack of experimental data of wave boundary layer flows over mobile beds under full scale progressive surface waves.

The experimental work as presented in this paper was initiated to address this lack of knowledge. Using acoustic-based velocity measurement instruments and conductivity-based sediment concentrations probes, detailed velocity measurements have been obtained inside the wave boundary layer under full-scale surface waves for different mobile sand beds. The data provide new insights into the oscillatory and mean flow velocities within the wave boundary layer, including the sheet flow layer. The measurements are also used to evaluate existing models for wave boundary layer thickness and erosion depth and comparisons are made with corresponding results from oscillatory flow tunnel experiments.

The experimental set-up, instrumentation and test conditions are described in Section 3.2 of the paper. The experimental results for instantaneous and time-averaged velocities within the boundary layer, erosion depth and boundary layer thickness are presented in Section 3.3. This is followed in Section 3.4 by a comparison of results from the present progressive wave experiments with previously obtained results from oscillatory flow tunnel experiments. Finally, in Section 3.5 a discussion and conclusions are given.

## 3.2 Experimental set-up

### 3.2.1 Wave channel with sand bed

The experiments were carried out in the large wave flume, or Groβer Wellenkanal (GWK), of the Coastal Research Centre in Hannover, Germany, a joint research facility of the University of Hannover and the Technical University of Braunschweig. The flume has a length of 280 m and is 5 m wide and 7 m deep. In this flume, regular and irregular waves with heights from 0.5 to 2.5 m and periods of 2 to 15 s can be generated. The wave generator incorporates wave absorption for elimination of reflected waves at the paddle.

The experiments were carried out over three different measurement campaigns in 2007 and 2008, in which two different types of sand were placed in the flume. The sands used in these experiments can be characterised as medium and fine sand. More details on the sand characteristics and grain size distribution are given in Section 3.2.3. Figure 3.1 shows an overview of the flume with the wave paddle on the left and the artificial beach on the right. For the medium sand experiments, a 1 m deep horizontal sand bed was placed at approximately 50 to 175 m from the wave paddle, with a 1:20 sloping sand beach downstream. For the fine sand experiments, the horizontal part of the profile was replaced with a 0.85 m deep fine sand bed. The dashed vertical line underneath 'container I' in Figure 3.1 indicates the position of the instruments used for detailed velocity and concentration measurements (approximately 110 m from the wave paddle). A more detailed description of the instruments and experimental set-up is given in the next section.

The water level in the flume was 4.5 m above the flume bottom during the medium sand experiments and 4.35 m during the fine sand experiments, giving 3.5 m water depth above both initial horizontal sand beds.

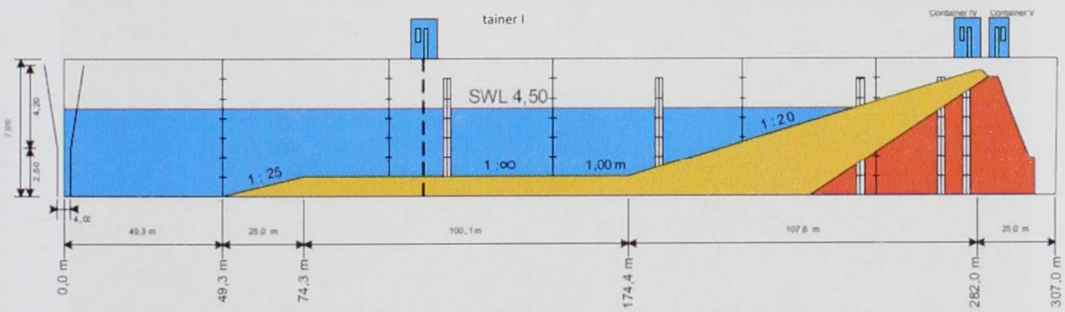


Figure 3.1. Sand bed set-up in the Large Wave Flume of the Coastal Research Centre, Hannover, Germany (set-up for medium sand bed shown).

### 3.2.2 Instruments and measurement set-up

**General overview**

For the detailed measurements near the sand bed in the wave boundary layer, special rigs were designed to obtain the required high spatial ($10^{-3}$ – $10^{-2}$ m) and high temporal ($10^{-3}$ – $10^{-1}$ s) measurement resolution, while at the same time avoiding flow disturbances as much as possible and being rigid enough to withstand the wave forces. The measurements were performed mainly from i) a wall-mounted instrument frame, and ii) a measuring tank buried underneath the sand surface, both provided with remotely-controlled vertical positioning systems with sub-mm accuracy. The majority of flow velocity and sediment concentration instruments were positioned on the wall frame.

A wide range of instruments was deployed from the frame for the experiment series, including acoustic velocity meters positioned near the bed (UVP and ADV-Vectrino), electromagnetic flow meters (EMF) higher in the water column (free stream), ripple profiler, transverse suction system (TSS) for time-averaged suspended sediment concentrations at several levels above the bed, acoustic backscatter sensor (ABS) for time-dependent concentration profiles and ultra-high concentration meter (UHCM) for time-dependent concentrations at selected points. Concentration measurements within the sheet-flow layer were carried out using conductivity-based CCM-probes deployed from a measuring tank buried under the sand surface. Close to the instrument frame, 3 additional EMFs were deployed from a second fixed frame attached to the flume wall. The two instrument frames are shown in Figure 3.2. The CCMs coming from beneath the sand bed are hardly visible, but penetrate the sand surface at a location between the UVPs and the Vectrino. Besides the instruments on the frames, 19 wave gauges were positioned along the flume to measure the wave characteristics. Net sand transport measurements were carried out along the flume bed by bed level profiling from a measuring carriage using the mass-conservation principle.

The present paper focuses on the boundary layer flow, using the velocity measurements from the UVPs and the ADV-Vectrino and using bed level information derived from the CCM measurements. More detail on the UVP, ADV and CCM measurements are presented below.

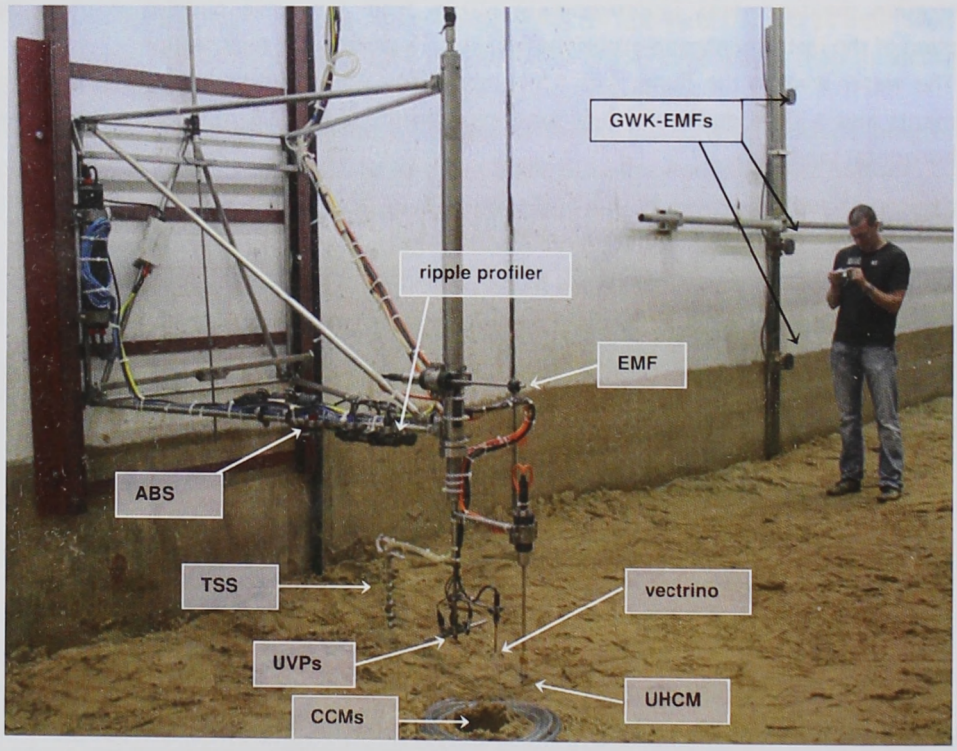


Figure 3.2. Overview of the 2 instrument frames in the Large Wave Flume. The CCM-tank is buried underneath the sand bed.

**CCM system**

The CCMs (manufactured by Deltares, The Netherlands) were vertically positioned into the sheet flow layer from a measuring tank buried in the sand bed. The probes have a measuring volume of approximately 1 mm high and 2 mm long and measure the electrical conductivity of the sand-

water mixture, which is inversely proportional to the sediment (volume) concentration. Deployment from a buried tank in the way used here is similar to that described by Ribbeirnk and Al-Salem (1995) for their measurements of concentrations in oscillatory sheet flow conditions. By penetrating the sheet flow layer coming from below instead of from above, disturbance of the flow is minimized. Ribberink et al. (2000) and Dohmen-Janssen and Hanes (2002) used the buried tank system for concentration measurements under progressive waves. For more technical details of the CCM probes and the tank system, reference is made to these publications. For the present experiments a new tank was constructed with 2 measuring rods, one for concentration measurements and one for bed-level measurement (Figure 3.3). Each rod can be vertically positioned with sub-mm accuracy independently from the other rod at pre-selected levels in the sheet flow layer. The vertical positioning is achieved via electrical servo-motors in the buried tank, controlled by a LabView programme which also controls position and CCM data acquisition (with a minimum sampling frequency of 50 Hz). The measuring accuracy of the bed level measurement using CCM is estimated to be in order of 1 mm. Together with the measurements of the no-flow bed level before and after each wave run, the CCM measurements provide crucial information for analysing the velocity measurements within the wave boundary layer.

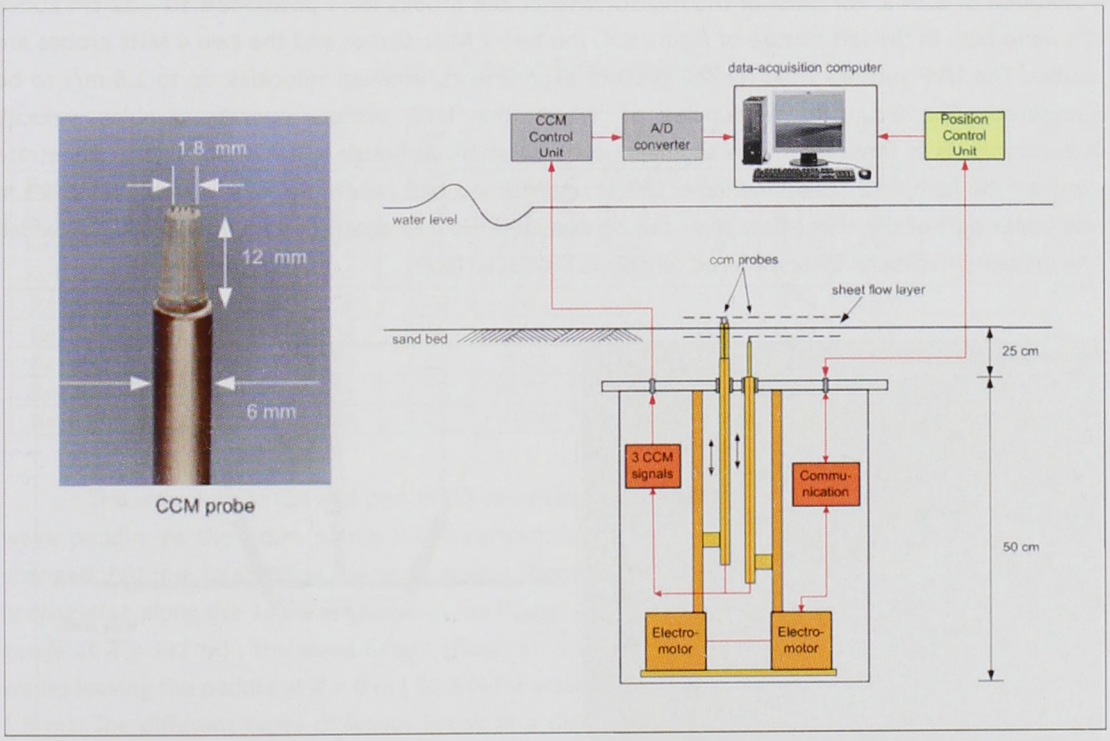


Figure 3.3. CCM tank system for measurement of sheet flow sand concentrations and the bed level.

**UVP and ADV-Vectrino**

Ultrasonic Velocity Profiler (MET-FLOW, 2002) operates through the acoustic Doppler principle. A transducer transmits a short emission of ultrasound, which travels along the measurement axis; the transducer switches to 'receiving' mode recording the energy scattered and echoed back from particles in the flow. The velocities measured are thus the velocities of particles inside the water, not

the water particles themselves. These can be sand grains but also other (smaller) particles that are naturally present in the water. The Doppler shift in the signal is used to determine the velocity. With the UVP, velocities at 128 locations along the beam axis are measured simultaneously, resulting in an instantaneous velocity profile with high spatial resolution. For the present experiments, 4 MHz and 2 MHz probes were used. For the 4 MHz probe, 128 measurements were recorded every 0.74 mm along the beam axis; for the 2 MHz probe, 128 measurements were recorded every 1.48 mm along the beam axis. The UVP measures the component of flow velocity along the beam axis. To obtain the actual velocity at a location, two downward-looking UVP probes were positioned at angles to the vertical axis, as shown in Figure 3.4. By combining instantaneous velocity measurements at the same height from the two UVPs, the time-dependent resultant velocity can be obtained over the vertical extent of UVP measurement. Combining the two UVP measurements in this way strictly requires the UVP measurement to be co-located, which only applies where the two beams intersect. In order to combine UVP at vertical locations other than at the intersection point, it is assumed that the flow is uniform between the measurement points (which is reasonable given the flat-bed condition of the bed throughout) and that the flow phase difference between the measurement points can be neglected (which is reasonable given that the maximum separation between the measuring points is 80 mm and the shortest wave length is 30 m). UVP data were obtained with a minimum time-resolution of 0.14 s. For most of the measurements, the probes were positioned 10 – 12 cm above the sand bed. In the left picture of Figure 3.4, the two 2 MHz probes and the two 4 MHz probes are visible. The UVP settings used for the present experiments, enabled velocities up to 1.8 m/s to be measured. The acoustic frequencies at which the UVP probes operate enables velocity measurements in flows with high sediment concentration. Although it is not possible to penetrate through the complete sheet-flow layer to the undisturbed bed (where velocity is zero), velocities in the upper part of the sheet-flow layer can be detected. How to determine the lowest level at which the measurements can be considered reliable is discussed later.

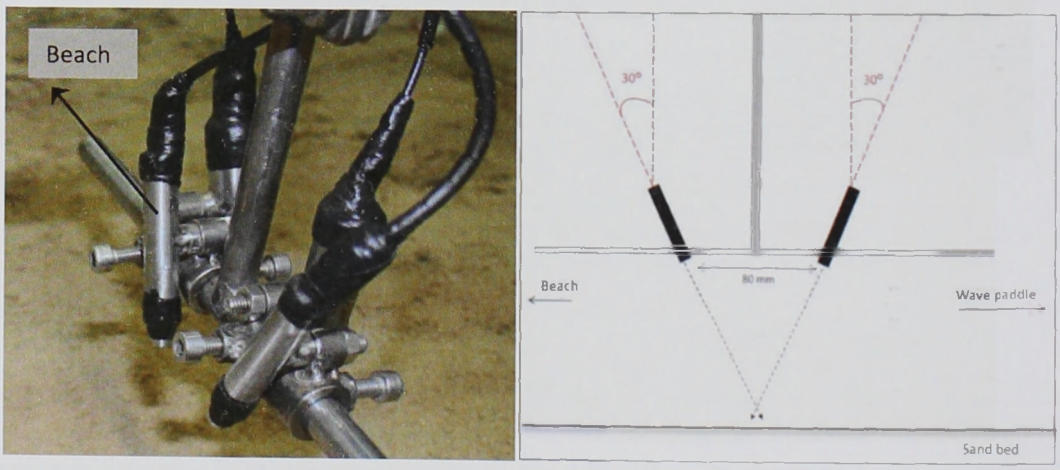


Figure 3.4. UVP probes set-up. Left: Two 4 MHz probes on the left and two 2 MHz probes on the right. Right: schematic side view of the 4 MHz probes.

Simultaneously with the UVP measurements, velocities were also measured in the free-stream and within the wave boundary layer using a small ADV (Vectrino, Nortek AS). The Vectrino measures three components of velocity at a single point with high sampling frequency of up to 200 Hz. For

these experiments, the Vectrino was positioned close to the UVPs (Figure 3.2), with its measurement point 70 mm below the UVP probes. This places the measurement point at the same level as the intersection of the beams of the two UVP probes (Figure 3.4). The UVPs and the Vectrino are connected to separate data–acquisition systems, synchronised by a common trigger. In Appendix II, a comparison is shown of free-stream and sheet-low layer velocity measurements obtained with UVP and with ADV-Vectrino; the measurements generally show very good agreement.

### 3.2.3 Experimental conditions

The majority of the tests were performed with regular "Corrected Shallow Water Trochoidal Waves (CSTW)". This wave shape is based on North Sea deep water wave measurements and was also used in the SISTEX1999 experiments (Ribberink et al., 2000; Dohmen-Janssen & Hanes, 2002). The waves generate orbital velocities with significant velocity-skewness (high onshore peak velocity, lower offshore peak velocity) and very low acceleration skewness. The test conditions considered for the present paper are presented in Table 3.1. Each condition was run for a number of hours, divided into a number of individual runs of between 0.5 and 1 hour duration. This resulted in a total of more than 60 hours of measurements. For practical reasons the UVP could not record continuously for the duration of a complete wave run; instead several UVP measurements of between 10 and 20 minutes each were performed for each run, giving a total of over 40 hours of UVP velocity measurements.

Table 3.1. Experimental conditions

| | $H$ (m) | $T$ (s) | $D_{50}$ (μm) | $U_{max}$ (m/s) | $U_{min}$ (m/s) | $<u>$ (m/s) | $R$ (-) | $\beta$ (-) | $\Psi_{max}$ (-) | time (hr) | # runs |
|---|---|---|---|---|---|---|---|---|---|---|---|
| Re1575m | 1.50 | 7.50 | 245 | 1.63 | -0.74 | -0.068 | 0.69 | 0.54 | 670 | 8.5 | 11 |
| Re1550m | 1.50 | 5.00 | 245 | 1.18 | -0.92 | 0.014 | 0.56 | 0.51 | 351 | 11 | 13 |
| Re1565m | 1.50 | 6.50 | 245 | 1.67 | -0.92 | -0.027 | 0.65 | 0.52 | 699 | 10 | 14 |
| Re1265m | 1.20 | 6.50 | 245 | 1.35 | -0.83 | 0.010 | 0.62 | 0.55 | 456 | 6 | 8 |
| Re1575f | 1.50 | 7.50 | 138 | 1.70 | -0.69 | -0.092 | 0.71 | 0.54 | 1298 | 4 | 7 |
| Re1550f | 1.50 | 5.00 | 138 | 1.28 | -1.02 | -0.028 | 0.56 | 0.53 | 731 | 5 | 10 |
| Re1565f | 1.50 | 6.50 | 138 | 1.55 | -0.83 | -0.058 | 0.65 | 0.52 | 1078 | 6 | 10 |
| Re1265f | 1.20 | 6.50 | 138 | 1.25 | -0.75 | -0.030 | 0.63 | 0.54 | 697 | 5 | 6 |
| Re1065f | 1.00 | 6.50 | 138 | 1.13 | -0.74 | -0.017 | 0.60 | 0.55 | 568 | 5 | 6 |

The wave height ($H$) and period ($T$) values in Table 3.1 are the input height and period at the wave paddle. At the point of the measurement frame (see Figure 3.1) the wave period has not changed, but due to shoaling the wave height slightly increased. Eekhout (2008) analysed the wave propagation along the 19 wave gauges in the flume. At the location of the measurement frame (wave gauge at $X$ = 111 m) , the wave height shows an increase of approximately 10 %, compared to the waves leaving the paddle at $X$ = 0 m ( 10.8 % for waves with $H$ = 1.2 m and 10.0 % for waves with $H$ = 1.5 m). The different types of waves break at a distance of $X$ = 180 to $X$ = 236 m from the wave paddle. More detail on wave propagation and deformation along the flume can be found in Eekhout (2008). $U_{max}$ and $U_{min}$ are the maximum onshore and offshore free stream orbital velocities and $<u>$ the mean flow velocity, measured outside the wave boundary layer (40 mm above the sand bed) at the location of the measurement frame (110 m from the wave paddle). Within each condition the variation in velocities measured during different runs varied between 3% and, at maximum, 10% over the total data-set obtained from all three measurement campaigns. The values of velocity skewness ($R$) in Table 3.1 were calculated from:

$$R = \frac{|U_{max}|}{|U_{max}| + |U_{min}|} \tag{3.1}$$

The values of the acceleration skewness ($\beta$) were calculated from:

$$\beta = \frac{|\dot{U}_{max}|}{|\dot{U}_{max}| + |\dot{U}_{min}|} \tag{3.2}$$

where $\dot{U}$ is the amplitude of the flow acceleration in the wave crest (max) and trough (min) direction. For all experiments, the degree of acceleration skewness was found to be much smaller than the velocity skewness. The values of the wave mobility number in Table 3.1 were calculated from:

$$\Psi_{max} = \frac{U_{max}^2}{(s-1)gD_{50}} \tag{3.3}$$

where $s = \rho_s / \rho$ is the relative sediment density, ($s$ = 2.65), $g$ the gravity acceleration and $D_{50}$ the median grain diameter of the sand. According to O'Donoghue et al. (2006), flat bed sheet-flow regime prevails when $\Psi_{max} > 300$, the ripple regime when $\Psi_{max} < 190$ and a transition regime prevails when $190 < \Psi_{max} < 300$. This corresponds well to the observations made during the present experiments, where sheet-flow sediment transport was observed for all conditions in Table 3.1.

The sand used in these experiments was well sorted quartz sand ($\rho$ = 2650 kg/m$^3$). The medium sand has the following characteristics: $D_{10}$ = 148 μm, $D_{50}$ = 245 μm and $D_{90}$ = 420 μm. During the experiments limited sorting took place both along the flume (coarsening towards the beach) as well as vertically inside the bed. The sieving analyses of various samples from the bed around the measurement frame after the experiments shows grain sizes all within ± 10% of the $D_{10}$, $D_{50}$ and $D_{90}$ to the pre-experiment values. This sand has similar $D_{50}$ as the medium sand used in the GWK experiments of Ribberink et al. (2000) and Dohmen-Janssen and Hanes (2002), the LOWT oscillatory flow tunnel experiments of Ribberink and Al-Salem (1994, 1995) and the AOFT oscillatory flow tunnel experiments of O'Donoghue and Wright (2004a, 2004b). The fine sand used in the present experiments has $D_{10}$ = 110 μm, $D_{50}$ = 138 μm and $D_{90}$ = 180 μm, with deviations from these values of less than 5% for post-experiment samples. The fine sand has similar $D_{50}$ to the fine sand used in the LOWT oscillatory flow tunnel experiments of Ribberink and Chen (1993) and the AOFT flow tunnel experiments of O'Donoghue and Wright (2004a, 2004b) and Campbell et al. (2006).

## 3.3 Results

### 3.3.1 Wave boundary layer velocities

A primary objective of the present experiments was to obtain detailed velocity measurements within the wave boundary layer and as far into the sheet-flow layer as possible.

Figures 3.5 and 3.6 show the near-bed velocity measurements for a wave with $H$ = 1.5 m and $T$ = 6.5 s (Re1565f), phase averaged over 50 waves. The positive values correspond to onshore velocities (towards the beach), the negative values correspond to offshore velocities. Figure 3.5 shows the measured time-dependent horizontal velocity at 7 vertical levels above the bed and Figure 3.6 shows the profiles of horizontal velocity at 23 phases of the wave ($\Delta\emptyset = \frac{1}{23}2\pi$), showing a profile approximately every 0.28 s for this 6.5 s wave. These results were obtained from the 4MHz probe, which gives the highest spatial and temporal resolution. The initial no-flow bed level is located at $z$ = 0 mm. The undisturbed bed level is measured before, during and after the experiments with the CCMs. The uppermost level ($z$ = 40 mm) in Figure 3.5 is located outside the wave boundary layer. From this level downward, the velocity decreases towards the bed.

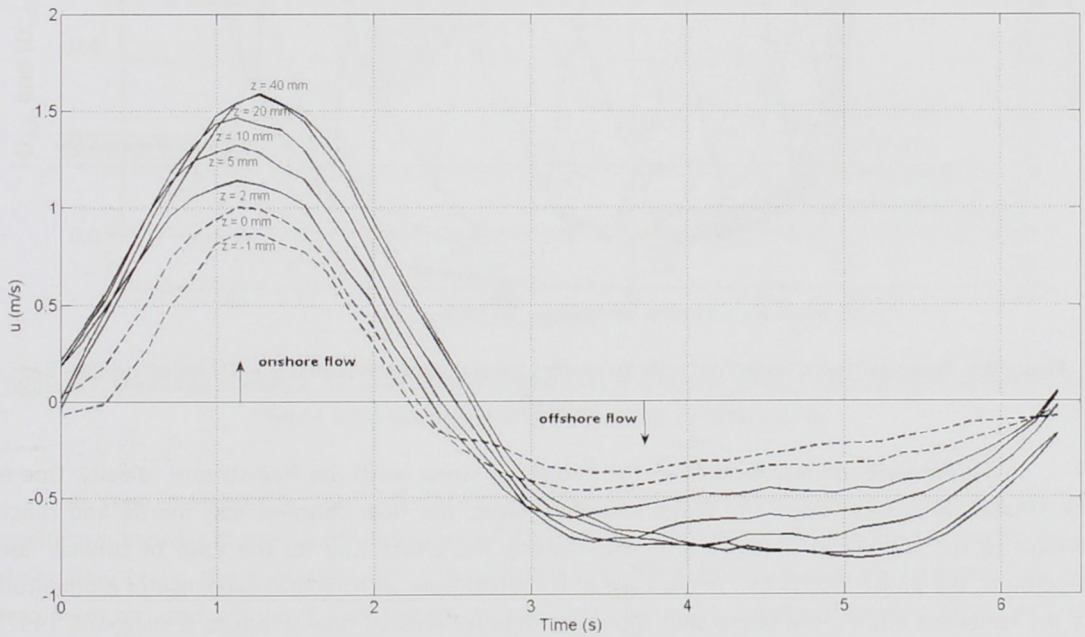


Figure 3.5. Time-series of horizontal velocity outside and inside the wave boundary layer for experiment Re1565f ($z$ = 0 corresponds to the initial, no-flow bed level).

In Figure 3.6, solid lines correspond to acceleration phases of the free-stream flow and the dashed lines correspond to deceleration phases. The UVP measurements are successful through the upper part of the sheet-flow layer, but not all the way down to the instantaneous undisturbed bed. The velocity profiles are considered reliable down to the point where the profile shows an inflection point (second derivative is zero). In Figure 3.6 this occurs at $z$ = -1 mm at the phase of maximum offshore free-stream velocity and at $z$ = -3 mm at the phase of maximum onshore free-stream velocity. Below the inflection point, the velocity profile is assumed to decrease linearly from its value

at the inflection point to zero at the level of the instantaneous erosion depth (see also O'Donoghue & Wright, 2004b), as indicated by the red lines for the maximum onshore and maximum offshore free-stream velocity phase in Figure 3.6. The instantaneous erosion depth was measured using the CCMs (see section 3.3.2). The upper level of the sheet-flow layer, defined as the level where the time-averaged sediment concentration in 8% by volume (Dohmen-Janssen, 1999) is indicated in Figure 3.6. Since the sediment concentrations inside the sheet-flow layer are much higher than above this layer, this level indicates where in the water column the vast majority of the sand transport takes place.

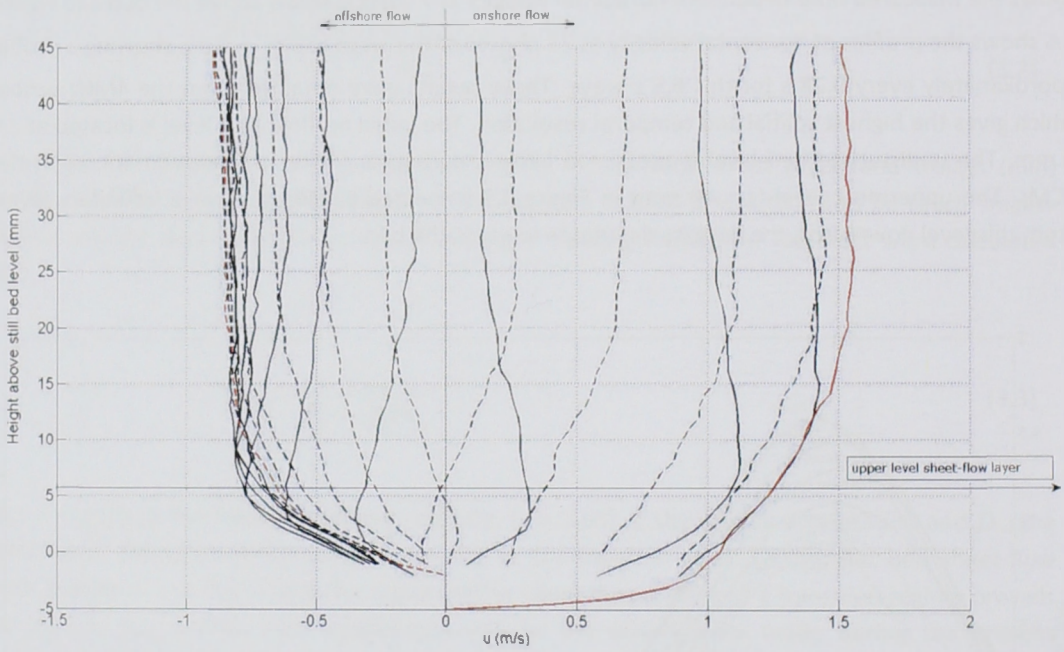


Figure 3.6. Phase-averaged horizontal velocity profiles for experiment Re1565f ($z$ = 0 is initial, no-flow bed level).

In oscillatory boundary layer flow, the bed shear stress leads the free-stream velocity. Due to the smaller velocities within the wave boundary layer, the flow contains less inertia and reacts quicker to the change in pressure gradient, causing the phase lead. In the case of laminar flow conditions, the phase lead is 45°. In the case of turbulent flow with vertical exchange of momentum by the turbulent eddies, the phase shift is smaller than for laminar flow (Fredsøe & Deigaard, 1992). The phase lead for turbulent flow conditions has been measured in experiments in oscillatory flow tunnels (McLean et al.,2001; Wright and O'Donoghue, 2002 and Campbell, 2006) and in flume experiments (Schretlen et al., 2008). In the present experiments the phase lead can be observed in Figure 3.5 through the time of the zero down-crossing and/or the time of peak onshore velocity. It is seen that as the bed is approached, the phase lead increases but then decreases once again deep into the sheet-flow layer. This effect, which is not predicted by traditional (clear water) boundary layer flow models, can be explained by an increase of inertia as the sediment concentrations increase rapidly inside the sheet-flow layer. This mobile-bed effect on the phase lead was also observed by McLean et al. (2001) and Wright and O'Donoghue (2002) in oscillatory flow tunnel experiments. In the present measurements with surface waves, the phase-lead of the zero-down-crossing is approximately 25° at the lowest measuring points in the sheet flow layer ($z \leq -1$ mm). This is

consistent with previous oscillatory flow tunnel results (20° - 26°) and is, as expected, less than the 45° phase lead of laminar flow.

The results shown in Figure 3.5 and 3.6 are from an experiment with fine sand ($D_{50}$ = 0.138 mm). The velocities from experiments with medium sand ($D_{50}$ = 0.245 mm) show similar results and behaviour. With different hydrodynamic conditions, the quantitative velocities vary but the boundary layer behaviour is similar for all wave runs and conditions. The flow velocity results of the other conditions in Table 1, are presented in Appendix III.

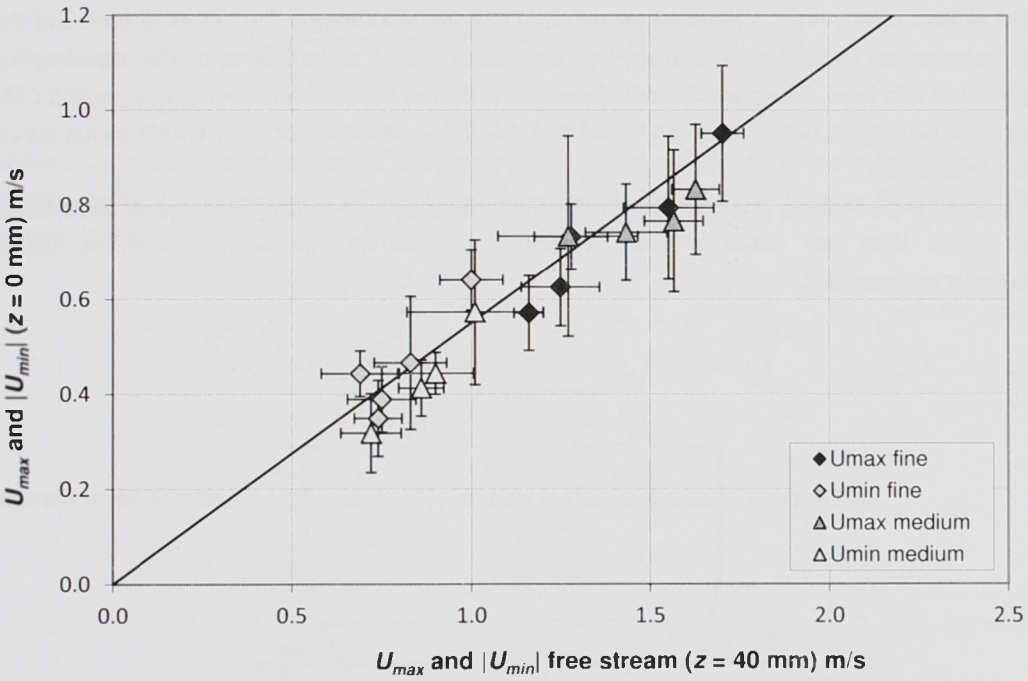


Figure 3.7. Measured maximum (on- and off-shore) velocities at $z$ = 0 mm versus maximum (on- and off-shore) free-stream velocities (at $z$ = 40 mm) for all experiments.

As seen in Figures 3.5 and 3.6, velocities at the initial, no-flow bed level ($z$ = 0 mm) are still significant. In order to get a better measure of the magnitudes of the maximum grain velocities in the sheet flow layer, the maximum on- and off-shore velocities at $z$ = 0 mm are compared to the maximum on- and off-shore free stream velocities in Figure 3.7. Each data-point represents the averaged data per condition in Table 3.1, with standard deviation error bars. For each condition several runs were analysed and for each individual run an ensemble averaged result over 50 waves was used. The velocity skewness of the waves is obvious, since the velocity values of the wave crests ($U_{max}$) are higher than the wave troughs ($U_{min}$). No systematic differences were found between the medium and fine sand results. It is shown that for the highest waves very large grain velocities up to 1 m/s are reached at the $z$ = 0 mm level. It is also shown that $U_{max}$ and $U_{min}$ at $z$ = 0 mm correlate strongly with $U_{max}$ and $U_{min}$ at the free-stream level, as expected. The best fit for this relation is $U_{max\,(z = 0\,mm)} = 0.55\ U_{max\,(free\ stream)}$ (see the solid line in Figure 3.7).

### 3.3.2 Erosion depth

During a wave cycle the level of the undisturbed bed fluctuates, caused by the periodic sediment pick-up and deposition processes. Minimum bed levels $z = z_{min}$ are reached two times per wave cycle, approximately at the moments of maximum onshore and maximum offshore velocity. Erosion depth $d_e$ is defined as the distance between the initial no-flow bed level $z = 0$ (without wave motion) and the instantaneous undisturbed bed level ($d_e = -z_{min}$) and is related to the maximum sediment load brought into motion by the waves. The CCMs are used during an individual run to track the level of the undisturbed bed during the crest or trough half wave cycle by lowering one of the CCM probes until a level is reached where the CCM signal no longer fluctuates in time and the voltage corresponds to that of an undisturbed bed. Since during certain parts of the experimental runs the mean bed level shows small gradual variations (in the order of mm's - cm's), a second CCM is required to keep track of the mean bed level and check the steadiness of the periodic signal during this measurement.

In these experiments, the high flow velocities underneath the wave crest generate a larger erosion depth than the lower offshore velocities underneath the wave trough as shown schematically in Figure 3.8.

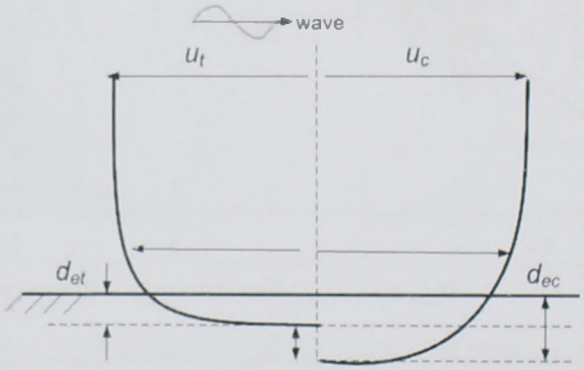


Figure 3.8. Velocity skewed wave leading to asymmetry between crest and trough erosion depth ($d_{ec} > d_{et}$).

The measured crest and trough maximum erosion depths, ($d_{ec}$ and $d_{et}$ respectively) are listed in Table 3.2, together with the corresponding Shields number.

Table 3.2. Measured erosion depths (crest and trough)

| | $D_{50}$ (μm) | $A$ (m) | $d_{ec}$ (mm) | $\theta_{crest}$ (-) | $d_{et}$ (mm) | $\theta_{trough}$ (-) |
|---|---|---|---|---|---|---|
| Re1575m | 245 | 1.95 | 5.3 | 5.67 | 2.3 | 1.55 |
| Re1550m | 245 | 0.94 | 2.6 | 1.76 | 1.4 | 1.47 |
| Re1565m | 245 | 1.72 | 5.1 | 4.46 | 2.0 | 1.60 |
| Re1265m | 245 | 1.39 | 2.3 | 1.65 | 1.4 | 0.94 |
| Re1575f | 138 | 2.03 | 6.5 | 8.75 | 3.5 | 1.70 |
| Re1550f | 138 | 1.02 | 4.3 | 5.66 | 2.4 | 2.56 |
| Re1565f | 138 | 1.61 | 5.2 | 8.46 | 2.3 | 1.82 |
| Re1265f | 138 | 1.29 | 3.8 | 3.03 | 1.5 | 1.59 |
| Re1065f | 138 | 1.16 | 2.6 | 2.79 | 1.0 | 1.20 |

Here, the maximum Shields number is calculated as follows:

$$\theta_{max} = \frac{0.5 f_w U_{max}^2}{\Delta g D_{50}} \qquad \text{for the wave crest} \qquad (3.4a)$$

$$\theta_{max} = \frac{0.5 f_w |U_{min}|^2}{\Delta g D_{50}} \qquad \text{for the wave trough} \qquad (3.4b)$$

where $U_{max}$ is the maximum on-shore velocity, $U_{min}$ the maximum off-shore velocity and $f_w$ is the friction coefficient determined by the Swart formulation (1974), based on an implicit relation of Jonsson (1966), with:

$$f_w = \exp\left[5.213\left(\frac{k_s}{A}\right)^{0.194} - 5.977\right], f_{w,max} = 0.3 \qquad (3.5)$$

where $A$ is the amplitude of the oscillatory motion in the free stream, defined by:

$$A = \frac{T U_{max}}{2\pi} \qquad (3.6)$$

Jonsson (1980) suggested an upper limit of 0.3 for $f_w$. The roughness height $k_s$ was determined using the following implicit relation for mobile beds with sheet-flow (Ribberink, 1998):

$$k_s = D_{50} \qquad \text{for} \quad \theta_{max} \leq 1 \qquad (3.7)$$

$$k_s = [1 + 6(\theta_{max} - 1)]D_{50} \qquad \text{for} \quad \theta_{max} > 1$$

with $\theta_{max} = \theta_{crest}$ for the wave crest and $\theta_{max} = \theta_{trough}$ for the wave trough.

Figure 3.9 presents the measured 'crest' and 'trough' erosion depths for all experiments, normalised with the grain diameter $D_{50}$, as a function of the maximum Shields number. The figure shows the average values from different runs per condition, including error bars based on standard deviations. The following power function provides a good fit with the new data:

$$\frac{d_e}{D_{50}} = \alpha \theta_{max}^{\beta} \qquad (3.8)$$

with $\alpha = 9.6$ and $\beta = 0.71$ for fine sand

with $\alpha = 5.8$ and $\beta = 0.81$ for medium sand

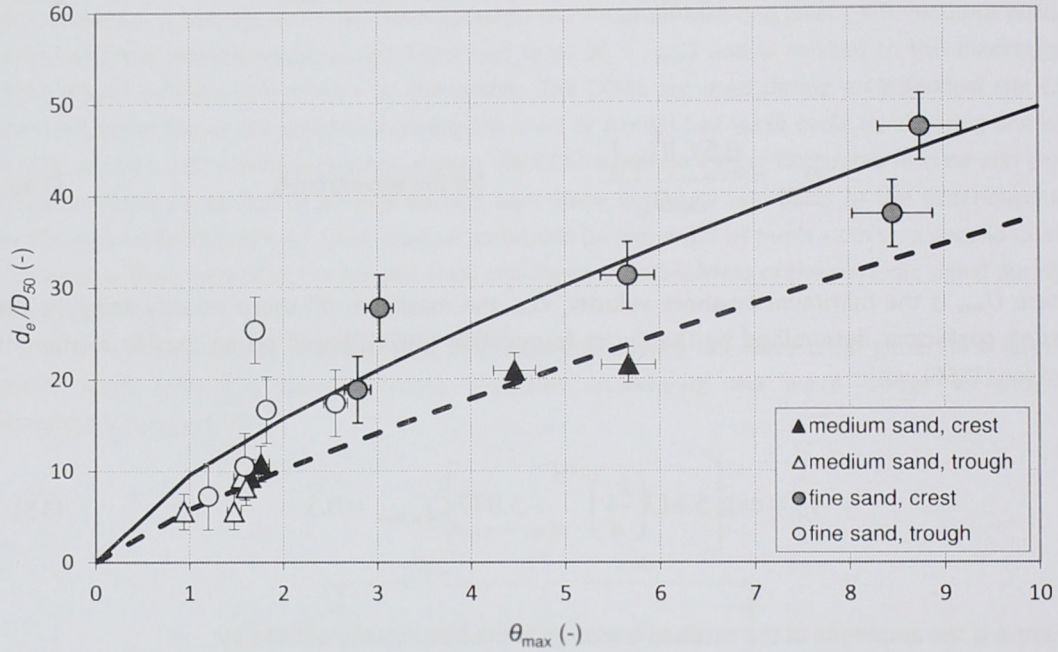


Figure 3.9. Non-dimensional erosion depths under wave crest and trough as function of the maximum Shields parameter with medium and fine sand. The measurements are presented by the circles (fine sand) and triangles (medium sand), the solid line represents the best fit power function (Eq. 3.7) for fine sand, the dashed line for medium sand.

The erosion depth (and with that the sheet flow layer) develops faster and becomes larger for fine sand cases than for medium sand. O'Donoghue and Wright (2004a) already concluded for oscillatory sheet flows that the (time-varying) erosion depth can be directly related to the (time-varying) Shields parameter. However, unsteady effects become increasingly important as the percentage of fine sand increases and their proposed relation is less accurate in the case of fine sand conditions. In Section 3.4 of this paper, more details are given of the comparison of erosion depth between oscillatory flows and surface waves.

### 3.3.3 Wave boundary layer thickness

The wave boundary layer is defined as that part of the flow which is affected by the presence of the bed. The wave boundary layer thickness ($\delta_b$) is most often defined as either the distance from the instantaneous undisturbed bed to the level of maximum velocity overshoot (e.g. Jensen et al., 1989) or the distance from the undisturbed bed to the level below the free-stream where the velocity deviates from the free-stream value by a certain percentage. In both cases the measurement is made at the phase of maximum free-stream velocity. In this paper, the first definition is used, mainly since this enables comparison of the results with existing oscillatory flow tunnel results (Campbell et al., 2006).

Figure 3.10 shows profiles of horizontal velocity corresponding to maximum onshore free-stream velocity for experiments Re1550, Re1565 and Re1575, in which fine and medium sand results are compared for the same wave condition. The velocity ($u$) is normalised against maximum onshore free stream velocity ($U_{max}$, measured at $z$ = 40 mm). The erosion depth where the velocity is zero is indicated in the figures. Because the measurements do not always show a clear velocity overshoot and due to the fluctuations in the measurements some uncertainty is present in determining the top of the wave boundary layer ($z = z_{top}$). However, for all cases it is clear that there are no large differences in the position of the top of the boundary layer between medium and fine sand results for the same flow condition. The wave boundary layer thickness is defined here as the distance between undisturbed bed level and the position of maximum velocity overshoot at the phase of maximum free-stream horizontal onshore velocity (see top graph in Figure 3.10):

$$\delta_b = z_{top} + d_e \tag{3.9}$$

Figure 3.10 shows that boundary layer velocities (normalised by free-stream maximum velocity) are lower for the medium sand compared with fine sand, for the same wave condition. This is especially obvious in the case of higher-velocity wave cases (Re1575 and Re1565), and may be explained by the fact that for the medium sand, the boundary layer flow experiences a rougher bed surface than for the finer sand. Also Campbell et al. (2006) found this for oscillatory flows when comparing velocity profiles with different bed roughness. Similar results have been obtained for the velocity profiles corresponding to maximum offshore velocity. The measured values of the (maximum) wave boundary layer thickness for the present experiments are presented in Table 3.3.

Table 3.3. Measured maximum wave boundary layer thickness.

| | $D_{50}$ (μm) | $A$ (m) | $\delta_b$ (mm) | $d_{ec}$ (mm) | $z_{top}$ (mm) |
|---|---|---|---|---|---|
| Re1575m | 245 | 1.95 | 46.3 | 5.3 | 41 |
| Re1550m | 245 | 0.94 | 20.6 | 2.6 | 18 |
| Re1565m | 245 | 1.72 | 32.1 | 5.1 | 27 |
| Re1265m | 245 | 1.39 | 21.3 | 2.3 | 19 |
| Re1575f | 138 | 2.03 | 40.5 | 6.5 | 34 |
| Re1550f | 138 | 1.02 | 24.3 | 4.3 | 20 |
| Re1565f | 138 | 1.61 | 31.2 | 5.2 | 26 |
| Re1265f | 138 | 1.29 | 23.8 | 3.8 | 20 |
| Re1065f | 138 | 1.16 | 21.6 | 2.6 | 19 |

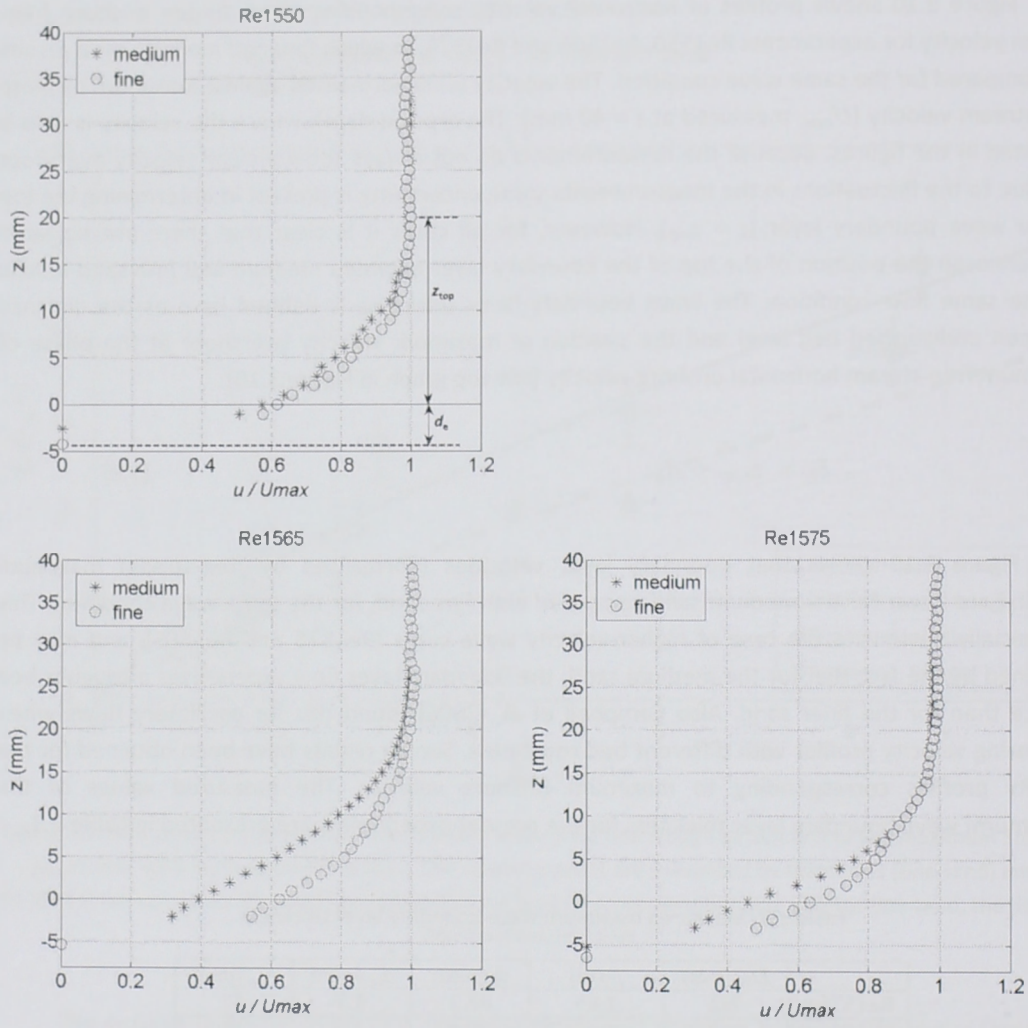


Figure 3.10. Profile of horizontal velocity at phase of maximum onshore free-stream velocity for 3 wave conditions, medium and fine sand.

To predict boundary layer thickness for different experimental conditions various empirical fits to previous datasets have been presented. Two of these are compared to the new experimental results:

$$\delta_b/k_N = 0.27\,(A/k_N)^{0.67} \qquad \text{(Sleath, 1987)} \qquad (3.10)$$

$$\delta_b/k_N = 0.09\,(A/k_N)^{0.82} \qquad \text{(Fredsøe \& Deigaard, 1992)} \qquad (3.11)$$

where $k_N$ is the Nikuradse equivalent grain roughness, taken to be equal to $2D_{50}$ by Sleath (1987) and $2.5D_{50}$ by Fredsøe & Deigaard (1992). In Figure 3.11 measured boundary layer thicknesses are compared to the two existing formulae. For this comparison the roughness height ($k_N$) is taken as

originally designed for the two formulas: $k_N = 2D_{50}$ for the Sleath model and $k_N = 2.5D_{50}$ for the Fredsøe & Deigaard model. The model of Fredsøe and Deigaard shows good overall agreement with the data, while the model of Sleath has the tendency to underpredict the wave boundary layer thickness slightly, especially for fine sand. Both models include a small grain-size influence (Sleath: $\delta_b \sim D_{50}^{0.33}$; Fredsøe and Deigaard: $\delta_b \sim D_{50}^{0.18}$). The smaller sensitivity of the Fredsøe and Deigaard model to grain size gives a better match to the present data.

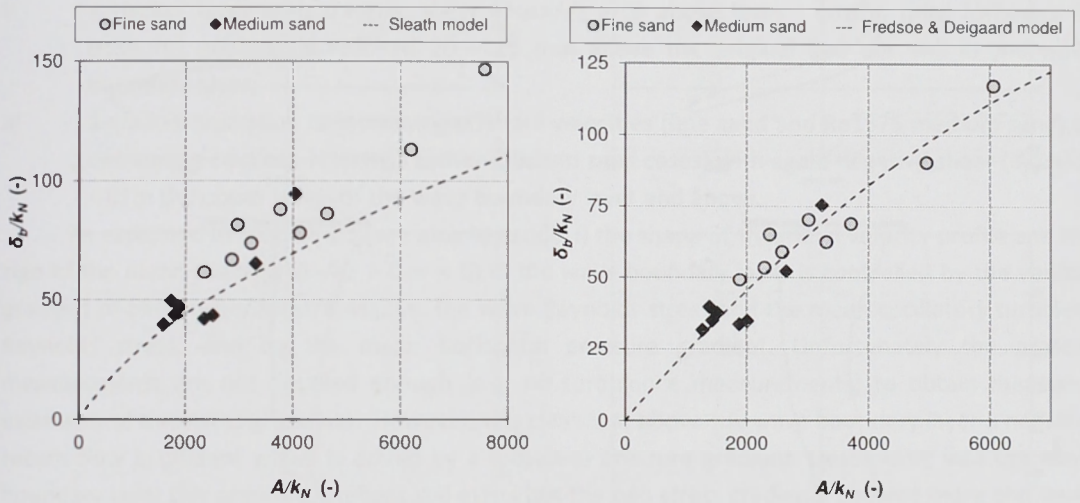


Figure 3.11. Dimensionless wave boundary layer thickness ($\delta_b/k_N$) against the dimensionless amplitude of the near-bed wave orbital motion ($A/k_N$) for both medium and fine sand conditions, compared to existing empirical relations by Sleath (1987) (left graph) and Fredsøe & Deigaard (1992) (right graph).

It is also investigated how the models perform when we use the 'mobile bed' roughness height as presented in the Equations (3.4a,b) to (3.7), instead of the grain roughness to calculate $A/k_N$ and $\delta_b/k_N$ for the experimental results. Both models then strongly overpredict the (relative) boundary layer thickness for all experiments (with a factor 1.3 to 2.4).

### 3.3.4 Wave boundary layer mean flow

In addition to the intra-wave velocities, the mean (i.e. period-averaged) velocity profile under full-scale surface wave conditions is of interest also. As discussed in the introduction, it is expected that this profile deviates from the mean velocity profile in oscillatory flow tunnels. Figure 3.12 shows the measured mean horizontal velocity profiles for all wave cases (Table 3.1), making distinction between the medium and fine sand conditions (solid and dashed lines respectively). As presented in Table 3.1, for condition Re1065 only the fine sand results are used, for the medium sand the bed was in the transition regime to a rippled bed. The mean velocity profiles presented in Figure 3.12 are the average result of 50 waves (from one representative experimental run). The profiles are cut off near the bed at the level of the wave trough erosion depth: above this level, flow is present during both half wave cycles: below it, only onshore motion is present during the positive half cycle.

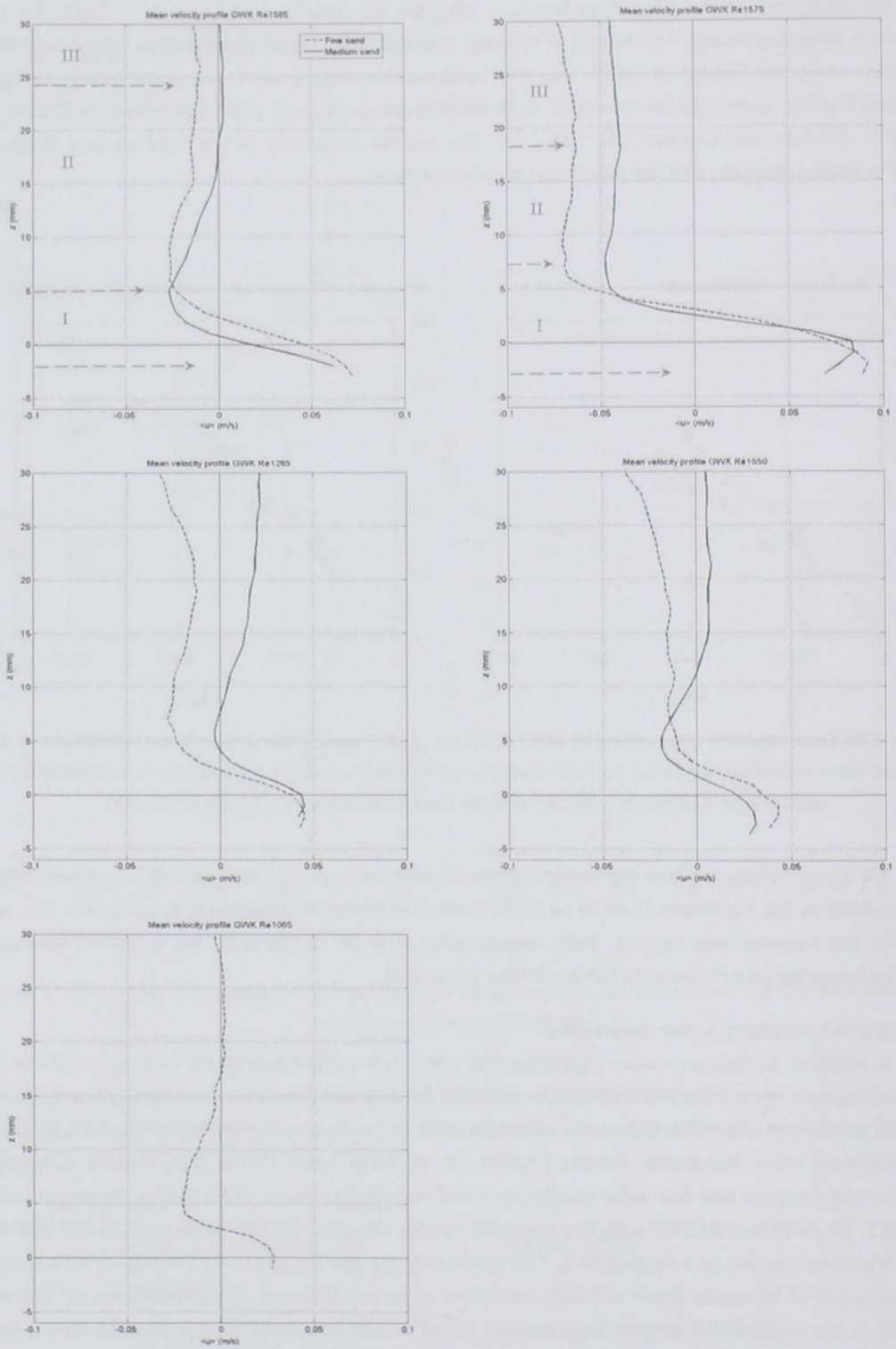


Figure 3.12. Mean flow velocity measurements inside the wave boundary layer under full scale surface waves; fine sand (dashed line) and medium sand (solid line) conditions.

It can be observed in Figure 3.12 that for all conditions (all waves and both sands) the mean velocity profile has a similar characteristic shape with three maxima/minima and three layers with positive and negative shear in between (as indicated in top two graphs) (see also Kranenburg et al., 2011):

I a thin layer with strong negative shear ($d\langle u\rangle/dz < 0$, $z$ measured upwards positive from the no-flow bed level) in the sheet flow layer starting with an onshore maximum approximately at the original bed level or just below ($0 < z < d_e$) and ending with an offshore minimum a few millimetres above the original bed;

II a thicker layer with positive shear ($d\langle u\rangle/dz > 0$) above layer I until a third (offshore or onshore) extreme is reached 20 – 25 mm above the original bed but still in the wave boundary layer;

III a gradual transition to increasing offshore velocities (fine sand and Re1575 medium sand) or decreasing onshore velocities (other medium sand cases) with again negative shear ($d\langle u\rangle/dz < 0$) in the upper levels of the wave boundary layer and above.

As explained in Section 3.1 (see also Appendix I) the shape of the mean velocity profile and the sign of the mean shear ($d\langle u\rangle/dz > 0$ or $< 0$) in the wave boundary layer is controlled by the vertical gradient of two horizontal stresses, i.e. the wave Reynolds stress and the mean oscillatory turbulent Reynolds stress, and by the mean horizontal pressure gradient. Unfortunately the present measurements are not detailed enough (e.g. no turbulence measurements) to obtain measured estimates of the stress gradients. However, it is clear that above the wave boundary layer a negative return flow is present which is driven by a (positive) pressure gradient. Descending into the wave boundary layer this pressure gradient still exists but the two stress gradients become more and more important. The wave Reynolds stress (Longuet-Higgins, 1953) has a positive contribution (positive real wave streaming) and will force the negative return flow into the positive onshore direction. At the same time the mean oscillatory turbulent Reynolds stress has a negative contribution (negative streaming due to velocity skewness) and will force the mean flow more into the negative offshore direction (Trowbridge & Madsen, 1984; Davies & Villaret, 1999). For example, for Re1565 the positive real wave streaming seems to dominate in the upper layer III (for medium sand: transition to positive onshore streaming), while in layer II the negative skewness contribution seems to become more important and force the mean flow back in the negative offshore direction. For Re1575 with a larger wave period and larger velocity skewness (see Table 3.1) the negative skewness contribution is more dominant, no onshore streaming is measured in the layers II and III, but the three-layer structure is still visible.

It is likely that in layer I with high sediment concentrations (sheet flow layer) other processes, such as grain-grain and grain-flow interactions will also affect the forcing of the mean flow. The positive onshore mean flow as present at the lower levels of this layer, probably also belongs to the onshore streaming in the layer below, as induced by the erosion depth asymmetry. At these low elevations between the levels of the trough and crest erosion depth ($-d_{ec} < z < -d_{et}$) the mean horizontal flow is fully controlled by the wave crest orbital flow and is always onshore directed. This also holds for the mean (i.e. wave-averaged) sand transport in this layer (see Section 3.3.2 and Figure 3.8 for a schematic representation).

The characteristic shape of the mean velocity profile reoccurs for all measurement campaigns (2007, 2008 I and 2008 II), for both sands and at any time during a wave run. It is found that it makes no difference whether the results are obtained early or at the end of a 1-hour wave run, indicating that the near-bed mean flow in the wave boundary layer develops quickly (time-scale of minutes).

Figure 3.13 shows the mean velocity profiles of five different runs of the same wave condition (Re1575), which gives an idea of the measuring uncertainties and how well the conditions can be reproduced. These results are from various runs from both the 2007 and the 2008 measurement campaign (phase-averaged over 50 waves). Based on this comparison, the measurement uncertainty of the z-levels is estimated to be approximately plus/ minus 1.5 mm, while the mean velocities show a variation of plus/ minus 0.02 m/s. Overall, Figure 3.13 shows that, despite these variations, the three-layer shape is consistently present for all cases.

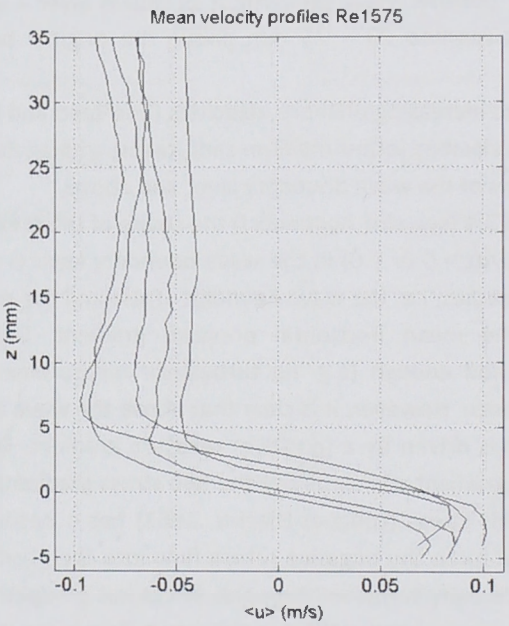


Figure 3.13. Mean flow velocity measurements inside the wave boundary layer from 5 different wave runs of the same hydrodynamic condition (Re1575) with fine sand.

Figure 3.14 shows how the mean velocity profile is affected by a variation in wave period (left graph) and wave height (right graph) for the fine sand conditions. In the left graph it can be seen that an increase in wave period, and with that an increase in velocity skewness (see Table 3.1), leads to an increase in the mean onshore component inside the sheet flow layer (layer I in Figure 3.12) and an increase in the mean off-shore component in layer II and (to a lesser extent) in layer III. In the right graph it is shown that an increase in wave height, and with that an increase in maximum flow velocities and velocity skewness (see Table 3.1), has a similar influence; an increase of the onshore flow component in layer I and to a smaller extent an increase in the offshore velocity component at higher levels. This consistent behaviour of the mean flow can be qualitatively explained by the changing balance between the onshore- and offshore-directed flow forces in the wave boundary layer, as discussed above. The negative or offshore contribution of the velocity skewness, coming with the increasing $T$ and $H$, seems to be responsible for the increase of the offshore streaming above the sheet flow layer (layers II and III). At the same time this increase in skewness and also $U_{max}$ leads to a larger erosion depth asymmetry and larger onshore streaming in the sheet flow layer (layer I).

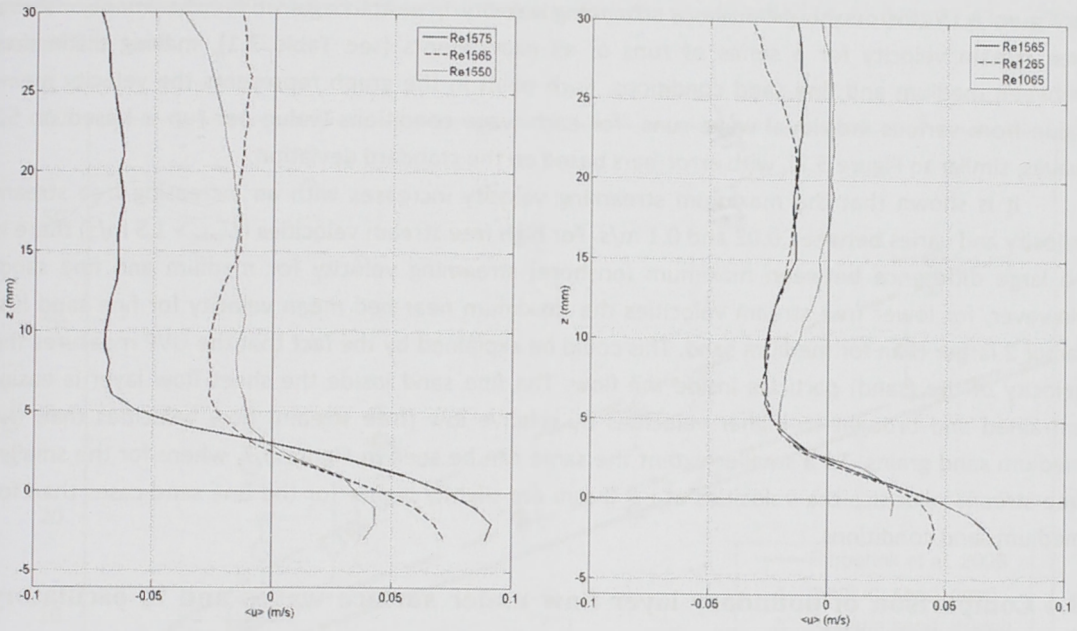


Figure 3.14. Mean flow velocity measurements inside the wave boundary layer with variation in wave period (left graph) and variation in wave height (right graph), all for fine sand conditions.

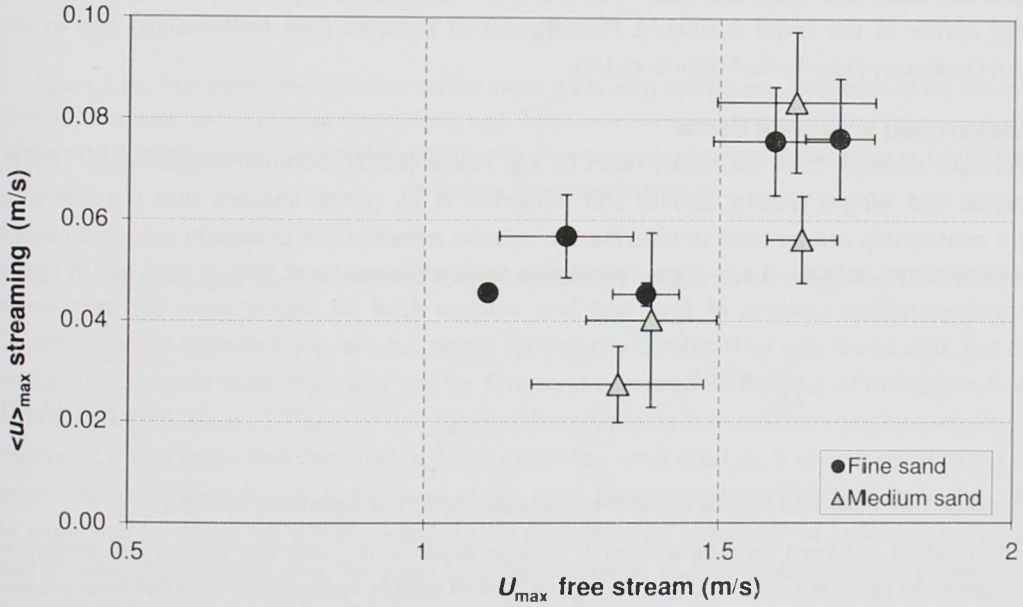


Figure 3.15. Maximum positive streaming velocity as a function of the maximum onshore velocity in the free stream.

Since most of the sediment is transported near the bed in the sheet flow layer, most of the sand grains will be transported with mean flow velocities as measured in layer I. Since the highest sediment concentrations will be present at levels $z < 0$ (see O'Donoghue and Wright, 2004a, 2004b) the onshore peak of the mean flow velocity in this layer is an interesting parameter for the sand flux.

In Figure 3.15 this maximum onshore streaming velocity is plotted against the maximum onshore free stream velocity for a series of runs of all experiments (see Table 3.1), making distinction between medium and fine sand conditions. Each point in the graph represents the velocity mean value from various individual wave runs for each wave conditions (value per run is based on 50 waves, similar to Figure 3.7), with error-bars based on the standard deviation.

It is shown that the maximum streaming velocity increases with an increasing free stream velocity and varies between 0.02 and 0.1 m/s. For high free stream velocities ($U_{max}$ > 1.5 m/s) there is no large difference between maximum (onshore) streaming velocity for medium and fine sand. However, for lower free stream velocities the maximum near-bed mean velocity for fine sand is a factor 2 larger than for medium sand. This could be explained by the fact that the UVP measures the velocity of the (sand) particles inside the flow. The fine sand inside the sheet flow layer is easier entrained and brought to higher velocities by relative low (free stream) flow velocities than the medium sand grains. To a smaller extent the same can be seen in Figure 3.7, where for the smaller free stream velocities the velocities at $z$ = 0 mm are slightly higher for the fine sand cases than for medium sand conditions.

## 3.4 Comparison of boundary layer flow under surface waves and in oscillatory flows

The similarity of bottom boundary layer sheet flow under progressive surface waves (wave channels) and in horizontal oscillatory flows (flow tunnels) is investigated by comparing erosion depth and boundary layer flow characteristics of the new (full-scale) experimental data with those measured earlier in the Large Oscillating Flow Tunnel of Deltares (The Netherlands) and in the Aberdeen Oscillatory Flow Tunnel (Scotland, UK).

### 3.4.1 Comparison of erosion depth

Previous research from oscillatory flows by e.g. Asano (1992), Dohmen-Janssen et al. (2001), O'Donoghue and Wright (2004a, 2004b) and Ribberink et al. (2008) showed that the following empirical relationship can be used to describe the relation between the maximum non-dimensional erosion depth $d_e/D_{50}$ and the wave-related maximum Shields parameter $\theta_{max}$ (see solid line in Figure 3.16):

$$\frac{d_e}{D_{50}} = 3.7\theta_{max} \qquad (3.12)$$

In this formula the maximum Shields number is calculated with the Equations 3.4 - 3.7.

The relation between (non-dimensional) erosion depth and maximum Shields for oscillatory flows, as given by Equation 3.12, is shown in Figure 3.16 to enable comparison with the new erosion depth results for progressive waves. Erosion depths under progressive waves show the same trend as the empirical relation for oscillatory flows of Ribberink et al. (2008), i.e. increasing erosion depth with increasing maximum Shields number. However, measured erosion depths under progressive waves have larger magnitudes than erosion depths observed in tunnel oscillatory flows. The largest increase is found for the fine sand experiments. It should be realised that Equation (3.12) was developed for only maximum (i.e. crest) erosion depths in velocity-skewed oscillatory flows. The new results from progressive waves presented in Figure 3.9 and 3.17 include maximum erosion depths for both the wave crests and wave troughs and it appears that Equation (3.12) is comparable to the medium sand

relation given for Equation 3.8, but clearly underestimates the present data for both half cycles in the case of fine sand.

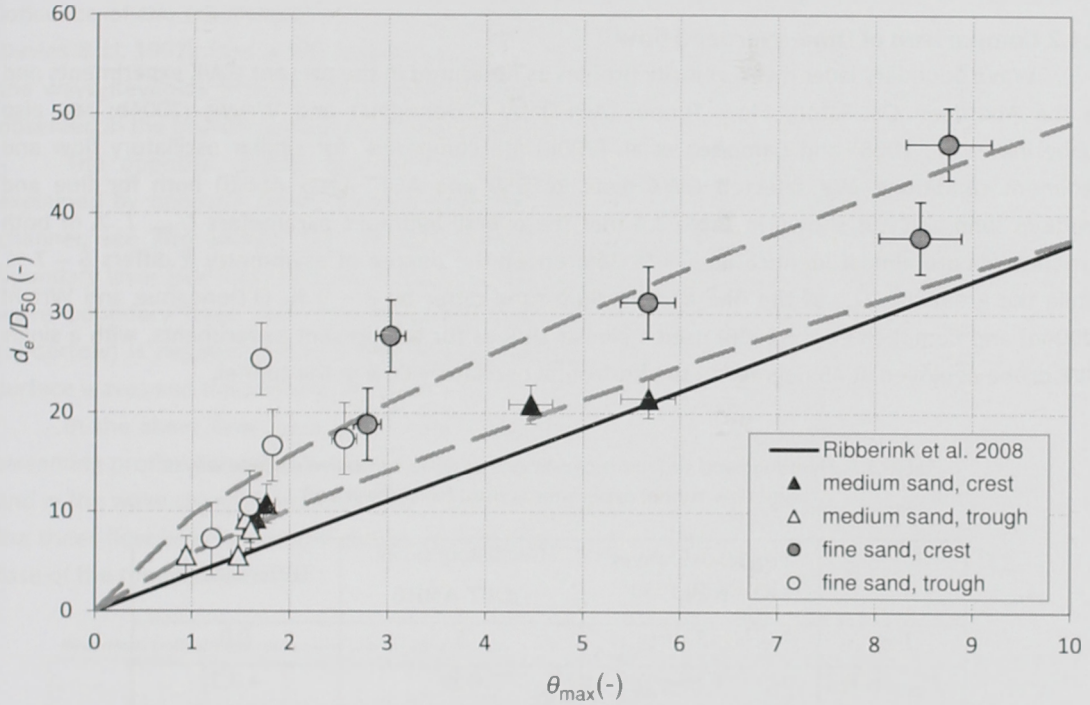


Figure 3.16. Non-dimensional erosion depths under wave crest and trough as function of the maximum Shields parameter for the present experiments with medium and fine sand (symbols) and relations as shown in Equation 3.8 (dashed lines). The solid line represents the empirical relation of Ribberink et al. (2008) based on oscillatory flow experiments.

In the new surface wave experiments a difference was found in erosion depth between the wave crest and wave trough for both medium and fine sand. In previous oscillatory flow tunnel experiments the asymmetry in erosion depth for velocity-skewed flow was found also, but only for medium and coarse sand cases and not for fine sand experiments (see e.g. O'Donoghue & Wright, 2004a; Ribberink et al., 2008). For fine sand and comparable free-stream velocity magnitudes and skewness, it was found that the erosion depth under the wave crest $d_{ec}$ is almost equal to the erosion depth under the wave trough $d_{et}$ for cases of fine sand. Ribberink et al. (2008) indicated that this may be explained by phase-lag effects, leading to a more gradual behaviour of sediment concentration and erosion/ deposition during the wave cycle for fine sand. As stated above, in the present surface-wave experiments $d_{e,crest}$ is always > $d_{e,trough}$, even for fine sand.

The reasons for the different erosion depth behaviour in oscillating flow tunnels and under progressive surface waves is likely to be the result of a combination of processes occuring: i) the additional onshore-directed wave Reynolds stress may lead to an additional onshore-offshore bed shear stress asymmetry under surface waves, ii) the vertical orbital flow under surface waves has an influence on the settling of (especially fine) sand and iii) horizontal advective sand fluxes, as present under progressive surface waves but not in oscillating flow tunnels, may play a role here (see Kranenburg et al., 2010). Which of these processes would be dominant has not been clarified in this

study. For further quantitative explanations it is recommended to analyse the experimental results with a process-based boundary layer flow and sediment model (e.g. Kranenburg et al., 2010; Hsu et al., 2004).

### 3.4.2 Comparison of time-averaged flow

Wave boundary layer mean velocity profiles as measured in the present GWK experiments and in the Aberdeen Oscillatory Flow Tunnel (AOFT) by O'Donoghue and Wright (2004b; see also Ribberink et al., 2008) and Campbell et al. (2006) are compared for similar oscillatory flow and sediment conditions. We selected GWK tests Re1550 and AOFT tests A5010 both for fine and medium sand and it is shown in Table 3.4 that the overall hydraulic parameters $U_{rms}$, $T$, $A$ of both experiments are almost identical (0 – 4 % difference), the degree of asymmetry $R$ differs 6 – 7 %, while the grain size $D_{50}$ of the fine and medium sand differ by 8 – 9 %. O'Donoghue and Wright (2004b) and Campbell et al. (2006) used a similar UVP as for the present experiments, with a single UVP probe deployed at 45 degrees to the horizontal oscillatory flow in the tunnel.

Table 3.4. Hydraulic and sediment conditions under progressive surface waves and flow tunnel experiments used for comparison

| | Progressive waves GWK Re1550 | Oscillatory flows AOFT A5010 | Difference (%) |
|---|---|---|---|
| $T$ (s) | 5 | 5 | 0.0 |
| $U_{rms}$ (m/s) | 0.86 | 0.89 | + 3.3 |
| $R$ (-) | 0.56 | 0.60 | + 6.7 |
| $A$ (m) | 1.02 | 1.00 | - 2.0 |
| $D_{50}$ (μm) | 138 | 150 | + 8.0 |
| | 245 | 270 | + 9.3 |

The time-dependent boundary layer velocity profiles and the wave boundary layer thickness in the new GWK experiments show a strong similarity with the oscillating flow tunnel results (not shown here). However, as was expected, differences are found in the mean velocity (streaming) profiles. Figure 3.17 shows a comparison of the measured mean velocity profiles in which the flow velocities are normalised with $U_{max}$ (maximum onshore free stream flow velocity). The left graph shows the mean velocity profiles for medium sand experiments in both facilities. Here, it is clear that for both cases an onshore-directed streaming is present in the lowest levels of the sheet flow layer (layer I: for $z < \approx 5$ mm). The shape of the profile, as well as the magnitude of the mean velocity is almost similar. Above the sheet flow layer both experiments show offshore streaming, but the negative mean velocity for the tunnel flow exceeds that of the surface wave condition. At higher elevations the velocity profiles differ with opposite mean velocity gradients $d\langle U\rangle/dz$. For the tunnel case $d\langle U\rangle/dz > 0$ and the negative streaming gradually decreases with increasing distance from the bed; for the progressive wave a layer III is present with $d\langle U\rangle/dz < 0$; the two profiles intersect near the edge of the wave boundary layer (approximately $z$ = 25 mm for this condition). The fine sand experiments show similar shape differences in the mean velocity profiles above the sheet flow layer (right graph of Figure 3.17). Again the negative streaming in the tunnel case strongly exceeds the streaming in the progressive wave case and the velocity gradients also show similar differences.

However, the transition to positive onshore streaming when descending into the sheet flow layer does not occur in the oscillating flow tunnel, instead negative streaming persists here.

The large negative streaming in the tunnel above the sheet flow layer can be explained by the influence of the (oscillatory) net turbulent Reynolds stress, induced by the velocity skewness (see Davies & Li, 1997). Due to the absence of vertical orbital motion, the onshore streaming induced by the wave Reynolds stress is not present in tunnels. This also explains the more positive streaming observed in the present surface wave experiments.

The opposite velocity gradients in the upper parts of the wave boundary layer can be explained by opposite mean pressure gradients $\partial\langle p\rangle/\partial x$ ($< 0$ in the tunnel and $> 0$ in the wave channel; see also Section 3.1). In the tunnel a positive return flow is present above the wave boundary layer (see Ribberink and Al-Salem, 1995), which compensates the negative streaming in the wave boundary layer and this requires $\partial\langle p\rangle/\partial x < 0$. In the wave channel the return current (undertow) is negative because it compensates the mean Lagrangian mass flux generated by the surface waves and this requires $\partial\langle p\rangle/\partial x > 0$.

In the sheet flow layer ($z < 5$ mm) mobile bed and high concentration processes affect the streaming profile. For medium sand these processes seem to work out in a similar way in the tunnel and in the wave channel. However, for fine sand large differences are present, especially deep within the sheet-flow layer where the streaming is positive in the case of surface waves and negative in the case of the tunnel flow.

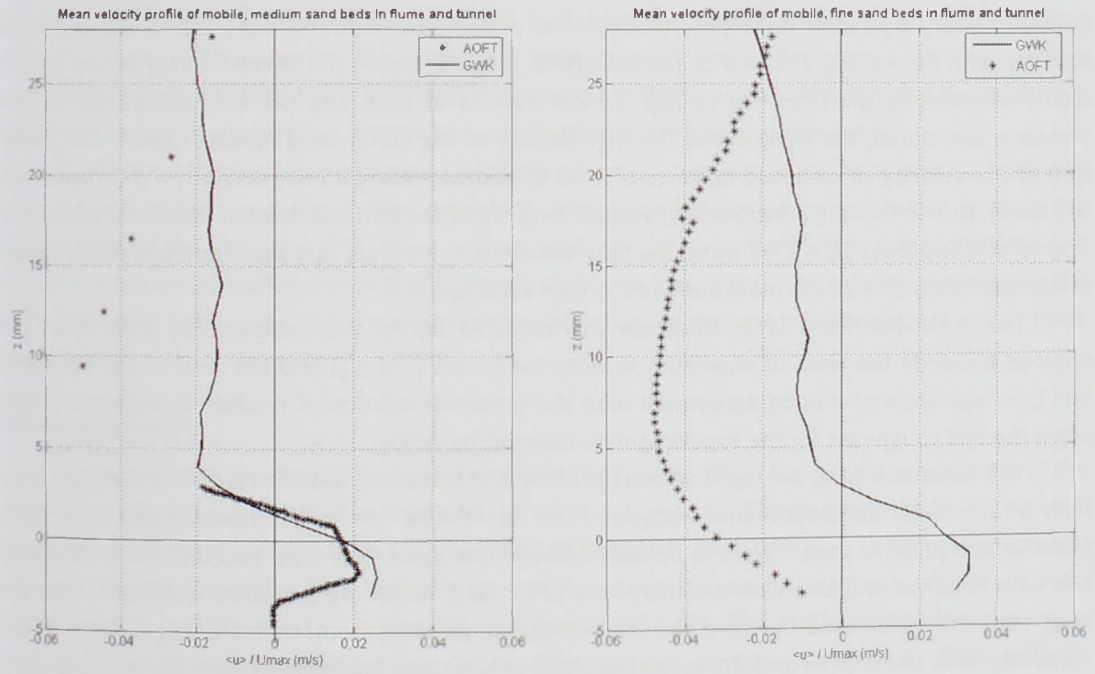


Figure 3.17. Mean flow velocity measurements inside the wave boundary layer under full-scale surface waves (GWK) and oscillatory flow (AOFT) for medium (left) and fine (right) sand conditions. (The oscillatory flow tunnel results for the medium sand are from Ribberink et al., 2008 and for the fine sand are from Campbell et al., 2006).

The different streaming behaviour for fine sand in the sheet flow layer in tunnels and under surface waves still needs further explanation. From the present experiments we can conclude that the different streaming coincides in a consistent way with a different erosion depth behaviour for fine sand (no crest/trough asymmetry and smaller magnitudes in tunnels). Moreover, the direction of the mean sand transport is different for both experiments ('onshore' under surface waves, 'offshore' in tunnels, see Schretlen et al., 2009, 2010).

A more extensive description and discussion of sediment concentration, sediment flux and sediment transport behaviour during the present GWK experiments will be presented in the following papers.

## 3.5 Conclusions

New experiments were carried out in the large-scale GWK wave channel under full scale non-breaking progressive surface waves above a horizontal mobile sand bed in the sheet flow regime. Using a 2-probe UVP system for velocity measurement combined with a CCM-probe system to determine instantaneous bed level, detailed velocity measurements were obtained inside the wave boundary layer (WBL). The measurements were carried out for a range of wave heights and wave periods, with a level of detail not previously achieved at this large scale.

The time-dependent horizontal oscillatory flows in the upper part of the WBL (above the sheet flow layer) show qualitatively the same behaviour as known from measurements in flow tunnels and from oscillatory boundary layer flow models. The phase-lead of the velocity shows the expected increase with decreasing distance to the bed. Near the bed, inside the sheet-flow layer, the flow is clearly affected by the presence of high concentrations of sand and the fluctuating level of the immobile bed during the wave cycle. The high density of the water-sand mixture causes the phase-lead of the velocity to decrease again to a value of approximately 25 degrees at $z$ = 0 (original still bed level). Due to the large (intra-wave) vertical mobility of the bed and erosion depths far below the original still bed level ($d_e$ = 1 – 7 mm), the flow velocities at $z$ = 0 are still significant and reach values of approximately 55% of the maximum free stream velocity.

The wave boundary layer thickness as measured during the experiments, defined as the distance between the level of maximum velocity overshoot ($z = z_{top}$) and the level of the immobile bed ($z = -d_e$), showed a good agreement with the empirical relation of Fredsøe & Deigaard (1992) when the bed roughness for the experiments is taken to be $2.5D_{50}$.

The measured time-averaged velocity profiles in the WBL show a characteristic vertical three-layer structure for all experiments, with 'onshore' as well as 'offshore' streaming and alternating negative and positive shear layers in between. Above the sheet flow layer two layers are observed, one with negative and one with positive shear ($d\langle u\rangle/dz$), which are explained qualitatively by the height-dependent balance between the mean pressure gradient (> 0), the vertical gradients of the wave Reynolds stress (> 0) and the mean (oscillatory) turbulent Reynolds stress (< 0). In lower parts of the sheet flow layer (pick-up layer $z$ < 0), the periodic vertical motion of the bed controls the streaming. Due to the velocity skewness of the wave-generated oscillatory flow the erosion depth during onshore motion always exceeds the erosion depth during the offshore motion. This directly leads to an onshore mean flow in the lowest levels of the sheet flow layer and in the upper sheet flow layer.

The characteristic three-layer structure of the WBL-streaming is observed during all experiments for medium as well as fine sand. Meanwhile, the structure shows systematic differences with the streaming profile shapes as measured in oscillating flow tunnels for similar velocity skewed oscillatory flows and similar sands. Above the sheet flow layer the streaming inside the wave boundary layer is generally more offshore directed in tunnels than under progressive surface waves, due to the absence of the wave Reynolds stress in tunnels. Above the wave boundary layer the opposite sign of the mean pressure gradient in tunnels (negative in tunnels, positive under progressive surface waves) leads to the opposite: an onshore mean current in oscillatory flow tunnels and an offshore mean current under surface waves (return flows).

For progressive surface waves generating velocity-skewed oscillatory flows, erosion-depth asymmetry appears to be a dominant mechanism responsible for 'onshore' streaming in the lowest part of the sheet flow layer ($z < 0$, pick-up layer), for medium as well as fine sand. In tunnels a very similar streaming profile is observed for medium sand, however for fine sand this onshore streaming is not observed and instead a negative streaming develops. The latter matches with the absence of erosion depth asymmetry with the presence of a negative mean sand transport in tunnels (instead of a positive mean transport under progressive surface waves).

The measured erosion depths increase with increasing maximum Shields number $\theta$ following a relation of the form $d_e/D_{50} = \alpha\theta^{\beta}$. For medium sand the erosion depths agree reasonable well with those measured in flow tunnels; they are only slightly larger and show a similar asymmetry. However, for fine sand conditions the erosion depths are systematically larger than in tunnels and the erosion depth asymmetry, which is absent in fine sand tunnel experiments, is present under these full-scale surface waves. The additional positive wave Reynolds stress under progressive surface waves may be responsible for an additional erosion depth asymmetry. But also the additional horizontal and vertical advection effects under surface waves may play a role here.

Further interpretation of the new surface wave measurements using detailed process-based wave boundary layer and sheet flow models is recommended for obtaining better quantitative explanations of the observed WBL flows. Future work on the data, concerning concentrations and net sand transport measurements will give more insight into how these flow velocity processes in the wave boundary layer under full scale surface waves influence the net sand transport under these conditions.

**Acknowledgements**

The experiments in the GWK are performed in the framework of the Access programme of the Integrated Infrastructure Initiative Hydralab-III of the European Community's Sixth Framework Programme (contract no. 022441) and the SANTOSS project. SANTOSS is a collaboration project between Twente University, The Netherlands and Aberdeen University, Scotland, with input from both Liverpool and Bangor University, UK and from DELTARES, The Netherlands. The project is funded by the Dutch Technology Foundation STW, applied science division of NWO and the technology program of the Ministry of Economic Affairs (TCB6586) and the UK's Engineering and Physical Sciences Research Council (EPSRC) (GR/T28089/01). Part of the instrumentation development and the data processing was carried out with funding from the project SANDS, a project of the European Union within the I3 project HYDRALAB III. The authors appreciate the contributions of the technical staff of the University of Utrecht, University of Twente and of the GWK (especially Henk Markies, Marcel van Maarsseveen, René Buijsrogge and Joachim Gruene). The people involved in completing the experiments, are thanked as well, in particular Maarten Kleinhans, Jebbe van der

Werf, Michel Zuijderwijk, Dominic van der A, Lorna Campbell, Luca Cavallaro, Joris Eekhout, Freek Huthoff, Tommer Vermaas and Christien Huisman. Suzanne Hulscher is thanked for the valuable comments to this paper.

## References

Asano, T. 1992. Observations of granular-fluid mixture under an oscillatory flow. *Proceedings of 23rd International Conference on Coastal Engineering*, ASCE, 1896-1909.

Campbell, L., T. O'Donoghue and J.S. Ribberink. 2006. Wave boundary layer velocities in oscillatory sheet flow. *Proceedings of 30th International Conference on Coastal Engineering*, ASCE, 2207-2219.

Craik, A.D.D., 1982. The drift velocity of water waves. *Journal of Fluid Mechanics*, 116, 187 – 205.

Davies, A.G. and Li, Z. 1997. Modelling sediment transport beneath regular symmetrical and asymmetrical waves above a plane bed. *Continental Shelf Research,* 17(5), 555-582.

Davies, A.G. and C. Villaret. 1999. Eulerian drift induced by progressive waves above rippled and very rough beds. *Journal of Geophysical Research*, 104(C1): 1465-1488.

Dibajnia, M. and A. Watanabe. 1998. Transport rate under irregular sheet flow conditions. *Coastal Engineering*, 35, 167-183.

Dohmen-Janssen, C.M. 1999. Grain size influence on sediment transport in oscillatory sheet flow – phase lags and mobile-bed effect. *PhD-thesis,* Delft University of technology Delft, The Netherlands. 246 pp.

Dohmen-Janssen, C.M., W.N. Hassan and J.S. Ribberink. 2001. Mobile-bed effects in oscillatory sheet flow. *Journal of Geophysical Research*, 106 (C11), 27103 – 27115.

Dohmen-Janssen, C.M., D.F. Kroekenstoel, W.N. Hassan and J.S. Ribberink, 2002. Phase lags in oscillatory sheet flow: experiments and bed load modelling. *Coastal Engineering*, 46, 61 – 87.

Dohmen-Janssen, C.M. and D.M. Hanes. 2002. Sheet flow dynamics under monochromatic nonbreaking waves. *Journal of Geophysical Research,* 107(C10), 3149.

Eekhout, J.P.C. 2008. Measurements and modelling of cross-shore morphodynamics. MSc Thesis, University of Twente, The Netherlands.

Fredsøe J. and R. Deigaard. 1992. Mechanics of coastal sediment transport. *Advanced Series on Coastal Engineering, 3*. World Scientific Publishing Co. Pte. Ltd., Singapore, 369 pp.

Gonzalez-Rodriguez, D. and O.S. Madsen. 2010. Prediction of net bedload transport rates obtained in oscillating water tunnels and applicability to real surf zone waves, *Proceedings of 32nd International Conference on Coastal Engineering,* ASCE, Shanghai, China.

Gonzalez-Rodriguez, D. and O.S. Madsen. 2011. Boundary-layer hydrodynamics and bedload sediment transport in oscillating water tunnels. *J. Fluid Mech.,* Vol. 667, pp 48 - 84

Hsu, T.J., J.T. Jenkins and Ph.L.-F. Liu. 2004. On two-phase sediment transport: sheet flow of massive particles. *Proc. R. Soc. Lond.* 460, 2223 – 2250.

Jensen, B.L., B.M. Sumer and J. Fredsøe. 1989. Turbulent oscillatory boundary layers at high Reynolds numbers. *Journal of Fluid Mechanics.*, 116, 265 – 297.

Jonsson, I.G. 1966. Wave boundary layer and friction factors. *Proceedings of 10th International Conference on Coastal Engineering,* 127 - 148.

Jonsson, I.G. 1980. A new approach to oscillatory rough turbulent boundary layers. *Ocean Engineering* 7, 109-152.

Kranenburg, W.M. , J.S. Ribberink and R.E. Uittenbogaard. 2010. Sand transport by surface waves: can streaming explain the onshore transport?, *Proceedings of 32nd International Conference on Coastal Engineering,* Shanghai, China.

Kranenburg, W.M., J.S. Ribberink and R.E. Uittenbogaard, 2011. Net currents in the wave boundary layer: balance of wave shape and free surface effects. *Proceedings of Coastal Sediments 2011*, Miami, USA, pp 1499 – 1513.

Longuet-Higgins, M.S. 1953. Mass transport in water waves. *Philosophical Transactions of the Royal Society of London. Series A, Mathematical and Physical Sciences*, 245(903): 535-581.

Nielsen, P. 1992. Coastal bottom boundary layers and sediment transport. *Advanced Series on Coastal Engineering, 4*. World Scientific Publishing Co. Pte. Ltd., Singapore, 324 pp.

McLean, S.R., J.S. Ribberink, C.M. Dohmen-Janssen and W.N. Hassan. 2001. Sand transport in oscillatory sheet flow with mean current. *Journal of Waterway, Port, Coastal and Ocean Engineering,* 127(3): 141-151.

MET-FLOW 2002. UVP Monitor Model UVP-DUO with Software version 3, User's Guide. Release 5, Lausanne, Switzerland.

O'Donoghue, T. and S. Wright. 2004a. Concentrations in oscillatory sheet flow for well sorted and graded sands. *Coastal Engineering*, 50, 117-138.

O'Donoghue, T. and S. Wright. 2004b. Flow tunnel measurements of velocities and sand flux in oscillatory sheet flow for well sorted and graded sands. *Coastal Engineering*, 51, 1163-1184.

O'Donoghue, T., J.S. Doucette, J.J. van der Werf and J.S. Ribberink. 2006. The dimensions of sand ripples in full-scale oscillatory flows. *Coastal Engineering*, 53, 997-1012.

Ribberink, J.S. and Z.W. Chen. 1993. Sediment transport of fine sand under asymmetric oscillatory flow. *Delft Hydraulics*, Report H840, Part VII, January. Delft, The Netherlands.

Ribberink, J.S. and A.A. Al-Salem. 1994. Sediment transport in oscillatory boundary layers in cases of rippled beds and sheet flow. *Journal of geophysical Research,* 99(C6), 12707-12727.

Ribberink, J.S. and A.A. Al-Salem. 1995. Sheet flow and suspension of sand in oscillatory boundary layers. *Coastal Engineering*, 25, 205 – 225.

Ribberink, J.S. 1998. Bed-load transport for steady flows and unsteady oscillatory flows. *Coastal Engineering*, 34, 59-82.

Ribberink, J.S., C.M. Dohmen-Janssen, D.M. Hanes, S.R. McLean and C. Vincent. 2000. Near-bed sand transport mechanics under waves – A large-scale flume experiment (Sistex99). *Proceedings of 27th International Conference on Coastal Engineering*, ASCE, 3263-3276.

Ribberink, J.S., J.J. van der Werf and T. O'Donoghue. 2008. Sand motion induced by oscillatory flows; sheet flow and vortex ripples. Journal of Turbulence, special issue on 'Particle-laden flow, from geophysical to Kolmogorov scales'. Euromech colloquim 477. Enschede, The Netherlands.

Schretlen, J.L.M., J.J. van der Werf, J.S. Ribberink, M. Kleinhans, W.M. Zuijderwijk and T. O'Donoghue. 2008. New high-resolution measurements of wave boundary layer flow under full-scale surface waves. *Proceedings of 31st International Conference on Coastal Engineering*, Hamburg, Germany.

Schretlen, J.L.M., J.S. Ribberink and T. O'Donoghue. 2009. Sand transport under full scale surface waves. *Proceedings of the Coastal Dynamics 2009 Impacts of human activities on dynamic coastal processes.* Tokyo, Japan.

Schretlen, J.L.M., J.S. Ribberink and T. O'Donoghue. 2010. Boundary layer flow and sand transport under full scale surface waves. *Proceedings of 32st International Conference on Coastal Engineering,* Shanghai, China

Sleath, J.F.A. 1987. Turbulent oscillatory flow over rough beds. *Journal of Fluid Mechanics.*, 182, 369 – 409.

Swart, D.H. 1974. Offshore sediment transport and equilibrium beach profiles. Delft Hydraulics Lab Publ No. 131.

Trowbridge, J. and O.S. Madsen. 1984a. Turbulent wave boundary layers 1. Model formulation and first-order solution. Journal of Geophysical Research, 89(C5): 7989-7997.

Trowbridge, J. and O.S. Madsen. 1984b. Turbulent wave boundary layers 2. Second-order theory and mass transport. Journal of Geophysical Research, 89(C5): 7999-8007.

Van der Werf, J.J. 2006. Sand transport over rippled beds in oscillatory flow. Ph.D. thesis, University of Twente, The Netherlands.

Van Rijn, L.C. 2007. Unified view of sediment transport by currents and waves I: Initiation of motion, bed roughness and bed-load transport. *Journal of Hydraulic Engineering*, 133(6), 649 – 667.

Wright, S. and T. O'Donoghue. 2002. Total sediment transport rate predictions in wave current sheet flow with graded sand. Oscillatory flow tunnel experiments at Aberdeen University. Experimental report EPSRC "LUBA" Project. University of Aberdeen, Aberdeen, UK.

## Appendix I Boundary layer streaming

Assuming a fixed bed and thus neglecting the influence of sand bed mobility on the flow and assuming uniform surface waves over a horizontal bottom, the Reynolds-averaged Navier-Stokes equations averaged over the wave cycle provide a description of the wave-induced mean flow. For the direction of the wave propagation *x*, the mean velocity distribution can be expressed as follows:

$$\frac{\partial}{\partial z}\left[\nu_t \frac{\partial \langle u \rangle}{\partial z}\right] = -\frac{\partial}{\partial z}\left[\langle \tilde{\nu}_t \frac{\partial \tilde{u}}{\partial z} \rangle\right] + \frac{\partial \langle \tilde{u}\tilde{w} \rangle}{\partial z} + \frac{1}{\rho}\frac{\partial \langle p \rangle}{\partial x} \qquad \text{(I)}$$

where the wave-averaged components are indicated with <..> and the time-dependent (intra wave) components with $\tilde{..}$, $z$ represents the level above the bed, $\nu_t$ the turbulent eddy viscosity, $u$ is the horizontal flow velocity, $w$ the vertical (orbital) flow velocity, $\rho$ is the density of the water and $p$ represents the pressure. The first term on the right-hand side of this equation represents the mean oscillatory turbulent Reynolds stress (Trowbridge & Madsen, 1984; Davies & Villaret, 1999), the second term represents the wave Reynolds stress and the third term the mean pressure gradient. The wave Reynolds stress is expected to be absent in horizontal oscillatory flows as occurring in tunnels. When the remaining terms are then vertically integrated with the boundary condition $\langle \frac{\partial \langle u \rangle}{\partial z} \rangle_{z=h} = 0$, with $h$ equals the level at half the tunnel height, the following equation results for oscillatory flow tunnel conditions:

$$\rho \langle \nu_t \rangle \frac{\partial \langle u \rangle}{\partial z} = -\rho \langle \tilde{\nu}_t \frac{\partial \tilde{u}}{\partial z} \rangle + \frac{\partial \langle p \rangle}{\partial x}[z-h] \qquad \text{(II)}$$

Here the first term on the right-hand side is equal to zero for sinusoidal oscillatory flows. For velocity skewed oscillatory flows the first term on the right-hand side of Equation II becomes negative. The resulting negative mean stress due to asymmetry of turbulence for the two half-wave cycles generates a negative current in the boundary layer. However, since tunnels do not allow a mean water flux, a negative mean pressure gradient is present to drive a small positive mean return flow. The resulting mean flow is negative near the bed in the boundary layer with a transition to a positive flow above the wave boundary layer. This coincides well with boundary layer flow measurements done in oscillatory flow tunnels by Ribberink & Al Salem (1995) and O'Donoghue & Wright (2004b). Davies & Li (1997) obtained the same result with a turbulent boundary layer model.

However, in the case of surface waves the wave Reynolds stress term is implemented again, and vertical integration of Equation I, with boundary condition $\langle \frac{\partial \langle u \rangle}{\partial z} \rangle_{z=h} = 0$ at the wave trough level $h$ leads to:

$$\rho \langle \nu_t \rangle \frac{\partial \langle u \rangle}{\partial z} = -\rho \langle \tilde{\nu}_t \frac{\partial \tilde{u}}{\partial z} \rangle + \rho[\langle \tilde{u}\tilde{w} \rangle - \langle \tilde{u}\tilde{w} \rangle_h] + \frac{\partial \langle p \rangle}{\partial x}[z-h] \qquad \text{(III)}$$

where the first term on the right-hand side remains negative. The third term generally includes now a positive mean pressure gradient $(\frac{\partial \langle p \rangle}{\partial x} > 0)$ which is required to drive the negative return flow to produce a zero mean water flux in the case of a closed boundary (e.g. a coast line or wave channel; see Longuet Higgins, 1953). Its influence inside the wave boundary layer is generally small (Craik,

1982). The wave Reynolds stress term $\langle \tilde{u}\tilde{w} \rangle$ is especially important inside the wave boundary layer, where it gradually decreases from a negative magnitude at the edge of the boundary layer to zero at the bed. The complete second term, which is not present in tunnel oscillatory flows, gives therefore an additional positive mean flow contribution. The question then is, which process is dominant and determines the sign of the net flow velocity profile. For laminar flow with constant viscosity the first term is zero and it is shown by Longuet-Higgins (1953) that the combination of the pressure gradient and wave Reynolds stress leads to an onshore-directed mean velocity inside the (lower part of the) wave boundary layer, then shifting to offshore direction above that. This implies that the presence of the wave Reynolds stress is dominant (near the bed), causing a net onshore velocity component near the bed. For turbulent wave boundary layers and skewed waves, this onshore-directed boundary layer streaming reduces due to the presence of the negative oscillatory turbulent Reynolds stress and can even lead to an offshore streaming for strongly velocity-skewed waves in shallow water (Trowbridge & Madsen, 1984 and Davies & Villaret, 1999).

## Appendix II Comparison between UVP and ADV-Vectrino

To check the UVP and ADV-Vectrino measuring instruments and their data-processing, a comparison is made between the measured horizontal velocities from the two instruments during the wave cycle at different positions above the bed and for 2 sand sizes. Figure II-1 shows horizontal velocity results from both the UVPs and the Vectrino combined. In total, results of three different hydrodynamic conditions and two sand types are presented (which are described in more detail in section 2.3 of the paper). In the two top graphs, the Vectrino data is retrieved with 50 Hz and later phase-averaged over 50 waves. As described above, the UVP data is retrieved with a sampling time of 0.11 s. The results of each measured UVP profile are interpolated in order to be able to combine the two at exactly the same level in the vertical. After combining the two signals and constructing the true horizontal velocity component, the results are also phase-averaged over 50 waves. The top left figure shows results of a wave with height 1.5 m and period 6.5 s. The top right graph shows the results of a wave with a height 1.2 m and period 6.5 s. The results shown in the two top graphs show some small differences between the Vectrino and UVP data, but overall, the agreement is good. The bottom two graphs shows Vectrino data, obtained with 200 Hz and phased-averaged over 50 waves, in combination with UVP data, processed as described before and again also phase-averaged over 50 waves (here with a smaller time resolution, due to different settings of the instrument). Both bottom graphs present results of waves with height 1.5 m and period 5.0 s. The bottom-left graph shows results of free-stream measurements and the bottom-right graph shows results measured inside the sheet-flow layer at 1.58 mm below the original still bed layer (pick-up layer). Again, there are some small differences between the results from the two instruments, but the overall agreement is good. For comparison, in the bottom right graph, the free-stream result measured with the EMF at 2 m above the bed is added.

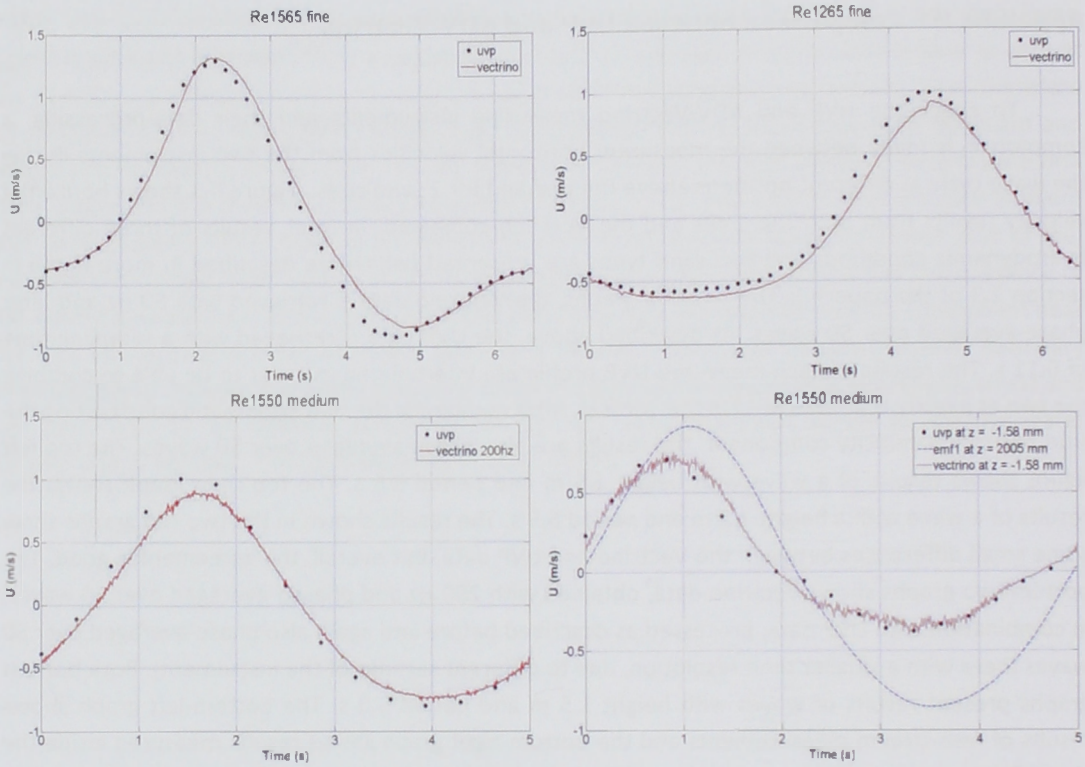


Figure II-1. Comparison of UVP and Vectrino results, measured inside the free stream for 3 different hydrodynamic conditions and 2 sand types (top graphs and lower left graph) and inside the sheet-flow layer (lower right graph, with EMF result of the free-stream). All results are phase-averaged over 50 waves.

## Appendix III Boundary layer flow velocities

Below, the horizontal flow velocity measurements inside the boundary layer for all conditions in Table 3.1 are presented. Slight variations to the $U_{max}$ and $U_{min}$ values as given in Table 1 are due to the fact that these are results from only 1 experimental run (ensemble-averaged over 50 waves, see also Figure 3.5).

Re1565 medium sand

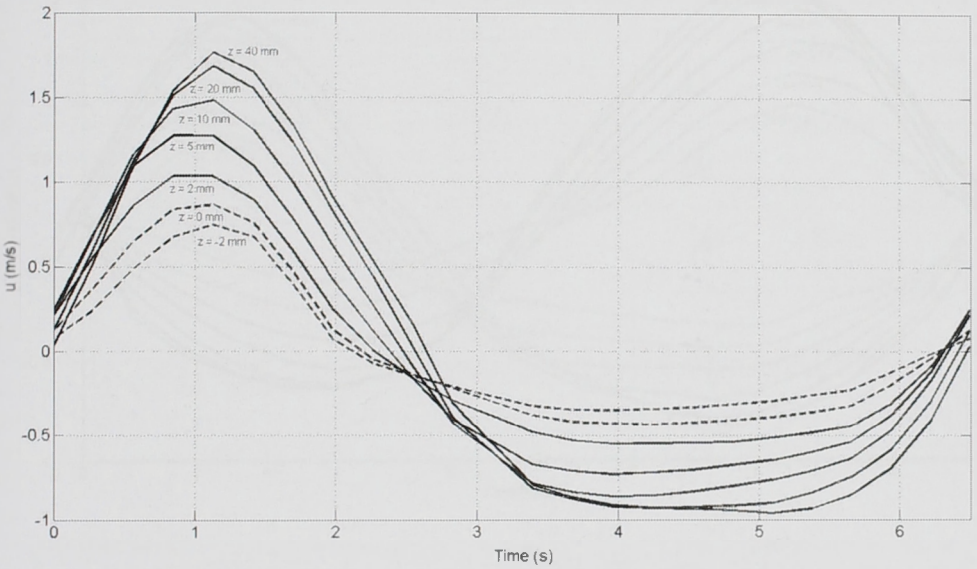


Re1265 medium sand

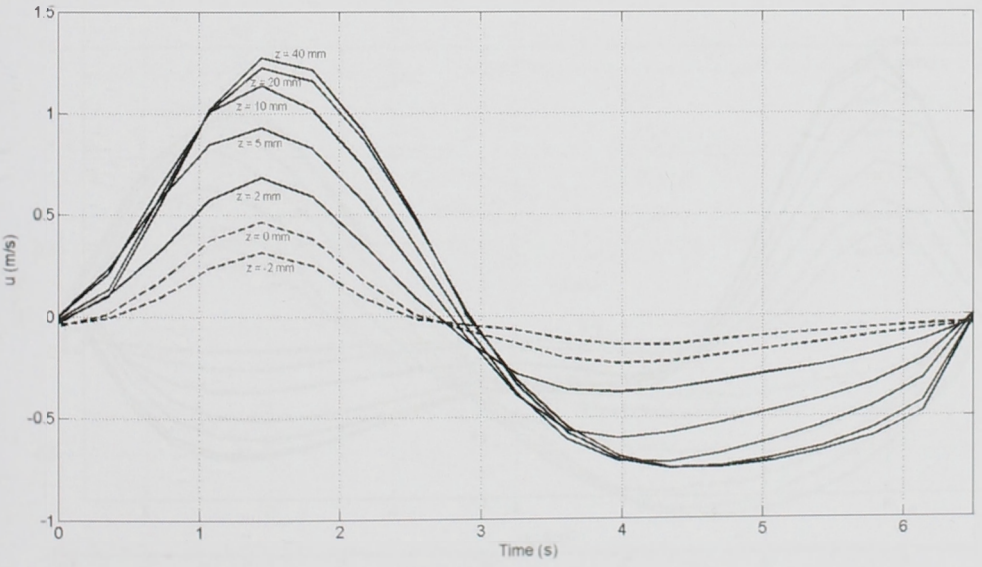

Re1550 medium sand

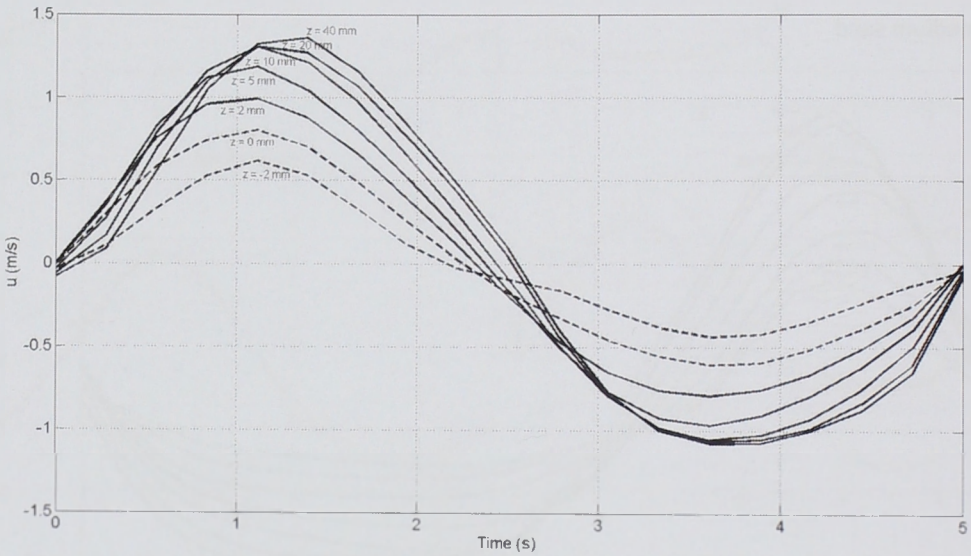


Re1575 medium sand

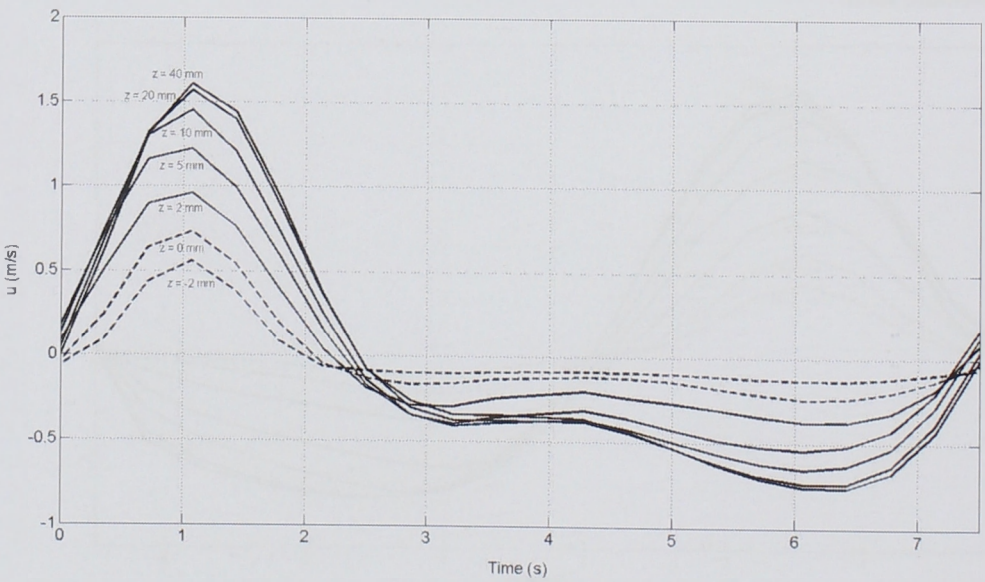

Re1265 fine sand

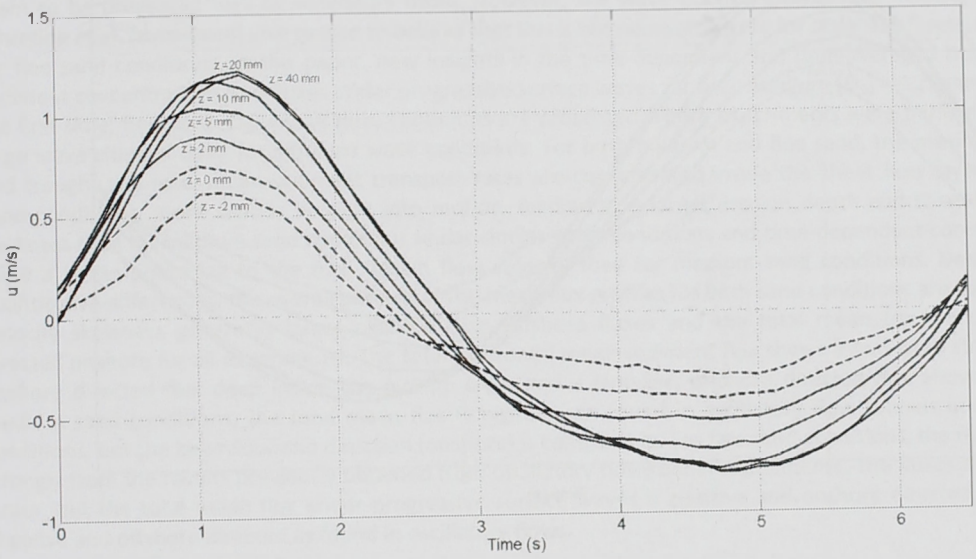


Re1065 fine sand

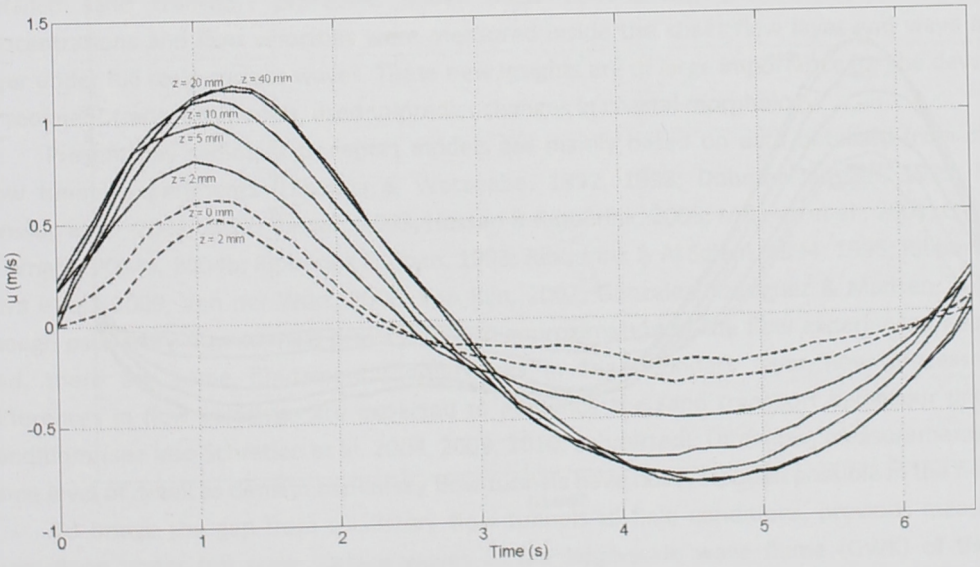

Re1550 fine sand

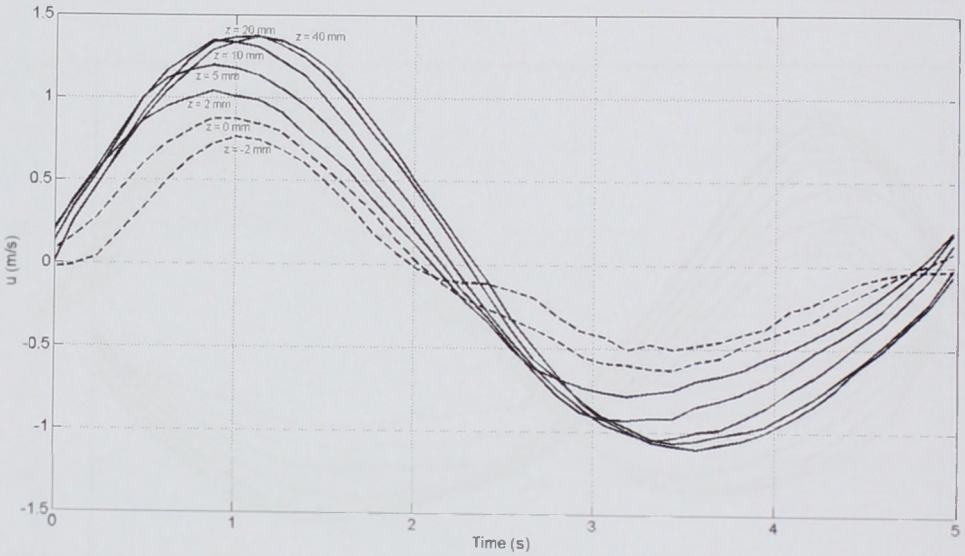


Re1575 fine sand

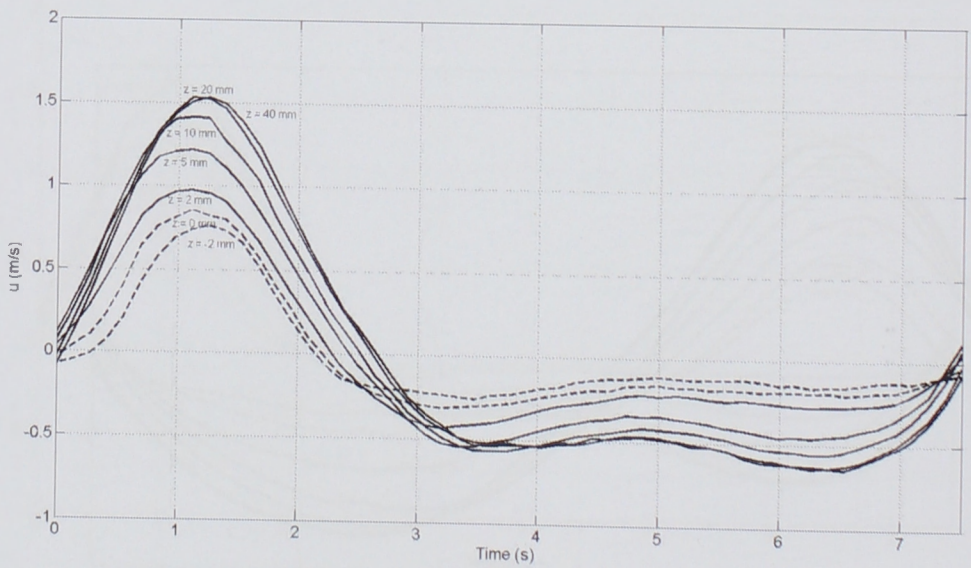

# 4. SAND CONCENTRATIONS AND FLUXES UNDER FULL SCALE SURFACE WAVES

**Abstract**

Existing models for wave-related (cross-shore) sand transport are primarily based on data from oscillatory flow tunnel experiments. However, theory and previous experiments indicate that flow differences between full scale surface waves and oscillatory flow tunnels may have a substantial effect on the net sand transport. For medium sand conditions, previous research showed that sheet flow layer concentrations under surface waves seem to be presented well by oscillatory flows. However, the wave boundary layer flow velocity results in Schretlen et al. (submitted) give reason to believe that this is not necessarily true for sediment fluxes, especially for fine sand conditions. In this paper, new insights in the time-dependent and time-averaged behaviour of sediment concentrations and fluxes under progressive surface waves for both medium ($D_{50}$ = 0.25 mm) and, for the first time, fine sand ($D_{50}$ = 0.14 mm) conditions are presented. These experiments were performed in the large wave channel GWK for different wave conditions. For both medium and fine sand, the maximum (crest and trough) and total mean sediment transport rates are concentrated inside the sheet flow layer. For fine sand conditions, more sand is brought into motion, leading to a larger erosion depth and sheet-flow layer thickness than for medium sand conditions under similar wave conditions and time-dependent concentrations show a larger phase lag to the free stream flow velocity than for medium sand conditions. Despite these quantitative differences, the overall pattern of the mean flux profiles for both sand conditions are comparable. Velocity skewness generates larger onshore than offshore fluxes and the total mean transport rates are directed onshore for all experiments. The total horizontal mean sediment flux shows a two-layer structure; an onshore directed flux deep inside the pick-up layer and a (smaller) offshore directed flux above that. For medium sand conditions, the total mean flux is higher than found in oscillatory flow tunnels under similar conditions, but the behaviour and direction (onshore) is comparable. For fine sand conditions, the results differ strongly from the results previously obtained from oscillatory flow tunnel experiments. The fluxes are not only larger, but the total mean flux under progressive surface waves is positive and onshore directed instead of negative and offshore directed as found in oscillatory flows.

## 4.1 Introduction

On the shoreface of wave-dominated coastal areas, the morphology is for a large part determined by small scale near-bed sand transport processes. Especially for sheet-flow conditions, when under high flow velocities, the vast majority of sand is transported in a thin layer (mm – cm thick) near the bed. The new measurements presented in this paper give new insights into the detailed sand transport processes under these conditions. For the first time, both sand concentrations and flow velocities were measured inside the sheet flow layer and wave boundary layer under full scale surface waves. These new insights are of large importance for the development of sediment transport models, used to predict changes in coastal morphology.

Present day sediment transport models are mainly based on data obtained from oscillatory flow tunnel experiments (Dibajnia & Watanabe, 1992, 1998; Dohmen-Janssen, 1999; Dohmen-Janssen et al., 2001, 2002; Hassan, 2003; Hassan & Ribberink, 2005; McLean et al., 2001; O'Donoghue & Wright, 2004a, 2004b; Ribberink & Chen, 1993; Ribberink & Al Salem, 1994; 1995; Ribberink, 1998; Silva et al.; 2009, Van der Werf, 2006; Van Rijn, 2007; Gonzalez-Rodriguez & Madsen, 2010). Even though oscillatory flow tunnels provide a good approximation of the flow experienced near the sea bed, there are some fundamental differences in the boundary layer flow processes. These differences in flow velocities are expected to influence the sand transport behaviour under these conditions (see also Schretlen et al. 2008, 2009, 2010, submitted). Until now, measurements with the same level of detail as done in oscillatory flow tunnels have not (yet) been possible in the field.

To bridge the gap from oscillatory flow tunnels to field conditions, previous measurements were done under full scale surface waves in the large-scale wave flume (GWK) of the Coastal Research Centre in Hannover, Germany (Ribberink et al., 2000; Dohmen-Janssen & Hanes, 2002; 2005). These measurements included detailed concentration measurements inside the sheet-flow

layer, flow velocity measurements in the free stream and wave crest velocity measurements inside the wave boundary layer (by cross-correlating CCM data), as well as net sand transport rates. These experiments were done with a horizontal mobile bed of medium sand ($D_{10}$ = 0.17 mm, $D_{50}$ = 0.24 mm, $D_{90}$ = 0.28 mm). The main conclusions of these experiments are that the behaviour of the sheet flow layer under surface waves is qualitatively similar to that in oscillatory flow tunnels, being: i) large concentration gradients exist over the sheet flow layer, ii) the sheet flow layer thickness is very similar to values measured in oscillatory flow tunnels and are well presented by the empirical relation of Sumer et al. (1996), iii) concentrations in the sheet flow layer are nearly coherent with the instantaneous near-bed hydrodynamics, including the velocity skewness (higher crest than trough velocities), iv) processes in the suspension layer show more unsteady behaviour than in the sheet flow layer and v) instantaneous sediment fluxes inside the sheet flow layer are at least an order of magnitude larger than in the suspension layer for these conditions. In those experiments, the detailed sheet-flow concentration measurements under full scale surface waves have only been performed for medium sand conditions. From oscillatory flow tunnel experiments it has been shown that grain size has a large influence on the sheet flow layer processes. O'Donoghue and Wright (2004a; 2004b) already concluded for oscillatory flow tunnel conditions that, also inside the sheet flow layer, the unsteady effects become increasingly important as the percentage of fine sand increases. The same would be expected under full-scale surface waves, but cannot be confirmed from existing surface wave experiments yet. In the new experiments presented here, all measurements are done for both medium and fine sand conditions. The sand used, was well sorted quartz sand with $D_{50}$ = 0.245 mm for the medium sand (comparable to that used in the above mentioned surface wave experiments and oscillatory flow tunnel experiments by Ribberink & Al-Salem (1994), O'Donoghue & Wright (2004a;2004b), Hassan & Ribberink (2005), Campbell et al. (2006) and $D_{50}$ = 0.138 mm for the fine sand conditions (comparable to that used in previous oscillatory flow tunnel experiments by Ribberink & Chen (1993), Wright (2002) Wright & O'Donoghue (2002), O'Donoghue & Wright (2004b), Campbell et al. (2006). This makes it possible to explore the influence of grain size on sheet flow layer sediment concentrations and fluxes under full scale surface waves. The results of the boundary layer flow velocity measurements of these experiments are presented in Schretlen et al. (submitted).

Even though sheet flow layer concentrations under surface waves seem to be represented well in oscillatory flow tunnels (at least for medium sand conditions), the wave boundary layer flow velocity results in Schretlen et al. (submitted) give reason to believe that this is not necessarily true for sediment fluxes, especially for fine sand conditions. The measurements presented in this paper were focused on the behaviour of sediment concentrations and sediment fluxes close to the bed, inside the wave boundary layer where the vast majority of the sand transport occurs. The aim is to obtain more detailed insights in the time-dependent and time-averaged behaviour of sediment concentrations and fluxes under progressive surface waves for different types of sediment.

Three different measurement campaigns were carried out in the large Wave Channel GWK in Hannover in the period 2007 – 2008 with different mobile sand beds resulting in over 60 hours of data. With the use of a new acoustic velocity measurement device (UVP) and with conductivity probes (CCM), for the first time, detailed high resolution flow velocity and concentration measurements were obtained inside the sheet flow layer under full-scale surface waves for both medium and fine mobile sand beds. The details of the experimental set-up, instrumentation and test conditions are described in Section 4.2 of this Chapter. This is followed by the experimental results in Section 4.3. The results are divided in i) time-averaged concentration profiles, ii) time-dependent

sediment concentrations and iii) fluxes (both time averaged as time dependent). The presentation of the new experiments is followed by a comparison with existing models for suspended and sheet-flow layer concentrations and sheet flow layer thickness and with oscillatory flow tunnel data in Section 4.4. Finally, the conclusion in Section 4.5 is used to give an overview of the findings from these new experimental results, on their own and in comparison to existing knowledge.

## 4.2 Methodology and experimental set-up

### 4.2.1 Experimental set-up

The experiments were carried out in the large wave flume, or Großer Wellenkanal (GWK), of the Coastal Research Centre in Hannover, Germany, a joint research facility of the University of Hannover and the Technical University of Braunschweig. The flume has a length of 280 m and is 5 m wide and 7 m deep. In this flume, regular and irregular waves with heights from 0.5 to 2.5 m and periods of 2 to 15 s can be generated. An online absorption system for preclusion of wave re-reflection is present at the wave generator.

The experiments were carried out during three different measurement campaigns in 2007 and 2008, in which two different types of sand were placed in the flume. The sands used in these experiments can be characterised as medium and fine sand. More details on the sand characteristics and grain size distributions are given in section 4.2.3. Figure 4.1 shows an overview of the flume with the wave paddle on the left and the artificial beach on the right. The sand bed as shown in this figure was used for the experiments with medium sand. A 1 m thick horizontal sand bed was placed from approximately 50 to 175 m from the wave paddle, with a 1:20 sand beach following at the far end (175 to 280 m from the wave paddle). For the fine sand experiments, the horizontal part of the profile was replaced with a 0.85 m thick fine sand bed. From approximately 200 m from the wave paddle, the 1:20 beach slope was kept intact to optimize wave absorption at the beach slope. The dashed vertical line in Figure 4.1 indicates the position of the instruments used for detailed velocity and concentration measurements (approximately 110 m from the wave paddle). A more detailed description of the instruments and experimental set-up will be given in the next section.

The water level in the flume was 4.5 m above the flume's bottom during the medium sand experiments and 4.35 m during the fine sand experiments, leading to 3.5 m water depth above both initial horizontal sand beds.

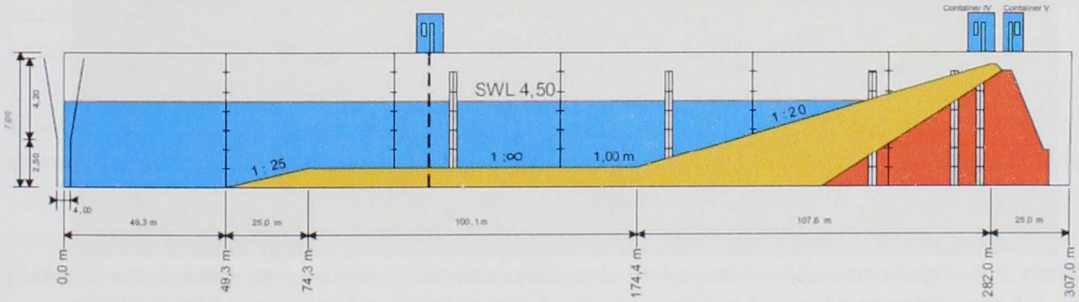


Figure 4.1. Overview of the Large Wave Flume of the Coastal Research Centre, Hannover, Germany.

### 4.2.2 Instruments and measurement set-up

#### General overview

For the detailed flow velocity and sand concentration measurements near the sand bed, special rigs were designed to achieve the required high spatial ($10^{-3}$ – $10^{-2}$ m) and high temporal ($10^{-3}$ – $10^{-1}$ s) measurement resolutions, while at the same time avoiding flow disturbances as much as

possible and being rigid enough to withstand the wave forces. The measurements were performed mainly from i) a wall measuring frame and ii) a measuring tank buried underneath the sand surface, both provided with remotely-controlled vertical positioning systems with sub-mm accuracy.

Sediment concentrations were measured with three different instruments, covering the range of concentrations from the lowest concentrations (0.5 gr/l) in the suspension layer to the highest values (up to 1600 gr/l) inside the sheet-flow layer. A Transverse Suction System (TSS), mounted on the rig, measured time-averaged suspended sand concentrations at several levels above the bed. Time-dependent concentrations were measured with a Ultra-High Concentration Meter (UHCM) at selected heights above the bed. Three Conductivity Concentration Meters (CCMs) were positioned inside a buried tank, to measure the high sediment concentrations inside the sheet-flow layer and detect the sand bed level before, during and after each experiment. Since the CCMs penetrate the sheet-flow layer from below instead of from above, disturbance of the flow was minimized. Flow velocity measurements were carried out with high-resolution acoustic velocity meters inside the wave boundary layer and in the free stream (UVPs, Vectrino) and with electromagnetic flow meters (EMFs) higher in the water column.

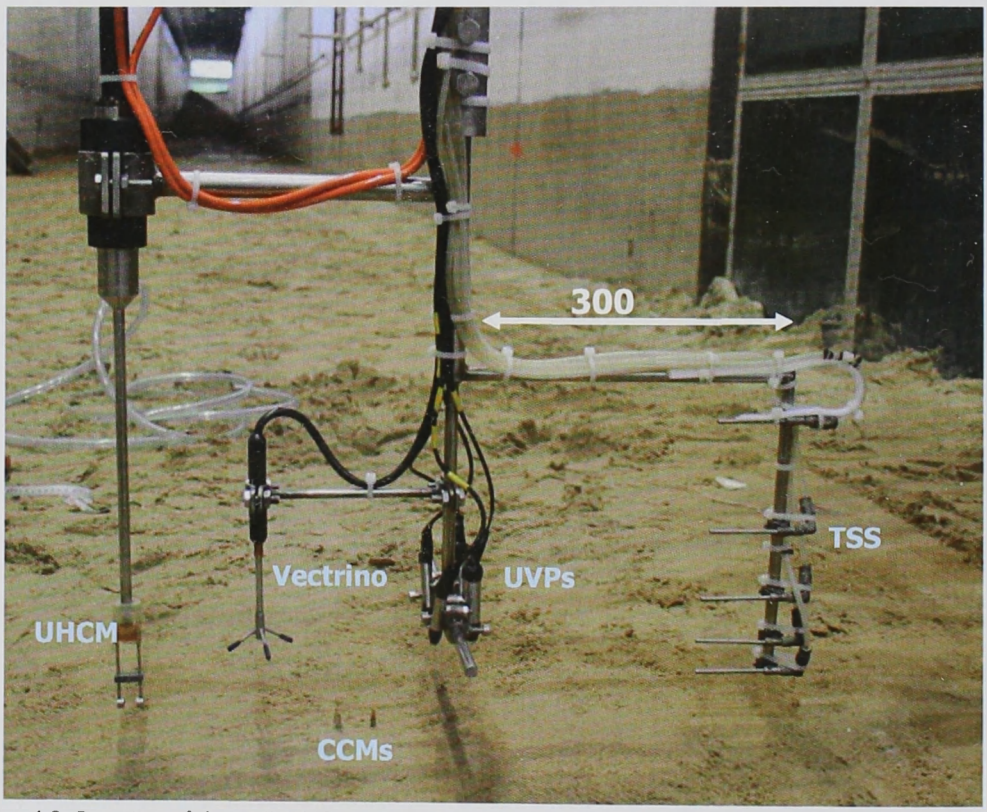


Figure 4.2. Overview of the wall sub-frame with instruments mounted in the Large Wave Flume. The CCM-tank is buried underneath the sand bed. For scale; the distance of the arm from centre to TSS is 300 mm.

Figure 4.2 shows the part of the wall-frame that can be positioned with sub-mm accuracy before, after and also during the measurements. From left to right, the UHCM, Vectrino, UVPs and TSS can be seen. In between the Vectrino and UVPs the three CCM tips, just penetrating the sand bed from below, are visible. The scale of the frame is made more clear by the given distance from the centre of the frame to the end of the TSS tubes, which is 300 mm. Apart from the instruments

positioned at one point in the flume, 19 wave gauges positioned along the flume, monitor the wave heights and wave deformation along the wave flume. To monitor the stability of the sand bed and formation of bed forms, a ripple profiler (echo-sounder) with a radius of 2 m was positioned on the wall frame. Net sand transport measurements were carried out along the flume bed by bed level profiling from a measuring carriage using the mass-conservation principle.

The present Chapter focuses on the sheet-flow layer concentrations and fluxes. Below, the instruments used for the concentration measurements (TSS, UHCM and CCMs) are described in more detail. A description of the wave boundary layer flow velocity measurements and used instruments was given in Schretlen et al. (submitted).

**Sediment concentration measurements**

The Transverse Suction System (TSS) is a simple method to measure time-averaged sediment concentrations. The principle is based on sucking samples in a direction normal to the ambient water motion at an intake velocity which, ideally, exceeds the ambient flow velocity more than three times (Bosman et al., 1987). Five intake nozzles, positioned at different heights, were used here to measure a concentration profile. Due to the fact that the sub-frame could be repositioned vertically, the position of the nozzles could be varied between approximately 2 to 60 cm above the sand bed for different experimental runs of the same wave condition. With the use of five pumps, the sand samples are collected, through the nozzles and connected tubes, into buckets. Afterwards the volume of the samples is determined by using calibrated tubes. As sand is heavier than water, water is sucked into the tubes easier than the sand. Because of this, the sample has a sand concentration that is systematically too low. To correct for this, the following calibration factor of Bosman et al. (1987) was used:

$$\beta_{ss} = 1 + \frac{1}{3} arctan\left(\frac{D_{50}}{D_r}\right) \tag{4.1}$$

where $D_r$ is a reference sand diameter of 0.09 mm. There are no calibration tables available for the very fine sand. Therefore, calibration is based on the relationship by Bosman et al. (1987) and a linear interpolation of existing Bosman tables. Besides the ability to measure the sediment concentrations, suction samples were also saved to determine the grain-sizes of the suspended sediment using the settling tube in the laboratory of the department of Physical Geography at Utrecht University. The principle and calibration of the settling tube is described in Kleinhans (1998).

The Ultra-High Concentration Meter (UHCM, produced by Deltares, The Netherlands) is an acoustical instrument for the measurement of sediment concentration, based on the principle of attenuation of sound by particles. The instrument is specifically applicable in flows with relative high sediment concentrations (up to 400 gr/ l for sand with a medium grain size of 0.2 mm). The output signal is proportional to the sediment volume concentration. Calibration depends on the distance between transmitter and receiver (constant for each probe), acoustic wave length and particle properties such as grain size. In these experiments, the UHCM was positioned on the movable sub-frame and measured concentrations just above the sheet flow layer (and CCMs) and below the lowest TSS suction tube (see Figure 4.2). A calibration for both sediments was carried out by the laboratory of Physical Geography at Utrecht University.

The principle of the Conductivity Concentration Meters (CCM, produced by Deltares, The Netherlands) is based on the conductivity change of a sand-water mixture due to the variation of the

quantity of non-conductive sand present in the measurement area. On top of the probe, four electrodes with a height of 1 mm and diameter of 0.3 mm are positioned. A constant AC electrical current is generated between the two outer electrodes and the voltage between the inner electrodes is measured. The distance between each of the electrodes is 0.6 mm. Due to the small measuring volume (< 2 mm) and the capability of measuring high sand concentrations (≈ 100 – 1600 g/l), this instrument is particularly suitable for concentration measurements inside the sheet-flow layer (see also Dohmen-Janssen, 1999). The CCM probes were placed in a measuring tank, buried in the sand bed and penetrated the sheet-flow layer from below (Figure 4.3). This method was used for the first time during oscillatory sheet flow measurements by Ribberink and Al-Salem (1995). By penetrating the sheet flow layer from below instead of from above, disturbance of the flow is minimized. The technique was extended later with a second probe to measure grain velocities using cross-correlation of the concentration signals (see McLean et al., 2001). Ribberink et al. (2000) applied the technique for the first time in a wave channel using a tank below the sand bed, see also Dohmen-Janssen and Hanes (2002). For more technical details of the CCM probes and the tank system, reference is made to these publications.

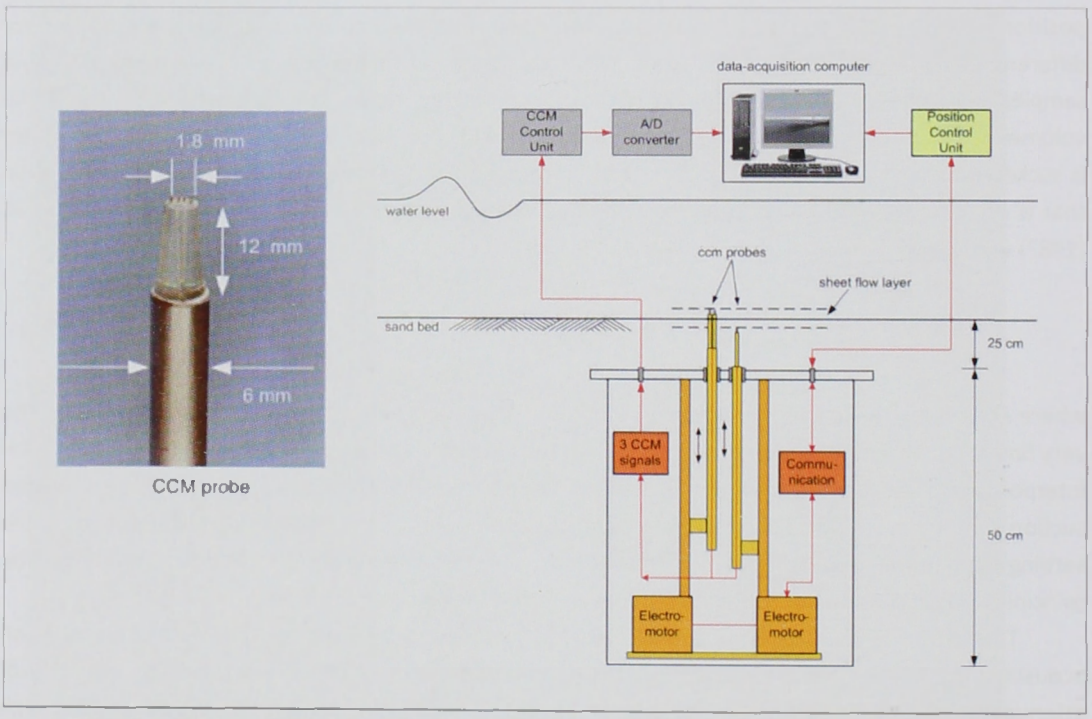


Figure 4.3. CCM tank system for measurement of the sheet flow concentrations and the bed level.

Apart from measuring the high sediment concentrations inside the sheet-flow layer, the CCMs can also be used to detect the sand bed level (changes) during the tests. For the current experiments a new tank was constructed with 2 measuring rods, having at least one for concentration measurements and one for bed-level measurement during the experiments. The rods can be vertically positioned with sub-mm accuracy independent from the other rod at pre-selected levels in the sheet flow layer. The vertical positioning is done with electrical servo-motors in the tank, which were operated from a PC in the measuring cabin next to the wave channel. The CCM measurements were monitored real-time and any changes in bed elevation were apparent during the experiments.

Together with the measurements of the still-bed level before and after each wave run, this provided crucial information for analysing the flow velocity measurements inside the wave boundary layer. The measuring accuracy of the bed-level measurement using CCM is estimated to be in the order of 1 mm. The vertical positions of the rods as well as the CCM signals were measured (with a minimum sampling frequency of 50 Hz) and stored together with the other measuring signals using a Labview data-acquisition system. See Figure 4.3 for a schematic overview of the CCM tank system and a photograph of a CCM probe.

### 4.2.3 Experimental conditions

The majority of the tests were performed with regular, corrected shallow water trochoidal waves (CSTW), varying in wave height ($H$) and period ($T$). This wave shape is based on North Sea deep water wave measurements and roughly comparable to second order Stokes waves. The wave-generated horizontal orbital flow is therefore velocity skewed and only minor acceleration skewed. The variations in wave height and period led to different bed regimes, i.e. rippled beds as well as flat beds with sheet flow. Besides these waves, a part of the tests was performed with second order Stokes waves and wave groups of irregular waves, based on a JONSWAP spectrum. This paper focuses on a selection of the regular CSTW conditions in only the sheet flow regime. Table 4.1 gives an overview of the experimental conditions. Each condition was run for a number of hours divided over different runs, resulting in over 60 hours of wave data (see also Schretlen et al., sumitted).

Table 4.1. Overview of selected experimental conditions.

| | $H$ (m) | $T$ (s) | $D_{10}$ (μm) | $D_{50}$ (μm) | $D_{90}$ (μm) | $U_{max}$ (m/s) | $U_{min}$ (m/s) | $<u>$ (m/s) | $R$ (-) | $\beta$ (-) | $\Psi_{max}$ (-) |
|---|---|---|---|---|---|---|---|---|---|---|---|
| Re1575m | 1.50 | 7.50 | 148 | 245 | 420 | 1.63 | -0.74 | -0.068 | 0.69 | 0.54 | 670 |
| Re1550m | 1.50 | 5.00 | 148 | 245 | 420 | 1.18 | -0.92 | 0.014 | 0.56 | 0.51 | 351 |
| Re1565m | 1.50 | 6.50 | 148 | 245 | 420 | 1.67 | -0.92 | -0.027 | 0.65 | 0.52 | 699 |
| Re1265m | 1.20 | 6.50 | 148 | 245 | 420 | 1.35 | -0.83 | 0.010 | 0.62 | 0.55 | 456 |
| Re1575f | 1.50 | 7.50 | 110 | 138 | 180 | 1.70 | -0.69 | -0.092 | 0.71 | 0.54 | 1298 |
| Re1550f | 1.50 | 5.00 | 110 | 138 | 180 | 1.28 | -1.02 | -0.028 | 0.56 | 0.53 | 731 |
| Re1565f | 1.50 | 6.50 | 110 | 138 | 180 | 1.55 | -0.83 | -0.058 | 0.65 | 0.52 | 1078 |
| Re1265f | 1.20 | 6.50 | 110 | 138 | 180 | 1.25 | -0.75 | -0.030 | 0.63 | 0.54 | 697 |
| Re1065f | 1.00 | 6.50 | 110 | 138 | 180 | 1.13 | -0.74 | -0.017 | 0.60 | 0.55 | 568 |

The wave height ($H$) and period ($T$) values in Table 4.1 are the input height and period at the wave paddle. At the point of the measurement frame (see Figure 4.1) the wave period has not changed, but due to shoaling the wave height slightly increased. Eekhout (2008) analysed the wave propagation along the 19 wave gauges in the flume. At the location of the measurement frame (wave gauge at $X$ = 111 m) , the wave height shows an increase of approximately 10 %, compared to the waves leaving the paddle at $X$ = 0 m ( 10.8 % for waves with $H$ = 1.2 m and 10.0 % for waves with $H$ = 1.5 m). The different types of waves break at a distance of $X$ = 180 to $X$ = 236 m from the wave paddle. More detail on wave propagation and deformation along the flume can be found in Eekhout (2008). $U_{max}$ and $U_{min}$ are the maximum onshore and offshore free stream orbital velocities and $<u>$ the mean flow velocity, measured just outside the wave boundary layer (40 mm above the sand bed) at the location of the measurement frame ($X$ = 110 m). Within each condition the variation in velocities measured during different runs varies from 3% to maximum 10% over all three measurement campaigns (spring 2007 – winter 2008). The degree of velocity skewness ($R$) is a function of the maximum on- and offshore velocity, defined as:

$$R = \frac{|U_{max}|}{|U_{max}| + |U_{min}|} \tag{4.2}$$

The values of the acceleration skewness ($\beta$) were calculated from:

$$\beta = \frac{|\dot{U}_{max}|}{|\dot{U}_{max}| + |\dot{U}_{min}|} \tag{4.3}$$

where $\dot{U}_{max}$ and $\dot{U}_{min}$ are the amplitudes of the flow acceleration in the wave crest (max) and trough (min) direction. For all experiments, the degree of acceleration skewness was found to be much smaller than the velocity skewness.

The wave mobility number is a parameter for the prediction of the transport regime and defined as follows;

$$\Psi_{max} = \frac{U_{max}^2}{(s-1)gD_{50}} \tag{4.4}$$

where $s = \rho_s / \rho$ is the relative sediment density, 2.65 in this case, g the gravity acceleration and $D_{50}$ the median grain diameter of the sand. According to O'Donoghue et al. (2006), a flat bed sheet-flow regime is present when $\Psi_{max} > 300$, ripple regime corresponds to $\Psi_{max} < 190$ and in between, $190 < \Psi_{max} < 300$, a transition regime is present. This corresponds well with the observations done during the present experiments, where sheet-flow sediment transport was observed for conditions Re1565, Re1265, Re1550 and Re1575 for both sands and for Re1065 for the fine sand. A transition towards the ripple regime was observed during condition Re1065 for the medium sand (and is not included in Table 4.1). During lower wave conditions (wave heights of 0.7 m) velocities decreased further and ripples were present for both medium and fine sand.

## 4.3 Experimental results

### 4.3.1 Time averaged sediment concentration profiles

The sand used for these experiments was well sorted quartz sand ($\rho$ = 2650 kg/m$^3$). Before the start of the experiments the grain size analyses of the sand resulted in the characteristics as shown in Table 4.1. More detailed results of the sediment analyses are shown in Figure 4.4. The left graphs show the vertical distribution of the $D_{10}$, $D_{50}$ and $D_{90}$ for all fine and medium suction samples. At the sand bed level ($z$ = 0 mm) the grain sizes of the bed material are presented. The right graphs show the grain size distribution of both the bed and suspended material. For the medium sand the difference between the suspended sand and bed material is far larger than for the fine sand and the medium sand (bed) material is less uniform. The medium sand conditions show relatively fine material in suspension, finer than the suspended material for the fine sand conditions. This could be due to the fact that the medium sand is less uniform, but more likely is that (also) the contents of the flume water, pumped from the Mittelland-canal, play a role here. The exact contribution of the latter is not analysed in further detail, the main results and analyses are concentrated near the bed (sheet-flow layer, $z < 2$ cm) where the transport process is concentrated (see also below).

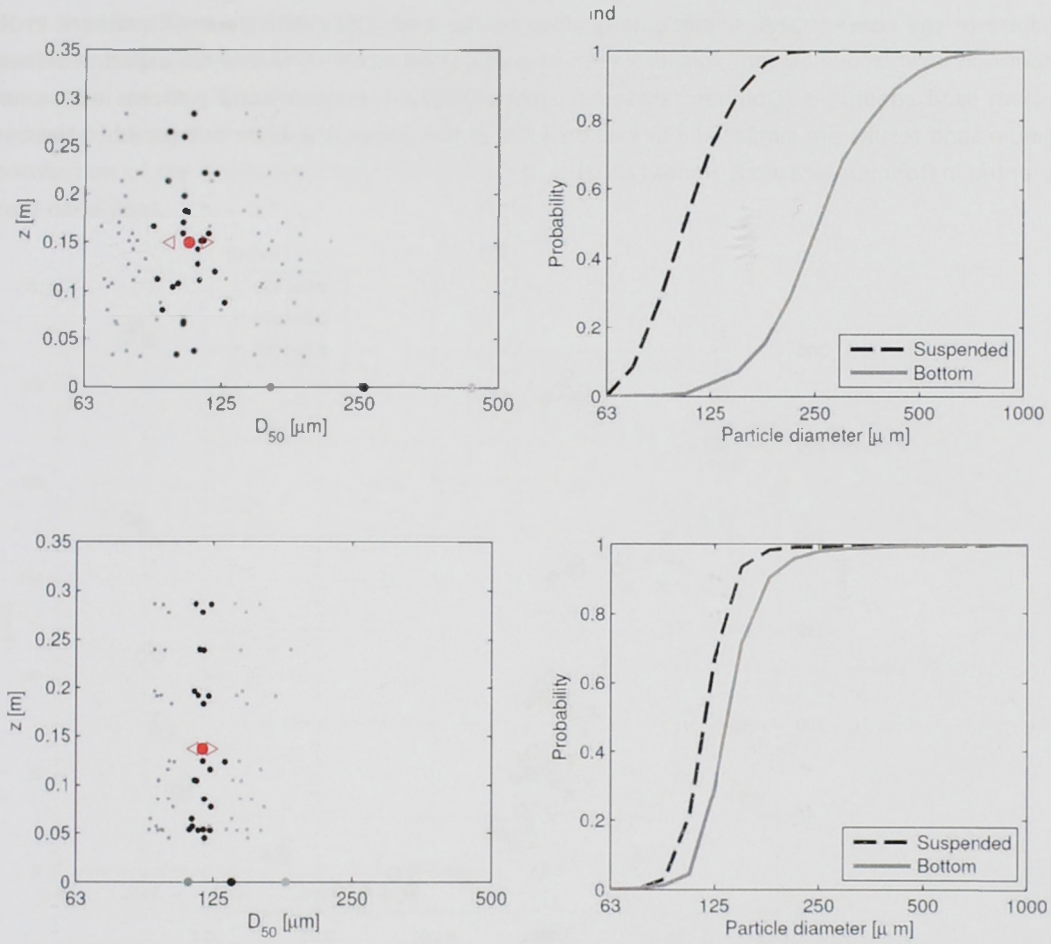


Figure 4.4. Left graphs: vertical distribution of $D_{10}$ (dark grey dots), $D_{50}$ (black dots) and $D_{90}$ (light grey dots) of suspended sediment from all regular wave conditions. The red dots and triangles represent respectively the median $D_{50}$ and standard deviation of all suspended sediment. The closed circles at z = 0 mm present the $D_{10}$, $D_{50}$ and $D_{90}$ of the bed material. Right graphs: sieve curves for the bed and suspended material. Top graphs present the medium sand results, the bottom graphs the fine sand results (from Huisman et al., 2009).

During the experiments some sorting occurred and the sieving analyses of sediment samples from the bed around the measurement frame ($X$ = 110 m) gave slightly varying results. It appeared that the sorting took place both along the flume (coarsening towards the beach) as well as vertically inside the bed (due to the formation of bed forms during the lower velocity conditions). However, since these deviations were less than 10 % for the medium sand and less than 5% for the fine sand cases, they were neglected in further analyses in the paper.

Time averaged suspended sediment concentrations of the fine sand experiments are shown in Figure 4.5 for different wave heights. In this graph the black diamonds represent a wave condition with wave height $H$ = 1.5 m and wave period $T$ = 6.5 s, the circles represent waves with $H$ = 1.2 m and $T$ = 6.5 s and the results of waves with $H$ = 1.0 m and $T$ = 6.5 s are presented by the crosses. The results are a combination of the five different suction tubes ($z$ > 30mm) and the UHCM measurements closer to the bed ($z$ < 50 mm). Each point of the TSS results represents one suction sample, taken over approximately 20 minutes during an experimental run and each point of UHCM results is found by ensemble averaging the time-dependent signal over 50 waves. The level $z$ = 0 mm is defined as the original still (no flow) bed level. The horizontal axis is a log scale, reflecting the large

gradient of the concentrations, particularly close to the bed. The relatively small gradient in the suspension layer above 50 mm was also seen in previous full scale surface wave experiments with medium sand conditions (Dohmen-Janssen & Hanes, 2002). The results and patterns of the new medium sand results are similar and in section 4.4.1 of this paper, these are compared to the ones presented in Dohmen-Janssen & Hanes (2002).

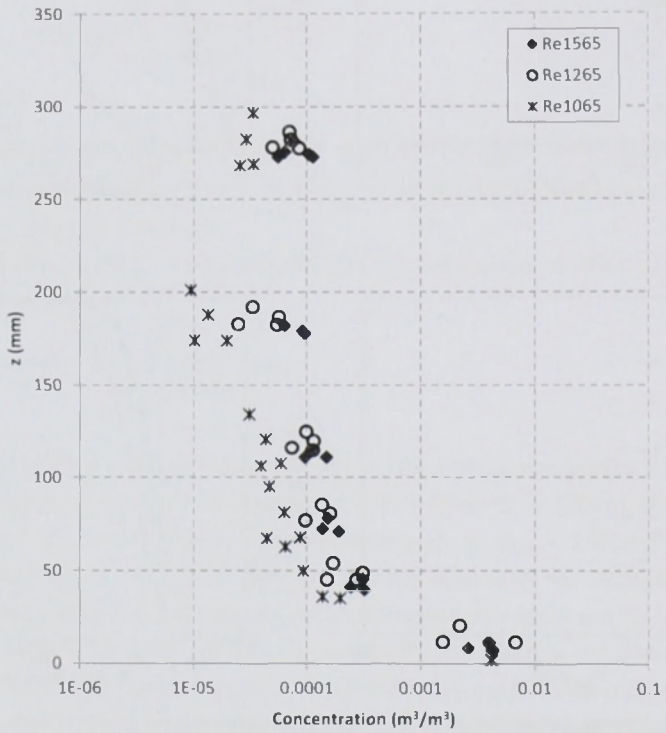


Figure 4.5. Time averaged suspended sand concentration profiles for wave conditions Re1565, Re1265 and Re1065 for fine sand.

For these fine sand results there is a small difference between the suspended sediment concentrations under conditions Re1565 and Re1265. The lower waves, with lower flow velocities, generate slightly lower concentrations of sediment in suspension. When the waves and flow velocities become even lower (Re1065), the sediment concentrations in suspension are, as expected, clearly decreasing as well. Figure 4.6 shows the suspended sediment concentrations and sheet-flow layer concentrations of two wave conditions with the same wave height but with different wave periods ($T$ = 6.5 s for Re1565 and $T$ = 7.5 s for Re1575). Similar to Figure 4.5, the vertical axis presents the distance from the original still bed level ($z$ = 0 mm) and the horizontal axis the sediment concentration ($m^3/m^3$) on a log-scale. The white circles represent the suspended TSS results, the grey diamonds the UHCM results and the crosses present the CCM results inside the sheet-flow layer. The high concentrations inside the sheet-flow layer ($z$ < 10 mm) measured with the CCMs from the buried tank, are the mean ensemble averaged results of up to 10 different experimental runs per condition. Here, it is shown that the difference in wave period, doesn't cause a significant difference in time averaged suspended sediment behaviour. Closer towards the bed (30 > $z$ > 10 mm), the UHCM results show that for the condition with a longer period and higher peak flow velocities (Re1575), just

above the sheet-flow layer the sediment concentrations are higher (compared to Re1565). Inside the sheet-flow layer (CCM measurements), more sediment is being brought into motion by the Re1575 waves than by the Re1565 waves, coinciding with the larger erosion depths for this condition, presented in Schretlen et al. (submitted). As a consequence of the large concentration gradient, the contribution of the suspended load to the total sand transport will be of minor importance under these conditions.

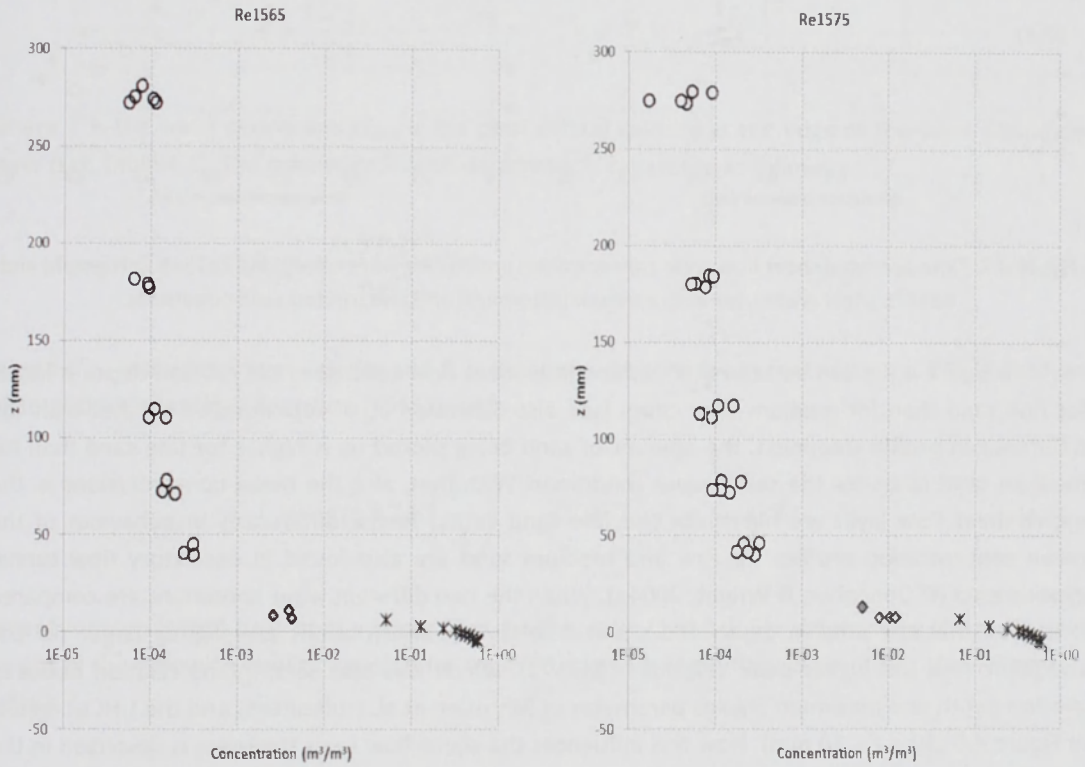


Figure 4.6. Time averaged concentration profiles (suspension layer and sheet flow layer) for wave conditions Re1565 (left graph) and Re1575 (right graph) for fine sand. Combined are the results from the TSS (circles), UHCM (diamonds) and CCM (crosses).

Figure 4.7 shows the time averaged sediment concentrations of both medium and fine sand results zoomed in on the sheet-flow layer only. The left graph shows the results of condition Re1565, for both medium and fine sand conditions, the right graph the same results for the hydrodynamic condition Re1575. The level $z$ = 0 mm is defined as the original still bed level. This level is determined by shifting the $z$ = 0 level (determined from the CCM measurements before and after each wave run) until the amount that is picked below the original bed level is equal to the amount entrained into the upper sheet flow layer determined by integration of the concentration profile). The upper level of the sheet flow layer is defined as the point where the time-averaged concentration reaches 8% (Dohmen-Janssen, 1999). The shift needed in the z-direction, varied from 0.08 mm to 0.52 mm for these 4 conditions.

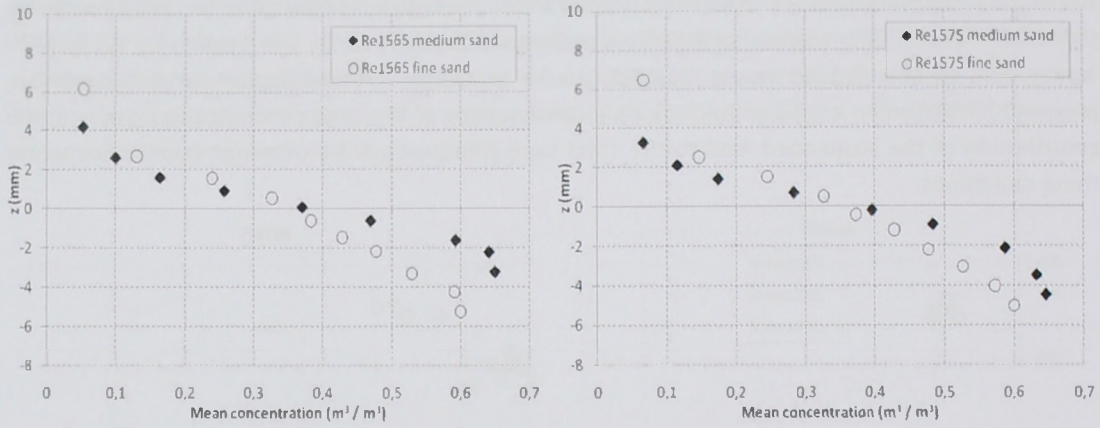


Figure 4.7. Time averaged sheet flow layer concentration profiles for wave conditions Re1565 (left graph) and Re1575 (right graph), for both medium (diamonds) and fine (circles) sand conditions.

In Figure 4.7 it can be seen that under these sheet-flow conditions the erosion depth is larger for fine sand than for medium sand cases (see also Schretlen et al. submitted). Together with the difference in profile steepness, the amount of sand being picked up is higher for fine sand than for medium sand cases for the same wave conditions. With that, also the mean concentrations in the upper sheet flow layer are higher for the fine sand cases. Similar differences in behaviour of the mean concentration profiles for fine and medium sand are also found in oscillatory flow tunnel experiments (O'Donoghue & Wright, 2004a). When the two different wave conditions are compared it is seen that the erosion depth and sheet flow layer concentrations are slightly larger for the condition with the higher peak velocities (Re1575), which was also seen in the relation between erosion depth and maximum Shields parameter in Schretlen et al. (submitted) and the UHCM results in Figure 4.6 ($30 < z < 10$ mm). How this influences the sheet-flow layer thickness is described in the next Section.

### 4.3.2 Sheet-flow layer thickness

The sheet flow layer can be divided in two different sections; the pick-up layer (from the erosion depth ($d_e$) up to the original still bed level ($z = 0$ mm)) and the upper sheet-flow layer (from the original still bed level up to the level where the concentration reaches 0.08 $m^3/m^3$). The thickness of the sheet flow layer ($\delta_s$), similar to the erosion depth, varies over the wave cycle. Table 4.2 shows the erosion depths ($d_e$) and the sheet-flow layer thickness ($\delta_s$) at the moment of the two flow velocity maxima of the wave (wave crest and wave trough) of the 4 conditions shown in Figure 4.7.

Table 4.2. Sheet flow layer thickness at the moment of maximum on- and offshore flow.

| | | $D_{50}$ (μm) | A (m) | $d_e$ (mm) | $\delta_s$ (mm) | $\theta_{max}$ (-) |
|---|---|---|---|---|---|---|
| Re1575m | crest | 245 | 1.95 | 5.3 | 10.3 | 5.67 |
| | trough | 245 | 0.88 | 2.3 | 4.8 | 1.55 |
| Re1565m | crest | 245 | 1.72 | 5.1 | 9.8 | 4.46 |
| | trough | 245 | 0.95 | 2.0 | 4.0 | 1.60 |
| Re1575f | crest | 138 | 2.03 | 6.5 | 12.8 | 8.75 |
| | trough | 138 | 0.82 | 3.5 | 8.7 | 1.70 |
| Re1565f | crest | 138 | 1.61 | 5.2 | 10.5 | 8.46 |
| | trough | 138 | 0.86 | 2.3 | 7.4 | 1.82 |

In previous research, various relationships for the (maximum) sheet flow layer thickness and (maximum) Shields parameter ($\theta_{max}$) are given, especially for steady flow and oscillatory flow tunnel cases (e.g. Sumer et al. (1996); Ribberink et al. (2008)). The maximum Shields parameter corresponding to the data is also shown in Table 4.2, together with the amplitude of the near-bed wave orbital motion at the edge of the wave boundary layer ($A$), which is defined as:

$$A = \frac{TU_{\max}}{2\pi} \tag{4.5}$$

where $T$ is the wave period and $U_{\max}$ is the peak orbital velocity at the edge of the wave boundary layer (see Table 4.1). The maximum Shields parameter is calculated as follows:

$$\theta_{\max} = \frac{0.5 f_w U_{\max}^2}{\Delta g D_{50}} \tag{4.6}$$

where $U_{max}$ is the maximum velocity and $f_w$ is determined by the Swart formulation (1974) (based on an implicit relationship of Jonsson (1966)), with:

$$f_w = \exp\left[5.213\left(\frac{k_s}{A}\right)^{0.194} - 5.977\right], f_{w,\max} = 0.3 \tag{4.7}$$

where Jonsson (1980) suggested a upper limit for the value $f_w$ of 0.3. For determining the roughness height $k_s$ the following implicit relation for mobile beds with sheet-flow is used (see also Ribberink, 1998):

$$k_s = D_{50} \qquad \text{for} \quad \theta_{max} \leq 1 \tag{4.8}$$
$$k_s = \left[1 + 6(\theta_{\max} - 1)\right] D_{50} \qquad \text{for} \quad \theta_{max} > 1$$

Figure 4.8 shows the relation between the measured dimensionless sheet flow layer thickness ($\delta_s/D_{50}$) and maximum Shields parameter ($\theta_{max}$). Similar as was shown for the erosion depth by Schretlen et al. (submitted), it is shown that the dimensionless sheet-flow layer thickness of fine sand conditions clearly exceeds the thickness of the layer for medium sand conditions. This occurs, in particular for smaller Shields parameter values i.e. smaller flow velocities under the wave trough. Following the dimensionless sheet flow layer thickness representation as a function of the Shields parameter as suggested in the literature, a (power) function with different variables for each sand type is applied to fit the data. The following power functions provide a good fit with the data:

$$\frac{\delta_s}{D_{50}} = \alpha \theta_{\max}^{\beta} \tag{4.9}$$

with $\alpha$ = 13.1 and $\beta$ = 0.70 for medium sand conditions
with $\alpha$ = 51.0 and $\beta$ = 0.23 for fine sand conditions.

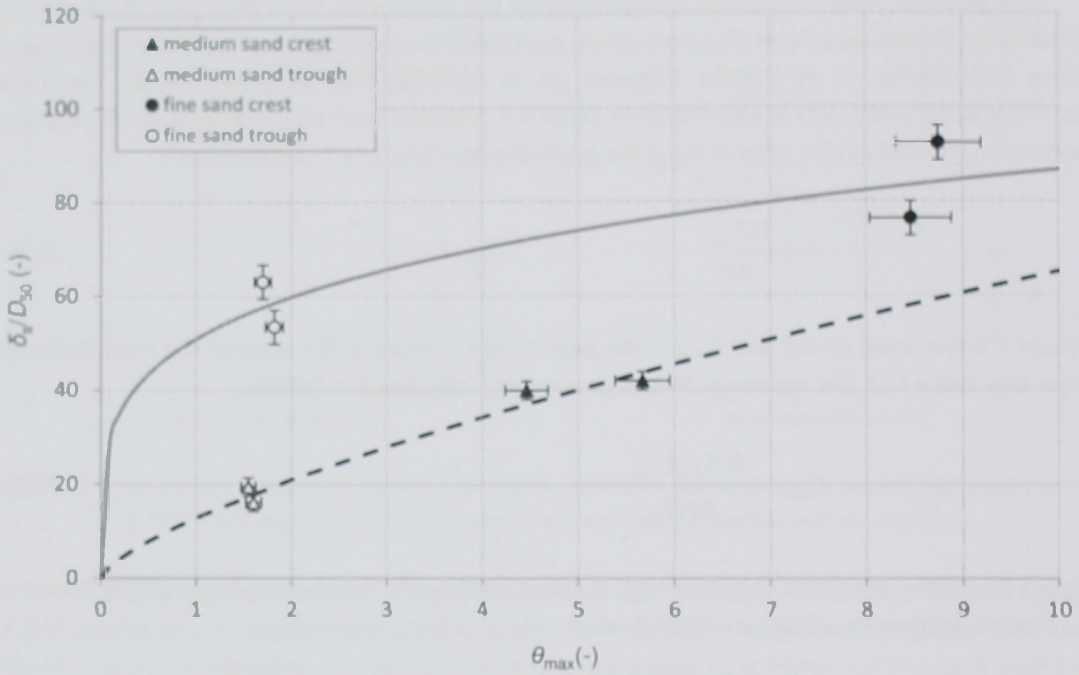


Figure 4.8. Non-dimensional sheet-flow layer thickness under wave crest and trough as function of the maximum Shields parameter for the Re1565 and Re1575 conditions with medium sand (triangles) and fine sand (circles). The solid line represents the power function for fine sand, the dashed line the function for medium sand (Eq. 8).

### 4.3.3 Time dependent sediment concentrations

Apart from the time-averaged sediment concentration profiles, also the time-dependent concentrations are determined. For both the fine and medium sand cases these are presented in Figure 4.9 (Re1565) and 4.10 (Re1575) at different levels inside the sheet-flow layer. The upper graph shows the horizontal free stream velocity measured just above the wave boundary layer ($z$ = 40 mm), ensemble averaged over 50 waves. The second graph shows the time dependent concentrations for fine sand conditions and the third graph the time dependent concentrations of the medium sand experiments. The concentrations are ensemble averaged as well. The number of waves over which this is done, depends on the available data, but varies between 35 and 400 waves for each $z$-level in the figures. For each concentration curve the height ($z$) is presented in relation to the original still bed level ($z$ = 0 mm). This original still bed level corresponds to the bed level shown in Figure 4.7, in Section 4.3.1. The time-dependent concentration measurements inside the sheet-flow layer show the following general behaviour for both sands, under both wave conditions:

- From the level of erosion depth up to the original still bed level, the concentrations decrease with increasing flow velocity. In this pick-up layer sand is being brought into motion and entrained into the upper sheet flow layer.
- In the upper sheet flow layer, from $z$ = 0 mm upwards, the sediment concentrations increase with increasing flow velocity.
- The velocity skewness of the waves is reflected in the asymmetry of the concentration signal. For the lowest parts of the pick-up layer, sand is only being brought into motion by the highest flow velocities, resulting in decreasing concentration under only the wave crest. High

in the upper sheet flow layer, the pattern continues where the highest concentrations occur due to the highest flow velocities underneath the wave crest.

However, there are also some differences caused by the variations in sediment or wave conditions.

- In the medium sand results of the condition Re1565 (lowest graph, Figure 4.9), it is shown that deep inside the sheet-flow layer, the concentration variation is coupled in a coherent instantaneous way to the velocity variation in the free stream. The phase of the peaks in the pick-up layer coincide with the peaks of the flow velocity. Higher up, in the upper sheet-flow layer, the phase lags of the concentration in relation to the flow velocity become larger. The concentration peak high up in the upper sheet flow layer ($z$ = 4,2 mm) lags 18 degrees behind the flow velocity peak. This behaviour is due to the fact that it takes time for the sediment grains to be picked up from the bed and moved higher up into the sheet flow layer. In general, the higher the elevation from the bed, the larger this phase lag becomes. When the medium sand results of conditions Re1575 are considered, this behaviour of phase lags is less pronounced. This could be due to the fact that for the larger wave periods, more time is available for the sediment pick-up process.
- When the fine sand results are considered, it is shown that through the complete sheet flow layer, the concentrations lag further behind the flow velocity than for the medium sand conditions. Apparently, the pick-up and settling process proceeds slower than for the medium sand. Under these conditions, unsteady effects would become more important throughout the complete sheet flow layer, than under conditions where the sand react more instantaneous to the flow velocity variation.
- Near the moment of on- to offshore flow reversal, short concentration peaks can be seen in the upper sheet flow layer. These are more pronounced for fine sand conditions than for medium sand, and larger under the waves with the highest peak velocities and largest velocity skewness (i.e. larger for the Re1575 waves than for the Re1565 conditions). Since these peaks cause an increase of concentrations in the upper sheet-flow layer, just before the offshore water movement, these peaks enlarge the phase lag effects and contribute to an increase of the offshore sand transport. The cause of these peaks is not yet known exactly. Ribberink et al. (2008) give the following comparison: the peaks occur near the moment of flow reversal when the bed shear stress is relatively small. A similarity seems to exist with the transition from laminar to fully turbulent oscillatory flows as observed in clear water oscillatory flow conditions over a smooth bed (Jensen et al., 1989). Here it was shown, that turbulent velocity fluctuations start to develop when the pressure gradient is against the flow direction in the deceleration phase just before flow reversal.

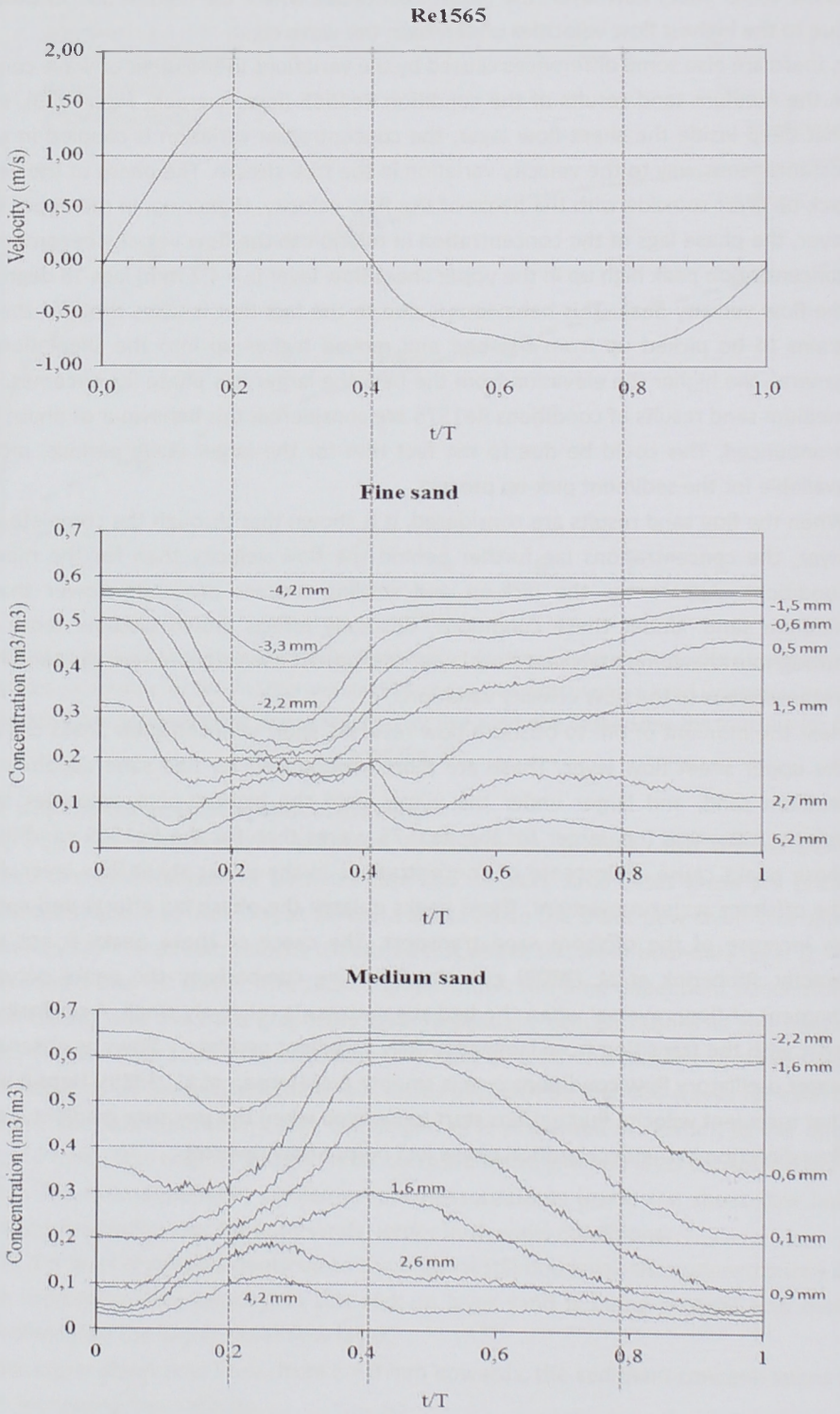


Figure 4.9. Measured ensemble averaged sediment concentrations at different levels inside the sheet flow layer for conditions Re1565, fine (middle graph) and medium (lowest graph) sand. The top graph presents the corresponding horizontal free stream velocity (measured at $z$ = 40 mm).

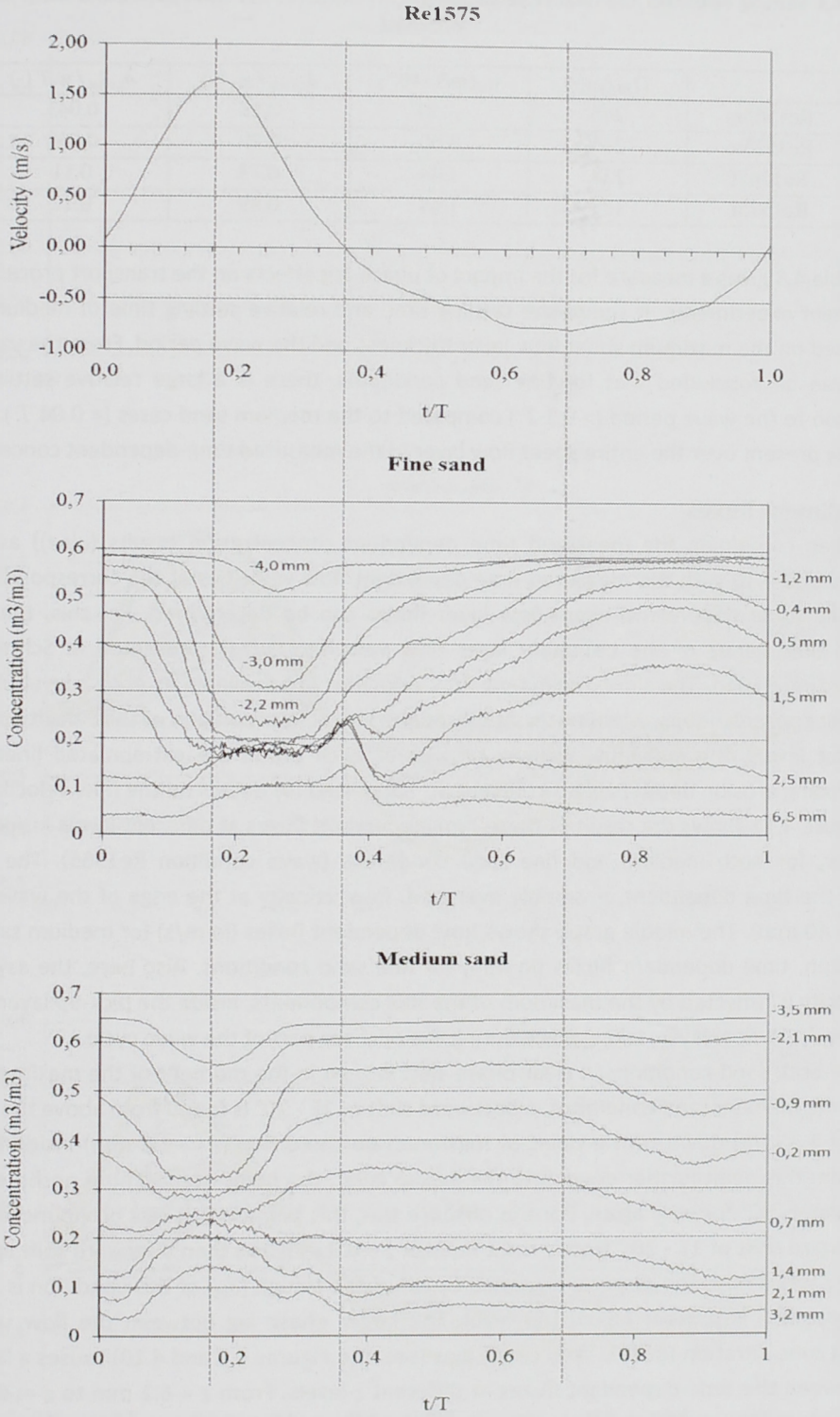


Figure 4.10. Measured ensemble averaged sediment concentrations at different levels inside the sheet flow layer for conditions Re1575, fine (middle graph) and medium (lowest graph) sand. The top graph presents the corresponding horizontal free stream velocity (measured at $z$ = 40 mm).

Table 4.3. Settling velocities and relative settling times in relation to the wave period and sheet flow layer thickness .

| | $D_{50}$ (μm) | $w_s$ (m/s · $10^{-2}$) | $\delta_{s,crest} / w_s$ (s) | $\delta_{s,crest} / w_s T$ (-) |
|---|---|---|---|---|
| Re1565m | 245 | 3.50 | 0.28 | 0.043 |
| Re1575m | 245 | 3.50 | 0.29 | 0.039 |
| Re1565f | 138 | 1.44 | 0.73 | 0.11 |
| Re1575f | 138 | 1.44 | 0.89 | 0.12 |

Table 4.3 gives a measure for the impact of phase-lag effects on the transport processes during the different experiments. It shows the settling time and relative settling time of medium and fine sand, based on the maximum sheet flow layer thickness and the wave period. From the values in the table it can be concluded that for fine sand conditions, there is a large relative settling time in comparison to the wave period (> 0.1 $T$ ) compared to the medium sand cases (≈ 0.04 $T$ ). This lag is constantly present over the entire sheet flow layer in the measured time-dependent concentrations.

### 4.3.4 Sediment fluxes

When combining the measured time dependent concentration results ($c(z,t)$) as shown in Figure 4.9 and 4.10 with the measured time dependent flow velocities at the corresponding z-levels ($u(z,t)$), the (time dependent) sheet-flow layer fluxes can be determined. For this, the ensemble averaged time series of the boundary layer flow velocities ($u(z,t)$) presented in Schretlen et al. (submitted) are used. The time-dependent flow velocities are available at each $z$-level of the time-dependent concentrations, when necessary through vertical interpolation of the velocity profiles. For the lowest levels, the individual velocity profiles at each phase are extrapolated linearly to the corresponding erosion depth (see Schretlen et al., submitted for details on the flow velocities).

Figure 4.11 shows the result of these time dependent fluxes at different levels inside the sheet flow layer, for both medium and fine sand conditions (wave condition Re1565). The top graph presents the time dependent, ensemble averaged, flow velocity at the edge of the wave boundary layer ($z$ = 40 mm). The middle graph shows time dependent fluxes (in m/s) for medium sand and the lower graph, time dependent fluxes (in m/s) for fine sand conditions. Also here, the asymmetry in flow velocity is reflected by the maximum of the flux components, inside the pick-up layer and inside the upper sheet-flow layer, taking place during the onshore part of the wave cycle.

For both sand conditions, a clear phase shift is seen in the moment of the maximum onshore flux. For the medium sand conditions, a backward shift of 15 - 20° is found from above the sheet-flow layer ($z$ = 4.2 mm) down to the point of maximum on-shore flux ($z$ = -1.6 mm) inside the pick-up layer. From this point further down into the pickup layer, the point of maximum onshore flux shifts approximately 30° forward again. For the offshore flux, this behaviour is less pronounced, but there is a backward shift of 15 - 20 ° from $z$ = 4.2 mm tot $z$ = 0.9 mm and then a forward shift again of 20 - 25° until $z$ = -1.6 mm. The maximum erosion depth of the trough ($d_{et}$) of this condition is 2.0 mm, so no offshore flux is present below this level. The larger phase lag between the flow velocity and sediment concentration for fine sand conditions (see also Figures 4.9 and 4.10) causes a larger phase shift between the time-dependent fluxes at different $z$-levels. From $z$ = 6.2 mm to $z$ = -0.6 mm the moment of maximum onshore flux shift 45 - 50° backwards, after which it shifts approximately 55° forwards again to $z$ = -5.3 mm.

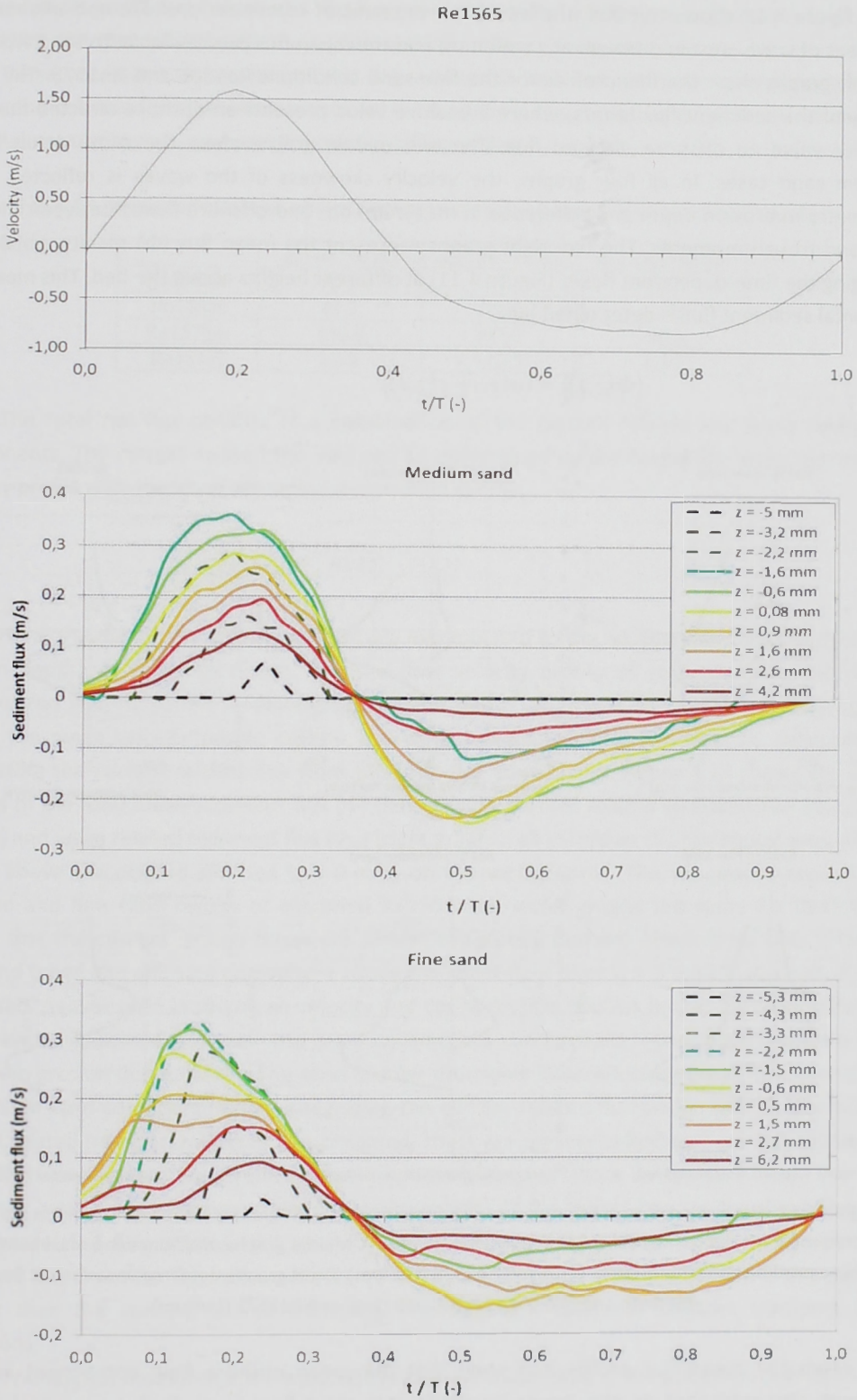


Figure 4.11. Measured ensemble averaged sediment fluxes at different levels inside the sheet flow layer for conditions Re1565, medium (middle graph) and fine (lowest graph) sand. The top graph presents the corresponding free stream velocity (measured at $z$ = 40 mm).

Figure 4.12 shows the flux profiles at the moment of maximum onshore and offshore flow (moment of wave crest and trough at $z$ = 40 mm) and the mean flux profiles for both sand types. The two left graphs show the flux profiles for the fine sand conditions Re1565 and Re1575. The X-axes represent the sediment flux in m/s, where a positive value presents an onshore directed flux and a negative value an offshore directed flux. The two middle graphs show the same result for the medium sand cases. In all four graphs, the velocity skewness of the waves is reflected by the asymmetry in erosion depth and difference in maximum on- and offshore fluxes between the wave crest and trough moments. The two right graphs represent the mean flux ($\Phi$) results, obtained by averaging the time-dependent fluxes (Figure 4.11) at different heights above the bed. This mean total horizontal sediment flux is determined by:

$$\langle \Phi(z,t) \rangle = \langle u(z,t) \cdot c(z,t) \rangle \tag{4.10}$$

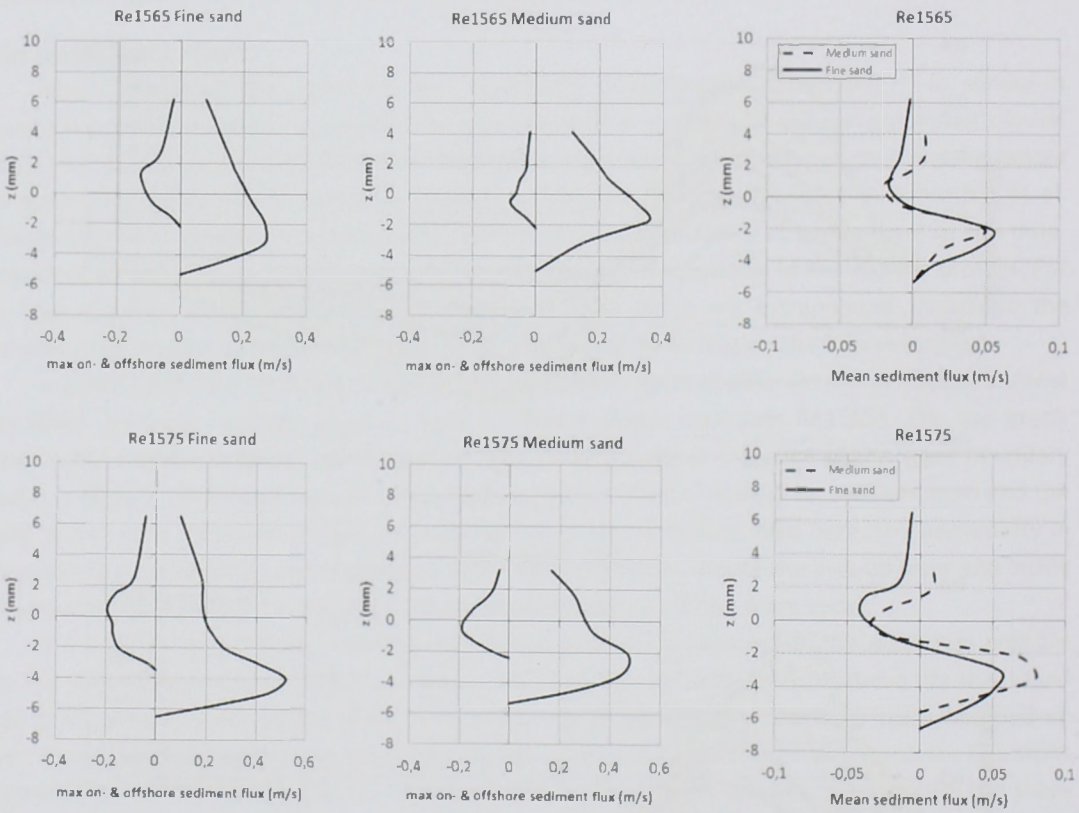


Figure 4.12. Vertical profiles of the measured sediment fluxes. Left graphs: fine sand maximum on- and offshore profile results for Re1565 (top) and Re1575 (bottom). Middle graphs: medium sand maximum on- and offshore profile results for Re1565 (top) and Re1575 (bottom). Right graphs: total mean sediment fluxes for medium and fine sand for Re1565 (top) and Re1575 (bottom).

From the mean flux profile it is seen that the mean onshore flow component and high sediment concentrations in the lower levels of the sheet-flow layer lead to an onshore flux component which is relatively large compared to the offshore fluxes at higher levels above the bed. This is seen for both the medium and fine sand conditions, which is in line with the concentration

profiles results presented before and the flow velocity results in Schretlen et al. (submitted). When integrating the mean flux profiles over the vertical, the net sand transport can be determined in $m^2/s$. These results are presented in Table 4.4, where the total net transport rates ($q_s$) are given in the second column. Positive values represent a net onshore flux, negative values a net offshore flux. The total net transport is onshore directed for all four cases.

Table 4.4. Measured total and current related transport and resulting wave related transport .

| | $q_s$ ($10^{-6}$ $m^2/s$) | $q_{s,c}$ ($10^{-6}$ $m^2/s$) | $q_{s,w}$ ($10^{-6}$ $m^2/s$) |
|---|---|---|---|
| Re1565m | 85.2 | 161.8 | -76.6 |
| Re1565f | 81.2 | 216.0 | -134.8 |
| Re1575m | 150.0 | 187.0 | -37.0 |
| Re1575f | 48.8 | 112.5 | -63.7 |

The total net flux consists of a combination of the current related and wave related flux components. The current related flux ($\Phi_c$) can be determined by combining the wave average flow velocity profile with the wave average concentration profile:

$$\langle \Phi_c(z) \rangle = \langle u(z) \rangle \cdot \langle c(z) \rangle \tag{4.11}$$

Here, the mean flow velocity profiles are extrapolated to the no-flow bed level (depending on erosion depth). In order to do so, first the flow velocity profile of each phase in the wave is extrapolated linearly to the instantaneous erosion depth, after that the profiles are averaged to obtain the mean velocity profile $<u(z)>$. The wave related flux ($\Phi_w$) can then be determined by subtracting the current related flux from the total flux component. Figure 4.13 shows the vertical profiles of the total mean sediment flux ($\Phi$) (left graphs), current related sediment flux ($\Phi_c$) (middle graphs) and wave related sediment flux ($\Phi_w$) (right graphs), all in m/s on the horizontal axes, with the height above the original still bed ($z$ = 0 mm) on the vertical axes. The top graphs represent the medium and fine sand results of condition Re1565, the lower graphs the same for Re1575. It is shown that the current related fluxes are almost completely onshore directed for both conditions and sand types, the offshore component above the sheet-flow layer ($z$ > 3 mm) is so small, it can be neglected. As was seen in the mean velocity and concentration profiles before, no large differences in behaviour appeared between the medium and fine sand results, apart from a slightly larger maximum erosion depth for the fine sand and for the higher flow velocities (Re1575) in comparison to medium sand conditions. When integrating the current related flux profile over the vertical, the current related transport rate in $m^2/s$ is obtained. These are presented in the 3$^{rd}$ column of Table 4.4.

The wave related flux profiles show a relatively large offshore component inside the sheet-flow layer, with a small onshore component above that. At the lowest level in the sheet-flow layer, the wave-related flux is (close to) zero. The 4$^{th}$ column in Table 4.4 gives the net wave-related transport rate in $m^2/s$. The net wave related transport is always negative (offshore directed), but smaller than the current related transport, resulting in a total net onshore transport for all conditions.

A number of measurement inaccuracies cause an uncertainty in the presented transport rates. The largest error is caused by the measurement of the z-level of the concentration and velocity measurements. This error is estimated to be 1 mm to both sides (up and down) at maximum. The flux profiles are recalculated with a shift of the flow velocity and concentration measurements of 2 mm in

relation to one another. The maximum error found in the transport rates when the z-levels are varied is 50 to 60 % to both sides. These relatively high numbers are due to the large gradients over height of the sediment concentration inside the whole sheet flow layer and flow velocity especially inside the pick-up layer. On top of that, the uncertainty of the velocity measurements was around ± 10% (see Schretlen et al., sumitted).

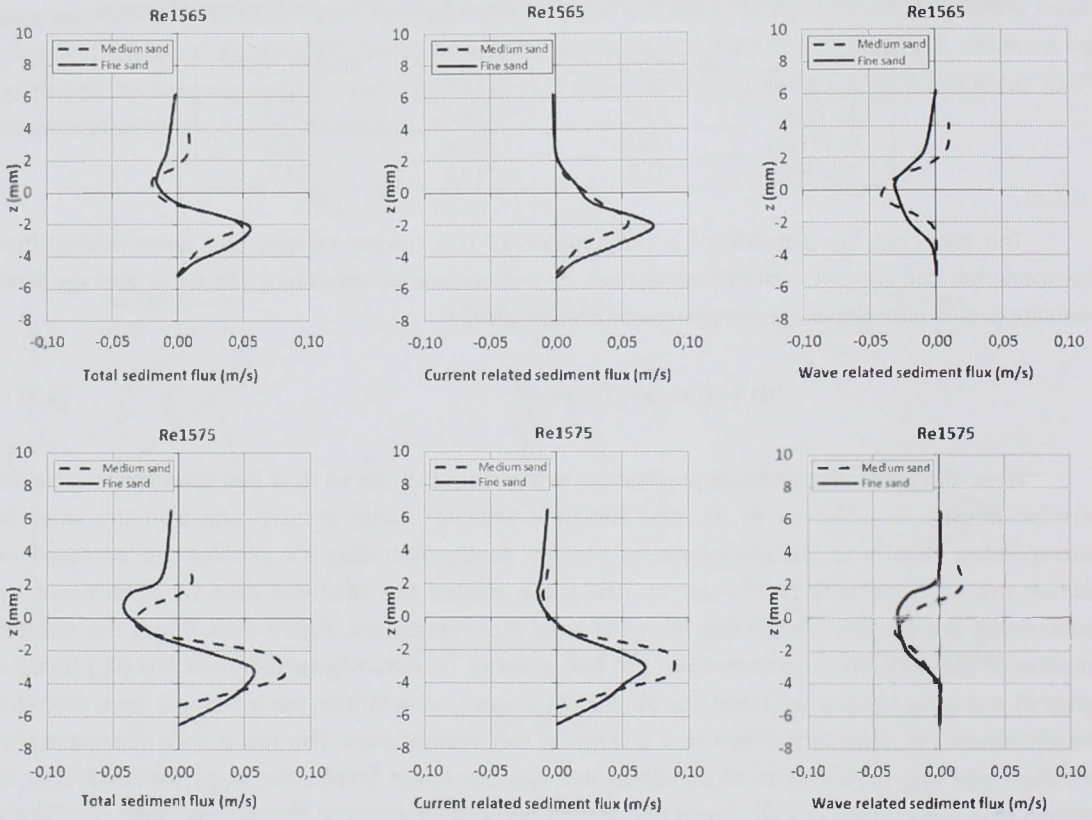


Figure 4.13. Vertical profiles of the measured total mean sediment flux (left graphs), current related sediment fluxes (middle graphs) and wave related sediment flux (right graphs) for both fine and medium sand conditions of the experiments Re1565 (top) and Re1575 (bottom).

As shown in Figures 4.12 and 4.13, the largest onshore part of the flux takes place in the lower levels of the sheet-flow layer (pick-up layer). Due to the velocity skewness (leading to differences in on- and offshore flow velocities and erosion depth asymmetry) there is only onshore movement of the sediment in the lowest levels of the pick-up layer (see also Schretlen et al., submitted). At the level above that (around $z$ = -2 mm), there is a shift from a net onshore flux towards a net offshore flux, followed by an offshore maximum in the upper sheet-flow layer ($0 < z < 1$ mm), followed by a fast decrease of the flux at levels $z > 2$ mm. The current related flux is concentrated in the pick-up layer, while the largest contribution of the wave-related flux is located around the transition from pick-up layer to upper sheet flow layer (around $z$ = 0 mm and slightly higher for fine sand than medium sand cases). Furthermore, it can be seen in Figures 4.12 and 4.13 that not only the onshore component inside the pick-up layer, but also the offshore component above the pick-up layer is larger for the Re1575 conditions than the Re1565 conditions. Here, the higher flow velocities (and

velocity skewness) generate more sediment being brought up in the upper sheet-flow layer and just above that. This was also shown by the UHCM results in Figure 4.6 and CCM results in Figure 4.7. For both fine sand conditions it can be seen that the erosion depth is larger and more sand is picked up than for the medium sand cases, but also more sand is brought (higher) in suspension, causing a larger off-shore flux component for the fine sand than for the medium sand conditions.

## 4.4 Sheet-flow layer concentration and fluxes under surface waves and in oscillatory flows.

In this section, the results of the new experiments are compared to existing knowledge from previous experiments (surface waves and oscillatory flow tunnels) and models.

Overall, the medium sand used in the new experiments can be considered similar to the medium sand of the GWK measurements described in e.g. Ribberink et al. (2000) and Dohmen-Janssen and Hanes (2002; 2005) or the oscillatory flow tunnel experiments of Ribberink and Al-Salem (1994, 1995) and O'Donoghue and Wright (2004a, 2004b); see Table 4.5. The fine sand is similar to the fine sand used in the oscillatory flow tunnel experiments of e.g. Ribberink and Chen (1993), O'Donoghue and Wright (2004a, 2004b) and Campbell et al. (2006), see also Table 4.5.

Table 4.5. Sediment conditions of the new and previous sheet-flow regime experiments

| | Medium sand | | | Fine sand | | |
|---|---|---|---|---|---|---|
| | $D_{10}$ (μm) | $D_{50}$ (μm) | $D_{90}$ (μm) | $D_{10}$ (μm) | $D_{50}$ (μm) | $D_{90}$ (μm) |
| New GWK experiments | 148 | 245 | 420 | 110 | 138 | 180 |
| Ribberink et al., 2000 | 170 | 240 | 280 | - | - | - |
| Ribberink & Al Salem 1994 | 150 | 210 | 320 | - | - | - |
| O'Donoghue & Wright 2004 | 170 | 270 | 390 | 100 | 130 | 170 |
| Campbell et al., 2006 | 170 | 270 | 390 | 100 | 150 | 170 |
| Ribberink & Chen, 1993 | - | - | - | 100 | 130 | 180 |

### 4.4.1 Time averaged suspended sediment concentration profiles

Various expressions are derived to describe suspended sediment concentrations (e.g. Smith, 1977; Fredsoe & Deigaard, 1992). Smith (1977) gives the following relation (based on the advection-diffusion equation) for the time-averaged concentration profile of suspended sediment:

$$\langle C(z) \rangle = C_a \left( \frac{z_a}{z} \right)^{\alpha} \tag{4.12}$$

Ribberink & Al-Salem (1994) found, based on oscillatory flow tunnel experiments, that this concentration distribution generally provides a good fit for suspended sediment above oscillatory sheet flow layers. The value of α is almost constant for a wide range of flow velocities; α = 2.1 (± 5%). Together with this, they derived an empirical relation for the reference concentration $C_a$ at a reference level $z_a$ of 10 mm above the bed:

$$C_a = a u_{rms}{}^{n} \tag{4.13}$$

with $n$ = 2.4 and $a$ = $4.26 \cdot 10^{-3}$ $(s/m)^{2.4}$. Since this relation is expected to change for the grain size (i.e. not valid for fine sand conditions), a comparison to the new experimental results is only done for the medium sand conditions. Figure 4.14 shows the results for three medium sand conditions; Re1565

with $u_{rms}$ = 0.87 m/s (circles); Re1265 with $u_{rms}$ = 0.80 m/s (crosses) and Re1575 with $u_{rms}$ = 0.71 m/s (diamonds). The calculated concentrations are presented by the lines. From the calculated results it can be seen that the results lie closely together, but the concentrations decrease with a decreasing $u_{rms}$. This pattern is less obvious in the experimental data due to some scatter of the data points. When comparing the data points to the calculated results, it can be concluded that under surface waves, the suspended concentrations are higher than under oscillatory flow tunnel conditions and the decrease of the concentration with height is much smaller (the further away from the bed, the larger the difference between the data points and calculated lines becomes). Closer to the bed, the differences between the concentrations under surface waves and in oscillatory flow tunnels is expected to be smaller, more details on this are presented later in this section. A similar comparison was made by Dohmen-Janssen & Hanes (2002) for lower $u_{rms}$ (≈ 0.6 m/s) and slightly different sand. The concentrations were lower for those cases, but they showed the same trend as found in the present tests.

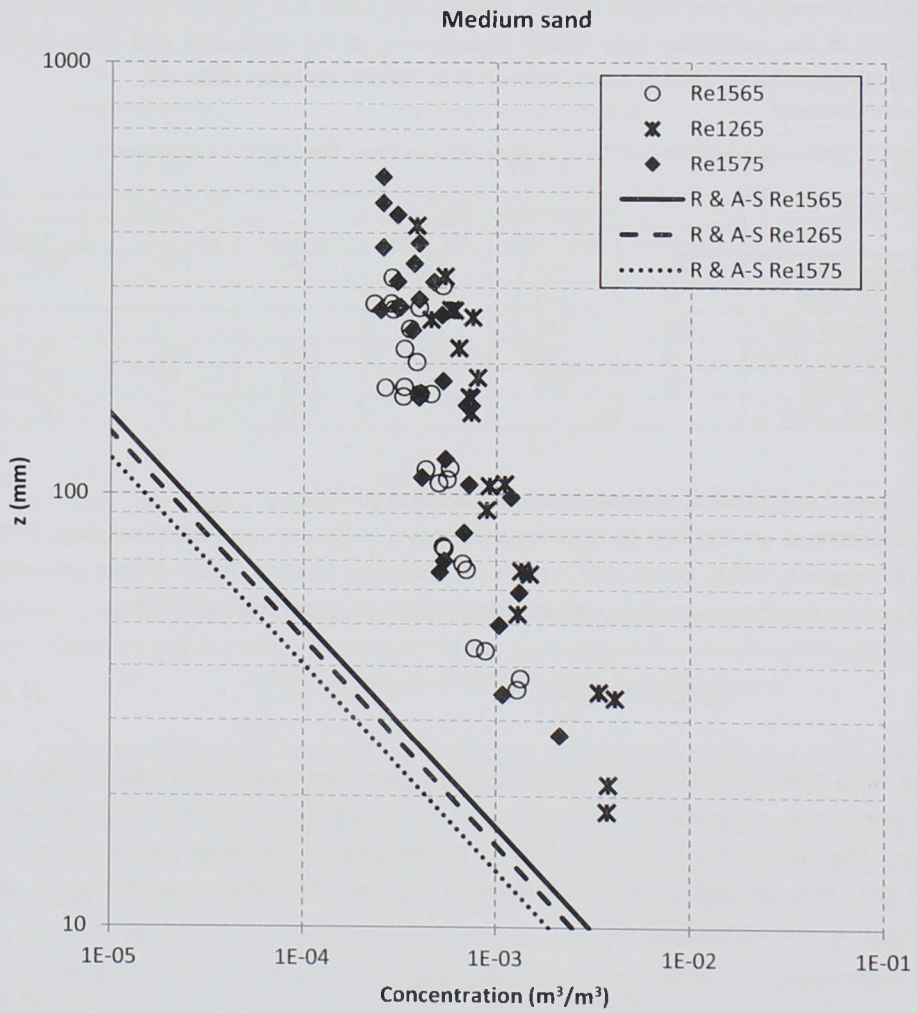


Figure 4.14. Measured suspended sediment profiles for medium sand conditions (Re1575, Re1565 and Re1265), compared to the empirical relation found by Ribberink & Al-Salem (1994) for oscillatory flow tunnel data.

### 4.4.2 Sheet-flow layer thickness

According to Dohmen-Janssen & Hanes (2002), the sheet flow layer thickness under full scale surface waves (with medium sand) is very similar to that found in oscillatory flow tunnels and is presented well by the empirical relation of Sumer et al. (1996) for steady flow. In Ribberink et al. (2008) it was shown that also the sheet flow layer thickness measured in oscillatory flow tunnels corresponds well with the relation of Sumer et al. (1996). Based on a large dataset Ribberink et al. (2008) give a linear relation for the sheet flow layer thickness and maximum Shields parameter $\theta_{max}$ under oscillatory flow conditions:

$$\frac{\delta_s}{D_{50}} = \beta\theta_{max} \qquad \text{with } \beta = 10.6 \qquad (4.14)$$

where $\theta_{max}$ is calculated with the equations 4.5 - 4.8. Figure 4.15 shows the relation between the measured dimensionless sheet flow layer thickness ($\delta_s/D_{50}$) and maximum Shields parameter ($\theta_{max}$) for the new surface wave experiments, in comparison with the relation given by Ribberink et al. (2008).

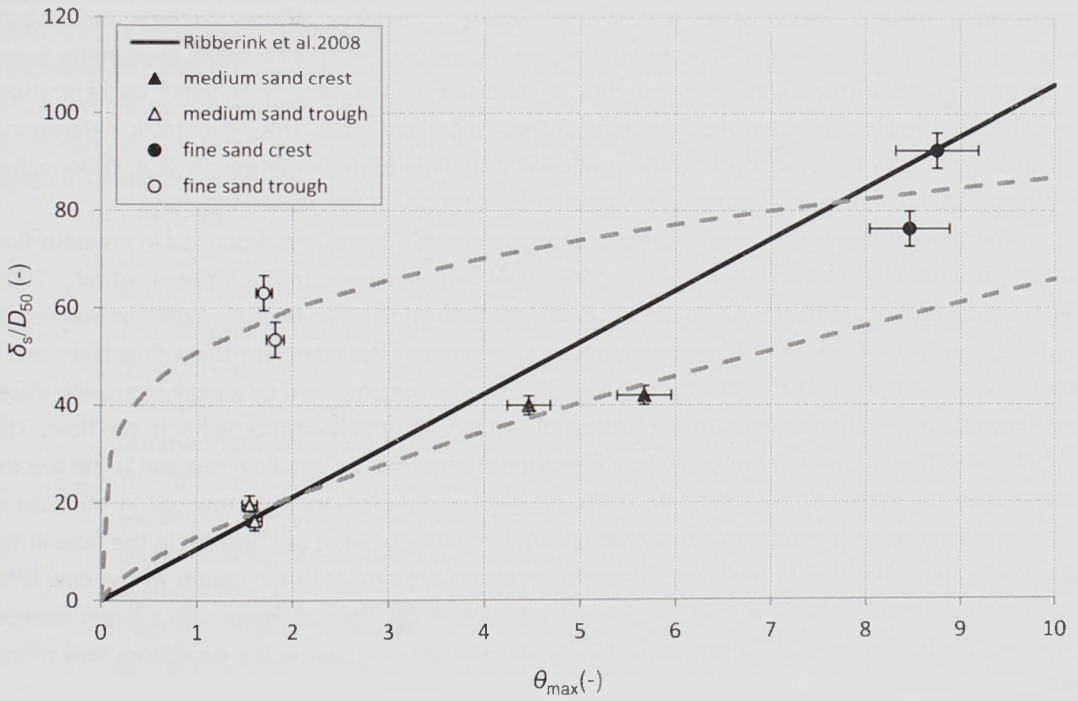


Figure 4.15. Non-dimensional sheet-flow layer thickness under wave crest and trough as function of the maximum Shields parameter for the Re1565 and Re1575 conditions with medium and fine sand (symbols). The solid line represents the Ribberink et al. (2008) function (Eq. 14).

In Figure 4.15 it can be seen that the relation of Ribberink et al. (2008) fits part of the data reasonably. There is some scatter, but more important, despite the fact that grain sizes are taken into account, the difference between the fine and medium sand results as described in Section 4.3.2 are not adequately represented by the model. The measured sheet-flow layer thickness is larger for

the fine sand cases than for medium sand (see also Table 4.2 and Figure 4.8). In particular for fine sand and small Shields parameter values, i.e. smaller flow velocities under the wave trough, the sheet flow layer thickness as observed under surface waves strongly exceeds the thickness under oscillatory flow conditions. Because of this, different empirical relations for fine and medium sand, such as Equation 4.9, are preferable. Similar behaviour (but with somewhat smaller differences) was found for the erosion depths ($d_e$), presented by Schretlen et al. (submitted).

### 4.4.3 Sheet-flow layer sediment concentrations

In a qualitative sense, the time-dependent concentration behaviour in the sheet flow layer, illustrated and described in Section 4.3.3, corresponds with the described behaviour and results from previous measurements in both oscillatory flow tunnels and under full scale surface waves (e.g. O'Donoghue & Wright, 2004a; Hassan & Ribberink, 2005; Dohmen-Janssen & Hanes, 2002).

The pattern of the pick-up layer and upper sheet flow layer and response of the sediment to flow velocities of the velocity skewed waves are similar to the behaviour described by those mentioned above. Ribberink et al. (2000) and Dohmen-Janssen & Hanes (2002) already concluded that for medium sand cases the behaviour of the sheet flow layer under waves is qualitatively similar to that in horizontal oscillatory flow tunnels. The present experiments have shown that the same cannot be concluded for fine sand cases. Similar to the results of the oscillatory flow tunnel experiments by e.g. O'Donoghue and Wright (2004a), unsteady effects become increasingly important as the percentage of fine sand in the bed increases. The erosion depth asymmetry found in the fine sand surface wave experiments is reflected in the time-dependent concentrations behaviour of the pick-up layer (middle graphs of Figures 4.9 and 4.10). This asymmetric behaviour is not seen in the pick-up layer concentrations of oscillatory flow tunnel experiments (e.g. O'Donoghue & Wright, 2004a), where no erosion depth asymmetry is found for fine sand conditions.

The short concentration peaks at flow reversal were also found and described in previous flow tunnel experiments (Ribberink & Chen, 1993; Dohmen-Janssen, 1999; McLean et al., 2001; O'Donoghue & Wright, 2004a). O'Donoghue & Wright (2004a) showed by their experimental results that the concentration peak at flow reversal occurs throughout the complete sheet flow layer and is most obvious at the top of the sheet flow layer. This peak is not matched by a peak in erosion depth and they relate this phenomenon to the settling of sediment from elevations higher in the flow. This is in line with the fact that in the oscillatory flow tunnel experiments, the flow reversal peaks are the strongest in the cases of fine sand and at the moment of on-offshore flow reversal in the case of velocity skewed waves; condition when relative large volumes of sand are present in the flow in the top of and above the sheet flow layer. These observations are similar to the results of the new GWK experiments. Thereby the flow reversal peaks are strongest for the condition with a larger velocity skewness (Re1575 over Re1565, see Table 4.1), which was also the case in the oscillatory flow tunnel experiments.

### 4.4.4 Sediment fluxes

Previously under large scale surface waves, only the sediment concentrations could be measured throughout the complete sheet-flow layer and the obtained data from flow velocities was limited to only part of the wave cycle (crest velocities) and/ or wave boundary layer (Ribberink et al., 2000, Dohmen-Janssen & Hanes, 2002, 2005). Therefore it was not possible to construct a complete flux profile throughout the sheet-flow layer under these conditions. However, in oscillatory flow tunnels it has been possible to obtain this flow velocity data throughout the wave boundary layer and various experimental results consisted of sheet-flow layer fluxes, e.g. Ribberink & Al-Salem

(1995), Dohmen-Janssen (1999), Dohmen-Janssen et al. (2001, 2002), McLean et al. (2001), Hassan (2003), Wright (2002), O'Donoghue & Wright (2004b). Two main conclusions from these experiments are that:

- The far majority of the sediment flux takes place inside the sheet-flow layer, even though suspended sediment is present above this layer.
- Phase-lag effects play a crucial role in the magnitude and direction of the flux, especially for conditions with fine sediment (small fall velocity), short wave periods and/or large sheet-flow layer thickness.

In Figure 4.16 flux results of the oscillatory flow tunnel experiments from O'Donoghue & Wright (2004b) and Wright (2002) are compared to the new surface wave results. The reason to take these oscillatory flow tunnel experiments (MA7515 and FA7515), is that these are available for sand types which are comparable to both the medium and fine sand of the new experiments (see Table 4.5) and their designed wave conditions of the asymmetric wave with period $T$ = 7.5 s is closest to one of the new experimental conditions presented in detail in this paper (Re1575). For more details on the similarities and differences between these conditions and resulting fluxes, see also Table 4.6. In Figure 4.16, the two left graphs show the fine sand maximum on- and offshore fluxes for the surface waves (top) and oscillatory flow tunnel (bottom), the middle graphs show the same for the medium sand cases and the right graphs the total mean fluxes for medium (dashed line) and fine (solid line) sand cases for the surface waves (top graphs) and oscillatory flow tunnel (bottom). The maximum on- and offshore fluxes from the oscillatory flow tunnel experiments are available in measurement points (Wright, 2002), these are copied here together with a best-fit curve. The total fluxes can also be found in O'Donoghue & Wright (2004b). The following can be concluded from Figure 4.16 and Table 4.6:

- The erosion depths and sheet-flow layer thicknesses are larger for the surface wave conditions, but so are the maximum flow velocities and Shields parameter, details on this are described previously in this paper and in Schretlen et al. (submitted).
- The maximum on- and offshore fluxes and the total net fluxes, and with that the transport rates, are larger under surface waves than under similar oscillatory flow conditions. The larger transport rates were also found by Ribberink et al. (2000) and Dohmen-Janssen & Hanes (2002, 2005) for the medium sand conditions.
- The fine sand fluxes are not only larger, but also in the onshore direction, whereas the oscillatory flow tunnel results show a net offshore flux for these conditions.
- Under oscillatory flow tunnel conditions, the erosion depth asymmetry, generated by the asymmetry in flow velocity, is present under medium sand conditions, but not under fine sand conditions. O'Donoghue and Wright (2004b) and Ribberink et al. (2008) suggest that this is due to the phase-lag effects, which have a larger impact in the case of fine sand (smaller fall velocity). In the new experiments it is found that under surface wave conditions, the erosion depth asymmetry is also present in the case of fine sand (see also the Schretlen et al., submitted for more details). This strongly affects the shape of the maximum onshore, offshore and mean flux profiles (see also section 4.3.4 for more details). Especially the large positive mean flux in the pick-up layer is directly caused by erosion depth asymmetry for medium and fine sand.

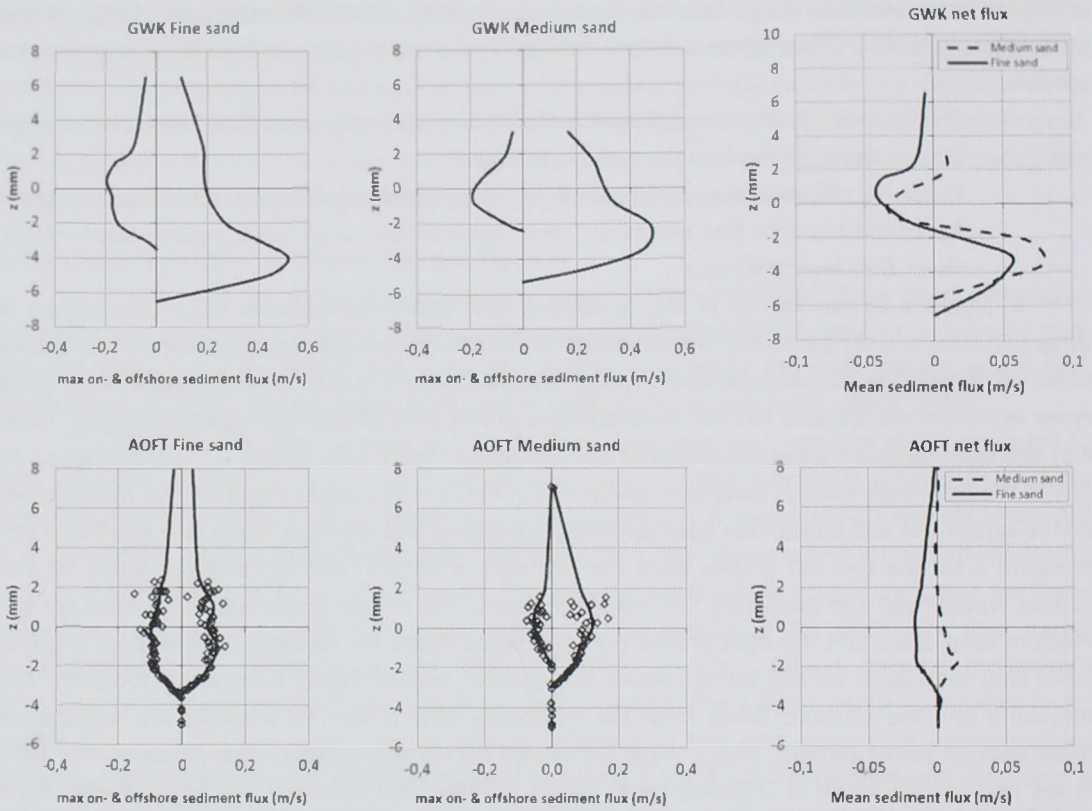


Figure 4.16. Vertical profiles of sediment fluxes, measured in GWK (Re1575, top graphs) and AOFT (A7515, bottom graphs) . Left graphs: fine sand maximum on- and offshore profiles results. Middle graphs: medium sand maximum on- and offshore profiles. Right graphs: total mean sediment fluxes for medium and fine sand.

Table 4.6. Comparison of GWK (Re1575m, Re1575f) and AOFT (MA7515, FA7515) flux results

| | $T$ (s) | $A$ (m) | $U_{max}$ (m/s) | $R$ (-) | $U_{rms}$ (m/s) | $\theta_m$ (-) | $d_e$ (mm) | $\delta_s$ (mm) | $q_N$ ($10^{-6}$ m$^2$/s) |
|---|---|---|---|---|---|---|---|---|---|
| Re1575m | 7.5 | 1.95 | 1.63 | 0.69 | 0.75 | 5.67 | 5.3 | 10.3 | 150.0 |
| Re1575f | 7.5 | 2.03 | 1.70 | 0.71 | 0.79 | 8.75 | 6.5 | 12.8 | 48.8 |
| MA7515 | 7.5 | 1.5 | 1.53 | 0.63 | 0.89 | 2.2 | 3.4 | 8.9 | 36 |
| FA7515 | 7.5 | 1.5 | 1.53 | 0.63 | 0.89 | 3.6 | 4.2 | 10.9 | -88 |

Ribberink et al. (2008) show that when the current-related flux and total mean flux of oscillatory flow tunnel experiments are compared, the current related flux has a dominant contribution to the total net transport rate, with positive values for the medium sand and negative values for the fine sand conditions. The current related flux seems to be dominated by the mean horizontal particle motion in the pick-up layer. In Figure 4.12 it can be seen that the wave-related flux in the new surface wave experiments, is of the same order of magnitude as the current-related flux and thus strongly affects the shape and magnitude of the total mean flux profile.

## 4.5 Conclusions

New experiments were carried out in the GWK wave channel under full scale non-breaking surface waves above a horizontal mobile sand bed in the sheet flow regime. These measurements were focused on the behaviour of sediment concentrations and sediment fluxes close to the bed, inside the wave boundary layer where the vast majority of the sand transport occurs. The

experiments give new, more detailed insights in the time-dependent and time averaged behaviour of sediment concentrations and fluxes inside the sheet flow layer for medium sand and, for the first time, fine sand conditions.

For both medium and fine sand, the maxima (crest and trough) and total mean sediment transport rates are concentrated inside the sheet flow layer. Above this layer and the wave boundary layer, there is sediment being moved in suspension, but the volume concentrations are too small to be of any significance to the total and time-dependent transport rates.

For fine sand conditions, more sand is being brought into motion, leading to a larger erosion depth and sheet-flow layer thickness than for medium sand conditions under similar wave conditions. Based on the measurements with both sand types, new empirical relations were presented for the erosion depth (Schretlen et al., submitted) and sheet flow layer thickness.

Velocity skewness leads to erosion depth asymmetry ($d_{e,crest} > d_{e,trough}$) for both sand types. Due to this, in the lowest levels of the pick-up layer the sediment is only transported during the onshore part of the wave cycle. This velocity skewness generates larger onshore than offshore fluxes and for all experiments (for both fine and medium sand) the total mean transport rates are directed onshore.

The total horizontal mean sediment flux shows a similar two-layer structure for both sand types; an onshore directed flux deep inside the pick-up layer and a (smaller) offshore directed flux above that. Due to the erosion depth asymmetry the onshore directed part of the total mean flux is highest in the lower parts of the pick-up layer. The highest offshore directed part of the total mean flux consist of a large wave-related part and a smaller (onshore directed) current-related part. The negative wave-related part is caused by an increase and decrease of pick-up layer concentrations during respectively positive onshore and negative offshore-directed velocities in the wave cycle ($< \tilde{u}\,\tilde{c} > <0$). The positive onshore-directed part of the mean flow (streaming) in the lower part of the wave boundary layer strongly contributes to the positive net transport rates inside the sheet flow layer.

Around the original bed level ($z$ = 0 mm) the sediment flux is more or less in phase with the free-stream flow velocities. Higher in the (upper) sheet flow layer and lower inside the pick-up layer the sediment fluxes show a lag in comparison to the free-stream velocities, caused by: i) delayed erosion of the sand bed (pick-up layer) and ii) the time necessary to entrain the sediment grains to a higher level.

For medium sand conditions, the behaviour of the measured sheet-flow layer processes is comparable to that found under oscillatory flow tunnel (OFT) conditions. The measured sediment fluxes of medium sand are larger than those of oscillatory flow tunnel experiments with comparable flow conditions. The direction of the total mean flux is, comparable to oscillatory flow tunnel results, onshore.

For fine sand conditions, some large differences between the surface wave and OFT results were found: i) the erosion depth is larger under surface waves, ii) under the wave trough sediment is entrained higher under surface waves and iii) erosion depth asymmetry is also found for fine sand conditions, which is not the case for comparable flows in OFTs. The maximum onshore and offshore fluxes are not only larger, but the total mean flux under progressive surface waves is positive and onshore directed instead of negative and offshore directed as found in OFTs. This is related to the measured erosion depth asymmetry which is not present for fine sand cases in OFTs. The research does not give a clear cause for these differences. It is likely that intra-wave advection processes of momentum and sediment (i.e. real wave streaming) which are not present in OFTs play a role here (see Kranenburg et al., 2010).

## References


Bosman, J.J., E.T.J.M. Van der Velden and C.H. Hulsbergen, 1987. Sediment concentration measurement by transverse suction. *Coastal Engineering* 11, 353-370.

Campbell, L., T. O'Donoghue and J.S. Ribberink. 2006. Wave boundary layer velocities in oscillatory sheet flow. *Proceedings of 30th International Conference on Coastal Engineering*, ASCE, 2207-2219.

Dibajnia, M. and A. Watanabe, 1992. Sheet flow under non-linear waves and currents. *Proceedings of the 23rd International Conference on Coastal Engineering*, Venice, Italy, pp. 2015-2028.

Dibajnia, M. and A. Watanabe. 1998. Transport rate under irregular sheet flow conditions. *Coastal Engineering*, 35, 167-183.

Dohmen-Janssen, C.M. 1999. Grain size influence on sediment transport in oscillatory sheet flow – phase lags and mobile-bed effect. *PhD-thesis*, Delft University of technology Delft, The Netherlands. 246 pp.

Dohmen-Janssen, C.M., W.N. Hassan and J.S. Ribberink. 2001. Mobile-bed effects in oscillatory sheet flow. *Journal of Geophysical Research*, 106 (C11), 27103 – 27115.

Dohmen-Janssen, C.M., D.F. Kroekenstoel, W.N. Hassan and J.S. Ribberink, 2002. Phase lags in oscillatory sheet flow: experiments and bed load modelling. *Coastal Engineering*, 46, 61 – 87.

Dohmen-Janssen, C.M. and D.M. Hanes. 2002. Sheet flow dynamics under monochromatic nonbreaking waves. *Journal of Geophysical Research*, 107(C10), 3149.

Dohmen-Janssen, C.M. and D.M. Hanes. 2005. Sheet flow and suspended sediment due to wave groups in a large wave flume. *Continental Shelf Research*, 25, 333 – 347.

Eekhout, J.P.C. 2008. Measurements and modelling of cross-shore morphodynamics. MSc Thesis, University of Twente, The Netherlands.

Fredsøe J. and R. Deigaard. 1992. Mechanics of coastal sediment transport. *Advanced Series on Coastal Engineering, 3.* World Scientific Publishing Co. Pte. Ltd., Singapore, 369 pp.

Gonzalez-Rodriguez, D. and O.S. Madsen. 2011. Boundary-layer hydrodynamics and bedload sediment transport in oscillating water tunnels. *J. Fluid Mech.*, Vol. 667, pp 48 - 84

Hassan W.N., 2003. Transport of size-graded and uniform sediments under oscillatory sheet-flow conditions. *PhD-thesis*, University of Twente, The Netherlands.

Hassan, W.N. and J.S. Ribberink, 2005. Transport processes of uniform and mixed sands in oscillatory sheet flow. *Coastal Engineering* 52, 745-770.

Huisman C., M.G. Kleinhans, B.G. Ruessink and M. Zuijderwijk,2009. Sediment concentrations from ABS measurements. *HYDRALAB - SANDS report*, Utrecht University, Faculty of Geosciences, Department of Physical Geography, The Netherlands.

Jensen, B.L., B.M. Sumer and J. Fredsøe. 1989. Turbulent oscillatory boundary layers at high Reynolds numbers. *Journal of Fluid Mechanics.*, 116, 265 – 297.

Jonsson, I.G. 1966. Wave boundary layer and friction factors. *Proceedings of 10th International Conference on Coastal Engineering*, 127 - 148.

Jonsson, I.G. 1980. A new approach to oscillatory rough turbulent boundary layers. *Ocean Engineering* 7, 109-152.

Kleinhans, M.G., 1998. Kalibratie van de valbuis Fysische Geografie Utrecht. *Tech. Rep., Netherlands Centre for Geo-ecological Research / Utrecht University Physical Geography*. ICG 98/13.

Kranenburg, W.M. , J.S. Ribberink and R.E. Uittenbogaard. 2010. Sand transport by surface waves: can streaming explain the onshore transport?, *Proceedings of 32nd International Conference on Coastal Engineering*, Shanghai, China.

McLean, S.R., J.S. Ribberink, C.M. Dohmen-Janssen and W.N. Hassan. 2001. Sand transport in oscillatory sheet flow with mean current. *Journal of Waterway, Port, Coastal and Ocean Engineering,* 127(3): 141-151.

O'Donoghue, T. and S. Wright. 2004a. Concentrations in oscillatory sheet flow for well sorted and graded sands. *Coastal Engineering*, 50, 117-138.

O'Donoghue, T. and S. Wright. 2004b. Flow tunnel measurements of velocities and sand flux in oscillatory sheet flow for well sorted and graded sands. *Coastal Engineering*, 51, 1163-1184.

O'Donoghue, T., J.S. Doucette, J.J. van der Werf and J.S. Ribberink. 2006. The dimensions of sand ripples in full-scale oscillatory flows. *Coastal Engineering*, 53, 997-1012.

Ribberink, J.S. and Z.W. Chen. 1993. Sediment transport of fine sand under asymmetric oscillatory flow. *Delft Hydraulics*, Report H840, Part VII, January. Delft, The Netherlands.

Ribberink, J.S. and A.A. Al-Salem. 1994. Sediment transport in oscillatory boundary layers in cases of rippled beds and sheet flow. *Journal of geophysical Research,* 99(C6), 12707-12727.

Ribberink, J.S. and A.A. Al-Salem. 1995. Sheet flow and suspension of sand in oscillatory boundary layers. *Coastal Engineering*, 25, 205 – 225.

Ribberink, J.S. 1998. Bed-load transport for steady flows and unsteady oscillatory flows. *Coastal Engineering*, 34, 59-82.

Ribberink, J.S., C.M. Dohmen-Janssen, D.M. Hanes, S.R. McLean and C. Vincent. 2000. Near-bed sand transport mechanics under waves – A large-scale flume experiment (Sistex99). *Proceedings of 27th International Conference on Coastal Engineering*, ASCE, 3263-3276.

Ribberink, J.S., J.J. van der Werf and T. O'Donoghue. 2008. Sand motion induced by oscillatory flows; sheet flow and vortex ripples. Journal of Turbulence, special issue on 'Particle-laden flow, from geophysical to Kolmogorov scales'. Euromech colloquim 477. Enschede, The Netherlands.

Schretlen, J.L.M., J.J. van der Werf, J.S. Ribberink, M. Kleinhans, W.M. Zuijderwijk and T. O'Donoghue. 2008. New high-resolution measurements of wave boundary layer flow under full-scale surface waves. *Proceedings of 31st International Conference on Coastal Engineering*, Hamburg, Germany.

Schretlen, J.L.M., J.S. Ribberink and T. O'Donoghue. 2009. Sand transport under full scale surface waves. *Proceedings of the Coastal Dynamics 2009 Impacts of human activities on dynamic coastal processes.* Tokyo, Japan.

Schretlen, J.L.M., J.S. Ribberink and T. O'Donoghue. 2010. Boundary layer flow and sand transport under full scale surface waves. *Proceedings of 32st International Conference on Coastal Engineering,* Shanghai, China.

Schretlen, J.L.M., J.S. Ribberink and T. O'Donoghue. Submitted. Boundary layer velocities measured above mobile beds under full scale progressive surface waves.

Silva, P.A., T. Abreu, H. Michallet, D. Hurther and F. Sano. 2009. Sheet flow layer structure under oscillatory flows. *Proceedings of the 6th IAHR River, Coastal and Estuarine Morphodynamics*, Santa Fe, Argentine, pp. 1057 – 1062.

Smith, J.D. 1977. Modelling of sediment transport on continental shelves. In: The Sea, volume 6, pp. 539 – 577, ed. by E.D. Goldberg et al., Wiley-Interscience, New York.

Sumer, B.M., A. Kozakiewicz, J. Fredsøe and R. Deigaard, 1996. Velocity and concentration profiles in sheet-flow layer of movable bed. *Journal of Fluid Mechanics* 182, 369-409.

Swart, D.H. 1974. Offshore sediment transport and equilibrium beach profiles. Delft Hydraulics Lab Publ No. 131.

Van der Werf, J.J. 2006. Sand transport over rippled beds in oscillatory flow. Ph.D. thesis, University of Twente, The Netherlands.

Van Rijn, L.C. 2007. Unified view of sediment transport by currents and waves I: Initiation of motion, bed roughness and bed-load transport. *Journal of Hydraulic Engineering*, 133(6), 649 – 667.

Wright, S. 2002. Well-sorted and graded sands in oscillatory sheet-flow. *PhD thesis*, Department of Engineering, University of Aberdeen, Aberdeen, UK.

Wright, S. and T. O'Donoghue. 2002. Total sediment transport rate predictions in wave current sheet flow with graded sand. Oscillatory flow tunnel experiments at Aberdeen University. *Experimental report EPSRC "LUBA" Project*. University of Aberdeen, UK.

# 5. SAND TRANSPORT RATES UNDER FULL SCALE SURFACE WAVES

**Abstract**

Many models developed to predict transport rates initiated by waves consist of (semi-) empirical formulas based on experimental data from oscillatory flow tunnel experiments. However, from previous research (e.g. Dohmen-Janssen & Hanes, 2002) it was concluded that surface wave effects may have a significant effect on the sand transport rates under sheet-flow conditions. In this paper, total net sand transport rates, measured under full scale surface waves are presented. The new transport data presented here i) are a valuable extension to the existing medium sand surface wave measurements (the amount of available data is more than doubled) and ii) give, apart from medium sand results ($D_{50}$ = 245 μm ) for the first time transport rates under full scale surface waves with a fine sand ($D_{50}$ = 138 μm ) mobile bed. These new results are compared to existing data and to two existing practical sand transport models (Nielsen, 2006 and Van Rijn, 2007), both quasi-steady empirical models that use different approaches to account for surface wave streaming effects. Finally, a new practical sand transport model which is recently developed (SANTOSS model) is described and compared to the data for surface waves. The new experiments show a linear increase in transport rates with an increase in the third-order moment of the time-dependent velocity in the free stream, for both the medium and fine sand. The transition from onshore to offshore net transport with increasing flow strength, as measured for fine sand conditions in oscillatory flow tunnels, is not observed under surface waves. This can probably be explained by the fact that phase lag effects of fine sand, responsible for the transition to offshore net transport, are now overruled by the presence of the positive mean flow and/or by intra-wave sediment advection effects. It is shown that the addition of individual surface wave processes in the semi-unsteady SANTOSS model, together with the large range of conditions for which the model is developed, make the model in principle better applicable for transport rate predictions than the other two models tested here.

## 5.1 Introduction

Most research aimed at the (natural) evaluation of coastal areas is in one way or another connected to sediment transport. Many models developed to predict transport rates initiated by waves, consist of (semi-) empirical formulas based on experimental data (e.g. Bailard, 1981; Dibajnia & Watanabe; 1992; Ribberink, 1998; Nielsen, 2006; Van der Werf, 2006; Van Rijn, 2007). The far majority of this data is obtained from oscillatory flow tunnel experiments. From previous research (e.g. Dohmen-Janssen & Hanes, 2002) it was concluded that the behaviour of the sheet flow layer under waves is qualitatively similar to that in horizontal flows. However, the boundary layer flow velocities and with that the sediment fluxes are found to be different in oscillatory flow tunnel and surface wave conditions (Ribberink et al., 2000; Dohmen-Janssen & Hanes, 2002; Schretlen et al., 2009, 2010, submitted, in progress). Ribberink et al. (2000) and Dohmen-Janssen & Hanes (2002) showed that the total net transport rates under surface waves show a linear relation with the third power of the flow velocity above the boundary layer, similar to transport rates in oscillatory flow tunnels, but the magnitudes of the transport rates under waves are approximately 2.5 times larger than found in oscillatory flow tunnels.

Research both in oscillatory flow tunnels (Dohmen-Janssen et al., 2001; McLean et al., 2001, O'Donoghue & Wright, 2004a; 2004b, Ribberink et al., 2008) and under full scale surface waves (Dohmen-Janssen & Hanes, 2002; Ribberink et al., 2008; Schretlen et al., in progress) has shown that under sheet-flow conditions, the far majority of sand is transported inside the sheet-flow layer. This would mean that the contribution of suspended sediment can be neglected in the total net transport rates and sheet flow layer / boundary layer flow processes play an important role. The hypothesis was given that the small onshore directed boundary layer streaming, present under surface waves but absent in oscillatory flow tunnels (Schretlen et al., submitted), may be held accountable for the (large) onshore directed transport under surface waves. The new flux measurements as described in Schretlen et al. (in progress) confirm this view for medium sand cases. For fine sand conditions the

total net fluxes inside the sheet flow layer also indicate an onshore directed transport. This is opposite to fine sand results found in oscillatory flow tunnels, where phase-lag effects were found to be dominant and a net offshore transport for fine sand conditions is observed (see e.g. Ribberink & Chen, 1993; O'Donoghue & Wright, 2004b).

In this paper, total net sand transport rates, measured independently from the detailed flow velocity and sand concentration measurements shown in Chapter 3 and 4 of this thesis (see also Schretlen et al., submitted; in progress), are presented and compared to those sheet-flow layer fluxes. The new transport data presented here i) are a valuable extension to the existing medium sand surface wave measurements (the amount of available data is more than doubled) and ii) give for the first time transport rates under full scale surface waves with a fine sand mobile bed. The main research question of this paper is whether the (small-scale) surface wave effects, found inside the wave boundary and sheet-flow layer may have a dominant effect on the total sand transport rates.

These new results are compared to existing data and to two existing practical sand transport models (Nielsen, 2006 and Van Rijn, 2007) that use different approaches to account for surface wave streaming effects. The theoretical background of these models is described as well.

Finally, a new practical sand transport model which is recently developed ( SANTOSS model, see: Van der Werf, 2007; Ribberink et al., 2010; Van der A et al., 2010) is described and compared to the data for surface waves. It is shown how the results of the new experiments contributed to the implementation of surface wave effects into this new transport formula and how this transport model performs in comparison to the existing ones.

## 5.2 Methodology and experimental set-up

### 5.2.1 Experimental set-up

The experiments were carried out in the large wave flume, or Groβer Wellenkanal (GWK), of the Coastal Research Centre in Hannover, Germany, a joined research facility of the University of Hannover and the Technical University of Braunschweig. The flume has a length of 280 m and is 5 m wide and 7 m deep. In this flume, regular and irregular waves with heights from 0.5 to 2.5 m and periods of 2 to 15 s can be generated. An online absorption system for preclusion of re-reflection is present at the wave generator.

Figure 5.1 shows an overview of the flume with the wave paddle on the left and an artificial beach on the right. For the three different measurement campaigns (2007, 2008 I, 2008 II), two different sand bed configurations were used. The sand bed, as shown in the top image of Figure 5.1, was used for the experiments with medium sand (2007 and 2008 II campaigns). A 1 m thick horizontal sand bed was placed from approximately 50 to 175 m from the wave paddle, with a 1:20 sand beach following at the far end (175 to 280 m from the wave paddle). For the experiments with fine sand (2008 I campaign, lower image Figure 5.1), the horizontal part of the medium sand profile was replaced with a 0.85 m thick fine sand bed, placed from approximately 50 to 170 m from the wave paddle. From approximately 200 m from the wave paddle, a 1:15 beach slope was now used to optimize wave absorption at the beach slope. By breaking up the total profile and assuring that no fine sand was transported beyond this point by the waves, the net sand transport measurements could be performed more accurately than with a sand profile over the total length of the flume. For practical reasons it was not possible to place the profile with the medium sand in a similar way. More detail on the sand types is given in section 5.2.2 of this paper.

The water level in the flume was 4.5 m above the flume bottom during the medium sand experiments and 4.35 m during the fine sand experiments, leading to 3.5 m water depth above both

initial horizontal sand beds. The dashed vertical line in Figure 5.1 indicates the position of the instruments used for detailed velocity and concentration measurements (approximately 110 m from the wave paddle). A detailed description of these instruments and the measurements is given in the previous two Chapters. This Chapter focuses on the net sand transport measurements. Details on the instruments and methodology used for these measurements are presented in the next section.

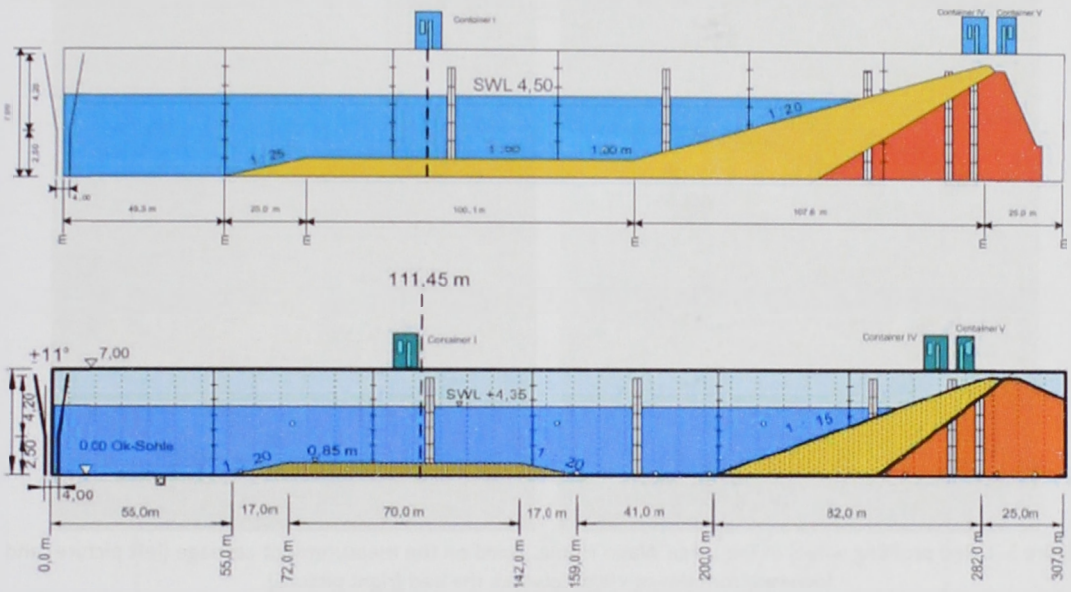


Figure 5.1. Overview of the Large Wave Flume of the Coastal Research Centre, Hannover, Germany.

### 5.2.2 Measuring instruments and experimental conditions

To be able to determine the net sand transport rates of the various wave conditions, detailed knowledge of sand bed (level) changes is essential. Before and after each wave run, bed level profiles were measured over the whole length of the flume. By applying the mass conservation principle to these measured profiles, the net sand transport rates from one or more wave runs could be obtained. This concept was used successfully before in oscillatory flow tunnels and in the same flume and described by e.g. Dohmen-Janssen (1999) and Dohmen-Janssen & Hanes (2002).

The bed level changes due to the waves were measured with two different techniques. In one campaign (2007), a bed level profiling wheel was used to obtain bed level profiles and in the other two campaigns (2008 I and 2008 II) echosounders were used to record the sand bed over the length of the flume. Figure 5.2 shows the GWK bed profiling wheel. The wheel is connected to the measurements carriage, which is moved along the flume's length in the middle of the flume. The wheel is then lowered towards the sand bed (right picture of Figure 5.2). The knowledge of the position of the carriage along the flume (through measurement of the rotation of one of the wheels of the carriage) and the vertical position of the wheel (obtained through the known relation between vertical distance and angle of the wheel frame) lead to a profile of the sediment bed along the flume. The advantage of this technique is that it can be applied with and without water present. Therefore, also the part of the profile above the still-water line, which was influenced by wave run-up can be measured. The disadvantage is that only one profile in the middle of the flume is measured. Any sand displacement across the profile can therefore not be accounted for. Even though only one profile

over the width was made, the results compare well to the results of the echosounders (see below for description) and previous measurements (Ribberink et al., 2000 and Dohmen-Janssen & Hanes, 2002). Especially for the flat bed, sheet flow conditions, there appeared to be little variation in the bed over the width of the flume.

Figure 5.2. Bed profiling wheel of the Large Wave Flume. Fixed on the measurement carriage (left picture) and lowered from the carriage towards the bed (right picture).

In both 2008 measurement campaigns (medium and fine sand conditions), the system of the profiling wheel was replaced by a system with echosounders (from Utrecht University). Two echosounders (1 MHz ultrasound) are attached at different lateral positions to the movable measurement carriage. When moving the carriage along the flume, two profiles are measured simultaneously. In total four bed level profiles, divided across the flume, are measured before and after each wave run (two times 2 echosounders). Figure 5.3 shows a cross-section of the flume (scale 1:40), with the position of the echosounders in red (0.625 m from the flume walls and 1.25 m from one another). Below that the measurement frame with instruments for the flow velocity and sediment concentration measurements and the sand bed with CCM-tank are visible. The latter are described in detail in Chapters 3 and 4. The vertical and horizontal accuracy of the echosounders is in the order of 1 cm. The echosounders can only be used if positioned under water. Therefore, the small section of the beach above medium water level cannot be taken into account. For the fine sand measurements, this doesn't influence the transport rate measurements, since these are calculated only over the horizontal fine sand bed section (see Figure 5.1b). For the medium sand the influence of this small section of the beach appeared to be negligible.

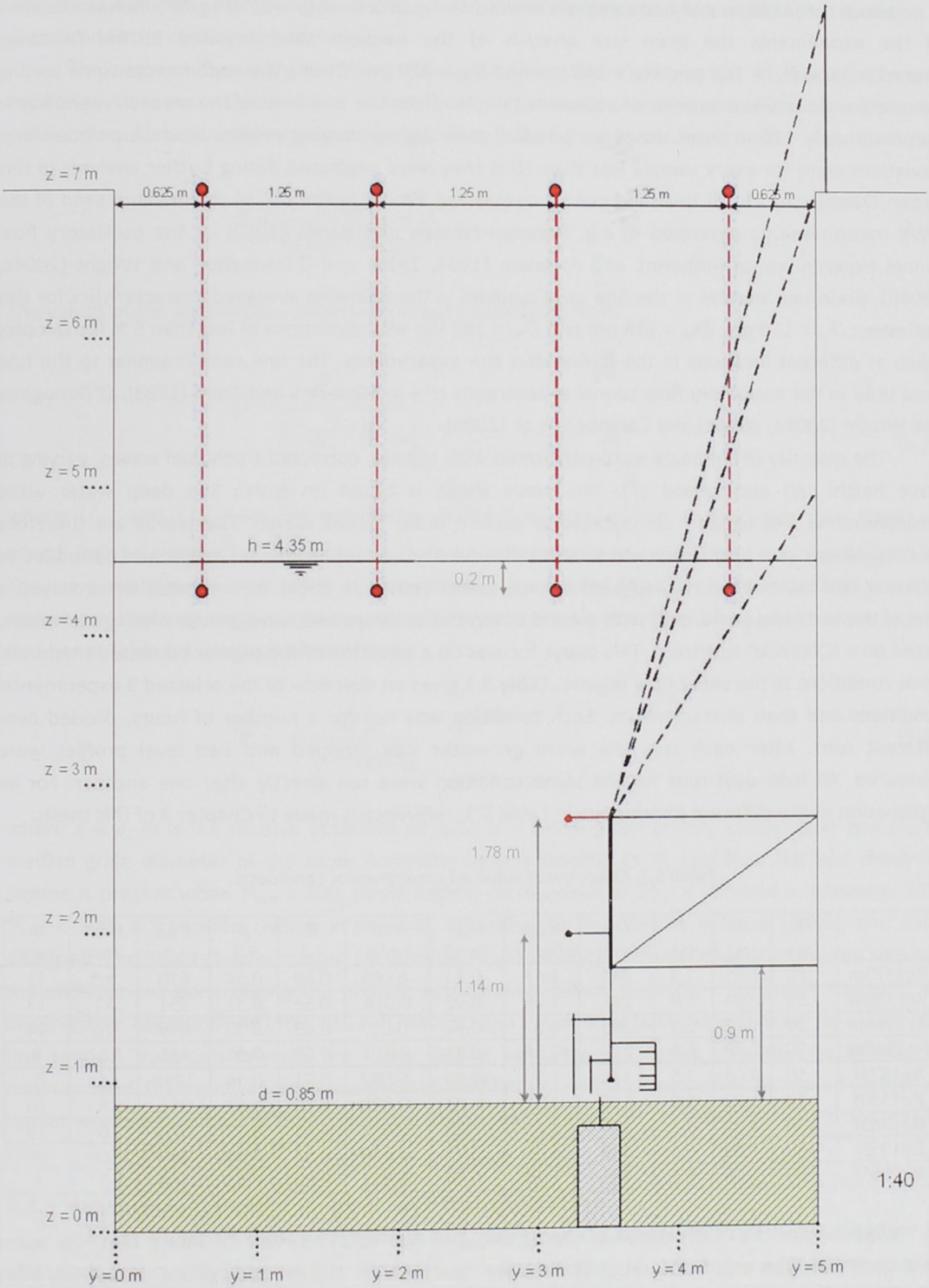


Figure 5.3 Cross section (scale 1:40) of the large wave channel (GWK) with the position of the echosounders in red, the measurement frame and sand bed with buried CCM-tank.

Both the medium and fine sands are well sorted quartz sand ($\rho$ = 2650 kg/m$^3$). Before the start of the experiments the grain size analysis of the medium sand resulted in the following characteristics; $D_{10}$ = 148 μm, $D_{50}$ = 245 μm and $D_{90}$ = 420 μm. During the experiments some sorting occurred and the sieve analysis of sediment samples from the bed around the measurement frame (approximately 110 m from the wave paddle) gave slightly varying results. However, since these deviations were for every sample less than 10 % they were neglected during further analyses in this paper. Overall, the $D_{50}$ of this sand can be considered similar to the $D_{50}$ of the medium sand of the GWK measurements described in e.g. Dohmen-Janssen and Hanes (2002) or the oscillatory flow tunnel experiments of Ribberink and Al-Salem (1994, 1995) and O'Donoghue and Wright (2004a, 2004b). Grain size analysis of the fine sand resulted in the following averaged characteristics for this sediment: $D_{10}$ = 110 μm, $D_{50}$ = 138 μm and $D_{90}$ = 180 μm with deviations of less than 5 % for samples taken at different locations in the flume after the experiments. The fine sand is similar to the fine sand used in the oscillatory flow tunnel experiments of e.g. Ribberink and Chen (1993), O'Donoghue and Wright (2004a, 2004b) and Campbell et al. (2006).

The majority of the tests were performed with regular, corrected trochoidal waves, varying in wave height ($H$) and period ($T$). This wave shape is based on North Sea deep water wave measurements and roughly comparable to second order Stokes waves. The waves are therefore velocity skewed and only minor acceleration skewed. The variations in wave height and period led to different bed regimes i.e. rippled beds as well as flat beds with sheet flow. Besides these waves, a part of the tests was performed with second order Stokes waves and wave groups of irregular waves, based on a JONSWAP spectrum. This paper focuses on a selection of the regular corrected trochoidal wave conditions in the sheet flow regime. Table 5.1 gives an overview of the selected 9 experimental conditions and their characteristics. Each condition was run for a number of hours, divided over different runs. After each run, the wave generator was stopped and bed level profiles were measured. All individual runs for the same condition were run directly after one another. For an explanation of the different parameters in Table 5.1, reference is made to Chapter 3 of this thesis.

Table 5.1. Overview of selected experimental conditions.

| | $H$ (m) | $A$ (m) | $T$ (s) | $D_{50}$ (μm) | $U_{max}$ (m/s) | $U_{min}$ (m/s) | $<u>$ (m/s) | $R$ (-) | $\beta$ (-) | $\Psi_{max}$ (-) | time (hr) | # runs |
|---|---|---|---|---|---|---|---|---|---|---|---|---|
| Re1575m | 1.50 | 1.95 | 7.5 | 245 | 1.63 | -0.74 | -0.068 | 0.69 | 0.54 | 670 | 8.5 | 11 |
| Re1550m | 1.50 | 0.94 | 5.0 | 245 | 1.18 | -0.92 | 0.014 | 0.56 | 0.51 | 351 | 11 | 13 |
| Re1565m | 1.50 | 1.72 | 6.5 | 245 | 1.67 | -0.92 | -0.027 | 0.65 | 0.52 | 699 | 10 | 14 |
| Re1265m | 1.20 | 1.39 | 6.5 | 245 | 1.35 | -0.83 | 0.010 | 0.62 | 0.55 | 456 | 6 | 8 |
| Re1575f | 1.50 | 2.03 | 7.5 | 138 | 1.70 | -0.69 | -0.092 | 0.71 | 0.54 | 1298 | 4 | 7 |
| Re1550f | 1.50 | 1.02 | 5.0 | 138 | 1.28 | -1.02 | -0.028 | 0.56 | 0.53 | 731 | 5 | 10 |
| Re1565f | 1.50 | 1.61 | 6.5 | 138 | 1.55 | -0.83 | -0.058 | 0.65 | 0.52 | 1078 | 6 | 10 |
| Re1265f | 1.20 | 1.29 | 6.5 | 138 | 1.25 | -0.75 | -0.030 | 0.63 | 0.54 | 697 | 5 | 6 |
| Re1065f | 1.00 | 1.16 | 6.5 | 138 | 1.13 | -0.74 | -0.017 | 0.60 | 0.55 | 568 | 5 | 6 |

Apart from the hydrodynamic conditions, also the total number of hours that the wave conditions were run and the number of different runs is given. The duration of the runs varies from 0.5 to 1 hour each, which means that bed profiles were measured after each half hour or hour of waves. The average net transport rates for one condition were determined from all measured profiles and, in case of the use of the echosounders, averaged over the 4 profiles over the width of the flume. This means that, for instance for condition Re1575m in Table 5.1, there are 40 transport

rate measurements. The average results of these measurements, with a standard deviation, is presented in the next section of this paper.

The degree of velocity skewness ($R$) and acceleration skewness ($\beta$) of the wave-induced oscillatory flow near the bed are a function of the maximum on- and offshore velocity and acceleration. The values of velocity skewness ($R$) in Table 3.1 were calculated from:

$$R = \frac{|U_{max}|}{|U_{max}| + |U_{min}|} \tag{5.1}$$

The values of the acceleration skewness ($\beta$) were calculated from:

$$\beta = \frac{|\dot{U}_{max}|}{|\dot{U}_{max}| + |\dot{U}_{min}|} \tag{5.2}$$

where $\dot{U}_{max}$ and $\dot{U}_{min}$ are the amplitudes of the flow acceleration in the wave crest (max) and trough (min) direction. For all conditions the amount of acceleration skewness was small ($\beta \leq 0.55$). The wave mobility number ($\Psi$) is a dimensionless parameter for the prediction of the transport regime and depends on the maximum flow velocity and grain size. The values of the wave mobility number in Table 5.1 were calculated from:

$$\Psi_{max} = \frac{U_{max}^2}{(s-1)gD_{50}} \tag{5.3}$$

where $s = \rho_s / \rho$ is the relative sediment density, ($s$ = 2.65), $g$ the gravity acceleration and $D_{50}$ the median grain diameter of the sand. According to O'Donoghue et al. (2006), a flat bed sheet-flow regime is present when $\Psi_{max} > 300$, ripple regime corresponds to $\Psi_{max} < 190$ and in between, $190 < \Psi_{max} < 300$, a transition regime is present. According to Van Rijn & Walstra (2003), bed forms disappear and sheet-flow is present for conditions with $\Psi \geq 250$. These values correspond well with the observations done during the present experiments, where sheet-flow sediment transport was observed for conditions Re1565, Re1265, Re1550 and Re1575 for both sands and for Re1065 for the fine sand. A transition towards the ripple regime was observed during condition Re1065 for the medium sand. During lower wave conditions (wave heights of 0.7 m) velocities decreased further and ripples where present for both medium and fine sand. These latter conditions are not be discussed in detail in the present paper.

### 5.2.3 Measurement methodology of sand transport rates

The net transport rates were determined, using a mass conservation technique. Before and after each test run, the bed profiles are measured. Considering a small section with length $\Delta x$ along the flume. The difference between sediment flowing into this section ($q_{sin}$) and the sediment flowing out of this section ($q_{sout}$) must be accounted for by changes in the bed elevation in that section per unit time, $\Delta z_b$ per unit of time $\Delta t$ as follows:

$$q_{\sin} - q_{sout} = \frac{\Delta\{z_b(1-\varepsilon_0)\}}{\Delta t}\Delta x \qquad (5.4)$$

where $q_s$ is the sediment transport rate in volume per unit width ($m^2/s$) and $\varepsilon_0$ is the porosity of the sand bed. This value of porosity may vary, but since this is not detectable during the measurements, a constant value of 0.4 is assumed (based on Van der Hout (1997) and Dohmen-Janssen & Hanes (2002)). Figure 5.4 shows two bed level profiles of fine sand conditions (see Figure 5.1b for the sand bed configuration) before and after 2 hours of regular, trochoidal waves (Re1565f). Both the horizontal and vertical axes are in meters. The values of the x-axis present the distance from the wave paddle. The grey line is before the wave-run, the black line after the wave-run. From this Figure it is shown that the overall transport direction is from left to right (onshore directed). In order to solve Equation 5.4 for small successive sections along the wave flume, at least one boundary condition must be known. During the experiments, no sand was transported against the direction of wave propagation. Therefore, net transport rates at the wave paddle-side (offshore) of the sand section (where the concrete bottom of the flume is detected by the echosounders) were set to zero.

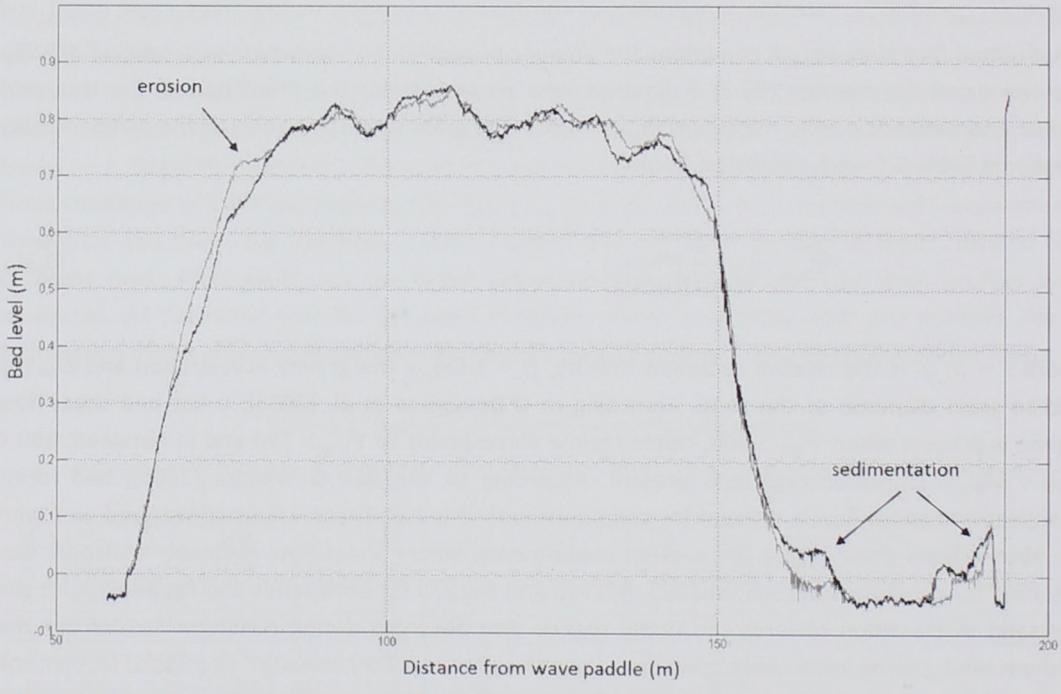


Figure 5.4. Sand bed profiles made with 1 echosounder (1 of total of 4 profiles over the width of the flume). Grey line: profile before the wave run. Black line: after 2 hours of regular trochoidal waves (Re1565f).

At approximately 110 m from the wave paddle, the instruments for the detailed flow velocity and sediment concentration measurements were positioned. The results of these measurements were discussed in detail in Chapter 3 and 4. To be able to compare these detailed flux measurements with the measured net sand transport rates by bed profiling, the transport rate results in this paper are the rates measured also at 110 m from the wave paddle. Since the scales are rather distorted in Figure 5.4, Figure 5.5 shows a more detailed view of the bed levels near the measuring location at $x$ = 110 m. From this figure it can be seen that the bed can be considered reasonable flat throughout these wave runs.

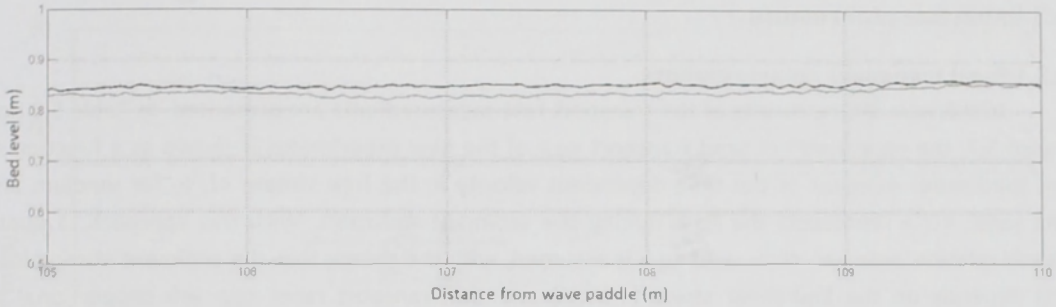


Figure 5.5. Sand bed profiles made with 1 echosounder, zoomed in at the location of the detailed measurements. Grey line; profile before the wave run. Black line: after 2 hours of regular trochoidal waves (Re1565f).

Figure 5.6 presents the sand transport rates determined from the bed profiles of experiment Re1565f, measured before and after 2 hours of wave action. The four different lines represent the results obtained from the four different echosounder profiles over the width of the flume. The far left side of the profiles is the concrete bed boundary where no sand comes in from locations closer to the paddle (see also Figure 5.4 and 5.1b). From there on, the transport is determined using Equation 5.4 (with horizontal steps $\Delta x$ = 1 cm). The difference between the four lines in Figure 5.6 is caused by measuring inaccuracies, porosity variations and lateral variations of the net transport. The average value of the four transport rate estimates at $x$ = 195 m is close to zero ($-4.87 \cdot 10^{-6}$ m$^2$/s), which could be expected at this onshore boundary of the sand bed. The variations of the measured net transport rates at the measuring location $x$ = 110 m is rather small ($\langle q_s \rangle \approx 50 - 70 \cdot 10^{-6}$ m$^2$/s).

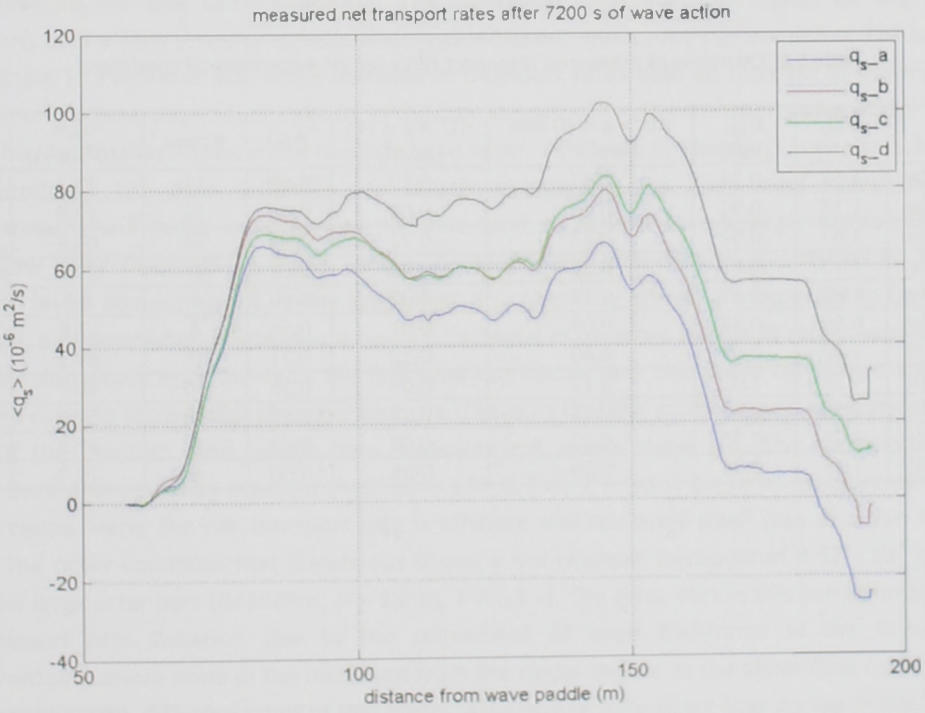


Figure 5.6. Sand transport rates along the fine sand bed. The 4 lines represent the 4 different profiles of the echosounders over the width of the flume. The transport in this figure is determined from bed profiles before and after 2 hours of regular trochoidal waves (Re1565f).

## 5.3 Experimental results

### 5.3.1 Sand transport measurements

In this section the results of the transport rate measurements are presented. In Table 5.2 and Figure 5.7, the measured net sand transport $<q_s>$ of the new experiments is shown as a function of the third-order moment of the time-dependent velocity in the free stream $<U^3>$, for medium and fine sand. $<U^3>$ represents the flow forcing the sediment transport. With this approach, a quasi-steady relation between $<U^3>$ and $<q_s>$ is assumed, with the theory that the sediment stirring load $L(t)$ depends on the bed-shear stress ($\sim U^2(t)$) and the transport rates $<q_s>$ are proportional to $U(t)*L(t)$ (see Bailard, 1981; Ribberink and Al-Salem, 1994). The third order velocity moment $<U^3>$ is calculated from the measured time-dependent flow velocities at $z$ = 1 m and $z$ = 40 mm above the sand bed. For the calculation the complete velocity signal is used, i.e. the orbital component ($\hat{u}$ ) of the flow plus the mean component ($<u>$). The reason to give $<U^3>$ at two different heights in the water column, is that the variation in height above the bed makes a big difference in values. When comparing the sand transport rates to previous experiments, later in this paper, most of the other experimental results (at least all of the existing surface wave data) are available in terms of $<U^3>$, measured higher above the sand bed than at $z$ = 40 mm. As can be seen here, despite all levels can be classified as 'in the free-stream', the height above the bed is important at should be taken into account when comparing sediment transport rates as a function of the third-order velocity moment. For Figure 5 it is decided to plot the transport rates $<q_s>$ as function of the third-order velocity moment $<U^3>$, measured at $z$ = 40 mm, since (unless mentioned differently) all free-stream flow velocity results presented in the new experiments are available at this level. Table 5.2 gives an overview of the conditions, with in the last three columns the number of wave runs, the mean transport rates and their standard deviation.

Table 5.2. Overview of measured transport rates for all experimental conditions.

| | $U_{max}$ (m/s) | $U_{min}$ (m/s) | $<U^3>$ z = 40 mm ($m^3/s^3$) | $<U^3>$ z = 1m ($m^3/s^3$) | $R$ (-) | # runs | $<q_s>$ ($10^{-6}$ $m^2/s$) | σ |
|---|---|---|---|---|---|---|---|---|
| Re1575m | 1.63 | -0.74 | 0.31 | 0.19 | 0.69 | 11 | 42.3 | 13.04 |
| Re1550m | 1.18 | -0.92 | 0.16 | 0.09 | 0.56 | 13 | 32.9 | 20.41 |
| Re1565m | 1.67 | -0.92 | 0.43 | 0.21 | 0.65 | 14 | 64.8 | 11.21 |
| Re1265m | 1.35 | -0.83 | 0.26 | 0.08 | 0.62 | 8 | 29.7 | 13.36 |
| Re1065m | 1.02 | -0.67 | 0.14 | 0.07 | 0.60 | 6 | 8.5 | 42.98 |
| Re0765m | 0.69 | -0.54 | 0.03 | 0.01 | 0.56 | 4 | -3.8 | 7.22 |
| Re1575f | 1.70 | -0.69 | 0.40 | 0.22 | 0.71 | 7 | 69.5 | 7.12 |
| Re1550f | 1.28 | -1.02 | 0.17 | 0.08 | 0.56 | 10 | 40.7 | 4.33 |
| Re1565f | 1.55 | -0.83 | 0.41 | 0.18 | 0.65 | 10 | 51.6 | 10.21 |
| Re1265f | 1.25 | -0.75 | 0.17 | 0.08 | 0.63 | 6 | 37.5 | 2.77 |
| Re1065f | 1.13 | -0.74 | 0.09 | 0.05 | 0.60 | 6 | 19.7 | 1.80 |

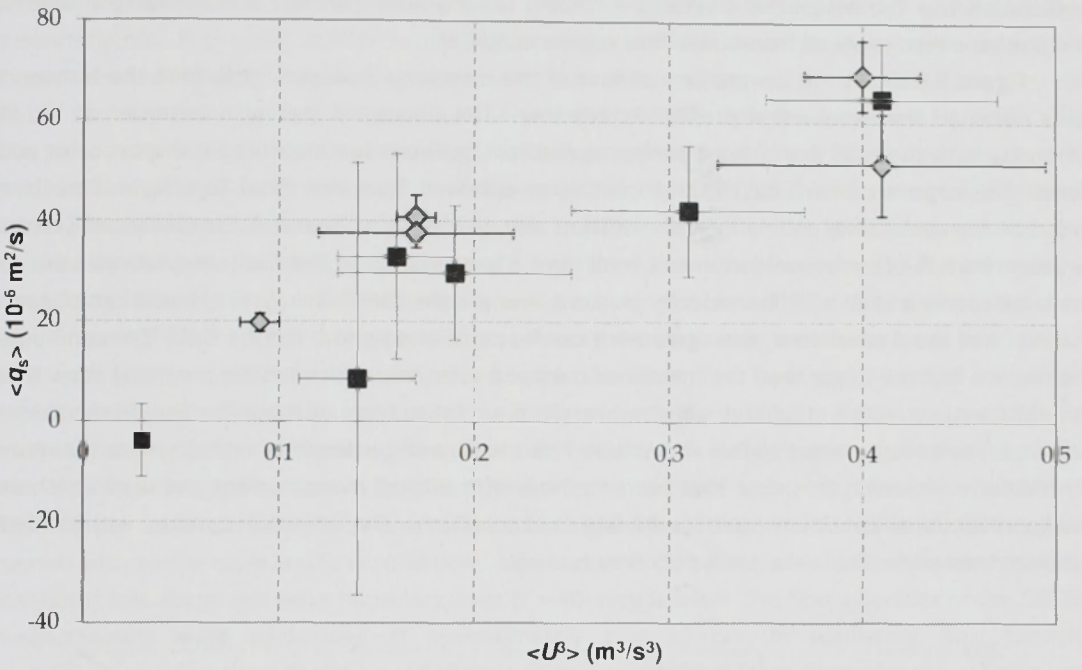


Figure 5.7. Measured sand transport rates for both medium sand (black squares) and fine sand (grey diamonds) conditions, with $<U^3>$ determined from flow velocity measurements at $z$ = 40 mm

The results from the new experiments are plotted in black squares (medium sand) and grey diamonds (fine sand). The vertical error bars reflect the standard deviation from all transport measurements for one wave condition. The horizontal error bars are based on the standard deviations of the flow velocity measurements of different wave runs per condition. For both sand types, there is a more or less linear increase in transport rates with an increase in the third-order moment of the time-dependent velocity in the free stream $<U^3>$. The transport rates of the fine sand are slightly larger than those of the medium sand cases. As shown in Chapter 3 (see also Schretlen et al., submitted), the flow velocities are largely comparable for both sand types. When the concentrations and fluxes are regarded, the fine sand conditions have a larger erosion depth and sheet flow layer thickness so, more sand is being brought into motion and stirred up to higher elevation levels above the bed. At the same time, the phase lag effects are expected to be larger for fine sand, a phenomenon which would cause a decrease in on-shore transport rates. Apparently, the larger erosion depth and stirring of the fine sand dominates over the phase lag effects, causing the fine sand cases to show a slightly larger onshore transport that the medium sand experiments.

Of the medium sand results, two measurement points stand out. The condition with the lowest third order velocity moment (Re0765m: $H$ = 0.7 m, $T$ = 6.5 s) presents measurements in the ripple regime. Here, the net transport rate is offshore and relatively small (see also Van der Werf, 2006). The other condition that stands out shows a net onshore transport of $8.52 \cdot 10^{-6}$ m$^2$/s with relatively large error bars (Re1065m: $H$ = 1.0 m, $T$ = 6.5 s). The error bars in this condition are caused by transport rate variation due to the movement of large bed-forms in the flume. These measurements where done in the transition from the ripple regime to the sheet-flow regime. During these experiments, different types of bed forms (with occasionally sheet-flow on top of the large bed forms) were observed. More detail on these non-sheet flow regime measurements can be found in Eekhout (2008). All other measurements were done in only the sheet-flow regime and these fit the

expectation that the net onshore velocity increases linearly with the third order velocity moment. The fine sand results are all from sheet-flow regime conditions.

Figure 5.8 shows the comparison of four of the measured transport rates with the transport rates obtained from mean flux profiles as determined in Chapter 4 (see also Schretlen et al., in progress), with the solid line being a perfect agreement between the measured transport rates and fluxes. The large error-bars for the transport rates obtained from the sheet-flow layer fluxes are based on the uncertainty estimation (50 – 60%) as also described in Chapter 4. Especially small errors in determination of the $z$-level (order of 1 mm) have a large impact on the flux transport rates due to the large concentration and flow velocity gradient over $z$ in the sheet-flow layer. Here it can be seen that for 3 of the 4 conditions, the agreement can be considered good, for the Re1575m condition, the flux is a factor 3 larger than the measured transport rate. Schretlen et al. (in progress) show that the net transport in this condition is the net result of a relative large onshore flux (inside the sheet-flow layer) and a large negative flux above that. This causes a larger absolute error than for the other 3 conditions. However, it is clear that both methods of transport measurement give a net onshore transport for the all conditions, also for the fine sand conditions. The latter is in contrast with the fine sand net transport rates in the oscillatory flow tunnels.

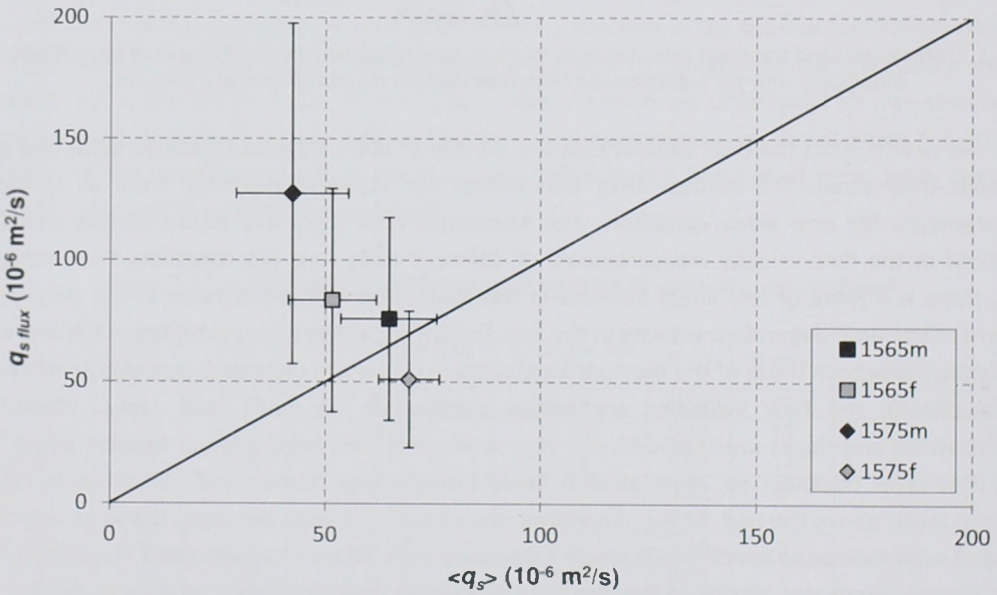


Figure 5.8. Comparison of the measured net transport rates determined through the mass conservation technique (horizontal axis) and the net transport rates calculated from the flow velocity and sheet-flow layer concentration measurements (vertical axis).

### 5.3.2 Sand transport rates under surface waves and oscillatory flows.

In this paragraph, the results of the new experiments are compared with results of previous experiments performed in both oscillatory flow tunnels and under surface waves. In the sheet-flow regime, the vast majority of sand is transported inside the sheet-flow layer, with by far the highest sediment concentrations in the pick-up layer. Therefore it may be expected that differences in relative small residual mean flows near the bed (e.g. boundary layer streaming) in the oscillatory flow tunnels and under surface waves influence the total net sand transport. Figure 5.9 and Table 5.3

present the comparison of the new medium sand transport rates to previous (medium sand) measurements. The black sqreuares present the new surface wave measurements with $<U^3>$ measured at $z$ = 40 mm, the white squares with $<U^3>$ measured at $z$ = 1 m . The black triangles the SISTEX surface wave experiments (see e.g. Ribberink et al. (2000); Dohmen-Janssen & Hanes (2002)), also performed in the GWK, Hannover. The grey circles represent oscillatory flow tunnel results with medium sand, taken from Ribberink & Al-Salem (1994), Wright (2002) and Hassan & Ribberink (2005). The new experiments show slightly smaller transport rates than the SISTEX experiments. This is primarily the case for the conditions with a high third order flow velocity (SISTEX mf and me conditions) where the two SISTEX conditions have a longer period ($T$ = 9.1 s) than the new experiments ($T$ = 6.5 – 7.5 s). In Chapter 4 it was already shown that an increase in wave period leads to a larger onshore sediment flux component inside the sheet flow layer and therefore to a larger onshore sediment transport rate. From the new experiments, no data with $T$ = 9.1 s is available for comparison. In relation to the oscillatory flow tunnel data, it is clearly shown that when the $<U^3>$ measured high in the free stream ($z$ = 1.0 m) is used, the net sand transport rates inside the sheet-flow regime under surface waves are consistently higher than those measured in oscillatory flow tunnels with similar sand and flow conditions. However, this difference does not exist when the $<U^3>$ measured just above the wave boundary layer ($z$ = 40 mm) is used. The flow velocities of the SISTEX measurements were performed at approximately $z$ = 10 cm. In oscillatory flow tunnels, measurements are bound to the height of the tunnel, varying from 50 to 80 cm for the experiments presented here.

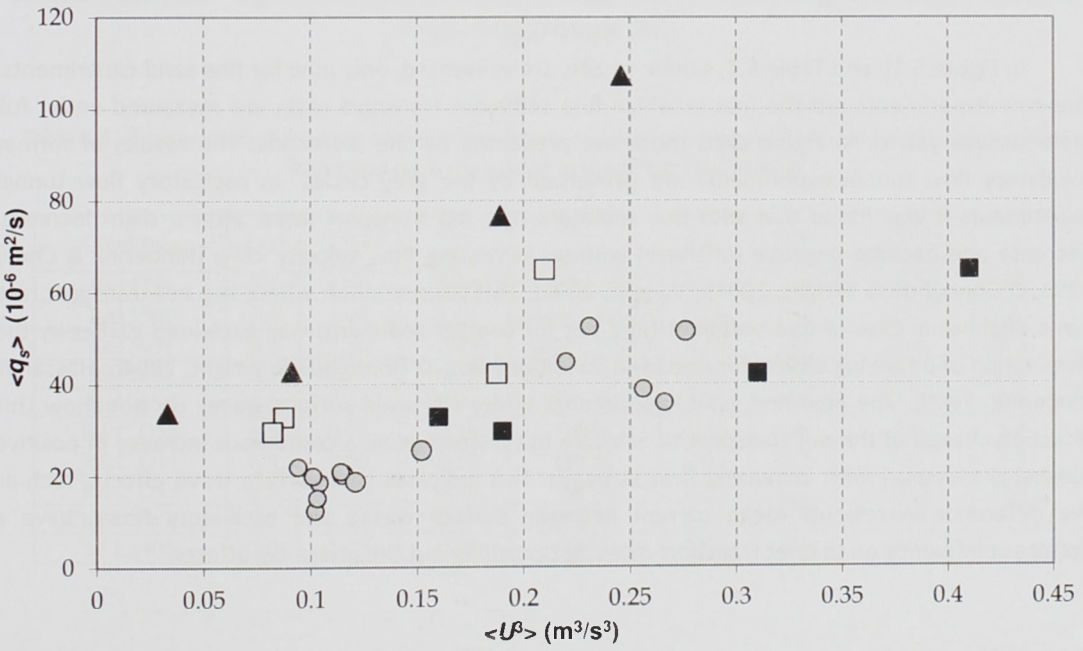


Figure 5.9. Measured sand transport rates for medium sand conditions from i) new flume experiments with $<U^3>$ at $z$ = 1 m (white squares), ii) from i) new flume experiments with $<U^3>$ at $z$ = 40 mm (black squares), iii) previous flume experiments (black triangles) (Ribberink et al., 2000; Dohmen-Janssen & Hanes, 2002; 2005) and iv) oscillatory flow tunnel experiments (grey circles) (Ribberink & Al Salem, 1994; Wright, 2002 and Hassan & Ribberink, 2005).

Table 5.3. Overview of measured transport rates for various medium sand experiments under full scale surface waves and oscillatory flows in the sheet-flow regime.

| Condition | $T$ (s) | $U_{max}$ (m/s) | $U_{min}$ (m/s) | $<U^3>$ ($m^3/s^3$) | $R$ (-) | $D_{50}$ (μm) | $<q_s>$ ($10^{-6}$ $m^2/s$) | $\sigma$ |
|---|---|---|---|---|---|---|---|---|
| Re1575m | 7.5 | 1.63 | -0.74 | 0.19 - 0.31 | 0.69 | 245 | 42.3 | 13.04 |
| Re1550m | 5.0 | 1.18 | -0.92 | 0.09 - 0.16 | 0.56 | 245 | 32.9 | 20.41 |
| Re1565m | 6.5 | 1.67 | -0.92 | 0.21 - 0.43 | 0.65 | 245 | 64.83 | 11.21 |
| Re1265m | 6.5 | 1.35 | -0.83 | 0.08 - 0.26 | 0.62 | 245 | 29.7 | 13.36 |
| Sistex mi | 6.5 | 0.98 | -0.79 | 0.033 | 0.55 | 240 | 33.8 | 16.4 |
| Sistex mh | 6.5 | 1.09 | -0.72 | 0.091 | 0.60 | 240 | 42.9 | 15.6 |
| Sistex mf | 9.1 | 1.31 | -0.70 | 0.189 | 0.65 | 240 | 76.7 | 6.4 |
| Sistex me | 9.1 | 1.45 | -0.64 | 0.246 | 0.69 | 240 | 107.3 | 17.7 |
| R&AS 7 | 6.5 | 0.95 | -0.50 | 0.102 | 0.66 | 210 | 12.42 | 0.94 |
| R&AS 8 | 6.5 | 1.31 | -0.70 | 0.256 | 0.66 | 210 | 38.86 | 2.34 |
| R&AS 10 | 9.1 | 0.96 | -0.53 | 0.104 | 0.66 | 210 | 18.56 | 2.25 |
| R&AS 11 | 9.1 | 1.25 | -0.69 | 0.220 | 0.66 | 210 | 44.83 | 1.88 |
| R&AS 13 | 6.5 | 1.20 | -0.90 | 0.114 | 0.57 | 210 | 21.0 | 2.43 |
| R&AS 14 | 9.1 | 1.19 | -0.92 | 0.094 | 0.56 | 210 | 22.0 | 4.52 |
| R&AS 15 | 5.0 | 0.98 | -0.54 | 0.103 | 0.64 | 210 | 15.2 | 2.49 |
| R&AS 16 | 12.0 | 1.03 | -0.63 | 0.101 | 0.62 | 210 | 20.0 | 1.34 |
| H&R C9 | 6.5 | 1.05 | -0.66 | 0.115 | 0.61 | 210 | 20.46 | 1.14 |
| H&R C1 | 6.5 | 1.07 | -0.57 | 0.121 | 0.65 | 210 | 18.74 | 2.53 |
| H&R C2 | 6.5 | 1.11 | -0.54 | 0.152 | 0.67 | 210 | 25.54 | 0.89 |
| H&R C11 | 6.5 | 1.39 | -0.87 | 0.276 | 0.62 | 210 | 51.47 | 2.36 |
| W Ma5010 | 5.0 | 1.53 | -0.90 | 0.231 | 0.63 | 270 | 52.6 | - |
| W Ma7515 | 7.5 | 1.53 | -0.90 | 0.266 | 0.63 | 270 | 35.9 | - |

In Figure 5.10 and Table 5.4, similar results are presented, only now for fine sand experiments. The new experiments are the first in which fine sediment transport rates are measured under full scale surface waves. In Figure 5.10 these are presented by the diamonds. The results of former oscillatory flow tunnel experiments are presented by the grey circles. In oscillatory flow tunnel experiments it was found that with fine sediment, the net transport rates, after a slight increase, decrease and become negative (offshore) with an increasing flow velocity $<U^3>$ (Ribberink & Chen, 1993; O'Donoghue & Wright, 2004b; Wright, 2002). This phenomenon where the net transport rate turns offshore in case of fine sediment (and not for coarser sediment) was explained earlier by the domination of phase lag effects for fine sand conditions (e.g. O'Donoghue & Wright, 2004b; Hassan & Ribberink, 2005). The new fine sand experiments under full scale surface waves do not show this direction change of the net transport to offshore but instead show a continuous increase of positive (onshore) transport with increasing flow strength. This indicates that surface wave effects, such as the difference in residual mean current between surface waves and oscillatory flows, have a dominant influence on the net transport rates by cancelling out the phase-lag effects.

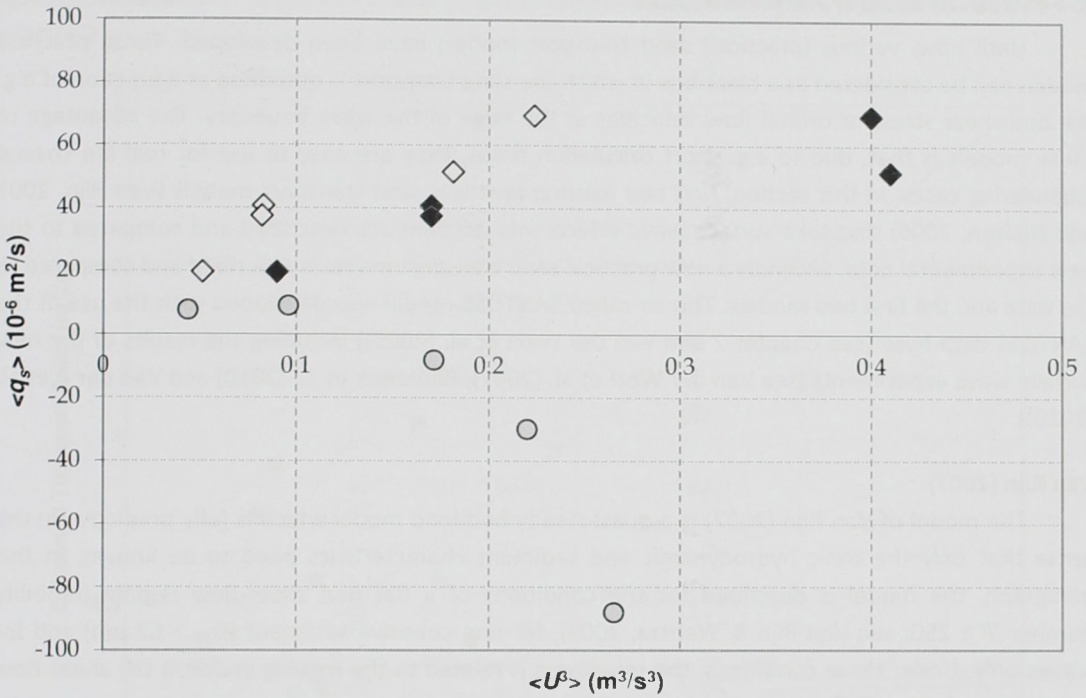


Figure 5.10. Measured sand transport rates for fine sand conditions from i) new flume experiments with $<U^3>$ at $z$ = 1 m (white diamonds), ii) new flume experiments with $<U^3>$ at $z$ = 40 mm (black diamonds) and iii) oscillatory flow tunnel experiments (grey circles) (Ribberink & Chen, 1993; O'Donoghue & Wright, 2004b and Wright & O'Donoghue, 2002).

Table 5.4. Overview of measured transport rates for various fine sand experiments under full scale surface waves and oscillatory flows in the sheet-flow regime.

| Condition | $T$ (s) | $U_{max}$ (m/s) | $U_{min}$ (m/s) | $<U^3>$ (m³/s³) | $R$ (-) | $D_{50}$ (μm) | $<q_s>$ ($10^{-6}$ m²/s) | $\sigma$ |
|---|---|---|---|---|---|---|---|---|
| Re1575f | 7.5 | 1.70 | -0.69 | 0.22 – 0.40 | 0.71 | 138 | 69.5 | 7.12 |
| Re1550f | 5.0 | 1.28 | -1.02 | 0.08 – 0.17 | 0.56 | 138 | 40.7 | 4.33 |
| Re1565f | 6.5 | 1.55 | -0.83 | 0.18 – 0.41 | 0.65 | 138 | 51.6 | 10.21 |
| Re1265f | 6.5 | 1.25 | -0.75 | 0.08 – 0.17 | 0.63 | 138 | 37.5 | 2.77 |
| Re1065f | 6.5 | 1.13 | -0.74 | 0.05 – 0.09 | 0.60 | 138 | 19.7 | 1.80 |
| R&C D14 | 6.5 | 0.79 | -0.48 | 0.044 | 0.62 | 128 | 7.6 | 1.4 |
| R&C D11 | 6.5 | 1.00 | -0.59 | 0.096 | 0.63 | 128 | 9.0 | 3.3 |
| R&C D13 | 6.5 | 1.30 | -0.76 | 0.220 | 0.63 | 128 | -30.2 | 6.6 |
| OD&W Fa7515 | 7.5 | 1.53 | -0.90 | 0.266 | 0.63 | 130 | -88.3 | - |
| W La406 | 4.0 | 1.28 | -0.75 | 0.171 | 0.63 | 130 | -8.1 | |

## 5.4 Practical sand transport models

Until now, various (practical) sand transport models have been developed. These practical models can be considered as a black box in which the sand transport is described as a function of e.g. the bed shear stress or orbital flow velocities at the edge of the wave boundary. The advantage of these models is that, due to e.g. short calculation times, they are easy to use for real life coastal engineering cases. In this section, first two existing practical sand transport models (Van Rijn, 2007 and Nielsen, 2006) that take surface wave effects into account are described and compared to the new experimental data. Secondly a new practical sand transport model is described and compared to the data and the first two models. This so-called SANTOSS-model was developed with the use of the SANTOSS data-base (see Chapter 2 and Van der Werf et al. (2009)) including the results of the new surface wave experiments (see Van der Werf et al. (2007); Ribberink et al. (2010) and Van der A et al. (2010)).

**Van Rijn (2007)**

The model of Van Rijn (2007) is a quasi-steady bed-load model which is fully predictive in the sense that only the basic hydrodynamic and sediment characteristics need to be known. In this paragraph, the model is described for the conditions of a flat bed sheet-flow regime (mobility number $\Psi \geq 250$; see Van Rijn & Walstra, 2003), for non-cohesive sediment ($D_{50} > 62$ µm) and for waves only. Under these conditions, the roughness is related to the moving grains in the sheet-flow layer.

The quasi steadiness of the model is reflected in the fact that it computes the instantaneous transport during the wave cycle with the use of instantaneous bed shear stress, based on the instantaneous velocity vector (see also Ribberink, 1998). The bed-load transport model for steady flow proposed by Van Rijn (1984a, 1993) is here slightly modified to better deal with (steady flow plus waves). A description of the model's formulae is given in Appendix I.

For the medium sand conditions ($D_{50} = 0.2 - 2$ mm), the assumption of quasi-steady behaviour is expected to be valid. For fine sand ($D_{50} < 0.2$ mm), phase lag effects between the shear stress and sediment concentration in the sheet-flow layer are important (see also Ribberink, 1998; Dohmen-Janssen, 1999), which would require a full unsteady or semi-unsteady model to present these effects. Using a phase-lag correction based on Dohmen-Janssen (1999) causes a gradual reduction of the net bed-load transport for finer sediments. The model is verified against field data (COAST3D project, Hoekstra et al., 2001) with a $D_{50}$ of 0.3 mm and overall, 80% of the predicted values are within a factor of 2 of the measured transport rates. When compared to laboratory data (Ribberink (1998); Dohmen-Janssen (1999) and Hassan et al. (1999)), the model predictions show a fairly good agreement with the medium sand measured data ($D_{50} = 0.21$ mm). The results for the fine sand data (e.g. Ribberink and Chen, 1993) comparison are not as good, part of the model results show transports in an opposite direction to the measurement results. Sensitivity computations for the sand range $0.13 \leq D_{50} \leq 0.46$ mm show that according to the model, the bed-load transport is only weakly dependent on particle size (Wong, 2010).

To simulate the new surface wave experiments, the hydrodynamic input for the model is a second order Stokes wave, based on the maximum on- and offshore (wave crest and trough) flow velocities, measured at the edge of the wave boundary layer (Wong, 2010).

Figure 5.11 presents the measured net sand transport rates of the new and existing surface wave experiments in relation to the rates calculated with the Van Rijn model. The black squares present the medium sand results, the grey diamonds the fine sand results. The solid line is a perfect

agreement between measurements and model calculations. The dashed line represent a variation of a factor 2.

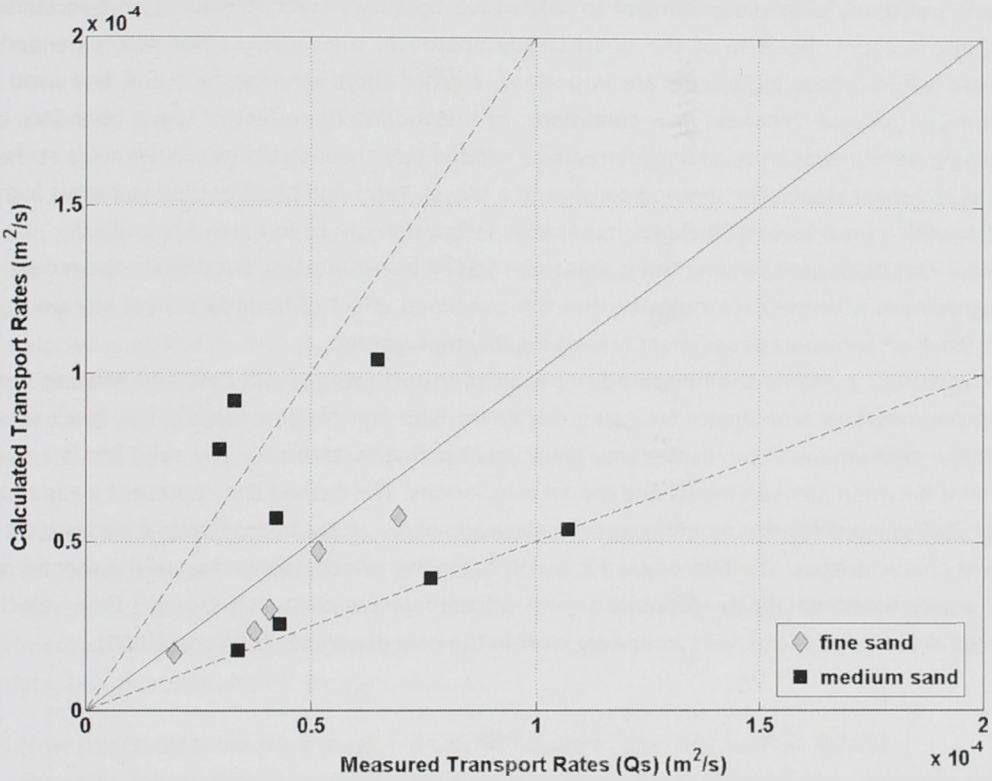


Figure 5.11. Measured GWK net transport rates, compared to the Van Rijn (2007) model.

From these results it can be seen that for most of the conditions, the results of the model calculations are within a factor 2 of the measured transport rates. Even though the model has a quasi-steady approach, surprisingly, the fine sand results show the best agreement. For the medium sand results, there is a distinction between the 4 points of the new experiments, which are overestimated by the model and the SISTEX-data (Ribberink et al., 2000; Dohmen-Janssen & Hanes, 2002) which are underestimated by the model. A sensitivity analysis (Wong, 2010) shows that the model is quite sensitive to an increase of the maximum onshore flow velocity ($U_{max}$), and to a far lesser extent sensitive for the wave period ($T$). Moreover, an increase in wave period leads to a small decrease in transport rates by the model, while the experimental results show the opposite (larger transport rates for an increase in wave period, see Section 5.3 and Chapter 3 and 4 (Schretlen et al., submitted; in progress).

A disadvantage of the model concept is that the influence of streaming is forced on the edge of the wave boundary layer. The new flow velocity and concentration measurements show that the influence of streaming and its influence on transport mainly occurs closer to the bed, in the lower levels of the wave boundary layer and inside the sheet-flow layer. When the model is run without the streaming, an underestimation of all data is shown, 66% of the data than fall outside the factor 2 range. The implementation of the wave boundary layer streaming component does increase onshore directed sand transport rates in a way that there is better agreement between the surface wave data and model calculations.

**Nielsen (2006) and Nielsen & Callaghan (2003)**

Similar to Van Rijn (2007) this is a quasi-steady model, designed to calculate instantaneous sediment transport, with the possibility to take wave boundary layer streaming and acceleration effects into account. Because of the quasi-steady approach, the model is not recommended for conditions where phase lag effects are important, e.g. for short wave periods and fine sand ($D_{50}$ <0.20 mm) in case of the sheet-flow conditions. In this model, the effect of wave boundary layer streaming is accounted for by adding a streaming related bed shear stress (wave Reynolds stress) to the total bed shear stress. The method consists of a Meyer-Peter and Mueller type transport formula operating with a time-varying Shields parameter. A description can be found in Appendix II.

Nielsen (2006) used (among other data) the SISTEX transport data to calibrate the model. The good agreement with the data indicates that the combined effect of boundary layer streaming and Lagrangian mass transport of sediment are reasonably represented.

Figure 5.12 presents the measured net sand transport rates of the new and existing surface wave experiments in relation to the rates calculated with the Nielsen model. The black squares present the medium sand results, the grey diamonds the fine sand results. The solid line is a perfect agreement between measurements and model calculations. The dashed line represent a variation of a factor 2. The input for the model are the measured values of the hydrodynamic parameters and sediment characteristics. The hydrodynamic input is (for the velocity skewed waves) a second order Stokes wave, based on the maximum on- and offshore (wave crest and trough) flow velocities, measured at the edge of the wave boundary layer in the new experiments (Wong, 2010).

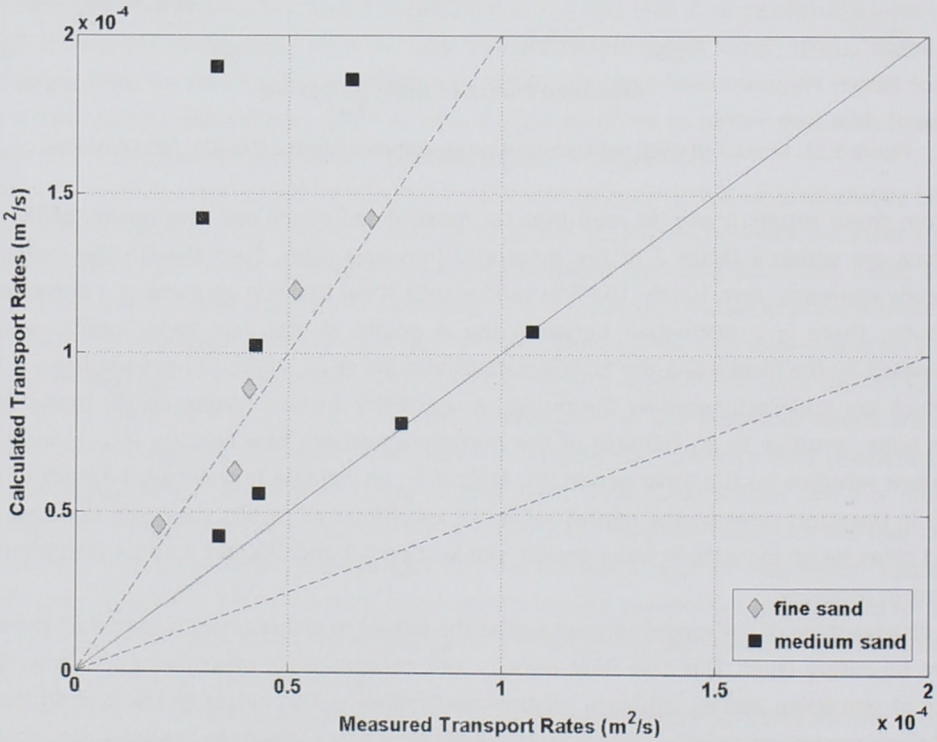


Figure 5.12. Measured GWK net transport rates, compared to the Nielsen (2006) model.

From Figure 5.12 it can be seen that there is almost perfect agreement between the model and the SISTEX-data (Ribberink et al., 2000), which makes sense, since this data is used by Nielsen

(2006) in the development of the model. However, the transport rates of the new data is clearly overestimated by the model, especially for three of the four medium sand conditions (Re1265m, Re1550m and Re1575m). The overestimation of medium sand conditions Re1565m and all fine sand conditions is close to a factor 2.

One reason for this overestimation may be the use of a friction factor for a mobile bed, which is considerably larger than the grain friction factor. Thereby, the Nielsen (2006) model is more sensitive to variations in peak onshore velocities and grain sizes (see Wong, 2010), more so than the Van Rijn (2007) model. Thereby, the model is more sensitive to a change in wave period $T$ than the Van Rijn model, and here, also an increase in wave period leads to a decrease of transport rates, opposite to the observed experimental results (see Section 5.3 and Chapter 3 and 4). When comparing the SISTEX-data to the medium sand results of the new experiments, the peak onshore flow velocity is higher in the new data and the wave period is higher for two of the SISTEX data-points. The Nielsen (2007) model calculates higher transport rates for conditions with higher flow velocities and shorter wave periods, but the measured transport rates of the new data are smaller than the SISTEX data. This could therefore explain the overestimation of the new medium sand data by the model.

Since the model has a quasi-steady approach, it is expected that the transport rates of fine sand results are overestimated because phase lag effects are not taken into account.

When the model is run without including the wave Reynolds stress, the data of the SISTEX experiments is underestimated (by a factor 2) and the model shows a very good agreement with the new data, but obviously not for the right reasons.

### 5.4.2 New practical transport model: SANTOSS model (Van der A et al., 2010)

Recently, a new general practical sand transport formula is developed. This SANTOSS model is designed to be applied for the near-bed sand transport for a wide range of sediment and hydrodynamic conditions, such as:

- Non-breaking waves with different shapes (velocity and/ or acceleration skewed) for a range of field-scale wave periods.
- Wave alone and current alone.
- Waves combined with currents under an angle.
- Large range of grain-sizes
- Sheet-flow and rippled-bed regime.

This model is developed with the use of the SANTOSS database (see Chapter 2 and Schretlen & Van der Werf, 2006; Van der Werf et al., 2009), which contains data from a large number of flume and oscillatory flow tunnel experiments, both existing and newly obtained in the SANTOSS project. Contrary to existing models (e.g. Van Rijn 2007; Nielsen, 2006), this model takes the following aspects into account:

- Phase-lag effects (semi-unsteady model)
- Sediment advection effects (Lagrangian grain motion and vertical orbital flow)
- The model is based on a much larger database with a wider range of conditions

The new data obtained from the SANTOSS experiments made it possible to develop a model which takes acceleration and surface wave effects into account. The aim of this paragraph is to show how the new SANTOSS model compares to the new experimental surface wave data. The work of Van der A (2010) describes the influence of acceleration effects and the implementation of those in the SANTOSS model.

The SANTOSS model is based on the concept of Dibajnia and Watanabe (1992, 1998). In short, the transport is calculated as follows: sediment loads stirred up during the wave crest and wave trough are calculated separately, based on the maximum bed shear stresses during the crest and trough. Whether these loads are transported during the same half cycle as in which they were stirred up, or by the next half cycle is determined by the phase-lag parameter. This parameter is calculated as the ratio of stirring height and settling distance during each half cycle. Stirring height and sediment load are calculated on the basis of the maximum (non-dimensional) bed-shear stress for each half cycle. The most important additions in relation to the scope of the surface wave conditions are:

- Lagrangian grain motion, which differs during the crest and trough period.
- Vertical orbital velocity affecting the grain settling velocity near the bed.
- Wave Reynolds stress

Below, a concise description of the model and it's elements concerning non-breaking, velocity skewed surface waves is given. A more detailed description of the model, its calibration and characteristics and performance under several different conditions (e.g. acceleration skewed waves, ripple regime, currents) can be found in Ribberink et al. (2010) and Van der A et al.(2010).

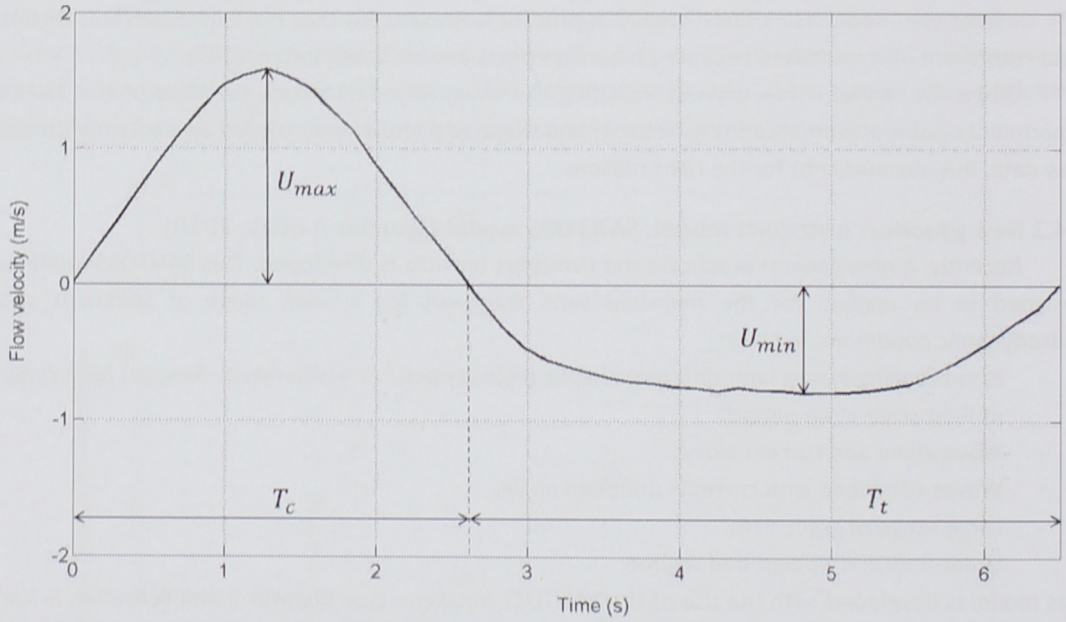


Figure 5.13 Flow velocity result from the new experiments (condition Re1565f at $z$ = 40 mm, see also Figure 5 in Chapter 2) with the input parameters as used in the SANTOSS model. The subscripts 'c' and 't' represent the crest and trough direction.

In Figure 5.13 , the wave's free-stream (horizontal) orbital velocity $u_w$ at the edge of the wave boundary layer (as measured in the new experiments, see Schretlen et al., submitted) is plotted against time ($t$). The model only uses the peak crest ($U_{max}$) and trough ($U_{min}$) orbital velocities. For the velocity-skewed waves as presented here, the crest velocity is larger than the trough velocity. This is expressed in the velocity skewness parameter $R$ (Equation 5.1) and the duration of the crest half-cycle ($T_c$) is smaller than the duration of the trough half cycle ($T_t$), see also Figure 5.13. In the model the periods $T_c$ and $T_t$ are calculated on the basis of standard shapes for velocity skewness (2nd order

Stokes). This makes it possible to calculate these time-lengths on the basis of the measured wave period $T$ and velocity-skewness $R$.

A more detailed description of the model, including the most important additions in relation to the scope of the surface wave conditions, is given in Appendix III. Contrary to the Van Rijn (2007) and Nielsen (2006) model, the SANTOSS model does not use a time-dependent velocity, only the (measured) maximum (crest and trough) flow velocities are used as input for the model.

Figure 5.14 shows the behaviour of the calculated dimensionless net transport $\Phi$ as a function of $U_{rms}$ for a typical progressive surface wave and flat bed conditions (see also Van der A et al., 2010), compared to a selection of the new experimental data with $T$ = 6.5 s, $R \approx 0.62$ and $\beta \approx 0.5$, Table 5.5 shows the settings of the model and the experimental parameters of the data. The two grain sizes (fine and medium sand) are distinguished. For medium sand, a distinction is made between the measurements of the 2007 and 2008 campaign for conditions Re1565m.

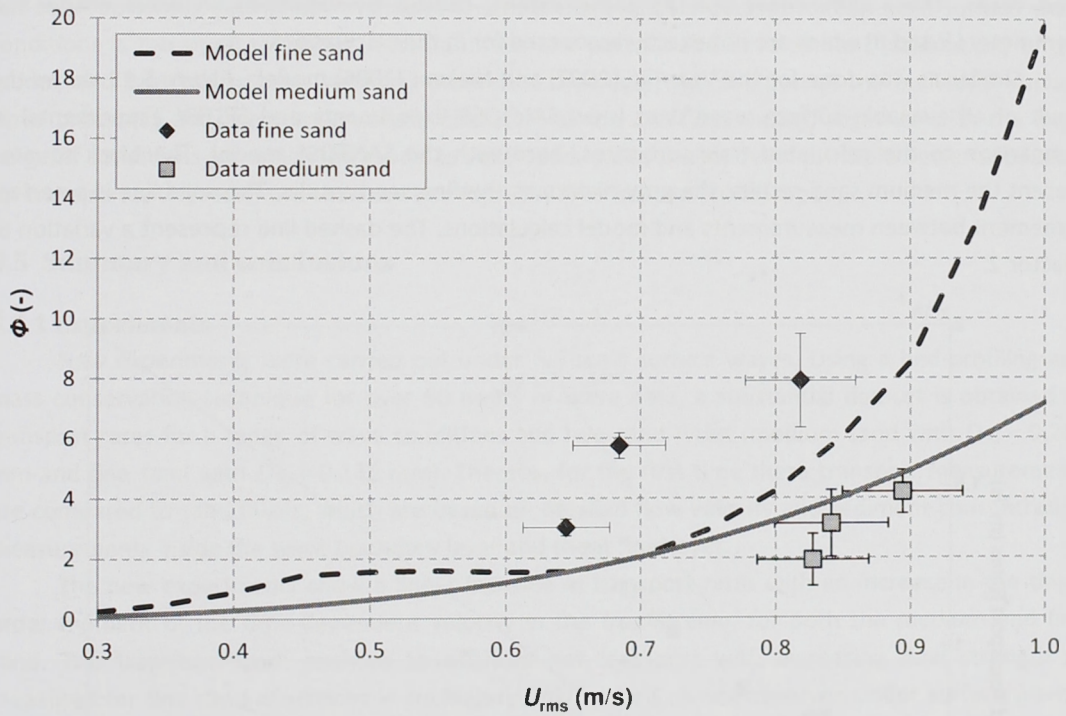


Figure 5.14 Non-dimensional transport rate as a function of $U_{rms}$ calculated with the SANTOSS model for a typical progressive surface wave for medium sand (solid line) and fine sand (dashed line) conditions. A comparison is made with a selection of the new data for fine sand (black diamonds) and medium sand (grey squares).

Table 5.5. Model settings for transport behaviour and experimental data for comparison.

| Condition | $T$ (s) | $U_{rms}$ (m/s) | $D_{50}$ (μm) | $R$ (-) | $\beta$ (-) | $\Phi$ (-) | $\sigma$ |
|---|---|---|---|---|---|---|---|
| Model settings | 6.5 | | 130 | 0.62 | 0.50 | | |
| Re1565f | 6.5 | 0.819 | 138 | 0.65 | 0.53 | 7.91 | 1.565 |
| Re1265f | 6.5 | 0.684 | 138 | 0.63 | 0.54 | 5.75 | 0.425 |
| Re1065f | 6.5 | 0.645 | 138 | 0.60 | 0.55 | 3.02 | 0.276 |
| Model settings | 6.5 | | 250 | 0.62 | 0.50 | | |
| Re1565m07 | 6.5 | 0.894 | 245 | 0.65 | 0.52 | 4.20 | 0.727 |
| Re1565m08 | 6.5 | 0.841 | 245 | 0.64 | 0.52 | 3.14 | 1.117 |
| Re1265m | 6.5 | 0.828 | 245 | 0.62 | 0.55 | 1.93 | 0.866 |

Figure 5.14 shows reasonable agreement between the behaviour of the model and the data. Both show a larger transport rate for the fine sand than for the medium sand and an increase of transport rates with an increasing $U_{rms}$. This trend can also be observed in the experimental data. However, the model shows some overestimation for medium sand and an underestimation for fine sand cases. These differences are, to some extent, caused by variations in wave shape and asymmetry ($R$ and $\beta$) which are not exactly accounted for in the calculations.

Similar as was done for the Van Rijn (2007) and Nielsen (2006) models, Figure 5.15 shows the result of all available surface wave data (new SANTOSS experiments and SISTEX experiments) in comparison to the calculated transport rates, here with the SANTOSS model. The black squares present the medium sand results, the grey diamonds the fine sand results. The solid line is a perfect agreement between measurements and model calculations. The dashed line represent a variation of a factor 2.

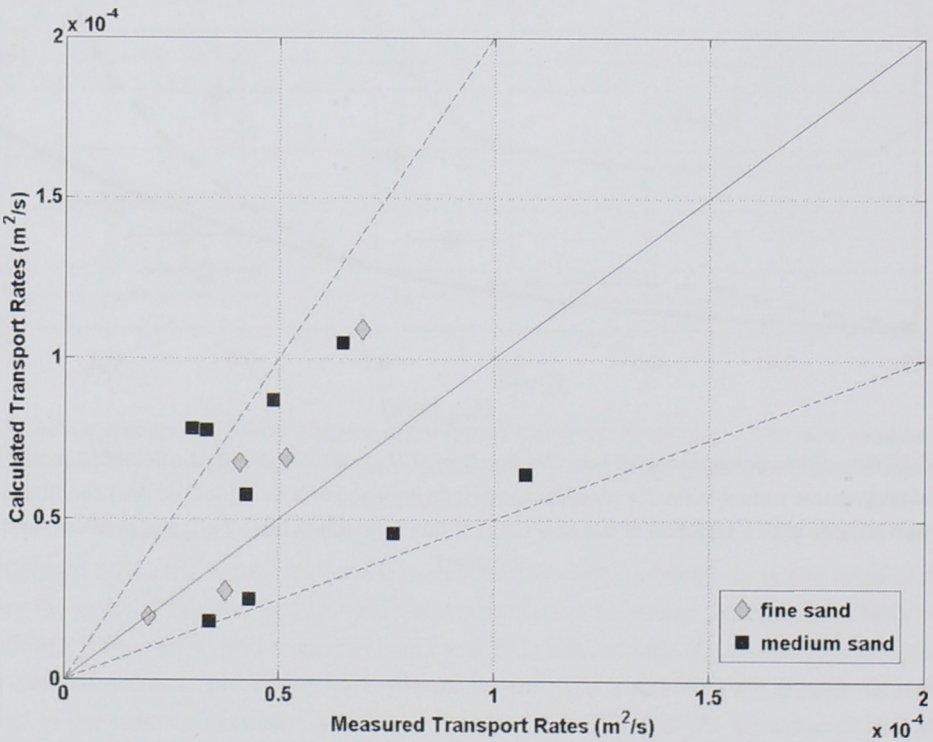


Figure 5.15. Measured GWK net transport rates, compared to the SANTOSS (2010) model.

Overall, this model gives the best result of the three practical sand transport models used in this paper. The fine sand conditions are all within a factor 2, which makes the performance of the model better than that of Nielsen (2006) and comparable to that of Van Rijn (2007). Very similar to the Van Rijn (2007) model, the medium sand results of the SISTEX experiments are underestimated by almost exactly a factor 2. The medium sand results of the new experiments are all more or less a factor 2 overestimated by the model.

When a semi-unsteady version of the SANTOSS model is run with only the streaming component added as wave surface wave effect, the model is not capable to generate the onshore directed transport rates for fine sand conditions. When the additional advection processes (Lagrangian motion and vertical orbital velocities) are added, the direction of the predicted sand transport rates changes to from offshore onshore for fine sand cases as well. The relevance of the different surface wave processes were also investigated by Kranenburg et al. (2010).

The data of the SISTEX and new SANTOSS full-scale surface wave experiments is not only used to test, but also to develop the model. It would be recommended to test the model against new data, but as of now, this data is not available. Thereby, the available dataset for full-scale surface wave conditions is too small to split it in half and use one part for the development (calibration) of the model, and one half to test (validate) the model. However, the addition of the individual surface wave processes and the semi-unsteady character of the SANTOSS model, together with the large range of conditions for which the model is developed, make the model in principle better applicable for transport rate predictions than the Van Rijn (2007) or Nielsen (2006) model.

## 5.5 Summary and conclusions

### 5.5.1 Experiments

New experiments were carried out under full-scale surface waves. Using a bed-profiling and mass conservation technique for over 60 hours of wave data, a substantial dataset is obtained of transport rates for a range of wave conditions and two sand types (medium sand with $D_{50}$ = 0.245 mm and fine sand with $D_{50}$ = 0.138 mm). Thereby, for the first time these transport measurements are compared to sand fluxes, which are based on detailed flow velocity and sediment concentration measurements inside the wave boundary layer and sheet flow layer.

The new experiments show a linear increase in transport rates with an increase in the third-order moment of the time-dependent velocity in the free stream, for both the medium and fine sand. The transition from onshore to offshore net transport with increasing flow strength as measured for fine sand conditions in oscillatory flow tunnels, is not observed under surface waves. This can probably be explained by the fact that phase lag effects of fine sand, responsible for the transition to offshore net transport, are now overruled by the presence of the positive mean flow and / or by intra-wave sediment advection effects. Further research could focus on the question whether the phase-lag effects and surface wave effects could, in general, compensate for one another, i.e. also for various other types of sand and wave conditions.

Previous research showed that under sheet flow conditions the far majority of sand is transported inside the sheet flow layer, close to the bed. This is confirmed by the current experiments. The new experiments show slightly smaller transport rates than the SISTEX experiments. This is primarily the case for the conditions with a high third order flow velocity (SISTEX mf and me conditions) which have a longer period ($T$ = 9.1 s) than the new experiments ($T$ = 6.5 – 7.5 s). In Chapter 4 (see also Schretlen et al., in progress) it was already shown that an increase in wave

period leads to a larger onshore sediment flux component inside the sheet flow layer and therefore to larger onshore sediment transport rates.

### 5.5.2 Practical sand transport models

The new and existing surface wave transport rate data are compared to three practical sand transport models. The Van Rijn (2007) and Nielsen (2006) models are both quasi-steady empirical models and have a method to account for streaming effects under surface waves. The newly developed SANTOSS model (Van der A, 2010) is a semi-unsteady model which includes additional surface wave effects by adding boundary layer streaming and sediment advection effects (vertical and horizontal).

The Van Rijn (2007) model includes wave induced streaming effects by adding a wave induced streaming velocity to the instantaneous orbital velocity at the edge of the wave boundary layer. Despite the quasi-steady approach, it gives good agreement for the fine sand transport rates. This is probably caused by a compensation of the phase-lag effects with surface wave effects in the data, leading to a net transport rate (which happens to be) close to the quasi-steady model predictions. For the medium sand cases, it underestimated the transport rates of the SISTEX transport rates and overestimates the medium sand cases of the new experiments.

The Nielsen (2006) model includes wave induced streaming effects by adding a streaming related bed shear stress (wave Reynolds stress) to the total bed shear stress. The model shows almost perfect agreement with the SISTEX-data, which makes sense since this data is used by Nielsen (2006) for the development of the model. However, the transport rates of the new data are clearly overestimated by the model. Similar to the Van Rijn (2007) model, the fine sand transport rates are predicted better than the medium sand cases (smaller overestimation).

The SANTOSS model gives the best result of the three practical sand transport models used here. The fine sand conditions are all predicted within a factor 2, which makes the performance of the model better than that of Nielsen (2006) and comparable to that of Van Rijn (2007). With the notification that here, semi-unsteady processes such as phase lag effects are taken into account, which was not done by the Van Rijn (2007) model. Thereby, the addition of the individual surface wave processes, the semi-unsteady character of the SANTOSS model and the large range of conditions for which the model is developed, make the model in principle better applicable for transport rate predictions than the Van Rijn (2007) or Nielsen (2006) model.

According to all three models higher peak onshore flow velocity and shorter wave periods would cause a larger transport rate, while the experiments show the opposite effect of the wave period. Due to this model behaviour, the new medium sand results are overestimated in comparison with the SISTEX results (which have lower peak flow velocities and longer wave periods than the new data). The approach of Nielsen (2006) to add an extra bed shear stress is in principle an improvement for surface wave cases, but re-calibration with more data than the SISTEX data points might lead to better predictions, at least for medium sand cases where the instantaneous approach is valid. The overestimation of the fine sand cases makes sense, since no phase lag effects are taken into account, which would lead to a decrease in the net transport rates.

Apart from these full scale surface wave data, the SANTOSS model is developed with, and tested against, a far larger database (Van der Werf et al. (2009), Ribberink et al. (2010), Van der A et al. (2010)), including oscillatory (sheet) flow conditions (including acceleration and velocity skewed conditions), the ripple regime, combined waves and currents and current alone cases. For all conditions, the model is capable of predicting 65% to 87% of the transport rates within a factor 2 of

the measurements and close to 100 % of all transport rates within a factor 5 (85 to 99%). Here, the model performs clearly better than the other two for the entire SANTOSS database. In comparison to the Van Rijn (2007) and Nielsen (2006) model, the SANTOSS model is the only one capable of predicting the correct direction of sediment transport for all experimental data. This direction is offshore for velocity skewed fine sand oscillatory flow tunnel experiments and for part of the wave plus current data and it is onshore for all other oscillatory flow tunnel data and the surface wave experiments. The model is currently being implemented in a cross-shore morphological model to further test its validity and compare its performance with existing transport formula. Future work is aimed at i) further improvement of modelling surface wave effects and ii) extending the model to irregular wave and breaking wave conditions (Van der A et al. (2010)).

## References


Bailard, J.A. 1981. Observations of granular-fluid mixture under an oscillatory sheet flow. *Proceedings of 23rd International Conference on Coastal Engineering*, 1896 – 1909.

Bijker, E.W., J.P.Th. Kalkwijk and T. Pieters. 1974. Mass transport in gravity waves on a sloping bottom. *Proceedings of 14th International Conference on Coastal Engineering*, 447 – 465.

Campbell, L., T. O'Donoghue and J.S. Ribberink. 2006. Wave boundary layer velocities in oscillatory sheet flow. *Proceedings of 30th International Conference on Coastal Engineering*, ASCE, 2207-2219, San Diego, U.S.A.

Davies, A.G. and C. Villaret. 1997. Oscillatory flow over rippled beds: Boundary layer structure and wave-induced Eulerian drift. Gravity waves in water of finite depth, advances in fluid mechanics. *J. N. Hunt, ed.*, Computational Mechanics Publications, Southampton, U.K., 215 – 254.

Davies, A.G. and C. Villaret. 1999. Eulerian drift induced by progressive waves above rippled and very rough beds. *Journal of Geophysical Research*, 104(C1): 1465-1488.

Dibajnia, M. and A. Watanabe, 1992. Sheet flow under non-linear waves and currents. *Proceedings of the 23rd International Conference on Coastal Engineering*, Venice, Italy, pp. 2015-2028.

Dibajnia, M. and A. Watanabe. 1998. Transport rate under irregular sheet flow conditions. *Coastal Engineering*, 35, 167-183.

Dohmen-Janssen, C.M. 1999. Grain size influence on sediment transport in oscillatory sheet flow – phase lags and mobile-bed effect. *PhD-thesis,* Delft University of technology Delft, The Netherlands. 246 pp.

Dohmen-Janssen, C.M., W.N. Hassan and J.S. Ribberink. 2001. Mobile-bed effects in oscillatory sheet flow. *Journal of Geophysical Research,* 106 (C11), 27103 – 27115.

Dohmen-Janssen, C.M. and D.M. Hanes. 2002. Sheet flow dynamics under monochromatic nonbreaking waves. *Journal of Geophysical Research,* 107(C10), 3149.

Dohmen-Janssen, C.M. and D.M. Hanes. 2005. Sheet flow and suspended sediment due to wave groups in a large wave flume. *Continental Shelf Research*, 25, 333 – 347.

Eekhout, J.P.C. 2008. Measurements and modeling of cross-shore morphodynamics. *MSc thesis*. University of Twente, The Netherlands.

Guard, P. & Nielsen, P. 2010. Personal communication, with regard to Wong (2010), MSc thesis.

Hassan, W.N. et al. (1999). Gradation effects on sand transport under oscillatory sheet flow conditions. *Rep. No. Z2099.10,* Delft Hydraulics, Delft,. The Netherlands.

Hassan, W.N. and J.S. Ribberink, 2005. Transport processes of uniform and mixed sands in oscillatory sheet flow. *Coastal Engineering* 52, 745-770.

Hoekstra, P., P. Bell, P. van Santen and N. Roode. 2001. Intertidal bedforms and bedload transport measurements on Spratt Sand, Teignmouth (U.K.), *Coastal Dynamics*, Lund, Sweden, 1028 – 1037.

Kranenburg, W.M., J.S. Ribberink and R.E. Uittenbogaard. 2010. Sand transport by surface waves: can streaming explain the onshore transport? *Proceedings of 32nd International Conference on Coastal Engineering*, Shanghai, China.

Madsen, O.S. and W.D. Grant. 1976. Sediment transport in the coastal environment. *MIT Ralph M. Parsons Lab., Rep. 209,* Cambridge, U.S.A.

McLean, S.R., J.S. Ribberink, C.M. Dohmen-Janssen and W.N. Hassan. 2001. Sand transport tin oscillatory sheet flow with mean current. *Journal of Waterw., Port. Coast. Ocean Engineering.* ASCE, 127 (3), 141 – 151.

Nielsen, P. 1992. Coastal bottom boundary layers and sediment transport. World Scientific Publishing Co. Pte. Ltd., Singapore, 324 p.

Nielsen, P. and D.P. Callaghan. 2003. Shear stress and sediment transport calculations for sheet flow under waves. *Coastal Engineering*, 47, 347 – 354.

Nielsen, P. 2006. Sheet flow sediment transport under waves with acceleration skewness and boundary layer streaming. *Coastal Engineering*, 53, 749 – 758.

O'Donoghue, T. and S. Wright. 2004a. Concentrations in oscillatory sheet flow for well sorted and graded sands. *Coastal Engineering*, 50, 117-138.

O'Donoghue, T. and S. Wright. 2004b. Flow tunnel measurements of velocities and sand flux in oscillatory sheet flow for well sorted and graded sands. *Coastal Engineering*, 51, 1163-1184.

O'Donoghue, T., J.S. Doucette, J.J. van der Werf and J.S. Ribberink. 2006. The dimensions of sand ripples in full-scale oscillatory flows. *Coastal Engineering*, 53, 997-1012.

Ribberink, J.S. and Z.W. Chen. 1993. Sediment transport of fine sand under asymmetric oscillatory flow. *Delft Hydraulics*, Report H840, Part VII, January. Delft, The Netherlands.

Ribberink, J.S. and A.A. Al-Salem. 1994. Sediment transport in oscillatory boundary layers in cases of rippled beds and sheet flow. *Journal of geophysical Research,* 99(C6), 12707-12727.

Ribberink, J.S. and A.A. Al-Salem. 1995. Sheet flow and suspension of sand in oscillatory boundary layers. *Coastal Engineering*, 25, 205 – 225.

Ribberink, J.S. 1998. Bed-load transport for steady flows and unsteady oscillatory flows. *Coastal Engineering*, 34, 59-82.

Ribberink, J.S., C.M. Dohmen-Janssen, D.M. Hanes, S.R. McLean and C. Vincent. 2000. Near-bed sand transport mechanics under waves – A large-scale flume experiment (Sistex99). *Proceedings of 27th International Conference on Coastal Engineering*, ASCE, 3263-3276.

Ribberink, J.S., D.A. van der A and R.H. Buijsrogge. 2010. SANTOSS transport model – A new formula for sand transport under waves and currents. *Report SANTOSS_UT_IR3*, University of Twente, The Netherlands.

Schretlen, J.L.M. and J.J. van der Werf. 2006. SANTOSS Database, Existing data from experiments in oscillatory flow tunnels and large wave flumes. *Report SANTOSS_UT_IR1. Civil Engineering & Management Research Report (Int. rep. 2006R-008/WEM-009).* University of Twente, The Netherlands

Schretlen, J.L.M., J.S. Ribberink & T. O'Donoghue. 2009. Sand transport under full-scale surface waves. *Proceedings of Coastal Dynamics 2009*, Tokyo, Japan. World Scientific, paper 123.

Schretlen, J.L.M., J.S. Ribberink & T. O'Donoghue. 2010. Boundary layer flow and sand transport under full scale surface waves. *Proceedings of 32nd International Conference on Coastal Engineering*, Shanghai, China.

Schretlen, J.L.M., J.S. Ribberink and T. O'Donoghue. Submitted. Boundary layer velocities measured above mobile beds under full scale progressive surface waves.

Soulsby, R. 1997. Dynamics of marine sands. Thomas Telford, London, U.K.

Swart, D.H. 1974. Offshore sediment transport and equilibrium beach profiles. Delft Hydraulics Lab Publ No. 131.

Van der A, D.A. 2010. Effects of acceleration skewness on oscillatory boundary layers and sheet flow sand transport. *PhD thesis*, University of Aberdeen, U.K.

Van der A, D.A., J.S. Ribberink, J.J. van der Werf and T. O'Donoghue. 2010. New practical model for sand transport induced by non-breaking waves and currents. *Proceedings of 32nd International Conference on Coastal Engineering*, Shanghai, China.

Van der Hout, G. 1997. Grain size and gradation effects on sediment transport under sheet flow conditions. *Report Z2137, Part III*, October 1997, Delft Hydraulics, Delft, The Netherlands.

Van der Werf, J.J. 2006. Sand transport over rippled beds in oscillatory flow. *PhD thesis*, University of Twente, The Netherlands

Van der Werf, J.J., J.S. Ribberink and T. O'Donoghue. 2007. Development of a new practical model for sand transport induced by non-breaking waves and currents. *Coastal Sediments 2007*, ASCE, New Orleans, USA. pp 42 – 55.

Van der Werf, J.J., J.L.M. Schretlen, J.S. Ribberink and T. O'Donoghue. 2009. Database of full-scale laboratory experiments on wave-driven sand transport processes, *Coastal Engineering* 56, 726 – 732.

Van Rijn, L.C. 1984a. Sediment transport part I: Bed load transport. *Journal of Hydraulic Engineering*, 110 (11), 1431 – 1456.

Van Rijn, L.C. 1993. Principles of sediment transport in rivers, estuaries and coastal areas. Aqua Publications, Blokzijl, The Netherlands.

Van Rijn, L.C. 2000. General view on sand transport by currents and waves. *Rep. No.Z2899.20 – Z2099.30 – Z2824.30*, Delft Hydraulics, Delft, The Netherlands.

Van Rijn, L.C. and D.J.R. Walstra. 2003. Modelling of sand transport in Delft3D-online. *Rep. No. Z3624*, Delft Hydraulics, Delft, The Netherlands.

Van Rijn, L.C. 2007. Unified view of sediment transport by currents and waves I: Initiation of motion, bed roughness and bed-load transport. *Journal of Hydraulic Engineering*, 133(6), 649 – 667.

Wong, W.H. 2010. A comparison of wave-dominated cross-shore sand transport models. *MSc thesis*. University of Twente, The Netherlands.

Wright, S. 2002. Well-sorted and graded sands in oscillatory sheet-flow. *PhD thesis*, Department of Engineering, University of Aberdeen, Aberdeen, UK.

Wright, S. and T. O'Donoghue. 2002. Total sediment transport rate predictions in wave current sheet flow with graded sand. Oscillatory flow tunnel experiments at Aberdeen University. Experimental report EPSRC "LUBA" Project. University of Aberdeen, Aberdeen, UK.

## Appendix I Van Rijn model

The bed-load transport model for steady flow proposed by Van Rijn (1984a, 1993) is slightly modified to better deal with steady flow plus waves, leading to:

$$q_b = \gamma \rho_s D_{50} D_*^{-0.3} \left(\frac{\tau'_{b,w}}{\rho}\right)^{0.5} \left[\frac{(\tau'_{b,w} - \tau_{b,cr})}{\tau_{b,cr}}\right]^n \frac{U_{\delta,w}}{|U_{\delta,w}|} \quad \text{(I.1)}$$

in which $\gamma$ = 0.5 and $n$ = 1, calibrated using measured data sets ($D_{50}$ > 0.2 mm) of the large-scale wave tunnel of Delft Hydraulics (now Deltares) (Ribberink, 1998; Van Rijn, 2000), $\rho_s$ is the sediment density, $\rho$ is the fluid density, $D_{50}$ is the mean particle size and $D_* = D_{50}[(s-1)g/\nu^2]^{1/3}$ , with $s$ being the relative density ($\rho_s/\rho$) and $\nu$ is the kinematic viscosity. $\tau_{b,cr}$ is the critical bed-shear stress according to Shields. The instantaneous grain-related bed-shear stress due to the waves ($\tau'_{b,w}$ ) is presented by:

$$\tau'_{b,w} = 0.5\rho f'_w (U_{\delta,w})^2 \quad \text{(I.2)}$$

where $U_{\delta,w}$ is the instantaneous velocity at the edge of the wave boundary layer, $\rho$ is the fluid density and the wave-related grain friction coefficient is presented by:

$$f'_w = \exp\left[-6 + 5.2\left(\frac{A}{k_{s,grain}}\right)^{-0.19}\right] \quad \text{(I.3)}$$

where $A$ is the peak orbital amplitude at the edge of the wave boundary layer and $k_{s,grain} = D_{90}$.

Wave induced streaming effects are included by adding a wave induced streaming velocity to the instantaneous orbital velocity at the edge of the wave boundary layer. This concept is based on the work of Davies & Villaret (1997, 1999), who have summarized model and experimental results involving plane rough beds in the turbulent flow regime, showing that the near-bed streaming depends highly on the bed roughness and wave asymmetry (see also Bijker et al., 1974). The relative bed-roughness is presented by $A / k_{s,w}$. Where $A$ is again the peak orbital amplitude at the edge of the wave boundary layer and Van Rijn (2007) suggests for sheet-flow conditions (mobility number $\Psi \geq 250$) that $k_{s,w} = 20 f_{cs} D_{50}$. For the medium and fine sands used in the new experiments, the value of $f_{cs}$ = 1 ($D_{50} \leq 0.5$ mm). In the new experiments the sheet-flow conditions lead to a large relative roughness ($A / k_{s,w} \geq 192$, see Table 5.1 for the values of $A$), which means for the model of van Rijn (2007) that the wave-induced boundary layer streaming is onshore directed (in line with Longuet-Higgins, 1953) and presented by:

$$u_{\delta,s} = 0.75\, U_{max}^2 / c \quad \text{(I.4)}$$

where $U_{max}$ is the peak orbital velocity at the edge of the wave boundary layer and $c$ is the wave celerity (= $(gh)^{0.5}$ for shallow water waves).

## Appendix II Nielsen model

The method consists of a Meyer-Peter and Mueller type transport formula operating on a time-varying Shields parameter, like:

$$\frac{q_s(t)}{\sqrt{(s-1)gD_{50}^3}} = 12[\theta(t) - 0.05]\sqrt{\theta(t)}\frac{u_\theta(t)}{|u_\theta(t)|} \qquad \text{for } \theta(t) > 0.05 \qquad \text{(II.1)}$$

This Shields parameter $\theta(t)$ accounts for both acceleration-asymmetry and boundary layer streaming (see further below), $s$ is the relative density, $D_{50}$ the mean grain diameter. The parameter $u_\theta(t)$ is a sediment mobilising velocity as presented in the Nielsen & Callaghan (2003) model:

$$u_\theta(t) = \sqrt{\frac{1}{2}f_{2.5}}\left(\cos\varphi_\tau u + \sin\varphi_\tau \frac{1}{\omega_p}\frac{du}{dt}\right) \qquad \text{(II.2)}$$

in which $f_{2.5}$ is the grain roughness friction factor:

$$f_{2.5} = \exp\left[5.5\left(\frac{2.5D_{50}}{A}\right)^{0.2} - 6.3\right] \qquad \text{(II.3)}$$

and

$$A = \frac{\sqrt{2}}{\omega_p}\sqrt{var\{u(t)\}} \qquad \text{(Ii.4)}$$

In all of the above, $u$ is the free stream velocity, $\omega_p$ is the peak angular frequency, $\frac{du}{dt}$ presents the acceleration and $\varphi_\tau$ is the angle which determines the ratio of the effect of sediment mobilizing forces due to drag and/ or acceleration. Based on a.o. the SISTEX data, the overall best fit of this angle appeared to be 47° (Guard & Nielsen, 2010).

To implement the effects of boundary layer streaming, a total, instantaneous Shields parameter $\theta(t)$ is based on $u_\theta(t)$ and the wave Reynolds stress $-\widetilde{u}\widetilde{w}$ , leading to:

$$\theta(t) = \left|\frac{|u_\theta|u_\theta - (\widetilde{u}\widetilde{w})}{(s-1)gD_{50}}\right| \qquad \text{(II.5)}$$

where

$$-(\widetilde{u}\widetilde{w}) = \frac{2}{3\pi}f_e A^3\omega^3/c \qquad \text{(II.6)}$$

and

$$f_e = \exp\left[5.5\left(\frac{170\sqrt{\hat{\theta}_{2.5} - .05D_{50}}}{A}\right)^{0.2} - 6.3\right] \qquad \text{(II.7)}$$

where $\hat{\theta}_{2.5}$ is peak value of the grain roughness Shields parameter corresponding to the friction factor formula (see also Nielsen, 1992). Contrary to Equation II.3, here not the grain roughness

($2.5D_{50}$) is used, but a larger roughness ($170\sqrt{\hat{\theta}_{2.5} - .05D_{50}}$ ) based on the mobile bed (sheet flow layer). The total Shields parameter (Equation II.5) is then used in the sheet-flow sediment transport formula, Equation II.1.

## Appendix III SANTOSS model

*Lagrangian grain motion, which differs during the crest and trough period*

For surface waves, sediment grains move with the wave during the wave crest and against the wave during the wave trough (Stokes drift or Lagrangian motion). In this way the grains experience a longer crest period $T_{c,sw}$ (= $T_c + \Delta T_c$) and a shorter trough period $T_{t,sw}$ (= $T_t - \Delta T_t$). The variable $\Delta T$ depends on the ratio of the wave propagation velocity $c$ and the horizontal grain displacement during the half wave-cycle $d_g$ and can be written as:

$$\Delta T = \frac{d_g}{c} \tag{III.1}$$

Assuming a sinusoidal wave shape for the half-cycle horizontal grain motion, the crest period extension and trough period reduction can be written as follows:

$$\Delta T_c = \frac{d_g}{c} = \left\{\frac{c}{\zeta u}\pi - 2\right\}^{-1} T \tag{III.2a}$$

$$\Delta T_t = \frac{d_g}{c} = \left\{\frac{c}{\zeta u}\pi - 2\right\}^{-1} T \tag{III.2b}$$

where $\zeta$ is the ratio of the horizontal grain-velocity amplitude and free-stream velocity amplitude. Figure III-1 shows results of the new experiments, where this ratio appears to be constant for a range of conditions (see also Chapter 3 and Schretlen et al., submitted). These are results from the wave boundary layer flow velocities, measured with UVPs. Therefore, these flow velocities are representative of the grain velocities inside the wave boundary layer. Based on these measurements, the reduction factor ($\zeta$) is found to be 0.55. The wave propagation velocity ($c = L/T$ ) is calculated using an explicit formulation as given by Soulsby (1997). The half-cycle wave periods are now calculated using the previous two Equations:

$$T_{c,sw} = T_c + \Delta T_c \tag{III.3a}$$

$$T_{t,sw} = T_t + \Delta T_t \tag{III.3b}$$

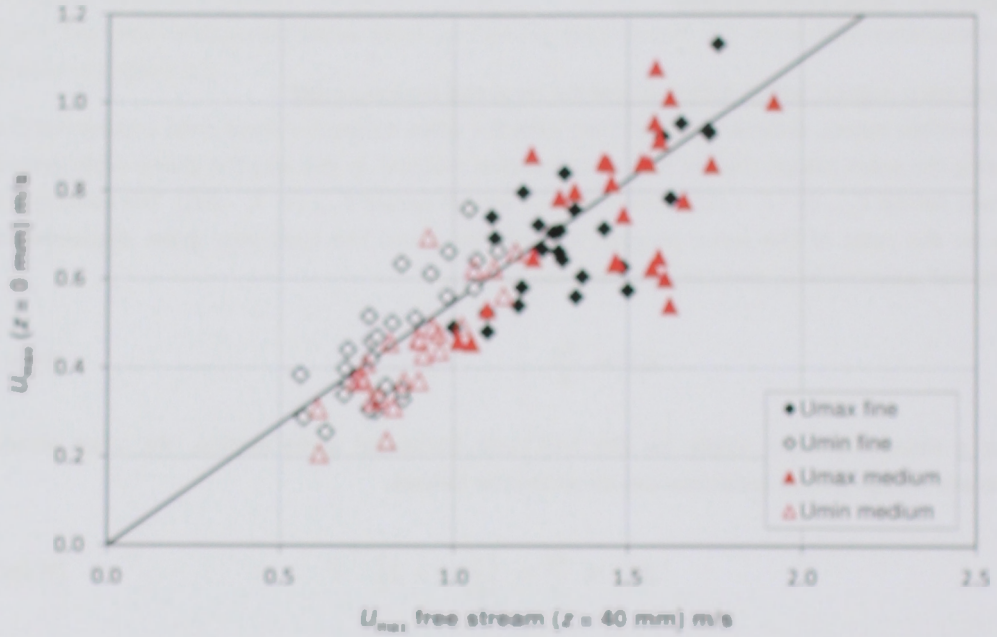


Figure III-1 The ratio between the maximum measured on- and offshore free stream velocity (at $z$ = 40 mm) and the maximum on- and offshore velocity at $z$ = 0 mm ($\zeta$ = 0.55).

*Vertical orbital velocity affecting the grain settling velocity near the bed.*

For surface waves, also a vertical orbital velocity ($w$) is present which affects the settling velocity of grains. Even relatively close to the bed, this directly influences the phase lag process (see also Kranenburg et al., 2010). In the new model, the vertical orbital velocity amplitude at elevation $z$ near the bed $w(z)$ is based on non-linear 2$^{nd}$-order Stokes wave theory. The sand settling velocities at crest and trough are then corrected with the vertical velocity at level $r_i$ as follows:

$$w_{sc} = w_s + w(r_i) \tag{III.4a}$$

$$w_{st} = \max(w_s - w(r_i), 0) \tag{III.4b}$$

with

$$r_i = \begin{cases} \varepsilon\eta & if \quad \eta > 0 \ \text{(ripple regime)} \\ \varepsilon\delta_{wl} & if \quad \eta = 0 \ \text{(sheet flow regime)} \end{cases} \tag{III.5}$$

in which $\varepsilon$ = 3 in the calibrated model (with subscript 'T' for either 'c' of crest or 't' of trough). Further on in this Section, the Equations (III.3)and (III.4) are implemented in the phase-lag parameters of the transport model.

*Wave Reynolds stress*

The magnitudes of the (non-dimensional) bed shear stress under the wave crest and trough are calculated trough the Shields parameters:

$$|\theta_c| = \frac{\frac{1}{2} f_{w\delta c} |U_{max}|^2}{(s-1) g D_{50}} \tag{III.6a}$$

$$|\theta_t| = \frac{\frac{1}{2} f_{w\delta t} |U_{min}|^2}{(s-1) g D_{50}} \tag{III.6b}$$

Where $s$ is the relative density ($\rho_s/\rho$), $g$ is the acceleration due to gravity and $D_{50}$ the median grain size of the sand bed.

For only velocity skewed waves without a superimposed current, the wave friction factor is similar for both the crest and trough and is defined as:

$$f_w = 0.00251 \exp\left[5.21 \left(\frac{A}{k_{s,w}}\right)^{-0.19}\right] \quad \text{for } \frac{A}{k_{s,w}} > 1.587 \tag{III.7}$$

$$f_w = 0.3 \quad \text{for } \frac{A}{k_{s,w}} \leq 1.587$$

The wave roughness height for sheet-flow conditions is defined as:

$$k_{sw} = \max\{D_{50}, D_{50}[\mu + 6(\langle|\theta|\rangle - 1)]\} \tag{III.8}$$

with

$$\mu = \begin{cases} 6 & \text{if } D_{50} \leq 0.15 \text{ mm} \\ \left[6 + (10^3 D_{50} - 0.15)\frac{(1-6)}{(0.20-0.15)}\right] & \text{if } 0.15 \text{ mm} < D_{50} < 0.20 \text{ mm} \\ 1 & \text{if } D_{50} \geq 0.20 \text{ mm} \end{cases} \tag{III.9}$$

with the mean absolute Shields parameter according to:

$$\langle|\theta|\rangle = \frac{\frac{1}{4} f_w U_{max}^2}{(s-1) g D_{50}} \tag{III.10}$$

The bed roughness for the sheet flow regime is solved iteratively since the Shields parameter also depends on the bed roughness (Ribberink, 1998). Apart from this calculated Shields parameter, for surface waves an additional (positive) wave Reynolds stress ($\theta_{wRe}$) is added. This will enhance the crest component and reduce the trough component of the bed shear stress (Shields parameter), leading to total maximum bed shear stresses defined as:

$$|\theta_{c\,sw}| = |\theta_c| + \theta_{wRe} \tag{III.11a}$$

$$|\theta_{t\,sw}| = |\theta_t| - \theta_{wRe} \tag{III.11b}$$

The wave Reynolds Shields parameter is

$$\theta_{wRe} = \frac{\tau_{wRe}}{\rho(s-1)gD_{50}} \tag{III.12}$$

with

$$\tau_{wRe} = \rho \frac{f_{wRe}}{2c} \alpha \hat{u}^3 \tag{III.13}$$

with $\alpha = 4/(3\pi) = 0.424$. The net transport rates are determined through:

$$\Phi = \frac{\langle q_s \rangle}{\sqrt{(s-1)gD_{50}^3}} = \frac{\sqrt{|\theta_{c,sw}|}T_{c,sw}(\Omega_{cc} + \Omega_{tc})\frac{\theta_{c,sw}}{|\theta_{c,sw}|} + \sqrt{|\theta_{t,sw}|}T_{t,sw}(\Omega_{tt} + \Omega_{ct})\frac{\theta_{t,sw}}{|\theta_{t,sw}|}}{T} \tag{III.14}$$

Following the approach of Dibajnia & Watanabe (1992), there are four contributions to the net sand transport:

i) The sand load that is entrained during the wave crest period and transported during the wave crest period:

$$\Omega_{cc} = \begin{cases} \Omega_c & \text{if} \quad P_c \leq 1 \\ \frac{1}{P_c}\Omega_c & \text{if} \quad P_c > 1 \end{cases} \tag{III.15}$$

ii) The sand load that is entrained during the wave crest period and transported during the wave trough period:

$$\Omega_{ct} = \begin{cases} 0 & \text{if} \quad P_c \leq 1 \\ \frac{(P_c-1)}{P_c}\Omega_c & \text{if} \quad P_c > 1 \end{cases} \tag{III.16}$$

iii) The sand load that is entrained during the wave trough period and transported during the wave trough period:

$$\Omega_{tt} = \begin{cases} \Omega_t & \text{if} \quad P_t \leq 1 \\ \frac{1}{P_t}\Omega_t & \text{if} \quad P_t > 1 \end{cases} \tag{III.17}$$

iv) The sand load that is entrained during the wave crest period and transported during the wave trough period:

$$\Omega_{tc} = \begin{cases} 0 & \text{if} \quad P_t \leq 1 \\ \frac{(P_t-1)}{P_t}\Omega_t & \text{if} \quad P_t > 1 \end{cases} \tag{III.18}$$

where the sand load is determined by

$$\Omega_i = \begin{cases} 0 & \text{if} \quad |\theta_i| \leq \theta_{cr} \\ m(|\theta_i| - \theta_{cr})^n & \text{if} \quad |\theta_i| > \theta_{cr} \end{cases} \tag{III.19}$$

where the critical Shields parameter is calculated following Soulsby (1997) and the coefficients $m$ = 9.48 and $n$ = 1.2.

The phase lag parameter ($P_i$), represents the ratio of a representative sediment stirring height and the sediment settling distance. With the addition of the Lagrangian grain motion effect

(crest/trough period correction) and with the settling velocity adjusted for surface waves, the phase-lag parameter for sheet-flow conditions is represented by:

$$P_c = 8\frac{\delta_{sc}}{T_{c,sw}w_{sc}} \qquad \text{(III.20a)}$$

$$P_t = 8\frac{\delta_{st}}{T_{t,sw}w_{st}} \qquad \text{(III.20b)}$$

The two corrections for surface wave effects have a similar influence: a reduction of the phase lag parameter for the crest $P_c$ and an increase of the parameter of the trough $P_t$, both lead to a shift of the net sand transport in the onshore direction.

# 6. DISCUSSION AND CONCLUSIONS

## 6.1 Discussion

### 6.1.1 Sand transport experiments

Full-scale surface wave experiments in which wave boundary layer flow velocities, sheet-flow layer concentrations and sand fluxes are measured in combination with the total sand transport rates were not performed before with the level of detail as presented in this thesis. The advantage of these large scale surface waves is that processes occurring under real waves are better represented than in small scale experiments. At the same time, due to these large scale conditions, the measurement accuracies as obtained in oscillatory flow tunnel experiments could not be reached here. The progression and deformation of the waves is not as easy to control as oscillatory flow and it is more difficult to perform measurements close to the bed with the required detail. Besides that, contrary to oscillatory flow tunnels and smaller flumes, what happens near the bed under 3.5 m of flume water cannot be checked visually (despite the windows at the side of the flume, the dirty canal water prevents a clear view of the bed). This while small variations in the sand bed and wave characteristics may have a large influence on the experimental results.

To minimize the effect of measurement uncertainties the following measures were taken in the design of the experiments; i) all wave conditions were repeated for a number of times (at least 6 runs per condition with a total duration of at least 5 hours), ii) the detailed measurements were repeated during these wave runs and different runs were compared for analyses, iii) a ripple profiler, pressure sensor, wave gauges and flow velocity meters high above the bed were used to monitor any changes in the wave conditions or the sand bed during the measurements. The measurements were done with regular waves and uniform sand since this makes it possible to systematically investigate the influence of parameters such as e.g. flow velocities, wave period, velocity skewness, and grain size. For future research it would be desirable to extend this to experiments with irregular waves and graded sediments, to get a more realistic result in comparison to field conditions. Dohmen-Janssen and Hanes (2005) showed for the SISTEX (medium sand) measurements, that under irregular waves, the quasi-steady behaviour of the transport rate is still valid. Whether this would be the same for fine sand conditions is still unknown. It should also be realized that due to the use of a horizontal mobile sand bed, bed slope effects on the flow, fluxes and transport rates were not investigated in the present work.

The research and new experiments were aimed at wave-dominated conditions in a (only) 5 m wide flume without tides and (other) longshore currents and the detailed measurements were only performed under non-breaking waves. It remains therefore unclear to what extent and how the wave boundary layer processes are influenced by the presence of an extra (by tides or breaking waves) generated turbulence above the wave boundary layer. Dohmen-Janssen (1999) showed with oscillatory flow tunnel experiments that a superimposed mean current on top of an oscillatory flow leads to higher suspended sediment concentrations above the wave boundary layer. However, the sheet-flow layer processes remain more or less similar and the sediment transport is still concentrated inside the sheet-flow layer. Fredsøe et al. (2003) showed in oscillatory flow tunnel experiments with a fixed bed that this 'extra' turbulence can influence the wave boundary layer flow and bed shear stress. Besides this, higher up in the water column, turbulence generated by breaking waves leads to extra entrainment of suspended sediment, which can then be transported offshore due to the undertow, leading to an important offshore component of the total sand transport rates

(Van Rijn, 2007). During the new experiments it was shown that in the free-stream, the mean velocity profile shows an increasing off-shore direction from the bed upwards, generated by the undertow (Eekhout, 2008). However, under the non-breaking waves at the location of the detailed measurements, the amount of sand being transported at these heights above the bed can be neglected in comparison with the transport rates inside the sheet-flow layer.

The flow velocity measurements show results deep inside the sheet-flow layer. Although, not completely into the lowest part of the pickup layer, where large parts of the transport are concentrated. Here, the sediment concentrations are too high to perform accurate velocity measurements with acoustic techniques and the flow velocities were therefore extrapolated to the level of erosion depth (where the flow velocity is zero). Also direct measurements of vertical flow velocities and with that of the wave Reynolds stress $< \tilde{u}\tilde{w} >$ in this layer were therefore not possible. Nevertheless, the new detailed measurements give, certainly in relation to knowledge from previous full scale surface wave experiments, new insights into the flow velocities and fluxes near the bed. No complete explanation could be given yet for everything which is observed, for instance:

- Is the larger erosion depth asymmetry under surface waves (especially for fine sand conditions) caused by a larger bed shear stress asymmetry due to wave boundary layer streaming?
- How do the high-concentration sheet-flow layer processes, such as grain-grain-flow interactions in the pick-up layer influence the oscillatory and mean flow in the wave boundary layer above?

It is also not fully clear why the new experiments show slightly smaller transport rates than the earlier SISTEX experiments. Although it is shown that it makes a large difference whether the third order velocity moment $<U^3>$, used for comparison of transport rates, is measured close to the edge of the wave boundary layer ($z$ = 40 mm) or higher up in the free-stream ($z \approx 1$ m), the $<q_s>$ - $<U^3>$ relation stays below the same relation for the SISTEX-experiments during which the velocities were measured at $z$ = 10 cm above the bed. A more detailed comparison of the datasets reveals that the differences primarily occur for the conditions with a high third order flow velocity moment $<U^3>$ (SISTEX mf and me conditions). For these cases the two SISTEX conditions have a longer wave period ($T$ = 9.1 s) than the new experiments ($T$ = 6.5 – 7.5 s). The flux measurements of the new experiments show a wave period influence which seems to be consistent with this: an increase in wave period leads to larger sediment fluxes inside the sheet flow layer and also to a larger onshore sediment transport rate. Such a period influence is neglected the $<q_s>$-$<U^3>$ transport relation and is also opposite to the period effect in $<q_s>$-bed shear stress relations (transport formulas). In the latter formulas a wave period increase leads to a decreasing relative roughness and bed shear stress and therefore to a decreasing net transport rate. The detailed sheet flow layer measurements with CCM show that this effect may be explained by the time-dependent sediment pick-up in the lower sheet flow layer. The wave period, controlling the available time for pick-up, may play a limiting role here, an effect which is not included in sand transport models so far.

The median grain size ($D_{50}$) of the sand used in the new medium sand experiments is comparable to that used in the SISTEX experiments (245 µm vs. 240 µm). However, the $D_{90}$ of the new experiments medium sand is clearly larger than that of the SISTEX experiments (420 µm vs. 280 µm). The present experiments show that coarser sediment leads to smaller erosion depths, smaller sheet-flow layer thickness and therefore smaller available sediment loads for transport. So this may explain the smaller transport rates for the new experiments in comparison with the SISTEX experiments with similar $<U^3>$.

### 6.1.2 Sand transport models

The new and existing surface wave transport rate data are compared to two existing practical sand transport models: Van Rijn (2007) and Nielsen (2006). Both are quasi-steady empirical models and have a method to account for streaming effects under surface waves. The Van Rijn (2007) model includes wave induced streaming effects by adding a mean (streaming) velocity to the instantaneous orbital velocity at the edge of the wave boundary layer. The Nielsen (2006) model includes wave induced streaming effects by adding a streaming related mean bed shear stress (wave Reynolds stress) to the instantaneous bed shear stress. The present experiments showed that i) the velocity (streaming) profile in the wave boundary layer has a complex layer structure, which is also strongly affected by the velocity skewness and ii) the vast majority of sand transport takes place very close to the bed, deep inside the sheet flow layer. Using an additional mean bed shear stress is therefore probably more suitable than using an additional mean velocity at the edge of the wave boundary layer to account for the surface wave streaming influence on the net transport rate.

The transport models used are generally classified as bed-load models. The classical definition of a bed-load layer is that of a layer of rolling grains in contact with the immobile bed. Above that a suspension layer may develop, dominated by turbulent diffusion and grain settling. This concept is not valid for sheet-flow conditions, where more grain layers with a high concentration are constantly moving close to the bed, influenced by time-dependent pick-up and settling processes. This leads to different views on how sheet-flow layer processes should be modelled:

- Sheet-flow layer as suspension with a bed-load formula added for the part closest to the bed (e.g. Davies & Li, 1997; Hassan & Ribberink, 2003).
- Quasi-steady bed load formulae, applied for the transport rates inside the complete sheet-flow layer, with the limitation that this is only valid for sediment with $D_{50} > 0.2$ mm (no phase lag effects) and also the lag in pick-up processes occurring with these sediments are not accounted for (e.g. Van Rijn, 2007; Nielsen, 2006).
- Semi-unsteady bed load formula for the complete sheet-flow layer. Here also phase-lag effects inside the sheet-flow layer (pick-up and entrainment) are accounted for in a parameterised way (Dibajnia and Watanabe, 1992; 1998; Dohmen-Janssen, 1999; Van der A et al., 2010).

Which concept is preferable may depend on the application of the model. For process-research aimed at the better understanding of physics, a concept such as developed by Davies & Li (1997) or more complex 2-phase models (e.g. Amoudry et al., 2008) could be preferred. However, for practical coastal erosion/ sedimentation studies these research models are still too (computer)time consuming and a robust semi-unsteady formula (e.g. Van der A et al., 2010) is probably preferable.

The validity of new practical sand transport formulas can be tested by morphodynamic experiments after implementing the new formula in a morphodynamic model. Van Rijn et al. (2011) performed a numerical simulation of erosion and accretion of plane sloping beaches by irregular wave attack in (full-scale) flume experiments. Three models (CROSMOR, UNIBEST-TC and DELFT3D) were used to simulate the experimental results focusing on the wave height distribution and morphological development of the beach profiles. One of their conclusions was that the model performance for the accretive test was less good than that for the erosive tests. It appeared that the onshore transport rates are underestimated by the current models. The results of the new experiments show that various transport mechanisms (e.g. wave boundary layer streaming and sediment advection processes) lead to a larger onshore transport rate than was assumed from previous oscillatory flow tunnel experiments. Thereby, Van der A (2010) showed that also

acceleration skewness leads to a larger onshore transport. It remains to be seen whether the new SANTOSS practical sand transport model, which takes these effects into account, leads to better predictions of these accretive beach tests.

## 6.2 Conclusions

As result of this research, for the first time detailed measurements of wave boundary layer flow and sheet-flow layer transport processes under full scale surface waves are presented. These results give new insights and provide quantitative data of sediment fluxes and net transport rates under velocity skewed surface waves for different wave conditions and types of sediment.

Below, more detailed conclusions are given with the use of the research questions as stated in the introduction of this thesis.

**Research questions**

**Database and design of the new experiments**

1. *What are the gaps in existing data and which gaps need to be covered with new experiments to obtain a better understanding of progressive surface wave effects on sand transport processes?*

With the construction of the SANTOSS database it became clear that the number of existing experiments enabling analysis of 'surface wave' effects is very limited. The available detailed full-scale surface wave data was limited to the SISTEX measurement campaign (see e.g. Ribberink et al., (2000) and Dohmen-Janssen & Hanes (2002)), which provides data for non-breaking surface waves in the sheet flow regime with a medium sand mobile bed. These experiments show a potential importance of surface wave effects for the net transport rates in coastal areas. However, it is also concluded that to be able to gain better understanding of these effects, more insight is needed in the details of the sand transport processes inside the sheet flow layer and wave boundary layer. The following data is therefore to be obtained from the new experiments:

- Detailed time-dependent and time-averaged flow velocity measurements throughout the complete wave boundary layer and the free-stream over the total wave cycle.
- Detailed time-dependent and time-averaged concentration and sediment flux measurements throughout the complete sheet flow layer and suspension layer over the total wave cycle.
- A set of measured total net sand transport rates.
- All three of the above under various hydrodynamic (wave) conditions and for both medium and fine sand mobile beds.

**Experimental set-up**

2. *How can we measure the wave boundary layer and sheet flow layer processes near the bed under full-scale progressive surface waves?*

A new measurement set-up (wall frames, buried tank with various instruments) was designed for these experiments. For the detailed measurements near the sand bed, special rigs were designed to achieve the required high spatial ($10^{-3}$ – $10^{-2}$ m) and high temporal ($10^{-3}$ – $10^{-1}$ s) measurement resolutions, while at the same time avoiding flow disturbances as much as possible and being rigid enough to withstand the wave forces. The UVPs used for the wave boundary layer flow velocities were used before for similar experiments under oscillatory flow tunnel conditions, but not yet under full scale surface waves. The complete measurement set-up made it possible to measure (time-

dependent) flow velocities inside the free-stream and wave boundary layer, (time-dependent) sediment concentrations inside the sheet-flow layer and suspension layer and the total net sand transport rates along the flume. It is the first time that such a complete and detailed data-set is obtained under full scale surface wave conditions with medium and fine sand mobile beds.

**Experimental results**

3. *To what extent do the wave boundary layer and sheet flow layer processes control the net sand transport under these wave conditions?*
4. *How does the grain size affect these wave boundary layer processes and the net sand transport rate?*
5. *How do these detailed processes and the net transport rates relate to the knowledge obtained from oscillatory flow tunnel experiments with similar conditions?*

The time-dependent horizontal oscillatory flows in the upper part of the wave boundary layer (above the sheet flow layer) show similar results for both the medium and fine sand conditions and qualitatively the same behaviour as known from measurements in flow tunnels and from oscillatory boundary layer flow models.

The measured mean velocity profiles in the wave boundary layer show a characteristic vertical three-layer structure for all experiments with 'onshore' as well as 'offshore' streaming and with alternating negative and positive shear layers in between. This pattern is present during all experiments for medium as well as fine sand. Meanwhile, the structure shows systematic differences with the streaming profile shapes as measured in oscillating flow tunnels for similar velocity skewed oscillatory flows and similar sands. Above the sheet flow layer the streaming is generally more offshore directed in tunnels than under progressive surface waves, which is explained by the absence of the wave Reynolds stress in tunnels. Above the wave boundary layer the opposite takes place due to the opposite sign of the mean pressure gradient in tunnels (negative in tunnels, positive under progressive surface waves).

For progressive surface waves generating velocity-skewed oscillatory flows, erosion-depth asymmetry appears to be a dominant mechanism responsible for 'onshore' streaming in the lowest part of the sheet flow layer ($z < 0$, pick-up layer) for medium as well as fine sand. For medium sand the erosion depths agree well with those measured in flow tunnels and also show a similar asymmetry. However, for fine sand erosion depth asymmetry is not only absent in tunnels but the erosion depths of the new surface wave experiments are also systematically larger than in tunnels. The additional wave Reynolds stress under progressive surface waves may be responsible for an additional erosion depth asymmetry. But also horizontal and vertical advection effects under surface waves, which are not present in tunnels, may play a role here. Based on the measurements, new empirical relations are presented for erosion depth and sheet-flow layer thickness.

For both types of sand, the total horizontal mean sediment flux shows a 2-layer structure, with an onshore directed flux in the lower part of the pick-up layer and a, slightly smaller, offshore directed part above that. The onshore directed part of the total mean flux is due to the erosion depth asymmetry, caused by the flow velocity skewness. Here, the current- and wave-related part of the flux are both positive and complement one another. The upper off-shore directed part of the total mean flux consists of a large negative wave-related part and a smaller positive current-related part. The negative wave related part is caused by increasing and decreasing pick-up layer concentrations

during respectively the positive onshore and negative offshore flow velocities during a wave cycle ($< \tilde{u}\tilde{c} > < 0$).

Especially for fine sand cases, the measured sediment fluxes differ strongly from previously obtained oscillatory flow tunnel results. The maximum on- and off-shore fluxes are not only larger, but the total mean flux appears to be positive and on-shore directed under progressive surface waves, instead of negative and off-shore directed in oscillatory flow tunnels. This difference in transport direction is consistent with the observed difference in erosion depth asymmetry. The latter is absent in oscillatory flows in the case of fine sand conditions. The current research did not give conclusive insights into the reason for this. It is likely that real wave streaming and other intra-wave advection processes, lacking in tunnels, play a role here.

The new experiments show a linear increase in transport rates with an increase in the third-order moment of the time-dependent velocity in the free stream, for both the medium and fine sand. The transition from onshore to offshore net transport with increasing flow strength as measured for fine sand conditions in oscillatory flow tunnels, is not observed under surface waves. A likely explanation for this difference is that phase lag effects of fine sand, responsible for the transition to offshore net transport, are now overruled by progressive surface wave effects, such as a larger 'onshore' mean bed shear stress (wave Reynolds stress) and the onshore directed wave boundary layer streaming. The wave Reynolds stress leads to additional crest and trough asymmetry of the bed shear stress, additional erosion depth asymmetry and thus to more onshore sand transport. The onshore streaming leads to an additional current-related sediment flux in the onshore direction. It is shown that, since the far majority of sand is transported inside the (lower) sheet flow layer, relatively small wave induced net currents may have an important effect on the sand transport rates under these conditions.

**Practical sand transport models**

6. *How do practical sand transport models account for surface wave effects and how can the new insights from the new experiments add to the development of an improved practical sand transport model?*

Three practical sand transport models were tested against the available transport measurements under full-scale surface waves; 2 quasi-steady models (Van Rijn, 2007 and Nielsen, 2006) and 1 semi-unsteady model (SANTOSS-model).

The quasi-steady models (Van Rijn, 2007 and Nielsen, 2006) assume that the intra-wave transport is coupled instantaneously to the intra-wave bed shear stress. For the application in surface wave conditions the models are provided with an additional onshore-directed mean velocity (streaming velocity in the Van Rijn model) or an additional onshore mean bed shear stress (wave Reynolds stress in the Nielsen model). Despite its quasi-steady approach, the model of van Rijn gives good predictions of the new flume transport data, also for fine sand conditions in which unsteady or phase-lag effects play a role. The model of Nielsen gives a systematic overprediction of the new data.

The SANTOSS model is a semi-unsteady model and gives in principle a better description of phase-lag effects on the net transport. Solely including onshore streaming in the transport formula was not sufficient to reverse the net transport of fine sand from offshore (in oscillatory flow tunnels) to onshore and to find agreement with the new surface wave data. It appeared that other surface wave effects, such as the influence of vertical orbital flow on the settling velocity and the Lagrangian motion of sand particles (advection effects) also play a role and should be included in the model.

The phase-lag effects and the advection processes seem to compensate each other to some extent for the investigated surface wave conditions in the experiments. It is not clear whether this compensation is a phenomenon which generally occurs for a wide range of (surface) wave and sediment conditions.

## 6.3 Recommendations

The new experiments as presented in this thesis filled some of the existing gaps in available sand transport data and knowledge. However, Van der Werf et al. (2009) clearly indicated that more experiments are still required; i) graded sand experiments, ii) wave-plus-current experiments and iii) and large scale surface wave experiments in the ripple regime. For future research it would be desirable to extend this also to experiments with irregular waves and sloping beds, to get a more realistic result in comparison to field conditions. Apart from these different experimental regimes and conditions non-breaking asymmetric surface waves represent only part of the shallow water coastal area where sand is being transported. To gain better overall knowledge on cross-shore transport rates, experiments should also be extended into the breaker zone, also including (acceleration skewed) bores and into the swash zone.

Implementing newly obtained knowledge on cross-shore sediment transport in morphodynamic models would be valuable to investigate how these processes interact with other dynamics such as long-shore currents, tides, sea bed and coastline morphology. In this way, the value of newly obtained knowledge and developed sand transport formula can be studied in practice by coastal engineers, scientists and managers, who need well-founded methods for predicting sand transport in coastal areas.

The newly developed SANTOSS practical model is currently being implemented in a cross-shore morphological model to further test its validity and compare its performance with existing transport formula. Future work is aimed at i) further improvement of modelling surface wave effects and ii) extending the model to irregular wave and breaking wave conditions (Van der A et al., 2010).

Further interpretation of the new surface wave measurements using detailed process-based wave boundary layer and sheet flow models is recommended for obtaining better quantitative explanations of the observed wave boundary layer flows and sheet flow layer processes, which cannot always be investigated from the measurements (see for instance Kranenburg et al.,2010). These process-based models are also relevant for further development of parameterizations of wave-induced sediment transport in morphodynamic models. Systematic exploration of the parameter space using validated process-based models is expected to give additional insight in the various real wave effects discussed above and their relative contribution to cross-shore sediment transport.

## References


Amoudry, L., T.-J. Hsu and P.L.-F. Liu. 2008. Two-phase model for sand transport in sheet flow regime. *Journal of Geophysical Research*, vol. 113, C03011.

Davies, A.G. and Li, Z. 1997. Modelling sediment transport beneath regular symmetrical and asymmetrical waves above a plane bed. *Continental Shelf Research,* 17(5), 555-582.

Dibajnia, M. and A. Watanabe, 1992. Sheet flow under non-linear waves and currents. *Proceedings of the 23rd International Conference on Coastal Engineering*, Venice, Italy, pp. 2015-2028.

Dibajnia, M. and A. Watanabe. 1998. Transport rate under irregular sheet flow conditions. *Coastal Engineering*, 35, 167-183.

Dohmen-Janssen, C.M. 1999. Grain size influence on sediment transport in oscillatory sheet flow – phase lags and mobile-bed effect. *PhD-thesis,* Delft University of technology Delft, The Netherlands. 246 pp.

Dohmen-Janssen, C.M. and D.M. Hanes. 2002. Sheet flow dynamics under monochromatic nonbreaking waves. *Journal of Geophysical Research,* 107(C10), 3149.

Dohmen-Janssen, C.M. and D.M. Hanes. 2005. Sheet flow and suspended sediment due to wave groups in a large wave flume. *Continental Shelf Research*, 25, 333 – 347.

Eekhout, J.P.C. 2008. Measurements and modeling of cross-shore morphodynamics. *MSc thesis.* University of Twente, The Netherlands.

Fredsøe, J., B.M. Sumer, A. Kozakiewicz, L.H.C. Chua and R. Deigaard. 2003. Effect of externally generated turbulence on wave boundary layer. *Coastal Engineering* 49, 155 – 183.

Hassan, W.N.M. and J.S. Ribberink. 2010. Modelling of sand transport under wave-generated sheet flows with a RANS diffusion model. *Coastal Engineering* 57, 19 – 29.

Kranenburg, W.M., J.S. Ribberink and R.E. Uittenbogaard. 2010. Sand transport by surface waves: can streaming explain the onshore transport? *Proceedings of 32nd International Conference on Coastal Engineering,* Shanghai, China.

Nielsen, P. 2006. Sheet flow sediment transport under waves with acceleration skewness and boundary layer streaming. *Coastal Engineering*, 53, 749 – 758.

Ribberink, J.S., C.M. Dohmen-Janssen, D.M. Hanes, S.R. McLean and C. Vincent. 2000. Near-bed sand transport mechanics under waves – A large-scale flume experiment (Sistex99). *Proceedings of 27th International Conference on Coastal Engineering*, ASCE, 3263-3276.

Van der A, D.A. 2010. Effects of acceleration skewness on oscillatory boundary layers and sheet flow sand transport. *PhD thesis*, University of Aberdeen, U.K.

Van der A, D.A., J.S. Ribberink, J.J. van der Werf and T. O'Donoghue. 2010. New practical model for sand transport induced by non-breaking waves and currents. *Proceedings of 32nd International Conference on Coastal Engineering*, Shanghai, China.

Van der Werf, J.J., J.L.M. Schretlen, J.S. Ribberink and T. O'Donoghue. 2009. Database of full-scale laboratory experiments on wave-driven sand transport processes, *Coastal Engineering* 56, 726 – 732.

Van Rijn, L.C. 2007. Unified view of sediment transport by currents and waves I: Initiation of motion, bed roughness and bed-load transport. *Journal of Hydraulic Engineering*, 133(6), 649 – 667.

Van Rijn, L.C., P.K. Tonnon and D.J.R. Walstra. 2011. Numerical modelling of erosion and accretion of plane sloping beaches at different scales. *Coastal Engineering* 58, 637 – 655.

## List of symbols

| | |
|---|---|
| $<...>$ | wave averaged components |
| $\tilde{...}$ | intra-wave components |
| | |
| $A$ | amplitude of the wave/peak orbital motion |
| $C, c$ | sediment concentration |
| $c(t)$ | intra-wave concentrations |
| $c(z)$ | time averaged concentration profile |
| $<c(z)>$ | wave averaged concentrations |
| $c$ | wave celerity |
| $D_{10}$ | grain diameter exceeded by 90% by weight of sample |
| $D_{50}$ | median grain diameter |
| $D_{90}$ | grain diameter exceeded by 10% by weight of sample |
| $d_e$ | erosion depth |
| $d_g$ | horizontal grain displacement |
| $f_w$ | wave friction coefficient |
| $g$ | gravity acceleration |
| $G_{tot}$ | total dry mass of sand |
| $h$ | water depth |
| $H$ | wave height |
| $k_N$ | Nikuradse equivalent grain roughness |
| $k_s$ | roughness height |
| $p$ | pressure |
| P | phase lag parameter |
| $q_s$ | sediment transport rate |
| $<q_s>$ | net sand transport rates |
| $R$ | velocity skewness |
| $s$ | relative sediment density ($\rho_s / \rho$) |
| $t$ | time |
| $T$ | wave period |
| $U, u$ | horizontal flow velocity |
| $u_{s,on}$ | Stokes drift caused by the surface waves |
| $u_{m,off}$ | undertow (return flow from the beach) |
| $u_{b,on}$ | boundary layer streaming |
| $u(t)$ | intra-wave velocities |
| $<u>$ | mean flow velocity |
| $<\bar{u}>$ | maximum current velocity |
| $U_{max}$ | maximum onshore free stream orbital velocity |
| $U_{min}$ | maximum offshore free stream orbital velocity |
| $<U^3>$ | third order velocity moment |
| $u_\theta$ | sediment mobilising velocity |
| $\dot{U}_{max}$ | amplitude of the flow acceleration in the wave crest direction |
| $\dot{U}_{min}$ | amplitude of the flow acceleration in the wave trough direction |

| | |
|---|---|
| $\Delta V_{ip}$ | total eroded sand volume (including pores), used in Mass Conservation Technique |
| $w$ | vertical flow velocity |
| $w_s$ | sediment settling velocity |
| $z$ | sand bed level / level above the bed |
| | |
| $\beta$ | acceleration skewness |
| $\delta_b$ | wave boundary layer thickness |
| $\delta_s$ | sheet flow layer thickness |
| $\varepsilon_0$ | bed porosity |
| $\zeta$ | ratio of the horizontal grain-velocity amplitude and free-stream velocity amplitude |
| $\eta$ | bed level elevation |
| $\theta$ | Shields parameter |
| $\nu_t$ | turbulent eddy viscosity |
| $\nu$ | kinematic viscosity coefficient |
| $\rho$ | density of water |
| $\rho_s$ | density of sediment |
| $\tau_{b,cr}$ | critical bed-shear stress according to Shields |
| $\tau'_{b,w}$ | instantaneous grain-related bed-shear stress due to the waves |
| $\varphi_\tau$ | angle which determines the ratio of the effect of sediment mobilizing forces due to drag and/ or acceleration |
| $\Phi$ | Flux |
| $\Psi_w$ | wave mobility number |
| $\omega_p$ | peak angular frequency |
| $\Omega$ | sand load that is entrained |

Subscripts

| | |
|---|---|
| cr | critical |
| max | maximum |
| min | minimum |
| t / trough | belonging to the wave trough |
| c / crest | belonging to the wave crest |
| on | onshore directed |
| off | offshore directed |
| r | reference |
| rms | root-mean-square |
| w / wave | wave related |
| c / current | current related |
| b | bed related |

## List of publications

### Journals

Werf, J.J. Van der, Schretlen, J.L.M., Ribberink, J.S. & O'Donoghue, T. 2009. Database of full-scale laboratory experiments on wave-driven sand transport processes, doi: 10.1016/j.coastaleng.2009.01.008. Coastal engineering, 56(7), 726-732.

Kranenburg, W.M., J.S. Ribberink, J.L.M. Schretlen & R. E. Uittenbogaard. Submitted. Sand transport beneath waves: the role of free surface effects.

Schretlen, J.L.M., J.S. Ribberink, W.M. Kranenburg & T. O'Donoghue. Submitted. Boundary layer velocities measured above mobile beds under full scale progressive surface waves.

### Proceedings

Schretlen, J.L.M., Ribberink, J.S., Kleinhans, M. & O'Donoghue, T. (2010). Boundary layer flow and sand transport under full scale surface waves. In J. Gruene & M. Klein Breteler (Eds.), Proceedings of the Hydralab III Joint user meeting, 2-4 February 2010, Hannover, Germany (pp. 37-40). Hannover: Forschungszentrum Kueste of University Hannover & Technical University Braunschweig.

Schretlen, J.L.M., Ribberink, J.S. & O'Donoghue, T. (2011). Boundary layer flow and sand transport under full scale surface waves, online http://journals.tdl.org/ICCE/article/view/1271. In J. McKee Smith & P. Lynett (Eds.), Proceedings of 32nd International Conference on Coastal Engineering (ICCE), 30 June - 5 July 2010, Shanghai (pp. 1-14). Shanghai: Coastal Engineering Research Council.

Schretlen, J.L.M., Ribberink, J.S. & O'Donoghue, T. (2009). Measurements and modelling of sand transport under full-scale surface waves. In M. Mizuguchi & S. Sato (Eds.), Proceedings of Coastal Dynamics 2009 Impacts of human activities on dynamic coastal processes, 7-11 September 2009, Tokyo, Japan (pp. 1-13). Singapore: World Scientific.

Schretlen, J.L.M., Werf, J.J. Van der, Ribberink, J.S., Kleinhans, M.G., Zuijderwijk, W.M. & O'Donoghue, T. (2009). New high-resolution measurements of wave boundary layer flow under full-scale survace waves. In J. McKee Smith (Ed.), Proceedings of the 31st International Conference Coastal Engineering 2008, 31 August - 5 September 2009, Hamburg, Germany (pp. 1559-1571). Singapore: World Scientific.

Schretlen, J.L.M., Werf, J.J. Van der, Ribberink, J.S., Uittenbogaard, R.E. & O'Donoghue, T. (2007). Surface wave effects on sheet-flow sand transport. In C.M. Dohmen-Janssen & S.J.M.H. Hulscher (Eds.), River, Coastal and Estuarine Morphodynamics, RCEM 2007, 17-21 September 2007, Enschede, The Netherlands, Vol I (pp. 329-335). London: Taylor & Francis Group.

**Abstracts**

Schretlen, J.L.M., Werf, J.J. Van der, Ribberink, J.S., Uittenboogaard, R.. & O'Donoghue, T. (2006). Modelling of cross-shore sand transport under non-breaking waves in sheet flow conditions. In ICCE2006, 30th International Conference, Book of abstracts San Diego, 2-8 September 2006 (pp. 352-352). San Diego.

Schretlen, J.L.M., Werf, J.J. Van der, Kleinhans, M., Eekhout, J.P., Zuijderwijk, W.M., Ribberink, J.S. & O'Donoghue, T. (2008). New high resolution flow and sand transport measurements under full-scale surface waves. In P. Hoekstra (Ed.), Book of abstracts NCK-days 2008, 27-28 March 2008, Delft, The Netherlands (pp. 38-38). Delft: NCK / Deltares.

Schretlen, J.L.M., Werf, J.J. Van der, Ribberink, J.S., Kleinhans, M., Zuijderwijk, M. & O'Donoghue, T. (2008). New high-resolution measurements of wave boundary layer flow and sand concentrations under full-scale surface waves. In J. McKee Smith (Ed.), Proceedings of the 31st International Conference on Coastal Engineering, Hamburg, Germany. (pp. 168-168). New Jersey: World Scientific.

Wong, Wing H., Ribberink, J.S., A, D. van der, Schretlen, J.L.M. & O'Donoghue, T. (2010). A new formula for sand transport under waves and currents. In Book of abstracts NCK-Days 2010, 25-26 March 2010, Westkapelle, The Netherlands (pp. 47-47). Delft: NCK.

**Reports**

Gent, M.R.A van, Coeveld, E.M., Rijn, L.C., Walstra, D.J.R., Graaff, J. van de, Reniers, A.J.H.M., Thiel de Vries, J.S.M. van, Ribberink, J.S., Schretlen, J.L.M. & Grasmeijer, B.T. (2006). Dune erosion. Measurement report large-scale model tests. (WL|Delft Hydraulics reports H4357). Delft, The Netherlands: WL|Delft Hydraulics.

Schretlen, J.L.M. & Werf, J.J. Van der (2006). SANTOSS Database, Existing data from experiments in oscillatory flow tunnels and large wave flumes. (Report SANTOSS_UT_IR1. Civil Engineering & Management Research Report2006R-008/WEM-009 ). Universiteit Twente.

## About the author

I was born on the 17th of April 1979 in Beesel, The Netherlands. Together with my sister I grew up in a small town. After finishing my primary education I went to Bisschoppelijk College Broekhin in Roermond, where I finished my 'VWO'-exams in 1998. Besides the social event called school, I enjoyed being in the outdoors, especially working with ponies and horses and our family camping trips.

From 1998 to 2004 I studied Physical Geography at Utrecht University, where apart from the study programme I spent time on the board of the student association for physical geography students Drift '66, organising the 'β-bedrijvendagen' and volunteering at riding lessons for disabled children. The work for my MSc thesis involved a field campaign and data-analyses in order to evaluate the tidal influences on the beach of Egmond aan Zee, The Netherlands. Before graduating, a fellow student and I decided to go to New Zealand to perform an extra research project at the University of Waikato and Muriwai beach, looking at sedimentary variations in space and through time at this field site.

In 2005 I started my PhD research at the Water Engineering and Management group at the University of Twente in Enschede. Since then, my boyfriend Freek and I moved from Utrecht to Enschede, we have both written a PhD thesis, and gained a lot of new friends and 4-legged housemates here in Twente. Besides work, I enjoy training (my own and other people's) horses, spending time with family and friends and find time for travelling whenever possible.

Since 2010 I have been working at the University of Twente as an assistant professor and coordinator of international affairs for the Civil Engineering and Management department. I will continue to do so for the coming period.

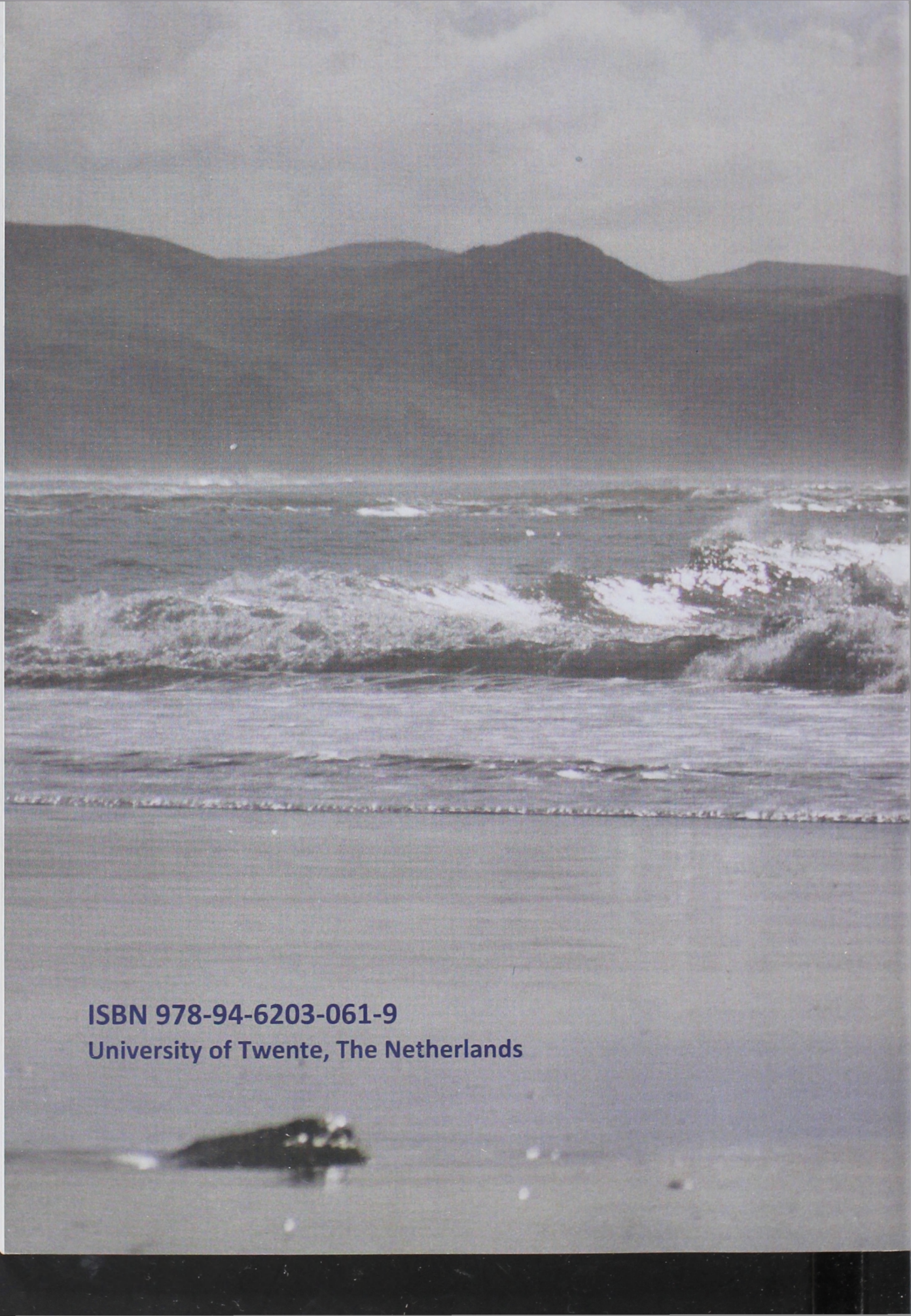

ISBN 978-94-6203-061-9
University of Twente, The Netherlands